TECHNICAL REPORT N-71-3

PROJECT OFFICER'S FINAL REPORT OPERATION DISTANT PLAIN, EVENTS 1, 2A 3, 4, AND 5; PROJECT 3.02A, EARTH MOTION AND STRESS MEASUREMENTS

by

J. K. Ingram

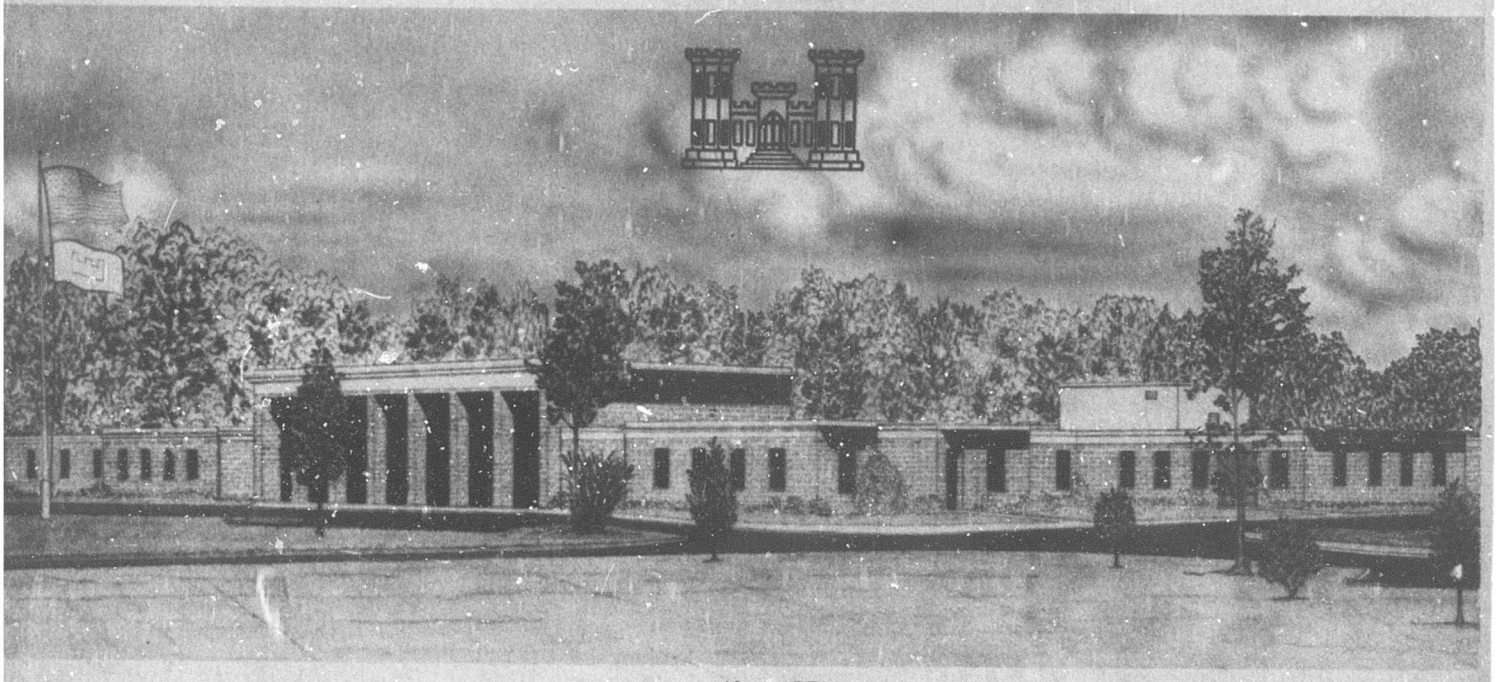

May 1971

Sponsored by Defense Atomic Support Agency

Conducted by U. S. Army Engineer Waterways Experiment Station, Vicksburg, Mississippi

177

Unclassified

Security Classification

DOCUMENT CONTROL DATA - R & D

(Security classification of title, body of abstract and indexing annotation must be entered when the overall report is classified)

1. ORIGINATING ACTIVITY (Corporate author) U. S. Army Engineer Waterways Experiment Station Vicksburg, Mississippi	2a. REPORT SECURITY CLASSIFICATION Unclassified 2b. GROUP

3. REPORT TITLE

PROJECT OFFICER'S FINAL REPORT, OPERATION DISTANT PLAIN, EVENTS 1, 2A, 3, 4, AND 5, PROJECT 3.02a, EARTH MOTION AND STRESS MEASUREMENTS

4. DESCRIPTIVE NOTES (Type of report and inclusive dates)

Final report

5. AUTHOR(S) (First name, middle initial, last name)

James K. Ingram

6. REPORT DATE	7a. TOTAL NO. OF PAGES	7b. NO. OF REFS
May 1971	185	15

8a. CONTRACT OR GRANT NO. b. PROJECT NO. c. NWER Subtask 96X4902 d.	9a. ORIGINATOR'S REPORT NUMBER(S) Technical Report N-71-3 9b. OTHER REPORT NO(S) (Any other numbers that may be assigned this report)

10. DISTRIBUTION STATEMENT

Approved for public release; distribution unlimited.

11. SUPPLEMENTARY NOTES	12. SPONSORING MILITARY ACTIVITY
	Defense Atomic Support Agency Washington, D. C.

13. ABSTRACT

Ground motions and stresses within the upper 10 feet of soil were measured on the Distant Plain events detonated in Canada in 1966-67. Ground motion measurements were unsuccessful for Event 1. Motion data of good quality were obtained for the remaining detonations (Events 2A, 3, 4, and 5). Vertical and horizontal acceleration and velocity and a limited number of vertical stress measurements were made. The surface gas bag, Event 2A, produced no crater. Airblast-induced ground motions for this event were greater than for Distant Plain Events 3 and 5 and Flat Top II and III as the result of significant explosive energy going directly into airblast formation rather than partitioning to the ground through crater formation. Events 3 and 5 and Flat Top II and III were identical in yield and geometry, but differed in site location. An additional variant, frozen ground, was introduced in Event 5. In spite of these variations, ground motions were similar in amplitude and waveform. Variances between Event 3 and Flat Top are attributed to slight differences in test site soils, explosive coupling, and instrument canister placement. The effect of frozen ground on Event 5 motions was generally limited to the horizontal vector near the surface. This was manifested as higher amplitude and frequency accelerations. The thin frozen surface layer allowed greater coupling of high-frequency components which are attenuated by dry alluvium. For Distant Plain Event 4, primary ground motions in the region of tree blowdown were down and away from the point of detonation at early times, then upward due to elastic rebound and, later, to refracted energy from depth. Measured upthrust motions were small and did not contribute significantly to blowdown.

DD FORM 1 NOV 68 1473 REPLACES DD FORM 1473, 1 JAN 64, WHICH IS OBSOLETE FOR ARMY USE.

Unclassified

Security Classification

14 KEY WORDS	LINK A		LINK B		LINK C	
	ROLE	WT	ROLE	WT	ROLE	WT
Distant Plain (Operation)						
Explosion effects						
Ground motion						
Soil stresses						

TECHNICAL REPORT N-71-3

PROJECT OFFICER'S FINAL REPORT OPERATION DISTANT PLAIN, EVENTS 1, 2A 3, 4, AND 5; PROJECT 3.02A, EARTH MOTION AND STRESS MEASUREMENTS

by

J. K. Ingram

May 1971

Sponsored by Defense Atomic Support Agency
NWER Subtask 96X4902

Conducted by U. S. Army Engineer Waterways Experiment Station, Vicksburg, Mississippi

ARMY-MRC VICKSBURG, MISS.

BLANK PAGE

THE CONTENTS OF THIS REPORT ARE NOT TO BE USED FOR ADVERTISING, PUBLICATION, OR PROMOTIONAL PURPOSES. CITATION OF TRADE NAMES DOES NOT CONSTITUTE AN OFFICIAL ENDORSEMENT OR APPROVAL OF THE USE OF SUCH COMMERCIAL PRODUCTS.

ABSTRACT

Ground motions and stresses within the upper 10 feet of soil were measured on the Distant Plain events detonated in Canada in 1966-67. Events 1, 2A, 3, and 5 were detonated at the Drowning Ford Test Site, Defence Research Establishment, Suffield (DRES), Alberta, Canada. Event 4 was detonated at a remote mountainous site near Hinton, Alberta.

Ground motion measurements were unsuccessful for the aboveground detonation (Event 1). Motion data of good quality were obtained for the remaining detonations of the test series (Events 2A, 3, 4, and 5). Acceleration and velocity measurements were made in the vertical and horizontal directions. In addition, a limited number of vertical stress measurements were made. Sixty-four data channels were successfully recorded on Event 2A, 32 for Event 3, 35 for Event 4, and 33 for Event 5. Data waveforms, except for Event 4, are included in Appendix A. Event 4 waveforms are included in Chapter 5.

Detonation of the surface gas bag, Event 2A, produced no crater. Airblast-induced ground motions for this event were greater than for Distant Plain Events 3 and 5 and Flat Top II and III. This was the result of significant explosive energy going directly into airblast formation rather than partitioning to the ground through crater formation.

Distant Plain Events 3 and 5 and Flat Top II and III were identical in yield and geometry, but differed in site location. An additional variant was introduced by Distant Plain Event 5 which was detonated in frozen ground. In spite of these variations, the ground motions were similar in amplitude and waveform. The variances between Distant Plain Event 3 and Flat Top are attributed to slight differences in test site soils, explosive coupling, and instrument canister placement.

The effect of the frozen ground on Distant Plain Event 5 motions was generally limited to the horizontal vector near the surface. This was manifested as higher amplitude and frequency accelerations than for unfrozen ground. The thin frozen surface layer allowed greater coupling of the high-frequency components which are attenuated by dry alluvium.

Distant Plain Event 4 primary ground motions in the region of tree

blowdown were down and away from the point of detonation at early times, then upward due to elastic rebound and, later, refracted energy from depth. Measured upthrust motions were small in the region instrumented and did not contribute significantly to the blowdown process.

PREFACE

This report describes the work conducted by the U. S. Army Engineer Waterways Experiment Station (WES) as Project 3.02a of the Operation Distant Plain Test Series, staged in Alberta, Canada, during 1966-1967. Project 3.02a was funded by the Defense Atomic Support Agency (DASA) under Nuclear Weapons Effects Research (NWER) Subtask 96X4902, and was conducted under the auspices of the Tripartite Technical Cooperation Program.

This work was conducted by personnel of the WES Nuclear Weapons Effects Division under the direction of Mr. G. L. Arbuthnot, Jr., Division Chief, Mr. L. F. Ingram, Chief, Physical Sciences Branch, and Mr. J. D. Day, Chief, Blast and Shock Section. This report was written by Mr. J. K. Ingram, Project Officer.

Messrs. L. T. Watson, Jr., G. P. Bonner, J. L. Pickens, and others of the Instrumentation Services Division provided field technical support in instrument checkout and data acquisition.

COL John R. Oswalt, Jr., CE, COL Levi A. Brown, CE, and COL Ernest D. Peixotto, CE, were Directors of the WES and Messrs. J. B. Tiffany and F. R. Brown were Technical Directors during the investigation and the preparation and publication of this report.

CONTENTS

TABLES

FIGURES

NOTATION

A_h	Horizontal particle acceleration, g's
A_r	Peak resultant particle acceleration, g's
A_v	Vertical particle acceleration, g's
c	Airblast propagation velocity, ft/sec
C_p	Peak stress propagation velocity, ft/sec
C_s	Seismic propagation velocity in the surface material, ft/sec
d	Measurement depth, feet
d_1	Shallower depth, feet
P	Stress at depth, psi
P_{so}	Surface overpressure, psi
P_1	Initial stress or stress at prior depth d_1, psi
R	Horizontal range, feet
T_a	Arrival time, msec
T_r	Rise time, seconds
U_h	Horizontal particle velocity, ft/sec
U_r	Peak resultant particle velocity, ft/sec
U_v	Vertical particle velocity, ft/sec
Z	Depth, feet
θ	The angle of the trailing wave intersection with the ground surface, degrees
ρ	Soil density, pcf

CONVERSION FACTORS, BRITISH TO METRIC UNITS OF MEASUREMENT

British units of measurement used in this report can be converted to metric units as follows.

Multiply	By	To Obtain
feet	0.3048	meters
inches	25.4	millimeters
pounds per cubic foot	16.01846	kilograms per cubic meter
pounds per square inch	6.894757	kilonewtons per square meter
tons	0.9071847	megagrams
Fahrenheit degrees	5/9	Celsius or Kelvin degrees[a]

[a] To obtain Celsius (C) temperature readings from Fahrenheit (F) readings, use the following formula: $C = (5/9)(F - 32)$. To obtain Kelvin (K) readings, use: $K = (5/9)(F - 32) + 273.15$.

CHAPTER 1

INTRODUCTION

1.1 BACKGROUND

Operation Distant Plain consisted of a series of high-explosive (HE) and detonable-gas experiments conducted in Alberta, Canada, during FY 1967 under the auspices of the Tripartite Technical Cooperation Program. This operation is a continuation of a test program begun in 1959 with a 5-ton[1] shot, and followed by a 20-ton shot in 1960, a 100-ton shot in 1961, and more recently, a 500-ton shot in 1964.

This current test series was designed to provide airblast, cratering, and ground-shock data from spherical shots above and at the surface in a particular soil type for both summer and winter conditions for testing prototype instrumentation, determining response of military equipment, and conducting experiments in blast biology. In addition, tree blowdown and defoliation data were to be obtained from a surface burst in a coniferous forest. Table 1.1 lists the events.

Event 1 was a spherical 20-ton TNT charge mounted on a tower with a height of burst (HOB) of 85 feet. Event 2 was a 20-ton-equivalent detonable-gas-filled balloon located at the same HOB and ground zero (GZ) as Event 1. Because of destruction of the gas balloon during the inflation process, Event 2 was rescheduled for testing in October 1966. Event 2A was a 20-ton-equivalent detonable-gas-filled bag (surface), similar to Event 2. Both Events 2 and 2A were to utilize remaining operable instrumentation from Event 1. These detonable-gas shots were aimed at producing blast and thermal effects for target response without creating ejecta and debris.

Both Events 3 and 5 were spherical 20-ton half-buried stacks of TNT. Event 3 served as a normal environmental control shot for an identical frozen-ground shot, Event 5, and to provide correlation with the Flat Top Series (Reference 1). Event 5 was detonated during the winter when the

---

[1] A table of factors for converting British units of measurement to metric units is presented on page 13.

ground was partially frozen. The main objectives of this event were to study cratering and ground-shock effects in a frozen medium. For Event 5, a unique test situation was hoped for: that the ground shock from the detonation would be induced into a three-layered system with a relatively slow-velocity layer sandwiched between the top (frozen) layer and the saturated layer at the water table. Complex ground-wave interactions were expected.

Little specific scientific knowledge has been assimilated on HE effects in a forested area. The mechanics of tree blowdown and defoliation need to be related to air shock and ground motions. Since the resultant conditions directly affect troop, helicopter, and surface vehicle movements, considerable effort has been directed toward this problem. A prototype shot, Blowdown I, was conducted in a tropical rain forest in Australia. Event 4 (Blowdown II) was designed to expand the empirical knowledge to include typical coniferous forest response.

A test site for Event 4 was selected near Hinton, Alberta, Canada, in the Dominion Forest Preserve. The soil of the area is primarily saturated glacial till in a clayey matrix intermixed with occasional thin layers of saturated clay, extending down to bedrock, perhaps at 100 feet. The upper 6 to 8 inches is mostly decaying organic material and root networks. The nature of the soil prevents deep root penetration so that the trees are only loosely anchored. Intuitively, it was felt that, because of these conditions, the directly transmitted ground shock from an explosive source would be transmitted to the root bundle and perhaps contribute to the blowdown mechanism.

1.2 OBJECTIVES AND SCOPE

The objectives of Project 3.02a were to measure earth motions and stresses produced by these detonations, and to analyze and correlate the results with data obtained on other similar shots (Flat Top II and III).

This report covers Project 3.02a participation in Events 1, 2A, and 3 (summer alluvium tests), the Event 4 forest shot (Blowdown II), and Event 5, the frozen-ground shot, of the Operation Distant Plain Test Series.

For each event, vertical and horizontal acceleration, velocity, and

displacement data were obtained for various ranges and depths. Vertical stress data were also obtained for all events except Event 4. The number of data channels employed on each shot is included in Table 1.1. The raw data obtained is given in Appendix A, except for Event 4. Event 4 data traces are given in Chapter 5.

1.3 PREDICTIONS

Predictions for instrument range settings were made from existing equations derived from one-dimensional theory and empirical data. Stress attenuation with depth was determined from the empirical expression developed in Reference 2.

$$P = P_1 \left(\frac{d}{d_1}\right)^{-0.37} \tag{1}$$

Where: P = stress at depth, psi

P_1 = initial stress or stress at shallower depth, psi

d = working depth, feet

d_1 = prior depth, feet

This equation permits incremental stresses to be calculated; however, an initial depth-stress input must be assumed. To set up initial conditions for solution, a depth of 0.5 foot, where the pressure level approximates the ground surface overpressure, was assumed.

Particle velocity was calculated from Equation 2, extracted from the Air Force Design Manual (Reference 3), using pressure inputs previously calculated from Equation 1 above.

$$U_r = \frac{P}{\rho C_p} \tag{2}$$

Where: U_r = peak resultant particle velocity, ft/sec

ρ = soil density (assumed to be approximately 100 pcf)

C_p = peak stress propagation velocity, ft/sec

Particle velocity rise times were calculated from Equation 3 (from Reference 3).

$$T_r = 0.001 + \frac{Z}{C_p} - \frac{Z}{C_s} \tag{3}$$

Where: T_r = rise time, sec

Z = depth, feet

C_s = seismic propagation velocity in the surface material, ft/sec

The peak resultant particle acceleration was predicted using Equation 4.

$$A_r = \frac{2U_r}{T_r} \tag{4}$$

Where: A_r = peak resultant particle acceleration, ft/sec/sec

For acceleration in g's Equation 4 becomes:

$$A_r = \frac{2U_r}{32.2T_r} \tag{5}$$

The angle θ is defined as the angle of the trailing wave intersection with the normal ground surface (Figure 1.1). This angle may be determined either graphically or by the expression:

$$\sin \theta = \frac{C_s}{c} \tag{6}$$

Where: c = airblast velocity, ft/sec

The included angle between the resultant and vertical vectors (Figure 1.1) is equivalent to θ, the trailing wave angle.

The vertical and horizontal acceleration components may now be calculated from Equations 7 and 8:

$$A_v = A_r \cos \theta \tag{7}$$

$$A_h = A_r \sin \theta \tag{8}$$

The vertical and horizontal particle velocity components may similarly be computed.

$$U_v = U_r \cos \theta \tag{9}$$

$$U_h = U_r \sin \theta \tag{10}$$

Table 1.2 lists the predicted values for airblast-induced ground motions computed for Project 3.02a.

TABLE 1.1 DISTANT PLAIN EVENTS

Event	Charge Configuration	Date	Location	No. Data Channels
1	20 tons, spherical, TNT, 8'-foot tower	7 July 1966	Browning Ford Test Range, DRES (Defence Research Establishment, Suffield)	69
2A	20-ton equivalent 62.5-foot radius, hemispherical, detonable gas (propane and oxygen), surface	22 July 1966	Browning Ford Test Range, DRES	69
3	20 tons, spherical, TNT, half-buried	27 July 1966	Browning Ford Test Range, DRES	94
4	50 tons, hemispherical, TNT, surface	16 August 1966	Hinton, Alberta	96
5	20 tons, spherical, TNT, half-buried	9 February 1967	Browning Ford Test Range, DRES	94

TABLE 1.2 PREDICTION DATA FOR AIRBLAST-INDUCED GROUND MOTIONS

Surface Overpressure P_{so}	Gage Depth d	Pressure at Depth P	Resultant Particle Velocity u_r	Rise Time τ_r	Resultant Particle Acceleration A_r	Horizontal Particle Velocity u_h	Horizontal Particle Acceleration A_h	Vertical Particle Velocity u_v	Vertical Particle Acceleration A_v
psi	feet	psi	ft/sec	seconds	g's	ft/sec	g's	ft/sec	g's
1,000	1.5	667.0	62.0	0.0025	1,540.0	--	--	62.0	1,540.0
	5.0	426.0	40.0	0.0060	415.0	--	--	40.0	415.0
	10.0	330.0	31.0	0.0110	174.0	--	--	31.0	174.0
550	1.5	364.0	34.0	0.0025	850.0	9.6	140.0	--	840.0
	5.0	234.0	22.0	0.0060	227.0	3.6	37.0	--	224.0
	10.0	182.0	17.0	0.0110	96.0	2.8	16.0	--	94.0
300	1.5	200.0	19.0	0.0025	470.0	4.2	104.0	--	468.0
	5.0	128.0	12.0	0.0060	124.0	2.6	28.0	--	121.0
	10.0	99.0	9.5	0.0110	53.0	2.1	12.0	--	52.0
	16.0	83.0	7.7	0.0145	29.0	1.5	5.6	--	28.0
200	1.5	133.0	12.0	0.0025	310.0	3.2	82.0	--	308.0
	5.0	86.0	8.0	0.0060	82.0	2.1	22.0	--	79.0
	10.0	66.0	6.2	0.0110	35.0	1.6	9.3	--	34.0
100	1.5	67.0	6.3	0.0025	160.0	2.2	56.0	--	149.0
	5.0	43.0	4.0	0.0060	42.0	1.4	15.0	--	39.0
	10.0	33.0	3.1	0.0110	17.0	1.1	5.9	--	16.0
60	1.5	35.0	3.1	0.0025	77.0	1.4	38.0	--	69.0
	5.0	21.0	1.9	0.0060	20.0	0.94	9.9	--	18.0
	10.0	16.0	1.5	0.0110	9.0	0.74	4.5	--	8.1
30	1.5	20.0	1.9	0.0025	47.0	1.1	28.0	--	36.0
	16.0	7.6	0.8	0.0145	2.6	0.48	1.5	--	2.1
20	1.5	13.0	1.2	0.0025	30.0	0.80	20.0	--	22.0
	5.0	8.0	0.8	0.0060	8.3	0.53	5.5	--	6.1
10	1.5	6.7	0.62	0.0025	15.0	0.49	12.0	--	9.5
5	1.5	3.4	0.33	0.0025	8.2	0.30	7.4	--	4.6

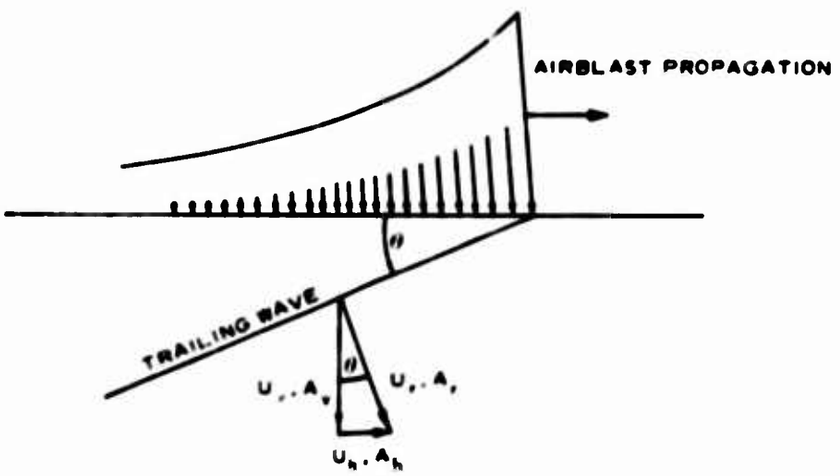

Figure 1.1 Wavefront diagram and force vectors.

CHAPTER 2

INSTRUMENTATION

2.1 DROWNING FORD TEST RANGE

2.1.1 Layout. Test operations for the summer series were to include Events 1, 2, 2A, and 3, held at the Defence Research Establishment, Suffield (DRES), Drowning Ford Test Range; Event 2 was postponed as mentioned in Section 1.1. Because of the compressed shot schedule, gages were emplaced and checked out at the Events 1 and 3 sites simultaneously. Gages recovered from Event 3 were immediately reused on Event 4. All gages were placed essentially along a single radial blast line in each test area (Figure 2.1). Gage signal cables were run in a covered trench to the recording instrumentation located in an 8- by 15-foot concrete bunker. The bunker was located approximately 1,200 feet from GZ. The cable runs were made in two steps. A trunkline approximately 700 feet long was permanently emplaced from the instrument bunker toward the test area, terminating in a hardened junction box. Individual gage cables were run in a covered trench from the placement locations to the junction box.

Events 1, 2, and 2A gagelines were first connected to the recording instrumentation through the junction box. After completion of Events 1 and 2A, the gagelines from the Event 3 site were connected in place of those from the previous setups.

Sixty-five channels of instrumentation were employed for Events 1 and 2A. The area instrumented was greater for these events because of planned measurements directly under the point of burst. The stresses expected to be generated by the high reflected overpressures from Shots 1 and 2A were of particular interest; therefore, the majority of the gages were in this region. Only the most distant stations were located in the mach reflection region. The overpressures expected ranged from 1,000 to 10 psi. The gage array is shown in Figure 2.2. Gages were positioned primarily at depths 1.5, 5.0, and 10.0 feet. Two additional horizontal velocity gages were included, one at the 16-foot depth and 80-foot range and one at the 18-foot depth and 210-foot range.

For each of the surface (i.e. half buried) bursts, Events 3 and 5,

34 instrument channels were used. Measurements were made in the surface overpressure region of 300 to 20 psi as shown in Figure 2.3. The array was designed to determine the different propagation phenomena expected between the frozen and unfrozen ground on Event 5. The array was positioned in order to remain generally in the elastic region of earth response. Projects 3.04a (Sandia Corporation) and 3.04b (Stanford Research Institute) obtained complementary data in the hydrodynamic and plastic (close-in) regions; however, these projects did not participate on Event 5.

2.1.2 Placement Methods. The particle motion canisters used at the Drowning Ford Test Range were placed in 8-inch-diameter augered boreholes. The holes in the Event 1 area were initially drilled by a local contractor using a mud drill. This method proved to be quite unsatisfactory due to the ragged nature of the hole and sidewall wetting. The holes had to be reamed out later by the DRES field crew using an air auger. This latter method was used for the remainder of the instrument holes at Drowning Ford.

In the process of drilling the holes, a fine, free-flowing gray sand was encountered at a depth of 8 to 12 feet. This sand layer, which made it quite difficult to place gage canisters deeper than this level, appeared to be extensive and was observed in all drill holes. Several 3-inch-diameter Shelby-tube samples were taken near the Event 1 area and were analyzed by the Eric H. Wang Civil Engineering Research Facility, Albuquerque, New Mexico. A description of the subsurface material (References 4 and 5) is given in Table 2.1.

The instrument placement technique was as follows. The bottom of the drill hole was tamped smooth and a thin layer of density-matched, low-strength grout was placed in the hole with a 4-inch-diameter plastic pipe. The instrument package was lowered into the hole with a placement tool, properly aligned, and leveled by optical and electrical reference. The canister was held in this position until initial set occurred in the grout. Sufficient additional grout was then added to cover the canister about 4 inches. After the grout had cured, dry masonry sand was rained into the hole and tamped in layers until the next instrument level was reached. Typical gage columns are shown in Figure 2.4.

The stress gages were placed in a separate hole parallel to the

particle motion gage canisters. Gages were placed downhole with a placement tool and the hole was backfilled with dry masonry sand as in the particle motion hole; however, no grout was used.

2.2 HINTON TEST SITE

Particle motion transducers recovered from canisters used in Events 1 and 2A were employed for Event 4. Twenty-four accelerometers and 12 velocity gages were used for a total of 36 channels. No stress gages were used for this test. Figures 2.5 and 2.6 show the Event 4 location plan and gage geometry.

Numerous obstacles were encountered in preparing the test site for gage emplacement. The nature of the glacial till was such that vertical gage holes were difficult to drill. Boulders and cobblestones held in a clayey matrix predominated the geology of the area. A backhoe was finally employed to cut a vertical trench to the desired depth for instrument placement. A cavity the size of the gage canister was then dug in the undisturbed sidewall. The canister was placed in the slot, properly aligned, and grouted in place (Figure 2.7). The trench was then backfilled and tamped. Cables were run in a shallow ditch in both sectors. The cleared sector cable was covered with sand and then indigenous soil. The forest trench was covered only with indigenous material.

Adverse weather conditions prevailed during most of the site preparation. Only 2-1/2 days of good weather were available for canister installation, and all but one of the canisters were emplaced in this period. Figure 2.8 shows the typical surface condition in the cleared sector.

2.3 EQUIPMENT

Ground shock was measured with velocity, acceleration, and earth stress gages. The motion gages (Pace A-18 accelerometers, Reference 6, and Sandia DX velocity gages, Reference 7), which were available commercially, were variable-reluctance-type gages. The stress gages (References 8 and 9) were designed and fabricated by the Waterways Experiment Station (WES). The motion gages and associated calibration and signal conditioning modules were assembled on-site and installed in sealed canisters. Usually,

one vertical and one horizontal accelerometer, and a horizontal velocity gage were employed in each can. The canisters were potted with wax to eliminate mount vibrations and prevent water leakage. The instrument package was designed to approximately match the density of the native alluvium. Soil density ranged from about 82 to 85 pcf for the ranges instrumented; the instrument canister density was 82.5 pcf.

All gages were calibrated in the laboratory before shipment to the test site. The accelerometers were statically calibrated on a spin table, the velocity gages by means of the free-fall method, and the stress gages in a static pressure chamber. All gages were electrically calibrated just prior to shot time. The stress gages were electrically calibrated at the amplifier; however, the particle motion gages were calibrated at the transducer.

The basic electronic system consisted of a 3-kHz carrier amplifier-demodulator system for the particle motion gages and a dc signal conditioner-amplifier system (operational amplifier) for the stress gages. Gage signals were recorded on both FM magnetic tape and light-beam galvanometer oscillographs. These methods have been used with a high degree of success on previous operations. All systems were activated by means of hard-wire signals provided by DRES through the Master Control Countdown System.

The 3-kHz carrier amplifier system response frequency is limited by the amplifier, but is flat up to 600 Hz. The amplifier system used with the stress gages was a dc signal conditioner and amplifier with a flat frequency response up to 20 kHz and a gain of 100. The frequency limiting factor here was the optical galvanometer of the recording oscillograph, which limited the signal frequency to about 2.5 kHz. This limitation is not imposed when coupling this electronic system to high-frequency magnetic tape recorders.

Two developmental accelerometers (Kaman Nuclear Model KA-1100) were mounted along with the Pace gages at the 1.5-foot depth at Locations D and F (Figure 2.1) in Event 2A. Both the Pace and Kaman gages are variable-reluctance gages. The Pace gage is a relatively low-frequency gage (up to 1,200 Hz, depending on range), whereas the Kaman gage is a higher

frequency gage with stated response up to 3,000 Hz, also dependent on range. Generally, the higher the acceleration tolerance of the gage (range), the higher its response frequency. Figure 2.9 shows the internal configuration of the Kaman gage. Signal conditioning for this gage was accomplished through an in-line signal conditioner/amplifier located at the gage. Gage balancing, calibration, and data recording were done in the Ballistic Research Laboratories (BRL) bunker by Kaman Nuclear and BRL personnel. The recorded waveforms and calibrations were provided by BRL.

2.4 GAGE ANNOTATION

The gages were alphanumerically coded by event number, horizontal range from GZ, depth of burial, sector, parameter, and orientation.

For example 2A 95 10 C AV

- 2 — Event
- 95 — Horizontal Range, ft
- 10 — Depth, ft
- C — Sector[1]
- A — Parameter
- V — Orientation

The parameters are identified as:
A = Acceleration
V = Velocity
E = Stress

and orientation as:
H = Horizontal radial
V = Vertical

Single and double integrations of measured data are indicated by the symbols $\int$ and $\iint$, respectively, preceding the gage designation.

2.5 DATA REDUCTION

The oscillographic paper was processed immediately after recovery, whereas the magnetic tape was scanned with an oscilloscope, then sent back to the WES for controlled playback and analysis.

Data reduction consisted of a system of digitizing the analog signal data, along with amplitude and timing code factors, processing the

---

[1] Used for Event 4 only: F = forested sector; C = cleared sector.

digitized data to punched cards for computer input, and running the card decks on the appropriate computer code. Computer input parameters were integrated (either singly or doubly) and processed to hard-copy printout and parameter versus time plots.

Data reduction techniques for Events 1 through 4 consisted of optically digitizing paper oscillograms with an electromechanical curve follower. Each time the scan field boundary was reached, the plot was advanced and reindexed. Paper stretch, reindexing, and operator error all contributed to accummulative error, increasing with length of scan. The accummulated error was compounded with numerical integration, necessary to obtain secondary and in some cases tertiary parameters.

By the time Event 5 data were ready for processing, a new analog-to-digital data converter was operational which could convert the FM analog magnetic tape into computer-compatible digital tape. This advanced processing technique greatly enhanced data reliability for this event.

Because of additional costs required to reprocess the bulk of the test data for increased accuracy, no reprocessing will be attempted.

TABLE 2.1 DESCRIPTION OF DROWNING FORD SOIL

Sample	Depth	Description
	feet	
1	0 to 3	Brown silty clay with considerable organic matter in the form of vertical root systems.
2	3 to 5.8	Tan silty clay, horizontal stratification, small amount of organic matter.
3	5.8 to 6.3	Light brown silty clay, horizontal stratification.
4	6.3 to 7.9	Light brown silty clay.
5	7.9 to 10.8	Alternating layers of light tan to light brown silty clay and fine, clean, gray sand.
6	10.8 to 13.3	Alternating layers of light tan to light brown silty clay and fine, clean, gray sand.

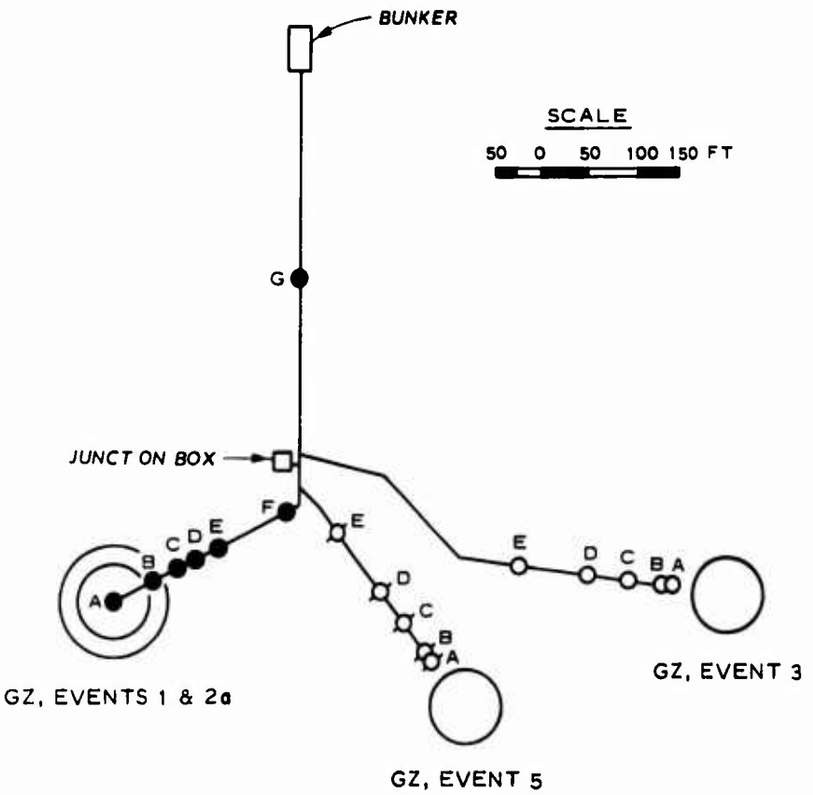

Figure 2.1 Field locations, Events 1, 2A, 3, and 5.

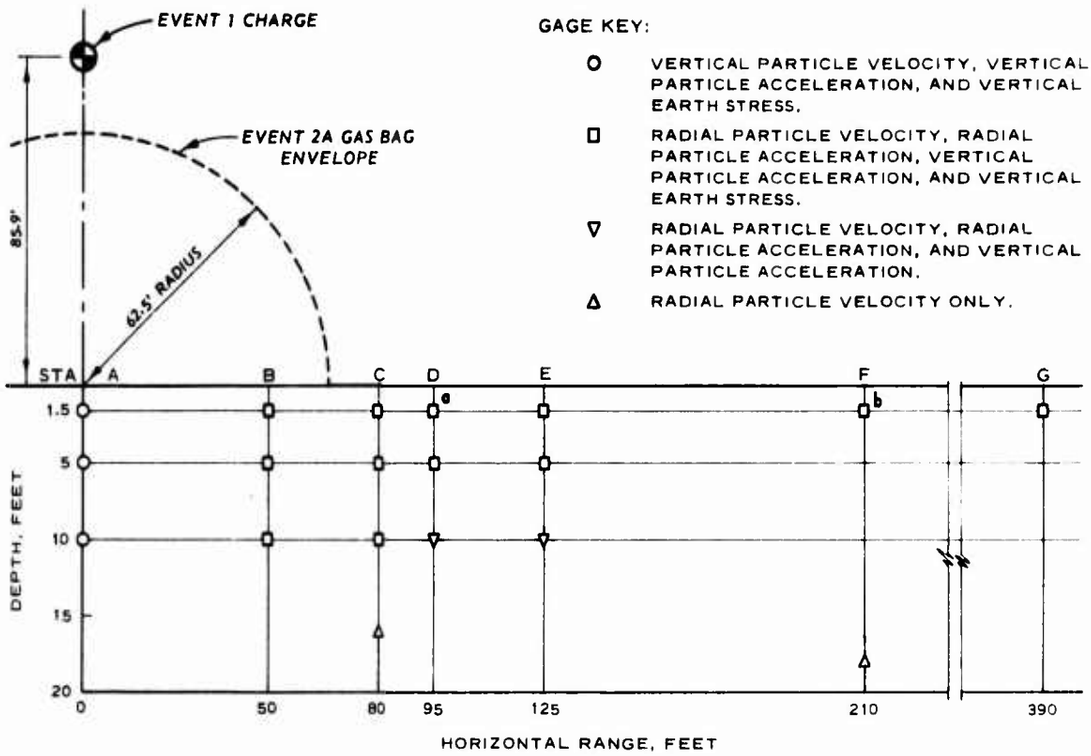

NOTE: 1. EVENT 2A GZ ACTUALLY LOCATED 10 FEET FROM EVENT 1 GZ ON A 79°28'11" ARC OFF NORTH.

2.

STATION	PREDICTED OVERPRESSURE, PSI	MEASURED OVERPRESSURE, PSI[d]	
		EVENT 1	EVENT 2A
A	1,000	600.0	-
B	500	400.0	-
C	300	230.0	120.0
D	200	170.0	75.0
E	100[c]	115.0	44.0
F	30[c]	33.0	21.0
G	10[c]	9.4	7.2

[a] A VERTICAL KAMAN NUCLEAR ACCELEROMETER WAS ALSO INCLUDED AT THIS LOCATION.

[b] A VERTICAL KAMAN NUCLEAR ACCELEROMETER WAS ALSO INCLUDED AT THIS LOCATION. TWO VERTICAL AND TWO HORIZONTAL ACCELEROMETERS WERE ALSO INCLUDED AT THIS RANGE BUT ON DIFFERENT AZIMUTHS.

[c] INCIDENT PRESSURE IN MACH REFLECTION REGION.

[d] BRL PROJECT 1.01.

Figure 2.2 Cross section of gage test plan, Events 1 and 2A.

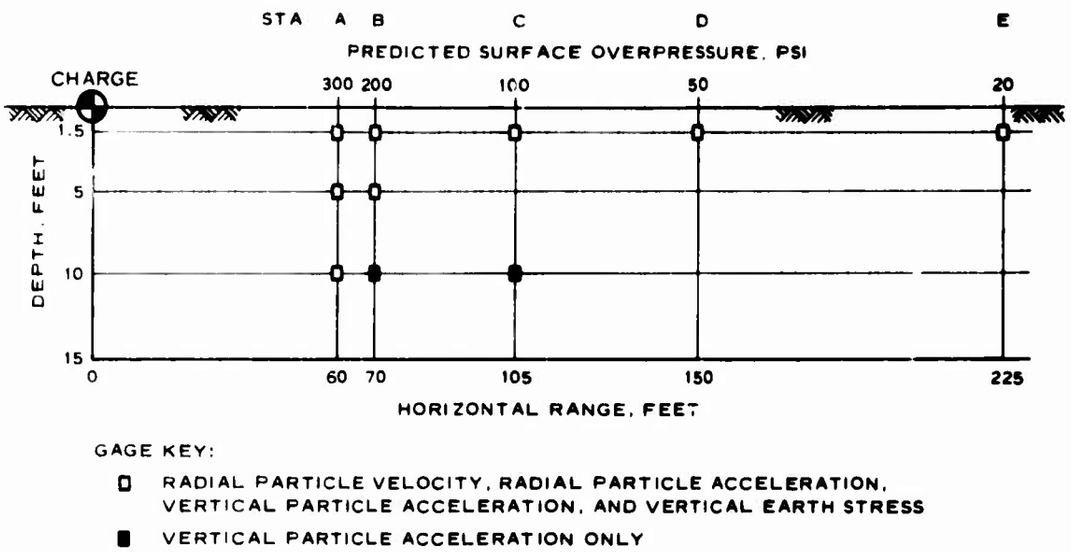

Figure 2.3 Cross section of gage test plan, Events 3 and 5.

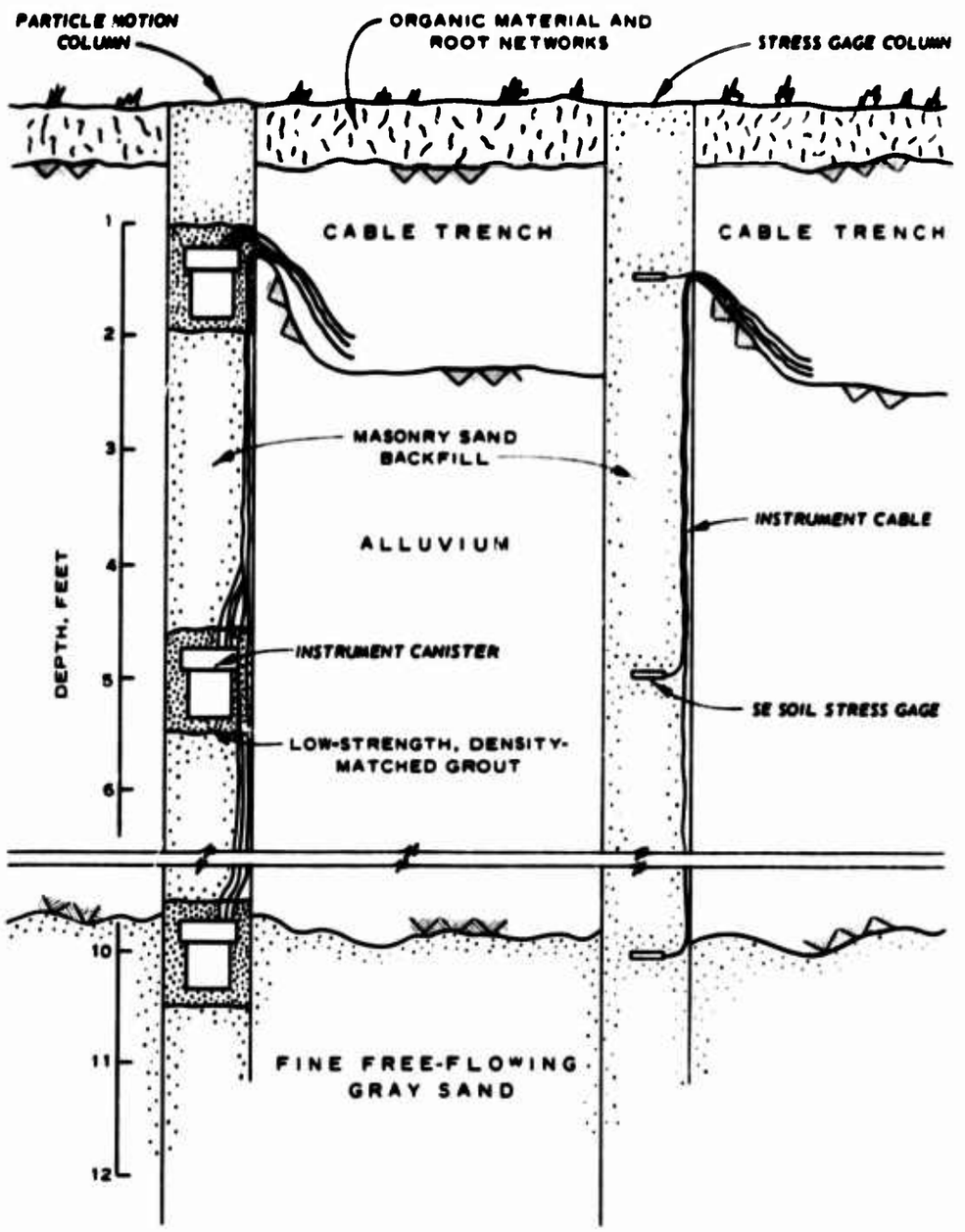

Figure 2.4 Typical gage columns, Drowning Ford Test Site.

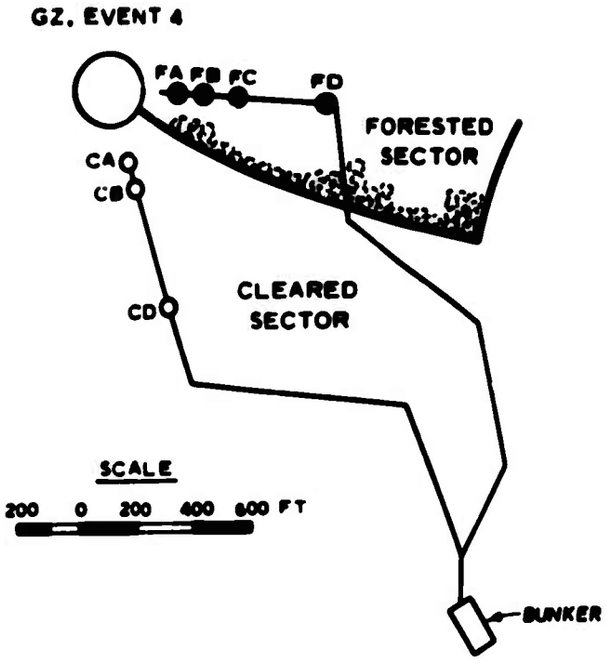

Figure 2.5 Field locations, Event 4.

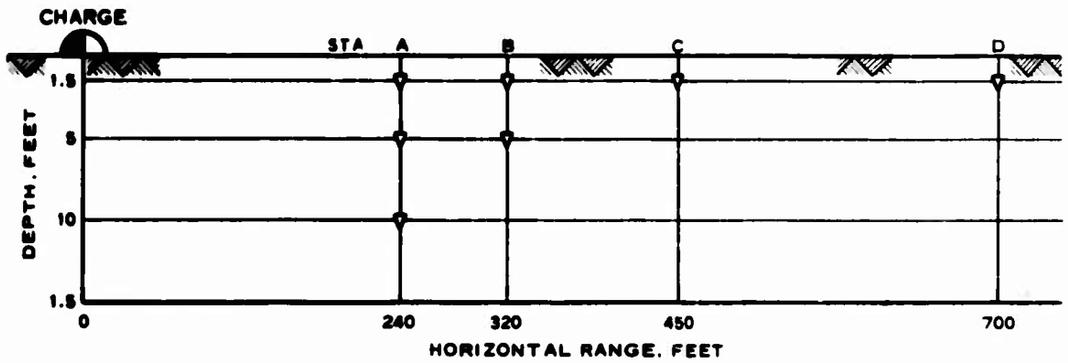

a. FORESTED SECTOR

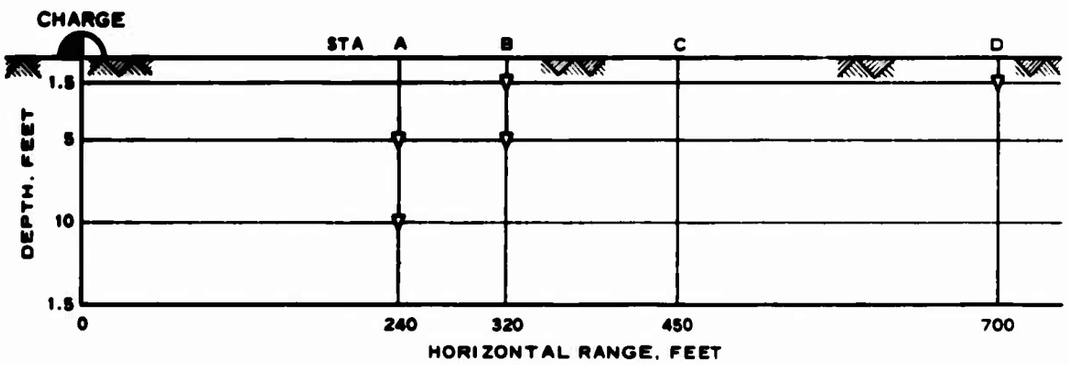

b. CLEARED SECTOR

GAGE KEY:

▼ RADIAL PARTICLE VELOCITY, RADIAL PARTICLE ACCELERATION, AND VERTICAL PARTICLE ACCELERATION

Figure 2.6 Cross section of gage test plan, Event 4.

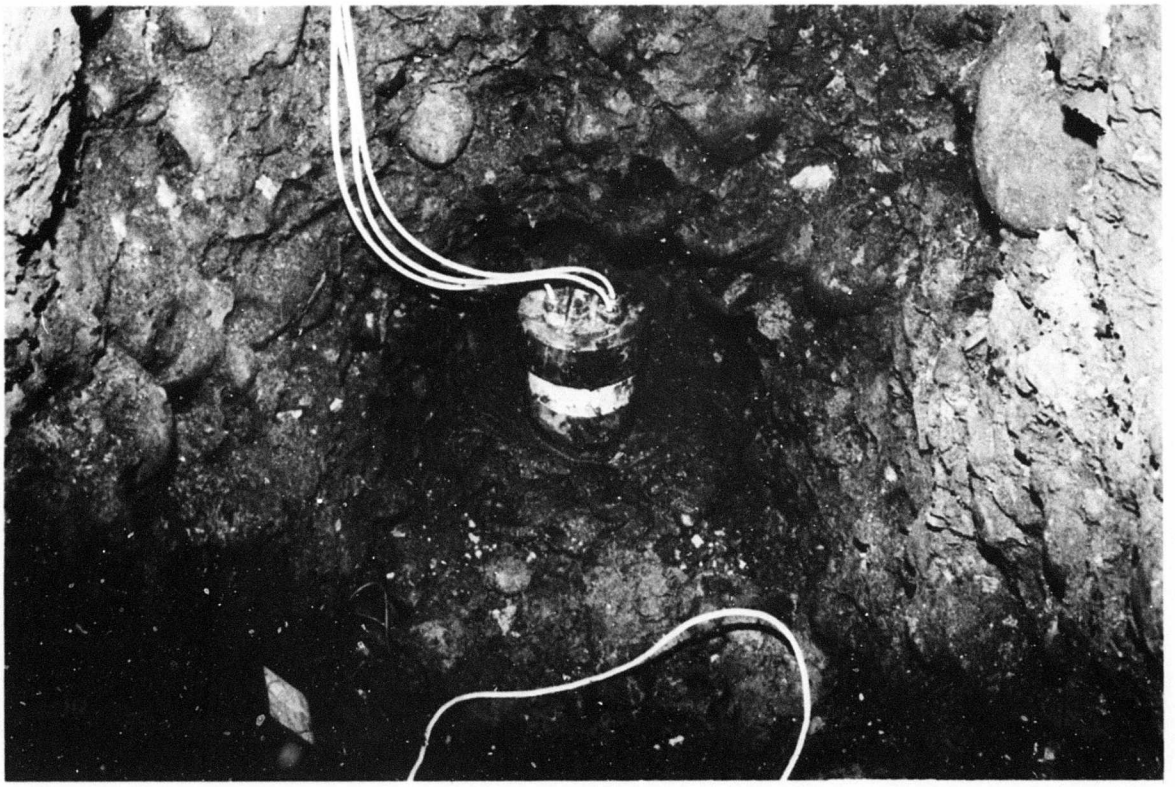

Figure 2.7 Partially grouted instrument canister, 10.0-foot depth, Event 4.

Figure 2.8 Photograph of cleared sector main blast line from GZ, preshot, Event 4.

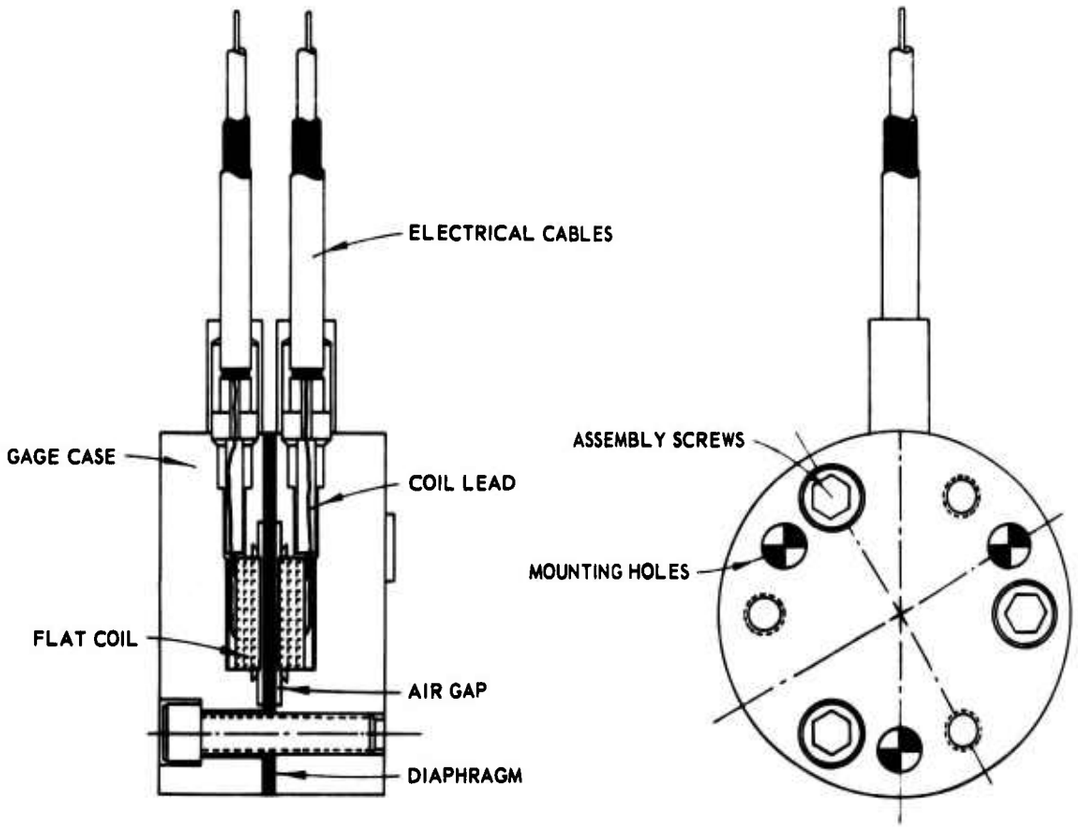

Figure 2.9 Kaman Nuclear experimental accelerometer.

CHAPTER 3

RESULTS, EVENTS 1 AND 2A

3.1 EVENT 1

No data were recorded by Project 3.02a for Event 1. All data channels were operable prior to evacuation of the instrument bunker for remote operation. Failure to properly receive and translate the -30-second primary start signal or the -2-second backup signal from DRES Control resulted in no recording equipment turn-on. Manual shorting of the DRES signal console relay (simulating a start signal) after the shot resulted in a normal turn-on of all systems. A check of the transducers confirmed all units were still in operable condition after the event.

It must be concluded that if either the -30-second primary or -2-second backup signal had been properly received and translated, data would have been acquired.

3.2 EVENT 2A

3.2.1 Data Recovery. Good data recovery was made on Event 2A. Sixty-four of sixty-five data channels yielded information. Peak values and arrival times are given in Tables 3.1 through 3.4.

3.2.2 Ground-Shock Arrival Time. Arrival times were obtained on all channels. The horizontal velocity calculated from propagation times recorded from the gages 1.5 feet deep underlying the gas bag was 8,500 ft/sec, which compares favorably with the computed gas detonation velocity of approximately 8,000 ft/sec. Near-surface horizontal propagation rates compared well with the airblast propagation outside the gas bag.

The seismic velocity of the upper 10 feet of soil was determined by seismic refraction survey before this shot to be approximately 800 ft/sec. The underlying layer, extending beyond 45 feet in depth, had an apparent velocity of 1,400 ft/sec. Propagation velocities for a string of vertical gages near the surface approximated 875 ft/sec and compared well with the seismic velocity for the upper layer. No significant effects of layering were detected in the data.

Figure 3.1 is a plot of near-surface (1.5-foot depth) ground-shock

arrival times versus horizontal range. Good comparison is noted between ground instrumentation and BRL surface airblast arrival (References 4 and 5).

Figure 3.2 is a shock-front diagram constructed from vertical motion and BRL surface airblast arrival times. Normal wavefront progression was observed outside the gas bag; however, an apparent anomaly is indicated for the region beneath the bag. The vertical wave front near the center of the bag appears to lag that near the edge. A possible cause for this occurrence could be a low density in the recompacted material in the area near the center of the bag. This area was dug out for the tower footings on Event 1 and the gas manifold on this event. Initial propagation through a less dense backfill would tend to lag that in a denser in situ material. However, it is doubtful that lag times on the order of those recorded could be effected over the short distance traveled. A mislocated canister was at once suspected since both motion gages were mounted together and yielded the same arrival time. But postshot inspection indicated that the gages were in their proper locations and the stress gages located in a parallel hole support the motion gage data.

3.2.3 Particle Acceleration. Table 3.1 lists the peak acceleration data for this event.

Vertical accelerations, as shown in Figure 3.3, varied from 702 g's directly under the bag to 7 g's at 390-foot range for the near-surface (1.5-foot depth) stations. Peak accelerations at the 5- and 10-foot depths progressively decreased with depth and range with a rate of attenuation like the near-surface stations. Outrunning ground motions were not observed over the ground range instrumented for this shot.

To determine the effect of the gas bag, vertical acceleration waveforms at progressive depths for selected stations beneath the gas bag and outside the bag are compared in Figure 3.4. The pulse width is noted to be less for gages near the edge of the gas bag than near the center or just outside.

Vertical acceleration and velocity were normalized to surface overpressure (Table 3.5) and plotted versus depth (Figure 3.5) to yield a family of response curves relating to the surface airblast loading.

Because points of measurement for surface airblast and ground motion instruments were not coincident, overpressures were derived by interpolation of the BRL data. No pressure data were available for regions within the gas bag; hence, ratios presented are related to positions beyond the bag radius.

Near-surface A_v/P_{so} ratios were as high as 2.13 g's/psi and exceeded unity except at the region of lowest overpressure. A trend of decreasing A_v/P_{so} and U_v/P_{so} ratios with increasing surface overpressure was indicated.

Waveforms for the developmental Kaman Nuclear accelerometers placed at 95- and 210-foot ranges can be compared with those for the Pace gages in Figure 3.6. Peak values are plotted in Figure 3.3. Good comparison in waveforms was noted; however, amplitude disparities were evident at both positions. The 95-foot-range Kaman gage measured exactly one-half the value of the Pace gage, whereas at the 210-foot range the Kaman gage reading was 1.5 times greater than the Pace gage reading. A calibration error is strongly suspected for the Kaman gages. The 95-foot-range Kaman gage apparently underread as compared with the data trend. The rise time for this gage was noted to be 1 msec longer than that for the Pace gage, indicating a possible damping problem. Rise times were identical for Pace and Kaman gages at the 210-foot range. Noise with a frequency of approximately 1,000 Hz was superimposed on the signal of the 210-foot-range Kaman gage. The source of this noise was not determined, but incomplete demodulation of carrier signal is suspected.

In conjunction with a General American Transportation Corporation (GATX) project for Event 1 (References 4 and 5), two vertical accelerometers were placed at the 210-foot range by WES. The GATX project was not part of Event 2A; however, since the depth and range of these gages gave a direct radial comparison with the vertical gage (2A-210-1.5-AV) in the main gageline, output signals were recorded. Waveforms are compared in Figure 3.7. The two auxiliary gages (2A-210-1.5-AV1 and 2A-210-1.5-AV2) compared well in both amplitude and waveform; however, a slight phase shift occurred between these and the primary gage (2A-210-1.5-AV). In addition, the initial pulse duration was much shorter for 2A-210-1.5-AV.

For horizontal acceleration (Figure 3.8), peak near-surface values varied from 58 g's directly under the gas bag to 4 g's at 390-foot range. Figure 3.8 shows a zone extending from 80- to 125-foot range in which there is considerable scatter in the data. A similarity was noted in the horizontal velocity data. The data points at 80- and 95-foot horizontal ranges (Gages 2A-80-1.5-AH and 2A-95-1.5-AH) appear quite low. Upon analyzing the waveforms (Figure 3.9), it was found that the initial peaks had apparently been clipped, possibly due to malfunction in the transducers or some unexpected response in the soil medium. Amplifier and recorder bandpass ranges were well above the data input and are, therefore, not considered sources of error.

It should be noted that peak value for the 10-foot depth at this range also shows a decreased value from the data trend.

3.2.4 Particle Velocity. Peak velocity data are listed in Table 3.2. Direct vertical particle velocity was measured only under the center of the bag at three depths. Peak values ranged from 33 ft/sec at 1.5-foot depth to 7.9 ft/sec at 10-foot depth. The integrated acceleration and measured velocity for these stations are in excellent agreement. Peak vertical velocities for all other stations were obtained by single integration of vertical accelerometer data, and are shown in Figure 3.10. Vertical velocity for the near-surface stations attenuated from 33 ft/sec directly under the bag to 0.5 ft/sec at 390-foot horizontal range. Peak downward velocity attenuated with both depth and range.

Maximum vertical velocity normalized to surface overpressure (Table 3.5) shows the near-surface ratio peaking at 21-psi overpressure, followed by a gentle decrease at higher overpressures. This trend is supported by data from other depths and by the acceleration ratio trends (Figure 3.5).

The peak outward horizontal velocity (Figure 3.11) attenuated relatively little with range at the 5-foot depth. At depths of 10 feet and below, the horizontal velocity showed a consistent pattern of attenuation with both depth and range. Peak measured horizontal velocity (approximately 4 to 5 ft/sec) was greatest at the 1.5-foot depth and 50-foot range (under the bag). No horizontal measurements were made closer than

this station to GZ. Integrated acceleration gave a comparable peak value of approximately 3.1 ft/sec. As noted earlier, the near-surface velocity data show an anomalous region at the same general range as do the horizontal acceleration values. A consistent trend does develop with increasing range; however, the rate of attenuation is quite low.

3.2.5 Displacement. Particle displacements were computed from numerical integration of acceleration and velocity parameters. Considerable scatter was apparent in the computed values. In many instances, reliable peak values could not be determined due to the shape of the computed curves, which were greatly affected by noise, drift (baseline shift), and error in numerical sampling. Computed values are listed in Table 3.3.

Vertical displacement attenuated with range outside the gas envelope at similar rates for all depths instrumented (Figure 3.12). Maximum transient displacement occurred at the center of the gas bag as expected and was on the order of 1.1 feet at 1.5-foot depth. This attenuated to a low of 0.004 foot at the farthest station (390-foot range).

Horizontal displacements ranged from 0.075 foot under the edge of the balloon (50-foot range) to 0.006 foot at 390-foot range and 1.5-foot depth. Significantly greater scatter was present in the horizontal data (Figure 3.13) than in the vertical.

3.2.6 Earth Stress. For the 1.5-foot depth, vertical stress was approximately 890 psi directly under the gas bag, decaying to 9 psi at the 390-foot range (Table 3.4). The near-surface measurements past 50-foot horizontal range are in good agreement with BRL surface airblast data (References 4 and 5), as shown in Figure 3.14. Stress decrease with depth was much more rapid than had been anticipated, producing only marginal output signals. Amplitude accuracy was consequently diminished, and relatively low confidence levels are placed on the data.

Near-surface waveforms are shown in Figure 3.15. Typical airblast loading profiles do not appear to develop in the ground-stress pulse until the wave front is in a free area, outside the containment zone (i.e., the zone directly beneath the gas bag).

Direct comparison is made between near-surface stress and surface airblast waveforms at 80- and 210-foot ranges in Figure 3.16. The loading

fronts appear to be retarded in the alluvium as evidenced by increasing rise times and rapid release of the energy shortly after peaking.

TABLE 3.1 ACCELERATION DATA, EVENT 2A

Gage	Ground Range	Depth	Arrival Time	Peak Positive Acceleration	Time of Peak
	feet	feet	msec	g's	msec
Vertical (Positive Downward):					
2A-0-1.5-AV	0	1.5	3.2	454	4.4
2A-0-5-AV		5.0	12.5	98.8	16.6
2A-0-10-AV		10.0	27.4	40.2	34.8
2A-50-1.5-AV	50	1.5	7.9	702	9.1
2A-50-5-AV		5.0	12.7	139	16.6
2A-50-10-AV		10.0	16.4	77.3	23.0
2A-80-1.5-AV	80	1.5	13.2	191	15.3
2A-80-5-AV		5.0	17.1	110	23.5
2A-80-10-AV		10.0	21.5	35.7	30.9
2A-95-1.5-AV	95	1.5	16.1	124	18.9
2A-95-5-AV		5.0	19.7	74.0	26.2
2A-95-10-AV		10.0	24.7	27.0	34.2
2A-125-1.5-AV	125	1.5	26.8	95.9	28.2
2A-125-10-AV		10.0	33.7	14.9	45.2
2A-210-1.5-AV	210	1.5	68.9	38.7	72.0
2A-210-1.5-AV1[a]		1.5	73.0	29.1	76.5
2A-210-1.5-AV2[a]		1.5	73.1	27.6	75.3
2A-390-1.5-AV	390	1.5	188	7.01	191
Horizontal (Positive Outward):					
2A-50-1.5-AH	50	1.5	7.6	58.3	9.3
2A-50-5-AH		5.0	11.3	42.8	15.8
2A-50-10-AH		10.0	16.7	18.3	22.8
2A-80-1.5-AH	80	1.5	14.2	10.6	--
2A-80-5-AH		5.0	19.0	20.7	23.0
2A-80-10-AH		10.0	27.0	7.47	30.5
2A-95-1.5-AH	95	1.5	15.7	11.7	19.5
2A-95-5-AH		5.0	23.3	28.0	26.2
2A-95-10-AH		10.0	28.9	8.49	34.0
2A-125-1.5-AH	125	1.5	27.0	22.6	28.7
2A-125-10-AH		10.0	33.8	5.52	44.4
2A-210-1.5-AH	210	1.5	68.6	5.54	70.3
2A-210-1.5-AH1[a]		1.5	70.8	6.30	72.7
2A-210-1.5-AH2[a]	Malfunction		--	--	--
2A-390-1.5-AH	390	1.5	188	4.2	194

[a] Located on different azimuth.

TABLE 3.2 VELOCITY DATA, EVENT 2A

Gage	Ground Range	Depth	Arrival Time	Peak Positive Velocity	Time of Peak
	feet	feet	msec	ft/sec	msec
Vertical (Positive Downward):					
2A-0-1.5-UV	0	1.5	3.8	34.4	34.7
∫2A-0-1.5-AV		1.5	3.6	41.3	34.3
2A-0-5-UV		5.0	16.9	15.0	40.4
∫2A-0-5-AV		5.0	12.4	14.7	38.9
2A-0-10-UV		10.0	28.6	7.60	39.0
∫2A-0-10-AV		10.0	27.4	7.60	38.9
∫2A-50-1.5-AV	50	1.5	7.9	17.9	11.4
∫2A-50-5-AV		5.0	12.7	10.6	38.5
∫2A-50-10-AV		10.0	16.4	7.17	37.9
∫2A-80-1.5-AV	80	1.5	13.2	11.4	18.4
∫2A-80-5-AV		5.0	17.1	7.67	37.4
∫2A-80-10-AV		10.0	21.5	4.68	36.2
∫2A-95-1.5-AV	95	1.5	16.1	8.64	51.6
∫2A-95-5-AV		5.0	19.7	4.40	37.4
∫2A-95-10-AV		10.0	24.7	3.12	37.8
∫2A-125-1.5-AV	125	1.5	24.8	4.03	39.4
∫2A-125-10-AV		10.0	33.7	2.30	48.0
∫2A-210-1.5-AV	210	1.5	68.9	2.10	71.0
∫2A-210-1.5-AV1[a]		1.5	73.0	3.09	74.4
∫2A-210-1.5-AV2[a]		1.5	73.1	3.09	75.0
∫2A-390-1.5-AV	390	1.5	198	0.49	199
Horizontal (Positive Outward):					
2A-50-1.5-UH	50	1.5	8.1	5[b]	1
∫2A-50-1.5-AH		1.5	7.6	3.12	37.7
2A-50-5-UH		5.0	13.9	1.48	16.4
∫2A-50-5-AH		5.0	11.3	1.42	16.4
2A-50-10-UH		10.0	16.3	0.90	21.8
∫2A-50-10-AH		10.0	16.7	0.92	25.7
2A-80-1.5-UH	80	1.5	12.4	1.55	18.1
∫2A-80-1.5-AH		1.5	14.2	0.68	--
2A-80-5-UH		5.0	19.0	1.20	24.0
∫2A-80-5-AH		5.0	19.0	1.04	24.3
2A-80-10-UH		10.0	29.2	0.56	36.4
∫2A-80-10-AH		10.0	27.0	0.73	38.7
2A-80-16-UH		16.0	29.8	0.54	44.2
2A-95-1.5-UH	95	1.5	16.0	0.68	21.0
∫2A-95-1.5-AH		1.5	15.7	0.72	1.7
2A-95-5-UH		5.0	21.6	1.18	26.7
∫2A-95-5-AH		5.0	23.3	0.88	26.4
2A-95-10-UH		10.0	29.3	0.29	34.4
∫2A-95-10-AH		10.0	28.9	0.53	35.3
2A-125-1.5-UH	125	1.5	27.4	0.60	31.6
∫2A-125-1.5-AH		1.5	27.0	0.38[b]	39.3
2A-125-10-UH		10.0	38.5	0.30	44.4
∫2A-125-10-AH		10.0	33.8	0.60[b]	45.7
2A-210-1.5-UH	210	1.5	69.6	0.45	71.0
∫2A-210-1.5-AH		1.5	68.6	0.31	71.4
∫2A-210-1.5-AH1[a]		1.5	70.8	0.46	73.4
2A-210-18-UH		18.0	78.9	0.10	114
2A-390-1.5-UH	390	1.5	189	0.24	191
∫2A-390-1.5-AH		1.5	188	0.15	194

[a] Located on different azimuth.
[b] Questionable.

Gage	Ground Range	Depth	Peak Positive Displacement
	feet	feet	feet
Vertical (Positive Upward):			
[illegible]		1.5	1.[illegible]
[illegible]		1.5	0.[illegible]
[illegible]		5.	0.[illegible]
[illegible]		5.	0.[illegible]
[illegible]		10.	0.110
[illegible]		10.0	0.094
[illegible]	50	1.5	0.[illegible]
[illegible]		5.0	0.101
[illegible]		10.0	0.122
[illegible]	80	1.5	0.138
[illegible]		5.0	0.107
[illegible]		10.0	0.077
[illegible]	95	1.5	0.147
[illegible]		5.0	0.059
[illegible]		10.0	0.044
[illegible]	125	1.5	0.180[a]
[illegible]		10.0	0.018
[illegible]	210	1.5	0.018
[illegible]		1.5	0.030
[illegible]		1.5	0.032
[illegible]	390	1.5	0.004
Horizontal (Positive Outward):			
[illegible]	50	1.5	0.075
[illegible]		5.0	0.034
∫∫2A-50-5-All	50	5.0	0.007
∫2A-50-10-UH		10.0	0.017
∫∫2A-50-10-All		10.0	0.039
∫2A-80-1.5-UH	80	1.5	0.060
∫∫2A-80-1.5-All		1.5	0.070[c]
∫2A-80-5-UH		5.0	d
∫∫2A-80-5-All		5.0	0.014
∫2A-80-10-UH		10.0	0.022
∫∫2A-80-10-All		10.0	0.014
∫2A-80-16-UH		16.0	0.026
∫2A-95-1.5-UH	95	1.5	0.040
∫2A-95-5-UH		5.0	0.024
∫∫2A-95-5-All		5.0	d
∫2A-95-10-UH		10.0	0.018
∫∫2A-95-10-All		10.0	0.029
∫2A-125-1.5-UH	125	1.5	0.048
∫∫2A-125-1.5-All		1.5	0.012
∫2A-125-10-UH		10.0	0.021
∫∫2A-125-10-All		10.0	0.024
∫2A-210-1.5-UH	210	1.5	0.008
∫∫2A-210-1.5-All		1.5	0.014
∫2A-210-18-UH		18.0	0.003
∫2A-390-1.5-UH	390	1.5	0.006
∫∫2A-390-1.5-All		1.5	d

[a] Questionable.
[b] Gages on different azimuth.
[c] Affected by [illegible].
[d] Negative positive shift.

TABLE 3.4 VERTICAL STRESS DATA, EVENT 2A

Gage	Ground Range	Depth	Arrival Time	Peak Stress	Time of Peak
	feet	feet	msec	psi	msec
2A-0-1.5-EV	0	1.5	4.2	889	14.6
2A-0-5-EV		5.0	8.6	210	30.8
2A-0-10-EV		10.0	24.5	113	39.4
2A-50-1.5-EV	50	1.5	9.5	130	11.4
2A-50-5-EV		5.0	15.4	5.72[a]	21.2
2A-50-10-EV		10.0	23.4	15.4	31.0
2A-80-1.5-EV	80	1.5	15.5	137	18.0
2A-80-5-EV		5.0	22.2	b	25.5
2A-80-10-EV		10.0	29.8	b	34.8
2A-95-1.5-EV	95	1.5	23.0	90.7	21.9
2A-95-5-EV		5.0	23.0	16.0	32.8
2A-125-1.5-EV	125	1.5	29.6	17.4[a]	36.9
2A-210-1.5-EV	210	1.5	69.5	17.5	73.2
2A-390-1.5-EV	390	1.5	188	9.0	198

[a] Questionable amplitude.
[b] Low signal, questionable waveform and amplitude.

TABLE 3.5 AIRBLAST-INDUCED VERTICAL ACCELERATION AND VELOCITY RATIOS, EVENT 2A

Overpressure	Gage Depth	Maximum Acceleration/Overpressure	Maximum Velocity/Overpressure
psi	feet	g's/psi	ft/sec/psi
120	1.5	1.59	0.096
	5.0	0.92	0.064
	10.0	0.30	0.042
73	1.5	1.70	0.118
	5.0	1.01	0.061
	10.0	0.37	0.043
45	1.5	2.13	0.134
	10.0	0.33	0.051
21	1.5	1.85	0.100
	1.5	1.39	0.147
	1.5	1.32	0.147
7.9	1.5	0.88	0.062

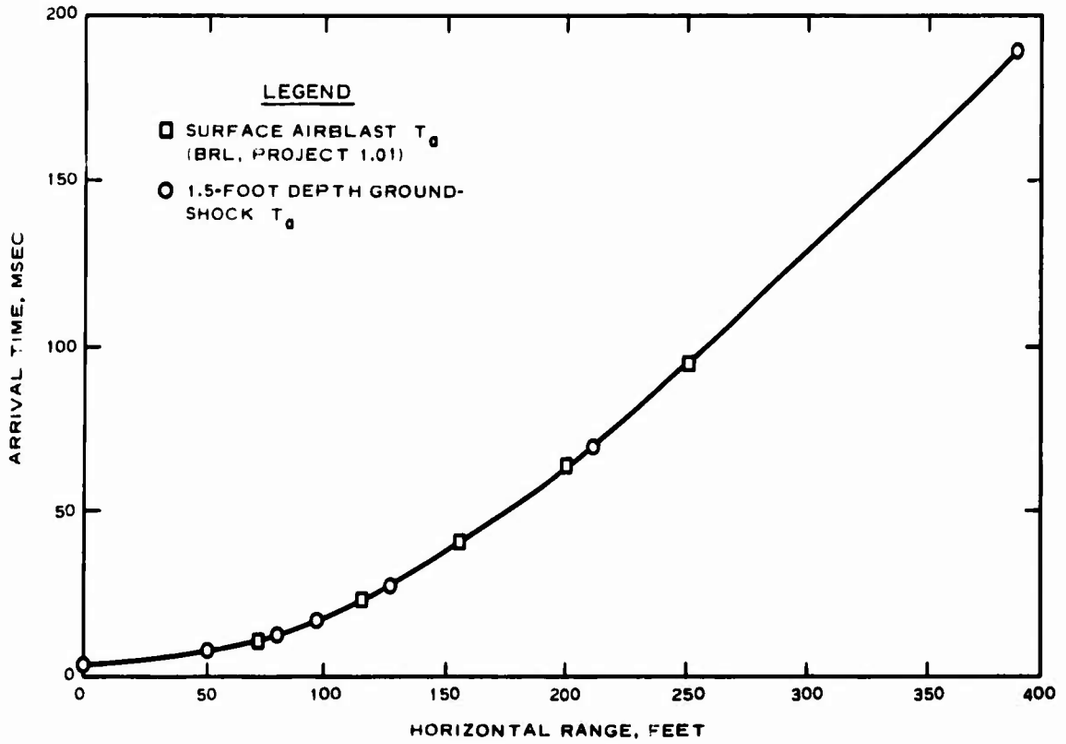

Figure 3.1 Ground-shock arrival time versus horizontal range, 1.5-foot depth, Event 2A.

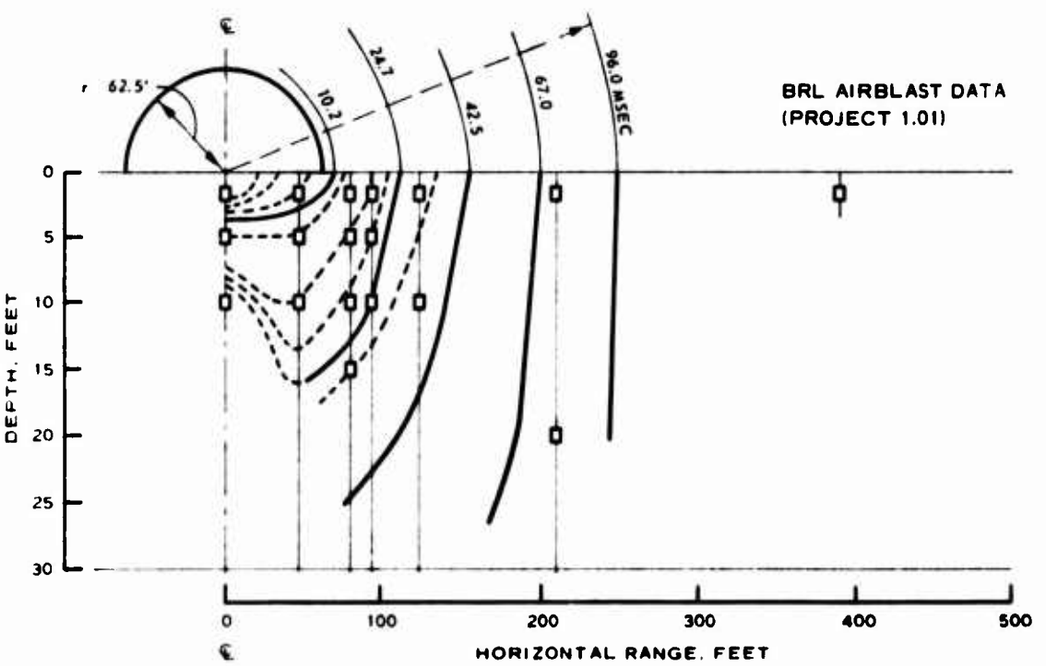

Figure 3.2 Ground-shock profile, Event 2A.

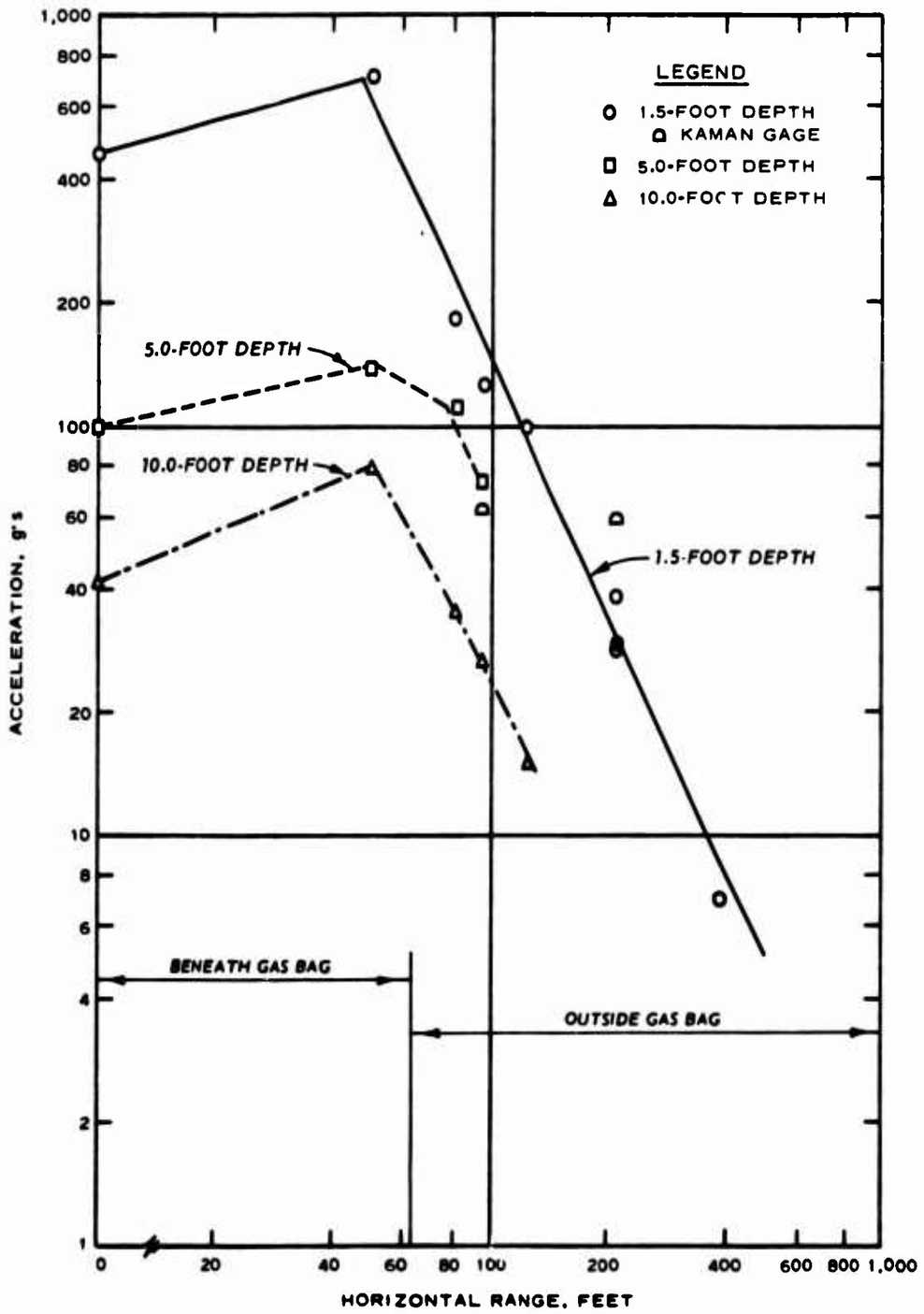

Figure 3.3 Peak airblast-induced downward acceleration versus horizontal range, Event 2A.

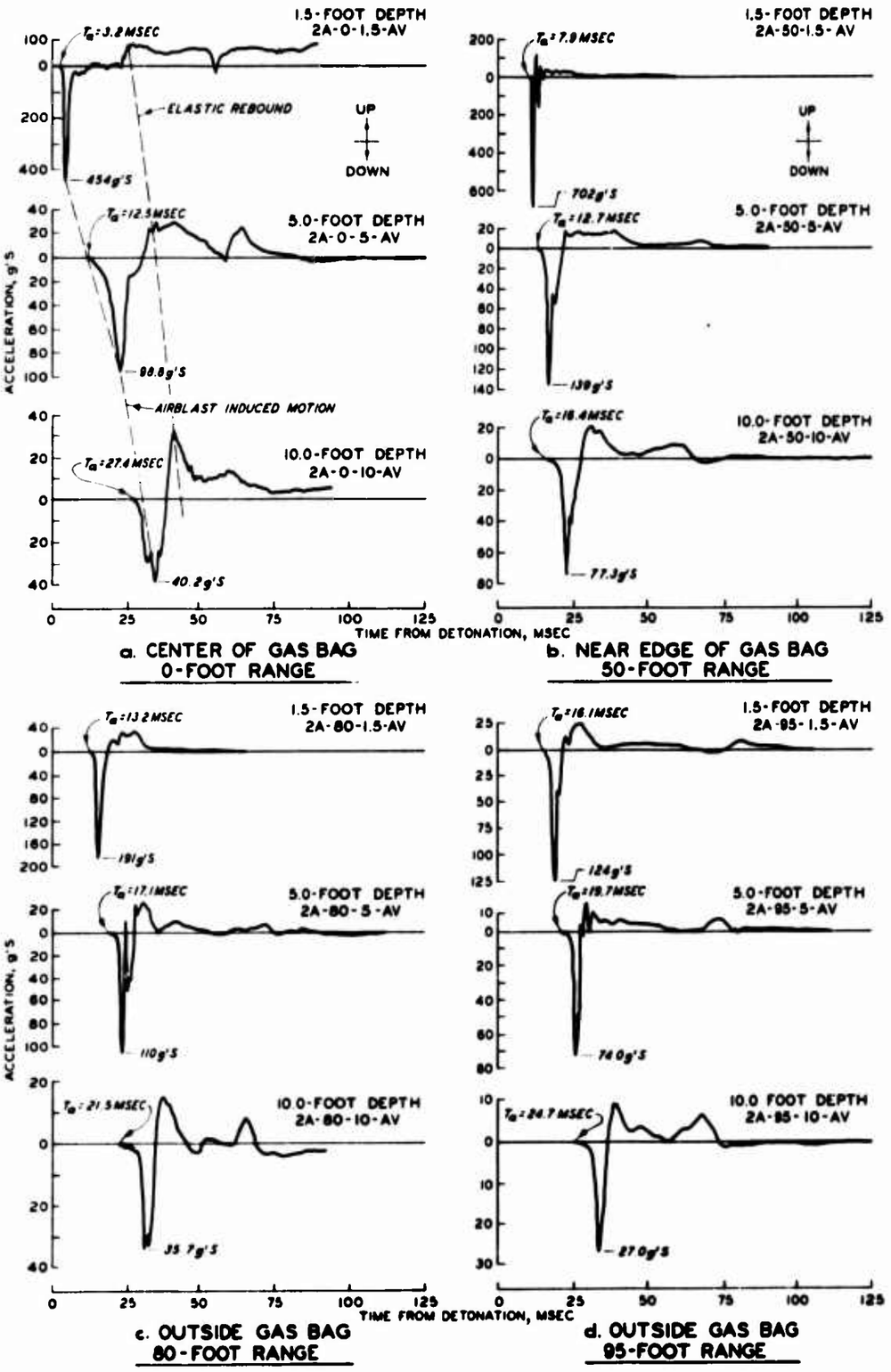

Figure 3.4 Vertical accelerograms, Event 2A.

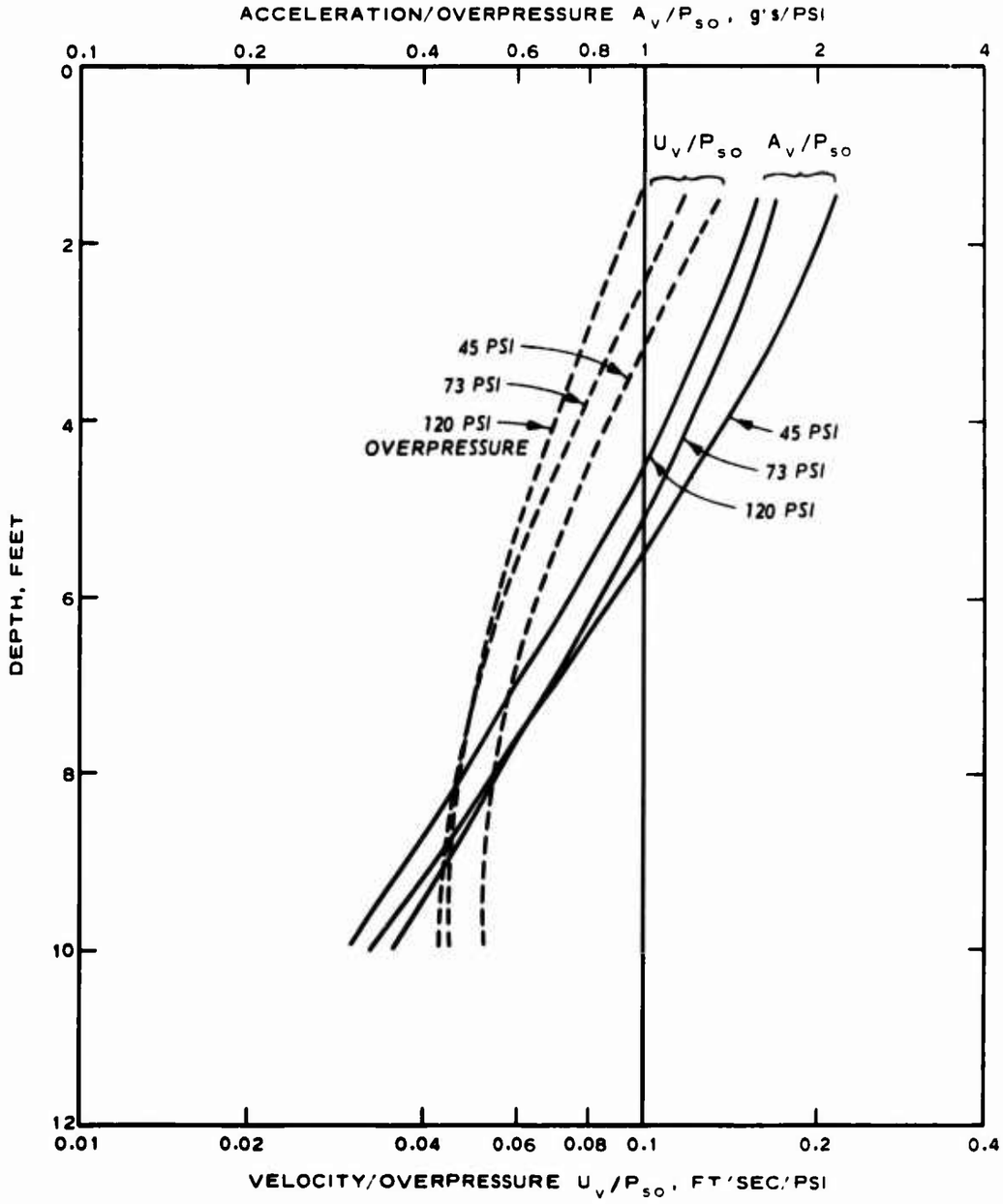

Figure 3.5 Ratio of maximum airblast-induced vertical acceleration and velocity to surface overpressure versus depth, Event 2A.

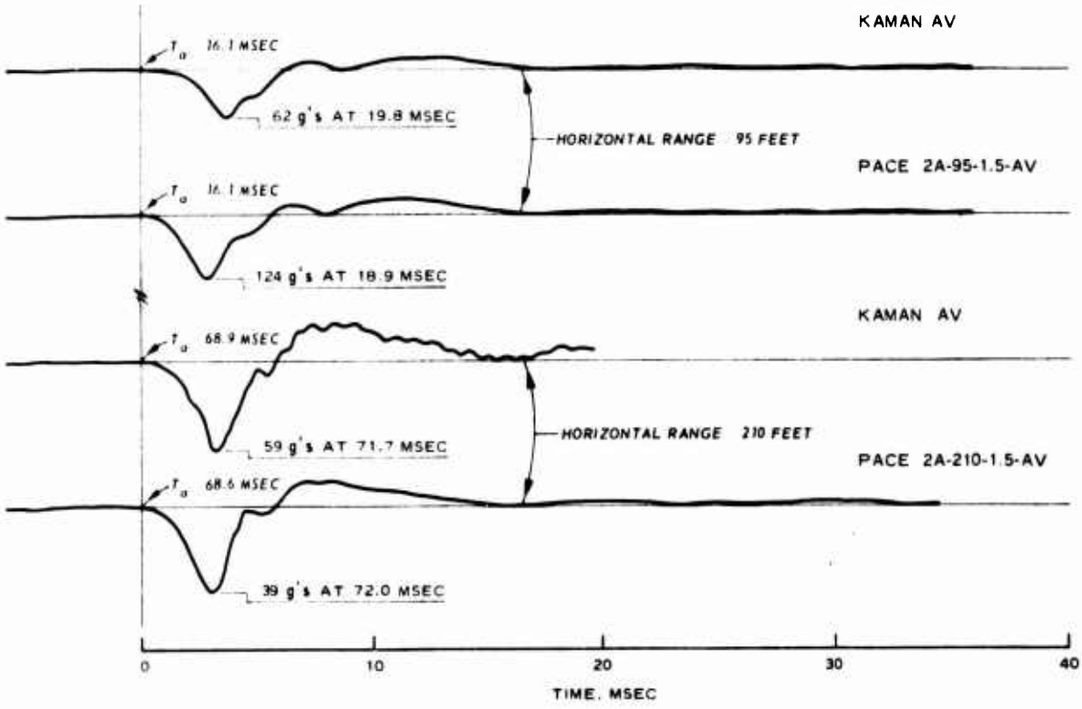

Figure 3.6 Vertical accelerogram comparisons, 1.5-foot depth, Kaman Nuclear and Pace transducers.

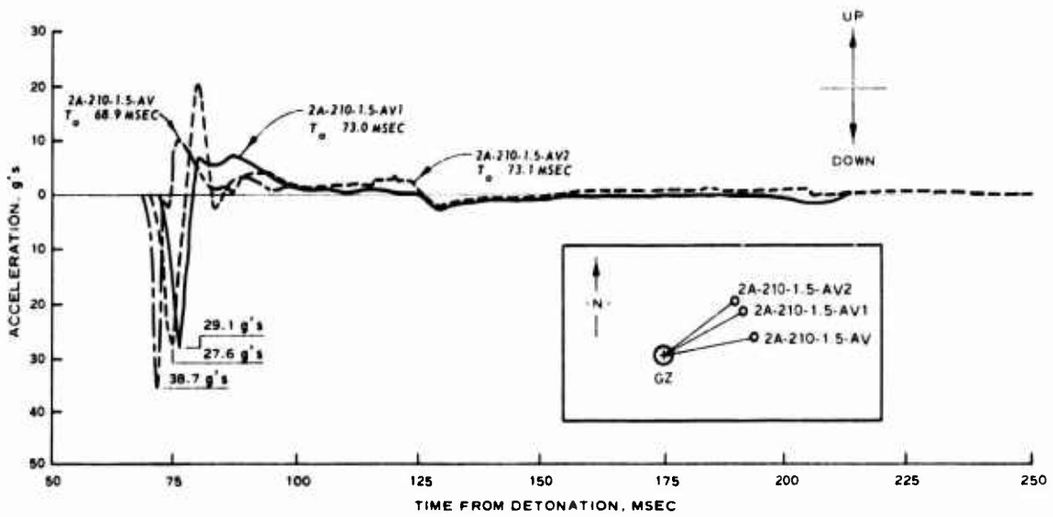

Figure 3.7 Vertical accelerograms, radially deployed gages, 1.5-foot depth, 210-foot horizontal range, Event 2A.

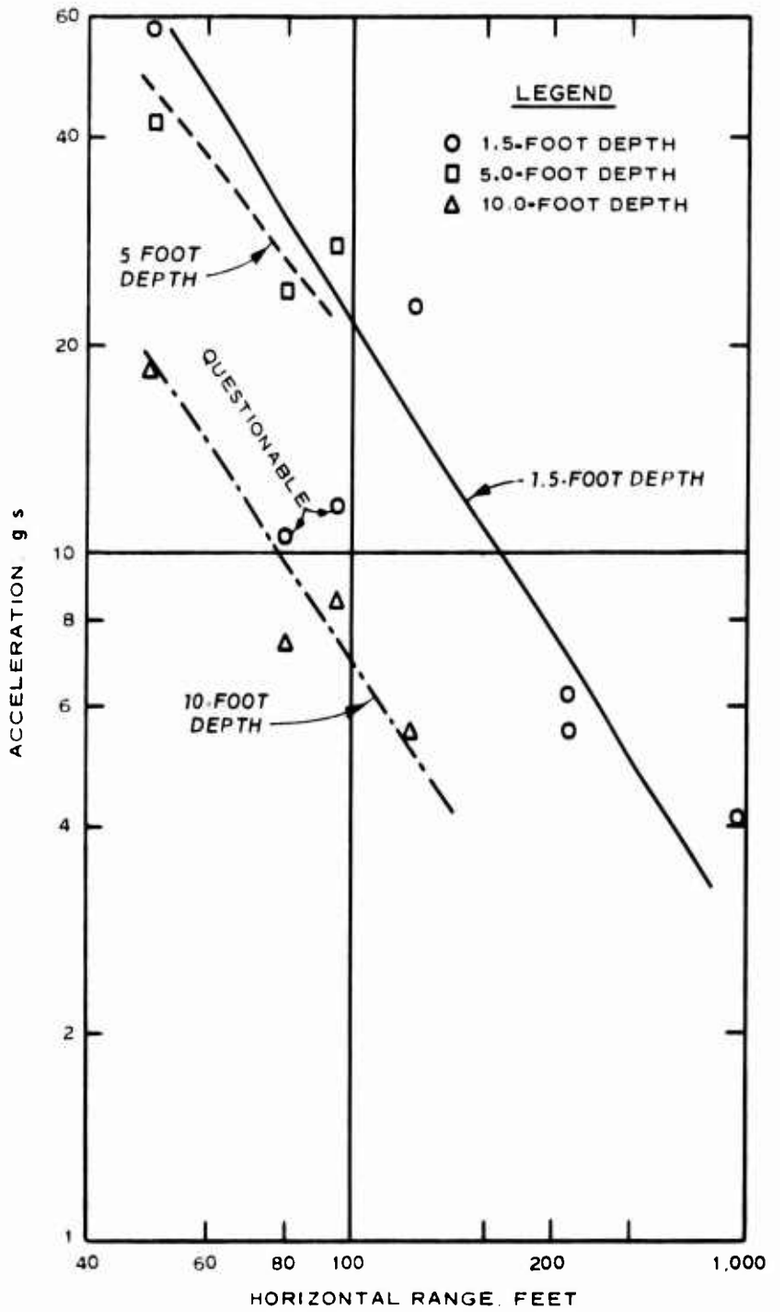

Figure 3.8 Peak airblast-induced outward acceleration versus horizontal range, Event 2A.

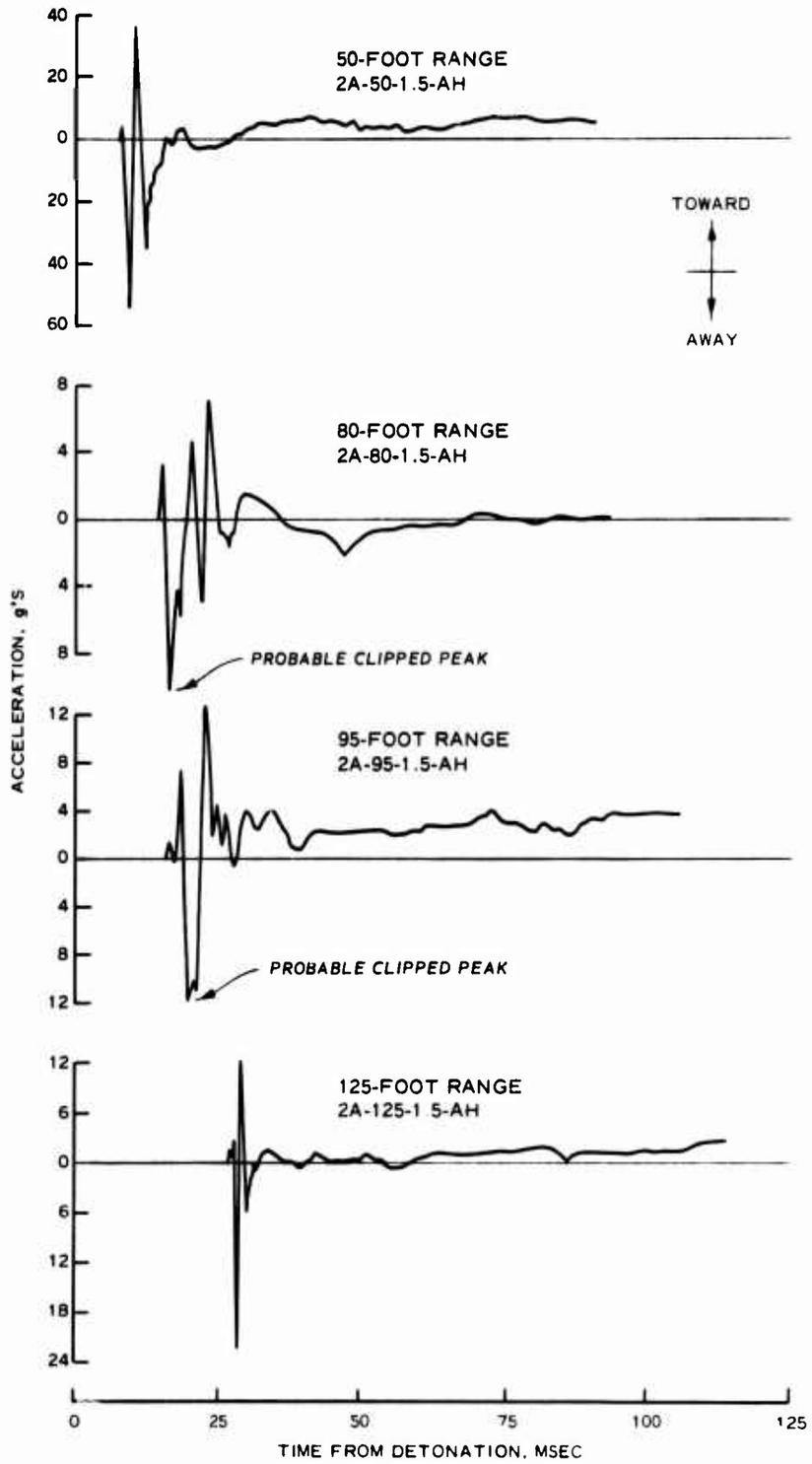

Figure 3.9 Horizontal accelerograms, 1.5-foot depth, Event 2A.

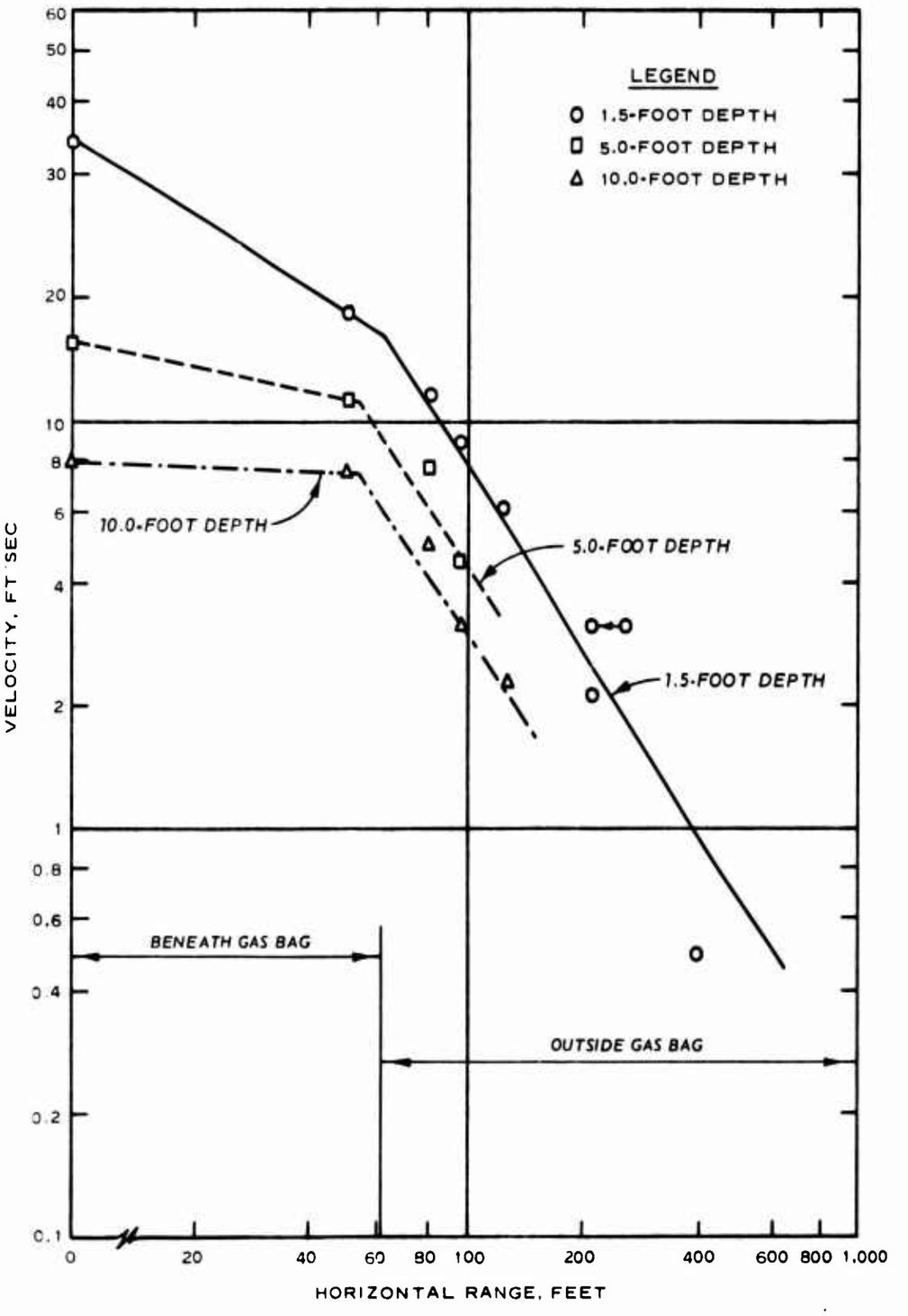

Figure 3.10 Peak airblast-induced downward particle velocity versus horizontal range, Event 2A. Except for those at 0 foot, points are based on integrated acceleration.

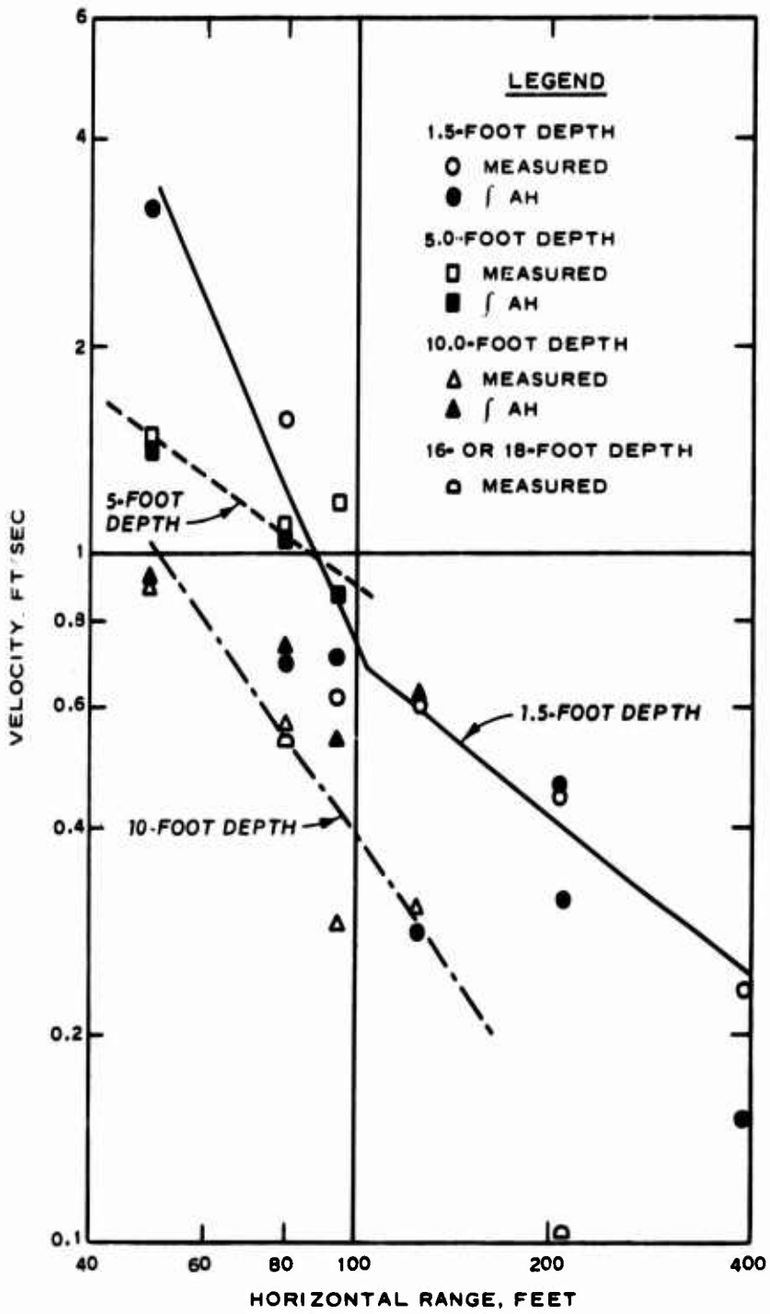

Figure 3.11 Peak airblast-induced outward particle velocity versus horizontal range, Event 2A.

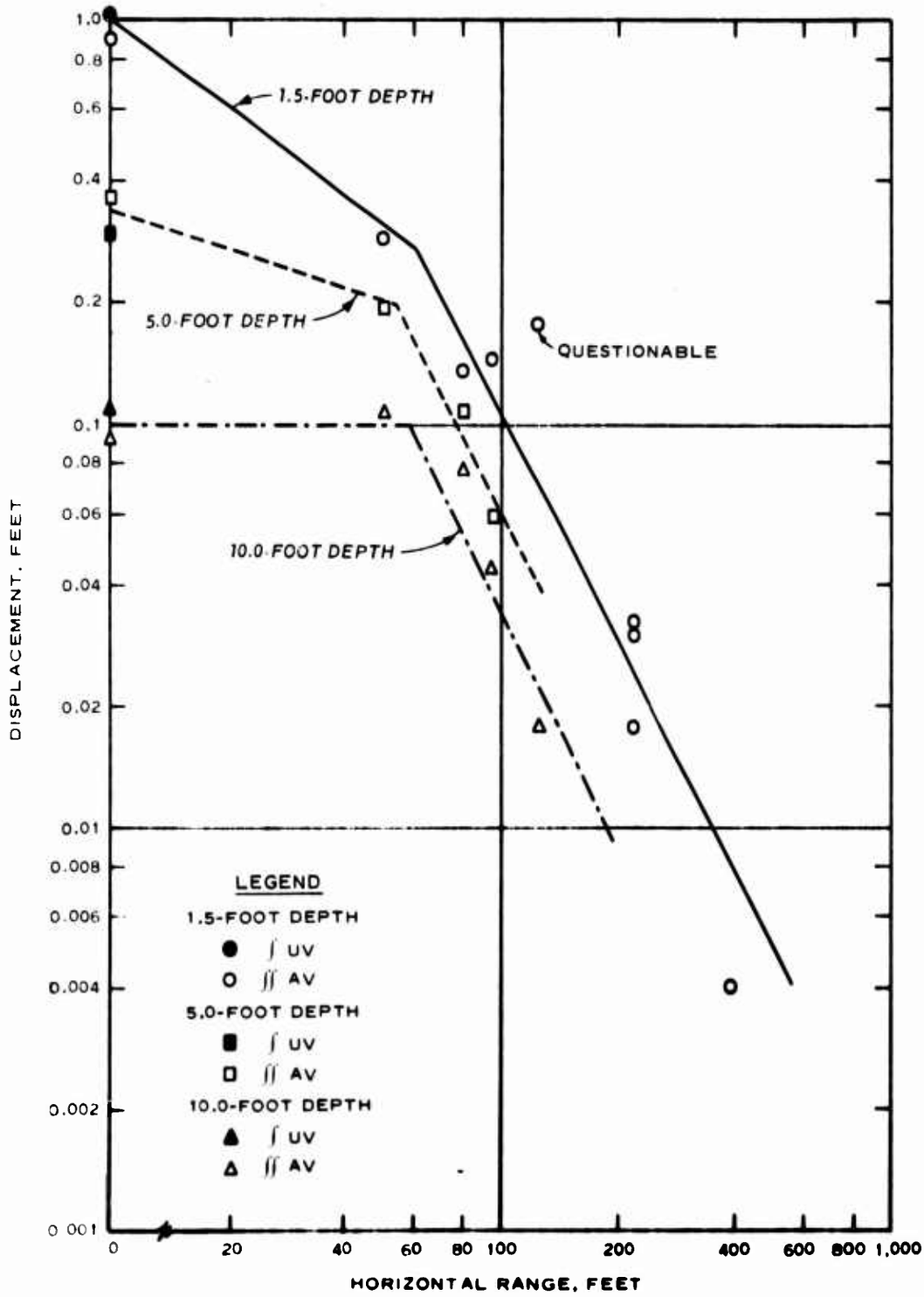

Figure 3.12 Peak airblast-induced downward displacement versus horizontal range, Event 2A.

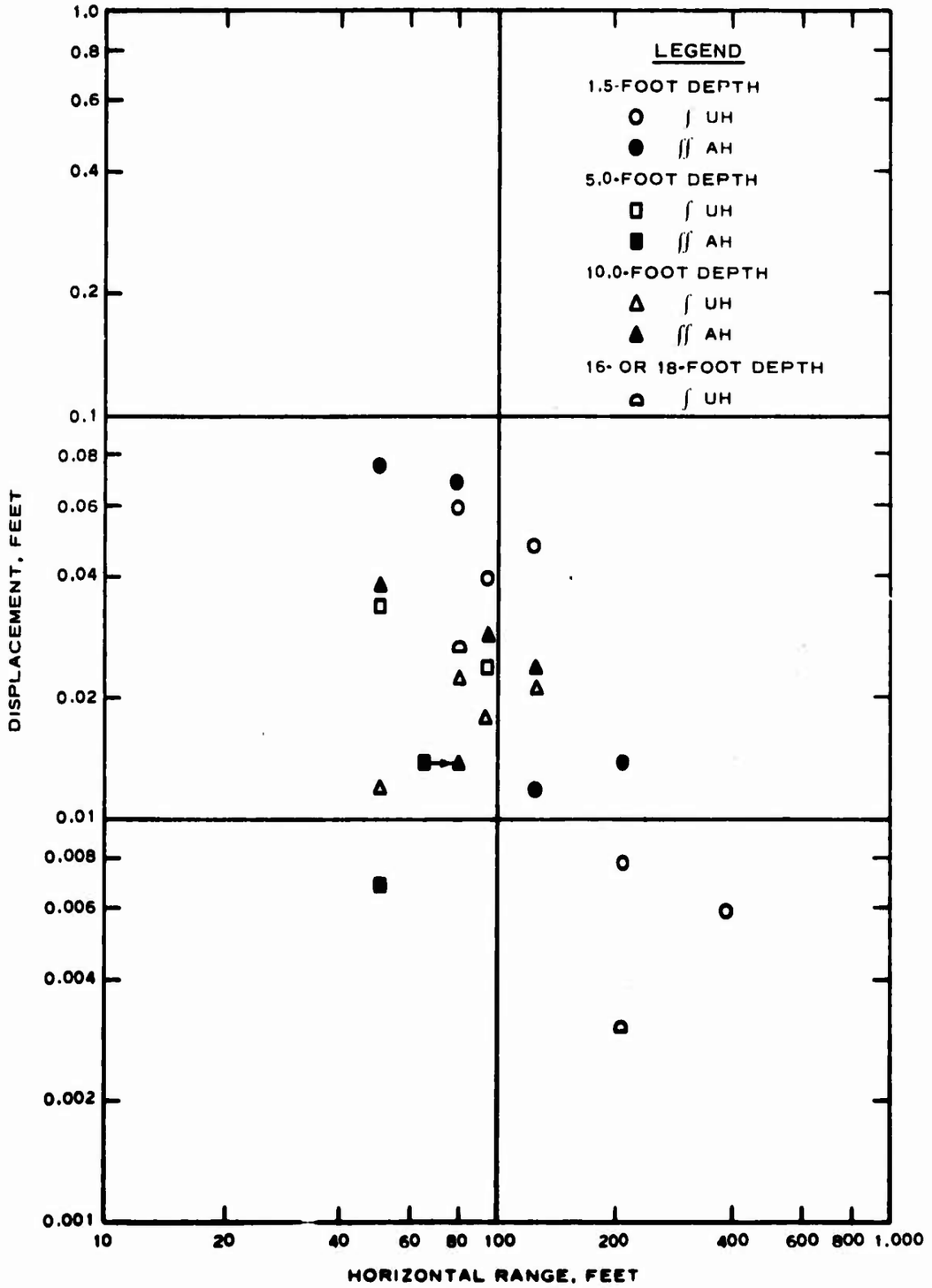

Figure 3.13 Peak airblast-induced outward displacement versus horizontal range, Event 2A.

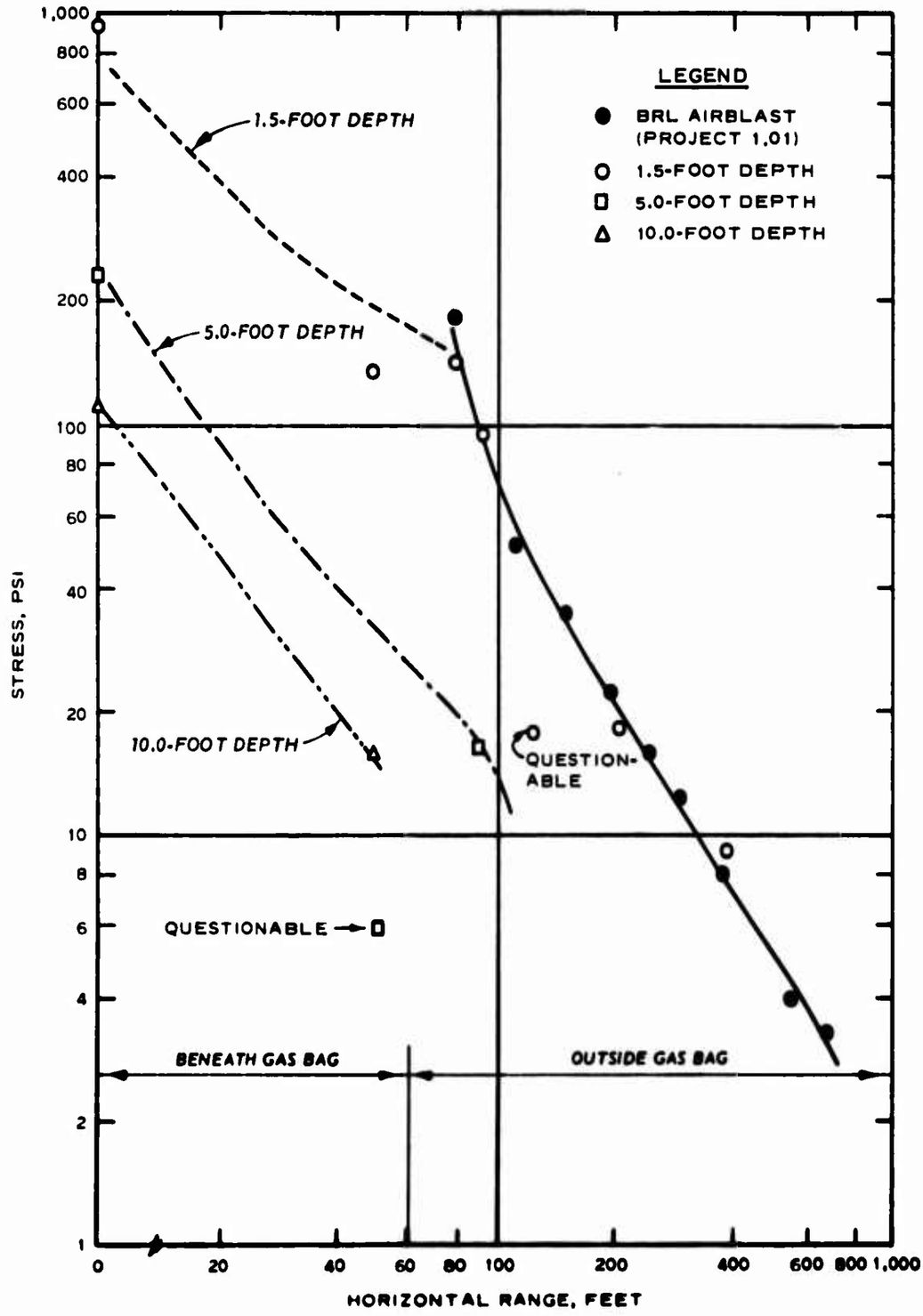

Figure 3.14 Peak airblast-induced vertical stress versus horizontal range, Event 2A.

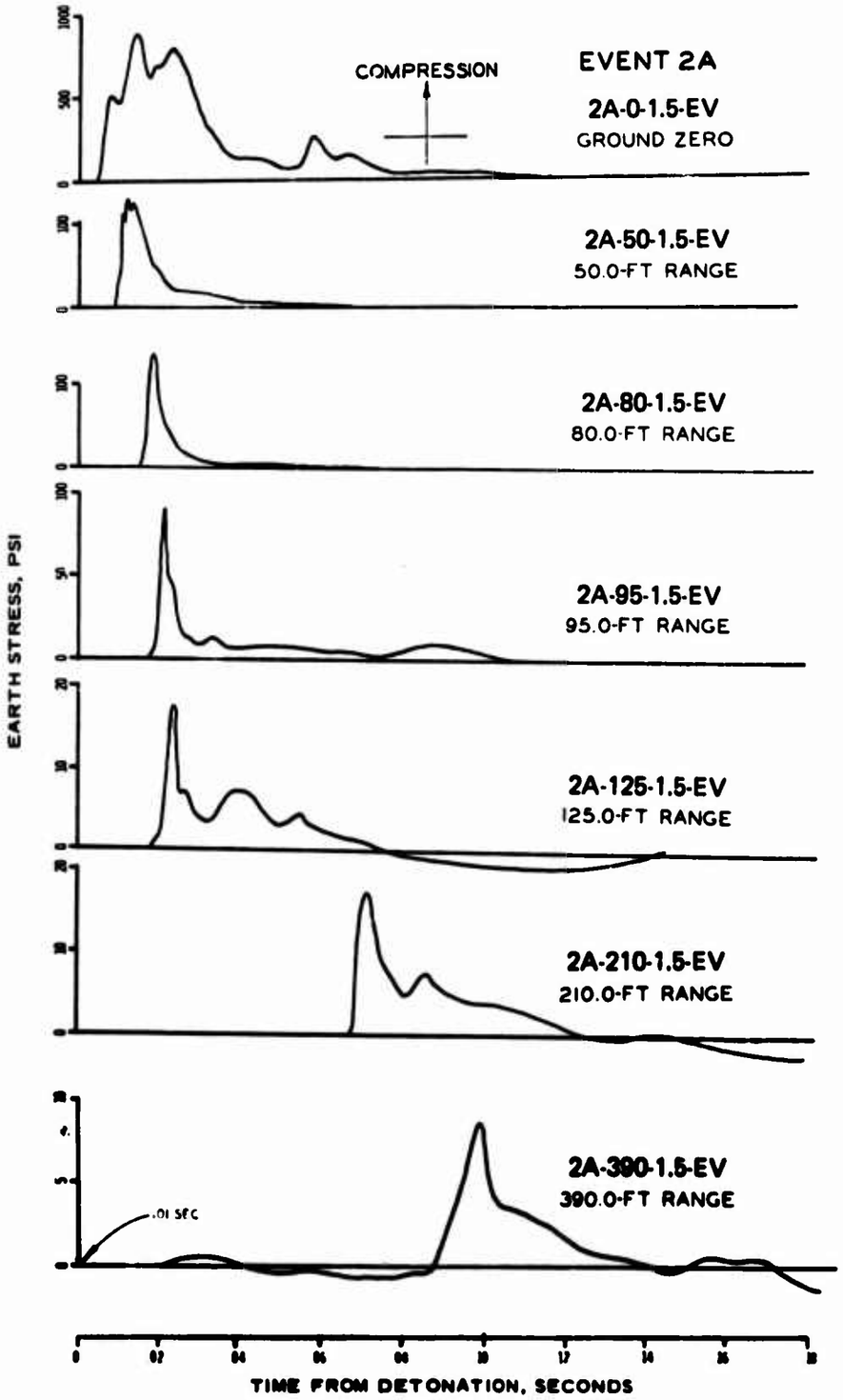

Figure 3.15 Vertical stress waveforms, 1.5-foot depth, Event 2A.

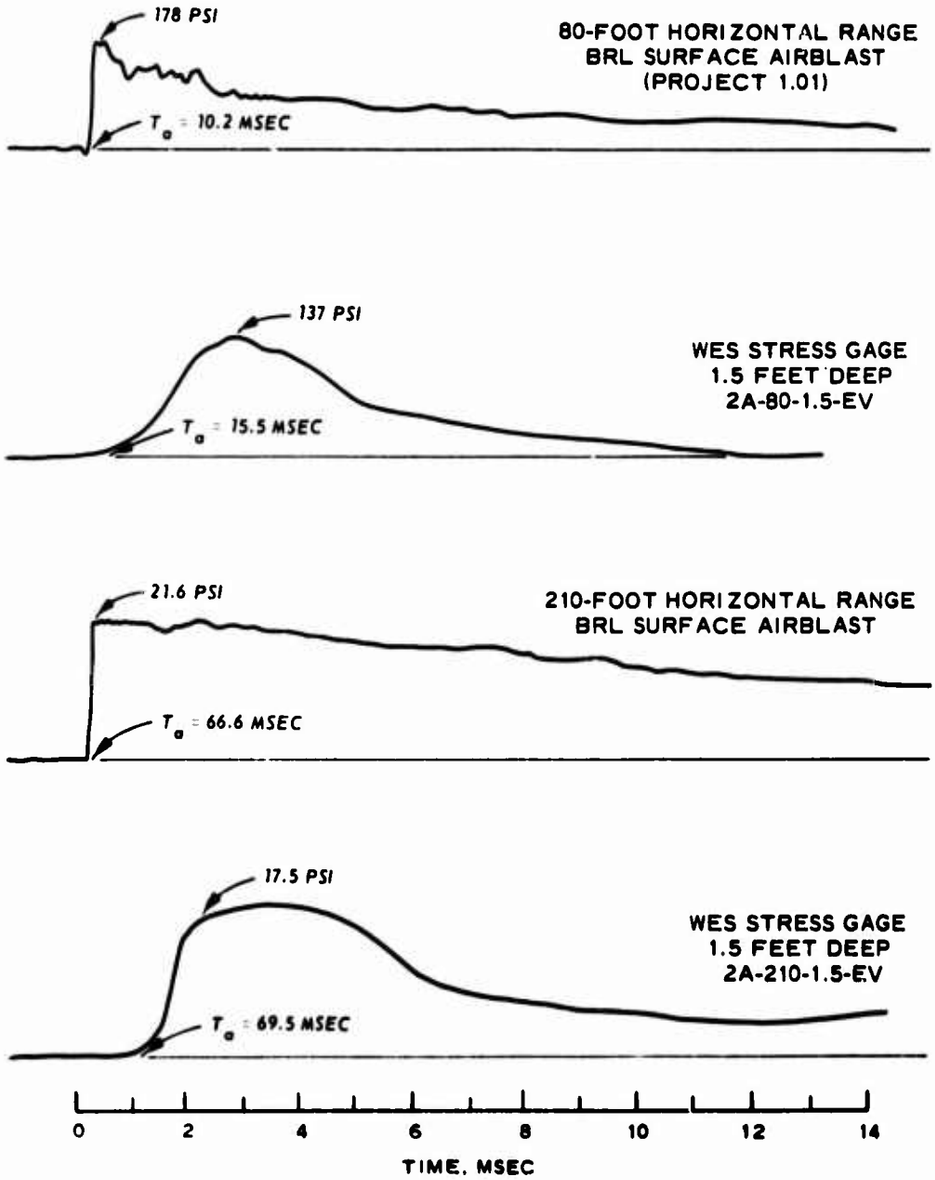

Figure 3.16 Comparison of surface airblast and near-surface (1.5-foot depth) stress waveforms, Event 2A.

CHAPTER 4

RESULTS, EVENTS 3 AND 5

4.1 SHOT CONDITIONS

An anomalous airblast wave was noted in Event 3. DRES high-speed photography showed a gas jet and associated bow wave which preceded the primary airblast wave and propagated along Projects 1.01 (BRL) and 3.02a (WES) gagelines. Project 1.01 noted a double-spiked pressure pulse (both spikes of similar magnitude at approximately 6 msec separation) at ground level, beginning at the 105-foot horizontal range and extending to about 310 feet (References 4, 5, and 10). No effects of this double-peaked wave were seen in the ground motion data, pointing out the integrating (smoothing) characteristics of the Drowning Ford alluvium on fast transient airblast inputs.

The winter conditions hoped for on Event 5 failed to materialize. There was practically no snow cover, only a thin layer of ice and slush. Ground temperatures were relatively high, approximately 20 F at a depth of 2 feet as measured in the WES instrument holes (Figure 4.1). Project 3.05 ground temperature measurements were somewhat lower than those made by WES. However, the Project 3.05 thermocouple lines were located along radii different from the ground motion gageline and were covered by more snow and ice, which would have insulated the ground better in those areas. Observation of preshot drillings from the test area indicated that only the upper 6 inches or so of the ground contained enough moisture to be considered truly frozen. No water table was detected. As a result of these conditions, the anticipated three-layered system, i.e., frozen upper layer, transitional zone, and saturated under layer, was not present. Therefore, major differences in ground-shock propagation between Events 3 and 5 were not expected.

4.2 DATA RECOVERY

Detonation of Event 5 occurred 3.5 seconds prematurely; as a consequence, the automatic channel calibrator was still in sequence since it was programmed to cut off at -2.5 seconds. Five gages recorded signals

while electrically offset in the calibration mode. The light-beam galvanometer oscillographs, which were programmed to switch from slow to fast record at -2 seconds, began recording in slow speed. The speed of these recorders increased as the data were being recorded, giving a nonlinear time base; however, the FM magnetic tape units were operating at normal speed and 33 of 34 data channels were successfully recorded. All data for this event were taken from tape playback. Determination of true zero or detonation time posed a problem. A small-amplitude electrical signal was detected on the fiducial channel which could have been generated by the detonation and fed back through the system. This signal was consistent with respect to time on all recorders and was determined to be actual event zero.

Of 34 channels of information, 32 were successfully recorded for Event 3 and 33 for Event 5. Peak values are listed in Tables 4.1 through 4.4.

For Event 3, Projects 3.04a and 3.04b obtained complementary data in the hydrodynamic and plastic (close-in) regions (References 4 and 5). However, these projects did not participate on Event 5.

4.3 GROUND-SHOCK ARRIVAL TIME

Arrival times are listed in Table 4.1 and near-surface (1.5-foot depth) arrival times versus distance are shown in Figure 4.2. Ground-shock arrival times for near-surface vertical accelerations were earlier for Event 5 than for Event 3 out to a range of 105 feet. First motion arrivals ranged from about 8 msec at the 60-foot station to 18 msec at 105 feet for Event 5 as compared to 11 msec and 21 msec for Event 3. At the 150-foot station, the arrival times for the two events were about equal, and at the 225-foot station, the arrival was slightly later for Event 5. From the 105-foot station outward, the first arrivals approximated those of the airblast for Event 3, but were outrunning slightly in Event 5.

A spatial shock-front diagram (Figure 4.3) constructed from BRL (Project 1.01) surface airblast-arrival data (References 4, 5, 10, 11, and 12), Sandia Corporation (Project 3.04b) hydrodynamic data (Reference 4), and WES (Project 3.02a) subsurface arrival measurements shows the wavefront propagation. Outrunning ground motion was observed at the 225-foot station

increasing horizontal range than the Event 3 ($R^{-1.33}$) or Flat Top data. Both Events 3 and 5 data fall below those of the Flat Top Series.

Ratios of airblast-induced vertical velocity to surface overpressure above the point of reference are listed in Table 4.6. Event 5 ratios did not exceed 0.032, while Event 3 values reached 0.061. Figure 4.18 shows these ratios as a function of the corresponding surface overpressure. Events 3 and 5 data trend similarly, the Event 5 data falling about 50 percent lower than Event 3. The Flat Top III data fall some 25 percent above the Event 3 points. All data are consistent at overpressures exceeding 40 psi, showing attenuation with increasing pressure.

4.5.2 Horizontal Velocity. Horizontal particle velocity waveforms are characterized by an initially outward-going pulse of relatively fast rise time and short duration induced by the surface airblast. This is followed by a later arriving pulse with longer rise time, higher amplitude, and considerable duration (approximately twice that of the airblast motion) produced by the crater-induced motion. Waveforms for Events 3 and 5 are compared in Figure 4.19. The Event 5 motions have higher frequencies and faster rise times for both airblast- and crater-induced phases than Event 3. Figure 4.20 shows measured near-surface horizontal velocity and integrated acceleration waveforms from Event 5. The amplitude of the 105-foot range waveform is quite high. This is an unreasonable value and was probably caused by a malfunction in the calibration module. Good waveform comparison is noted at later times between the measured and integrated data. Note the lower integrated value at 105-foot range as compared to the questioned value from the direct measurement.

Direct waveform comparison between Event 3 and Flat Top II and III was made for the 150-foot horizontal range. This composite plot is shown in Figure 4.21. Typically, the early airblast-induced motions showed scatter and waveform variance. Later direct-induced motions show general agreement.

Airblast-induced horizontal velocity is plotted as a function of range in Figure 4.22. Near-surface values tend to increase from 60- to 105-foot range, then rapidly decrease. Deeper stations show no clear trends.

Peak outward particle velocities from the direct-induced (late-arriving) ground shock for Events 3 and 5 and Flat Top II and III are

Event	Maximum Acceleration	Range	Minimum Acceleration	Range	Attenuation Rate
	g's	feet	g's	feet	
3	196	60	12	225	$R^{-2.00}$
5	164	60	20	225	$R^{-1.68}$
Flat Top II	145	65	27	150	--
Flat Top III	137	65	10	250	--

depth for Event 5 compared to Event 3 (Figures 4.7 and 4.14). The higher frequencies and amplitudes of Event 5 were influenced by the thin frozen surface layer which allowed greater coupling and transmission of the high-frequency shock components. The vertical component at this station was higher than the Event 3 measurement by a factor of 2, and the horizontal component by a factor of 3.

Ratios of peak near-surface vertical acceleration to surface overpressure for Events 3 and 5 and Flat Top II and III are listed in Table 4.5 and plotted in Figure 4.8. Data for Event 2A are also included in the figure for comparison. There is a general decrease in the ratio values around 100 psi for all events except Flat Top III, for which there was an increase. Averaged data indicate little attentuation between 10- and 200-psi overpressures. Flat Top measurement locations extended closer to the detonation point than did those on Distant Plain, and the A_v/P_{so} ratios tended to attenuate at this higher pressure region.

4.4.2 Vertical Acceleration for Deeper Gages. Event 3 acceleration pulse modification with depth is displayed in Figure 4.9. The initial downward spike diminishes in amplitude and broadens with increasing depth, and is no longer the predominant feature at the 10-foot level.

Vertical accelerograms for three locations at the 10-foot depth are compared in Figure 4.10 for Event 3. Initial downward motion was followed by an oscillating upward phase and finally a second downward pulse. The initial peaks at this depth attenuated little with increasing horizontal range. The third upward peak shows definite attenuation and is indicative of the direct (crater-induced) ground shock.

Events 3 and 5 waveforms for the 10-foot depth are compared at 60- and

70-foot horizontal ranges in Figure 4.11. Although a considerably higher frequency perturbation is imposed on the Event 5 waveforms, with corresponding faster rise times, the overall similarity between Events 3 and 5 is apparent.

4.4.3 Horizontal Acceleration. Event 5 horizontal acceleration waveforms for all 1.5-foot depth stations are shown in Figure 4.12. Waveform comparisons between Events 3 and 5 are shown for the 60- and 70-foot stations in Figure 4.13. The Event 5 waveforms exhibit higher frequency and amplitude components than the Event 3 signals.

Peak airblast-induced horizontal accelerations are plotted versus range for the near-surface gages in Figure 4.14. A trend of amplitude attenuation with increasing range is noted for the near-surface data. Event 5 values ranged from 34 g's at 60-foot horizontal range to 3 g's at 225-foot range for the near-surface stations. Comparable values from Event 3 ranged from 19 to 2 g's. Near-surface attenuation rates were nearly identical, $R^{-1.68}$ for Event 3 and $R^{-1.86}$ for Event 5.

4.5 PARTICLE VELOCITY

A composite velocity data listing for Events 3 and 5 is given in Table 4.2. No vertical velocity gages were used in either Event 3 or 5. Therefore, vertical velocities were computed by singly integrating vertical acceleration.

4.5.1 Vertical Velocity. Near-surface vertical velocity waveforms at 60-foot range are compared between Events 3 and 5 in Figure 4.15. Event 5 waveforms are characteristically of faster rise time and higher frequency in the airblast-induced phase than Event 3, but are otherwise similar in appearance. Near-surface vertical waveforms at various ranges are compared between Events 3 and 5 in Figure 4.16. Outrunning ground motion on Event 5 is indicated by the upward-going precursor on Gage 5-225-1.5-AV (225-foot range).

A plot of the computed peak airblast-induced (early time) velocity versus horizontal range is shown in Figure 4.17. This plot includes Events 3 and 5 and Flat Top II and III data for comparison. The Event 5 data are lower valued and appear to attenuate more rapidly ($R^{-1.84}$) with

increasing horizontal range than the Event 3 ($R^{-1.33}$) or Flat Top data. Both Events 3 and 5 data fall below those of the Flat Top Series.

Ratios of airblast-induced vertical velocity to surface overpressure above the point of reference are listed in Table 4.6. Event 5 ratios did not exceed 0.032, while Event 3 values reached 0.061. Figure 4.18 shows these ratios as a function of the corresponding surface overpressure. Events 3 and 5 data trend similarly, the Event 5 data falling about 50 percent lower than Event 3. The Flat Top III data fall some 25 percent above the Event 3 points. All data are consistent at overpressures exceeding 40 psi, showing attenuation with increasing pressure.

4.5.2 Horizontal Velocity. Horizontal particle velocity waveforms are characterized by an initially outward-going pulse of relatively fast rise time and short duration induced by the surface airblast. This is followed by a later arriving pulse with longer rise time, higher amplitude, and considerable duration (approximately twice that of the airblast motion) produced by the crater-induced motion. Waveforms for Events 3 and 5 are compared in Figure 4.19. The Event 5 motions have higher frequencies and faster rise times for both airblast- and crater-induced phases than Event 3. Figure 4.20 shows measured near-surface horizontal velocity and integrated acceleration waveforms from Event 5. The amplitude of the 105-foot range waveform is quite high. This is an unreasonable value and was probably caused by a malfunction in the calibration module. Good waveform comparison is noted at later times between the measured and integrated data. Note the lower integrated value at 105-foot range as compared to the questioned value from the direct measurement.

Direct waveform comparison between Event 3 and Flat Top II and III was made for the 150-foot horizontal range. This composite plot is shown in Figure 4.21. Typically, the early airblast-induced motions showed scatter and waveform variance. Later direct-induced motions show general agreement.

Airblast-induced horizontal velocity is plotted as a function of range in Figure 4.22. Near-surface values tend to increase from 60- to 105-foot range, then rapidly decrease. Deeper stations show no clear trends.

Peak outward particle velocities from the direct-induced (late-arriving) ground shock for Events 3 and 5 and Flat Top II and III are

plotted versus range in Figure 4.23. Event 5 near-surface values ranged from 7.8 ft/sec at 60-foot horizontal range to 0.33 ft/sec at 225-foot range. These compare to 7.3 ft/sec and 0.47 ft/sec for Event 3. Flat Top II values at 1-foot depth ranged from 3.7 ft/sec at 65-foot range to 0.43 ft/sec at 150-foot range. No Flat Top III data were available at 65-foot range; the 150-foot range value was 0.82 ft/sec. These data, as with the horizontal acceleration, attenuate with increasing horizontal range.

To achieve a degree of scaling, peak crater-induced particle velocity was ratioed to the square root of crater radius and plotted as a function of the ratio of range to crater radius. Comparison of Flat Top and Distant Plain data (Figure 4.24) shows similar slopes but varying offsets. Event 3 compared well with Flat Top III, Flat Top II data falling below these and Event 5 data falling above. The values are listed in Table 4.7.

4.6 DISPLACEMENT

All displacement data (Table 4.3) are derived from particle acceleration- and velocity-time histories. Confidence levels are less for displacement than for the measured parameter.

Peak vertical airblast- and crater-induced transient displacements are plotted as a function of range for Events 3 and 5 in Figure 4.25. Cratering-induced (upward) displacement predominated in both events, as for the Flat Top Series. The crater-induced motion predominated out to 150-foot range on Event 3 and out to 190-foot range on Event 5. Airblast-induced motion predominated beyond these ranges. Near-surface motion attenuations were similar for both events. The airblast-induced motion attenuated with range as $R^{-1.17}$ for Event 3 and as $R^{-1.55}$ for Event 5. Event 3 amplitudes were greater. Cratering motion attenuated about three times more rapidly than the airblast motion. Values were $R^{-4.24}$ for Event 3 and $R^{-4.60}$ for Event 5. Amplitudes were similar on both events.

Peak horizontal displacements (Figure 4.26) are about equal to the vertical values at ranges less than 100 feet. At greater ranges, the horizontal motions increase over the vertical. Event 3 horizontal displacements are generally higher than are those of Event 5. Attenuation with range (Figure 4.26) approximates $R^{-3.15}$ for Event 3 and $R^{-2.91}$ for Event 5.

4.7 STRESS

Peak stress data are tabulated in Table 4.4. The near-surface stresses appeared to attenuate with range roughly as did the airblast for Event 3. The Event 3 surface airblast attenuated with range as $R^{-0.94}$ and the near-surface stress approximately as $R^{-0.83}$. Event 5 airblast attenuated as $R^{-0.61}$ and near-surface stress as $R^{-2.20}$.

Signal levels from Events 3 and 5 stress gages were excessively low, resulting in poor resolution of late-time (low-amplitude) data. The stress waveforms for Event 3 show initial compression decaying to zero followed by a second compressive pulse. Waveforms from Event 5 are likewise initially compressive, but pulse to tension (apparent) after some 60 msec. For both cases, the second pulse is caused by the crater-induced ground shock (Figure 4.27). Typical waveforms are compared between Events 3 and 5 in Figure 4.28.

Since stress is a tensor quantity, motion vectors are indeterminate from its waveform. Velocity, however, is vector related and may be utilized to determine motion polarity or direction. Waveforms from similarly located vertical velocity gages compared with vertical stress waveforms clearly show the pulses are of opposite polarity, the first being airblast induced and downward, the second crater induced and upward. Both motions should be seen as compressive stress.

The cause of the second stress pulse sign reversal in Event 5 stress signals is unclear at this time. It may be related to unloading of some prestress in the gage diaphragms or mechanical edge-loading effects. Assuming a nominal prestress (due to placement, etc.), the diaphragms would respond linearly to the compressive loads that were applied. But, on unloading, the gage output would appear to go into tension (the recorded magnitude being highly improbable for soils of such low cohesion). In actuality, the diaphragms would be returning to the normal unloaded point below the initial prestress. Prestresses, unfortunately, were not measured. Gages were electrically nulled just prior to the event, thus effectively shifting the zero base if prestresses were indeed present. Under certain loading conditions, edge loads could induce strains in the sensors bonded

to the diaphragms, thus causing a spurious output, the polarity of the signal generated being dependent upon the sensor(s) most affected.

Theoretical computations (Reference 14) indicate that large amounts of energy are dissipated in the first few inches of dry alluvium such as that of Drowning Ford. This is in support of the at first surprisingly low stresses measured at relatively shallow depths. Higher scatter is to be expected in stress data for several reasons: (1) stress is perhaps the most sensitive parameter to variance in soil properties (stiffness, density, impedance, etc.); (2) it is difficult to achieve adequate and consistent coupling of the gage to the soil under field conditions; and (3) the state of stress will vary as the rate of loading varies and as the load vector changes.

TABLE 4.1 ACCELERATION DATA, EVENTS 3 AND 5

Gage, 3- or 5-	Ground Range	Depth	Arrival Time		Peak Positive Acceleration	
			Event 3	Event 5	Event 3	Event 5
	feet	feet	msec	msec	g's	g's
Vertical (Positive Downward):						
60-1.5-AV	60	1.5	10.6	8.17	195	165
60-5-AV		5.0	11.8	8.24	59.0	24.5
60-10-AV		10.0	16.8	13.3	12.4	12.5
70-1.5-AV	70	1.5	11.5	9.96	104	225
70-5-AV		5.0	14.2	10.9	29.8	30.3
70-10-AV		10.0	18.0	14.5	10.1	11.1
105-1.5-AV	105	1.5	21.0	18.3	53.9	58.3
105-10-AV		10.0	27.3	21.6	11.4	14.3
150-1.5-AV	150	1.5	38.7	38.7	44.2	36.5
225-1.5-AV	225	1.5	73.4	78.5	12.1	20.4
Horizontal (Positive Outward):						
60-1.5-AH	60	1.5	11.4	8.04	18.7	34.4
60-5-AH		5.0	12.4	[a]	12.2	[a]
60-10-AH		10.0	17.2	13.7	1.88	2.13
70-1.5-AH	70	1.5	11.8	9.88	14.0	44.3
70-5-AH		5.0	15.7	11.6	5.45	5.76
105-1.5-AH	105	1.5	21.8	16.9	7.99[b]	10.0[b]
150-1.5-AH	150	1.5	37.9	36.0	12.3	14.4
225-1.5-AH	225	1.5	74.4	77.2	1.91	3.40

[a] No signal recorded.
[b] Questionable.

TABLE 4.2 VELOCITY DATA, EVENTS 3 AND 5

Gage, 3- or 5-	Ground Range	Depth	Arrival Time		Peak Airblast-Induced Velocity		Peak Crater-Induced Velocity	
			Event 3	Event 5	Event 3	Event 5	Event 3	Event 5
	feet	feet	msec	msec	ft/sec	ft/sec	ft/sec	ft/sec
Vertical (Positive Downward):								
∫60-1.5-AV	60	1.5	10.6	8.17	9.17	6.02	--	--
∫60-5-AV		5.0	11.8	8.24	7.72	3.61	--	--
∫60-10-AV		10.0	16.8	13.3	2.64	2.64	--	--
∫70-1.5-AV	70	1.5	11.5	9.96	6.92	5.71	--	--
∫70-5-AV		5.0	14.2	10.9	4.02	3.37	--	--
∫70-10-AV		10.0	18.0	14.5	2.33	2.44	--	--
∫105-1.5-AV	105	1.5	21.0	18.3	5.08	2.21	--	--
∫105-10-AV		10.0	27.3	21.6	2.15	1.87	--	--
∫150-1.5-AV	150	1.5	38.7	38.7	3.26	1.24	--	--
∫225-1.5-AV	225	1.5	73.4	78.5	1.15	0.52	--	--
Horizontal (Positive Outward):								
60-1.5-UH	60	1.5	10.5	8.38	2.48	2.57	7.26	7.77
∫60-1.5-AH		1.5	11.4	8.04	8.78	8.03	--	--
60-5-UH		5.0	12.6	10.6	1.12	1.06	4.15	4.99
∫60-5-AH		5.0	12.4	[a]	4.26	[a]	--	[a]
60-10-UH		10.0	18.2	10.0	0.44	0.90	3.10	5.2
∫60-10-AH		10.0	17.2	13.7	4.93	[b]	--	[b]
70-1.5-UH	70	1.5	13.6	10.2	0.69	2.90	3.92	5.71
∫70-1.5-AH		1.5	11.8	9.88	[b]	6.00	--	--
70-5-UH		5.0	16.0[b]	11.2	0.40[b]	0.90	2.56	3.8
∫70-5-AH		5.0	15.7	11.6	3.0[b]	0.50	--	7.0
105-1.5-UH	105	1.5	23.1	18.6	5.55[b]	3.59	[c]	17.7[d]
∫105-1.5-AH		1.5	21.8	16.9	1.00	2.05	--	--
150-1.5-UH	150	1.5	40.5	38.7	0.90	1.82	0.45	0.96
∫150-1.5-AH		1.5	37.9	36.0	0.47	0.20	--	--
225-1.5-UH	225	1.5	75.0	75.9	0.26	0.22	0.47[b]	0.33
∫225-1.5-AH		1.5	74.4	77.2	0.54[b]	0.50	--	--

[a] No signal recorded.
[b] Questionable
[c] Clipped peak.
[d] Erroneous amplitude due to instrument tilt.

TABLE 4.3 DISPLACEMENT DATA, EVENTS 3 AND 5

Gage, 3- or 5-	Ground Range	Depth	Peak Airblast-Induced Displacement		Peak Crater-Induced Displacement	
			Event 3	Event 5	Event 3	Event 5
	feet	feet	feet	feet	feet	feet
Vertical (Positive Downward):						
∫∫60-1.5-AV	60	1.5	0.07	0.04	1.40	0.95
∫∫60-5-AV		5.0	0.07	0.03	0.76	0.45
∫∫60-10-AV		10.0	0.03	0.27	0.20	0.75
∫∫70-1.5-AV	70	1.5	0.04	0.76	0.50	0.20[a]
∫∫70-5-AV		5.0	0.04	0.30	0.40	0.28
∫∫70-10-AV		10.0	0.03	0.04	0.30	0.65
∫∫105-1.5-AV	105	1.5	0.05	None	0.20	0.05
∫∫105-10-AV		10.0	0.02	0.02	0.03	0.02
∫∫150-1.5-AV	150	1.5	0.03	None	0.02	0.03
∫∫225-1.5-AV	225	1.5	0.01	0.006	0.005[a]	0.007
Horizontal (Positive Outward):						
∫60-1.5-UH	60	1.5	a	a	1.90	0.92
∫∫60-1.5-AH		1.5	a	a	a	0.33
∫60-5-UH		5.0	a	a	0.87	0.68
∫∫60-5-AH		5.0	a	b	a	b
∫60-10-UH		10.0	a	a	0.47	0.60
∫∫60-10-AH		10.0	a	b	a	b
∫70-1.5-UH	70	1.5	a	a	0.92	0.54
∫∫70-1.5-AH		1.5	a	a	a	0.34
∫70-5-UH		5.0	b	b	0.29	0.30
∫∫70-5-AH		5.0	b	b	b	0.48
∫105-1.5-UH	105	1.5	b	b	b	b
∫∫105-1.5-AH		1.5	b	b	b	0.19
∫150-1.5-UH	150	1.5	b	b	0.71	0.12
∫∫150-1.5-AH		1.5	b	b	b	0.02
∫225-1.5-UH	225	1.5	b	b	0.03	0.02
∫∫225-1.5-AH		1.5	b	b	b	0.02

[a] No signal recorded.
[b] Questionable.

TABLE 4.4 VERTICAL STRESS DATA, EVENTS 3 AND 5

Gage, 3- or 5-	Ground Range	Depth	Arrival Time		Peak Airblast-Induced Stress	
			Event 3	Event 5	Event 3	Event 5
	feet	feet	msec	msec	psi	psi
60-1.5-EV	60	1.5	[a]	7.59	[a]	37.6
60-5-EV		5.0	[a]	8.14	[a]	9.9
60-10-EV		10.0	22.7[b]	16.8	3.8[b]	6.4
70-1.5-EV	70	1.5	11.4	10.7	63	29.2
70-5-EV		5.0	18.0	11.5	38	11.0
105-1.5-EV	105	1.5	24.3	18.8	20	25.0
150-1.5-EV	150	1.5	39.8	37.6	3.4	3.6
225-1.5-EV	225	1.5	78.0	77.4	9.3	3.7

[a] No signal recorded.
[b] Questionable.

TABLE 4.5 NEAR-SURFACE AIRBLAST-INDUCED VERTICAL ACCELERATION RATIOS, DISTANT PLAIN EVENTS 3 AND 5 AND FLAT TOP II AND III

Distant Plain Event 3		Distant Plain Event 5		Flat Top II		Flat Top III	
Overpressure	Maximum Acceleration/ Overpressure	Overpressure	Maximum Acceleration/ Overpressure	Overpressure	Maximum Acceleration/ Overpressure	Overpressure	Maximum Acceleration/ Overpressure
psi	g's/psi	psi	g's/psi	psi	g's/psi	psi	g's/psi
--	--	--	--	--	--	980	0.34
--	--	--	--	380	0.32	500	0.41
237[a]	0.82	224[a]	0.74	--	--	280	0.49
165	0.63	215	1.04	210	0.69	--	--
110	0.49	93.5	0.63	140	0.48	130	1.48
53.5	0.83	39.0	0.94	45.0	0.60	42.0	0.98
21.0	0.58	17.5	1.16	--	--	15.0	0.67

[a] Extrapolated.

TABLE 4.6 NEAR-SURFACE AIRBLAST-INDUCED VERTICAL VELOCITY RATIOS, DISTANT PLAIN EVENTS 3 AND 5 AND FLAT TOP II AND III

All velocity data listed are from integrated vertical acceleration.

Distant Plain Event 3		Distant Plain Event 5		Flat Top II		Flat Top III	
Overpressure	Maximum Velocity/ Overpressure	Overpressure	Maximum Velocity/ Overpressure	Overpressure	Maximum Velocity/ Overpressure	Overpressure	Maximum Velocity/ Overpressure
psi	ft/sec/psi	psi	ft/sec/psi	psi	ft/sec/psi	psi	ft/sec/psi
--	--	--	--	--	--	980	0.023
--	--	--	--	380	0.027	500	0.024
237	0.039	224	0.027	210	0.050	280	0.037
165	0.042	215	0.027	140	0.117	130	0.075
110	0.046	93.5	0.023	--	--	--	--
53.5	0.061	39.0	0.032	45	0.038	42	0.083
21.0	0.055	17.5	0.030	--	--	15	0.053

TABLE 4.7 NORMALIZED PEAK HORIZONTAL PARTICLE VELOCITY, EVENTS 3 AND 5

Crater Radius		Gage Range		Gage Depth		Range/ Crater Radius		Crater-Induced Velocity		Velocity/ Crater Radius$^{1/2}$	
Event 3	Event 5	Event 3	Event 5	Event 3	Event 5	Event 3	Event 5	Event 3	Event 5	Event 3	Event 5
feet	feet	feet	feet	feet	feet			ft/sec	ft/sec	ft/sec/ft$^{1/2}$	ft/sec/ft$^{1/2}$
35.1	32.8	60	60	1.5	1.5	1.71	1.83	7.26	7.77	1.23	1.36
35.1	32.8	60	60	5.0	5.0	1.71	1.83	4.15	4.99	0.70	0.88
35.1	32.8	60	60	10.0	10.0	1.71	1.83	3.10	10.0[b]	0.53	--
35.1	32.8	70	70	1.5	1.5	1.99	2.13	3.92	5.71	0.66	1.00
35.1	32.8	70	70	5.0	5.0	1.99	2.13	2.56	1.47	0.43	0.26
35.1	32.8	105	105	1.5	1.5	2.99	3.20	a	17.7[b]	--	--
35.1	32.8	150	150	1.5	1.5	4.27	4.58	0.45	0.96	0.08	0.17
35.1	32.8	225	225	1.5	1.5	6.42	6.86	0.47	0.33	0.08	0.06

[a] Clipped peak.
[b] Questionable.

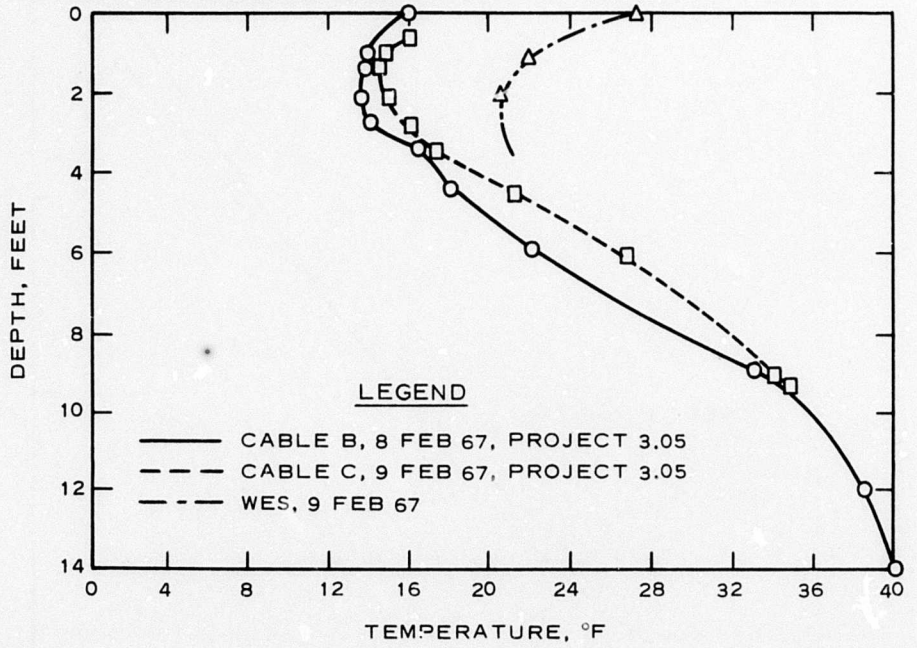

Figure 4.1 Preshot ground temperatures, Event 5. Project 3.05 temperatures were obtained by U. S. Army Cold Regions Research Engineering Laboratories (CRREL) and were supplied by J. Smith of CRREL.

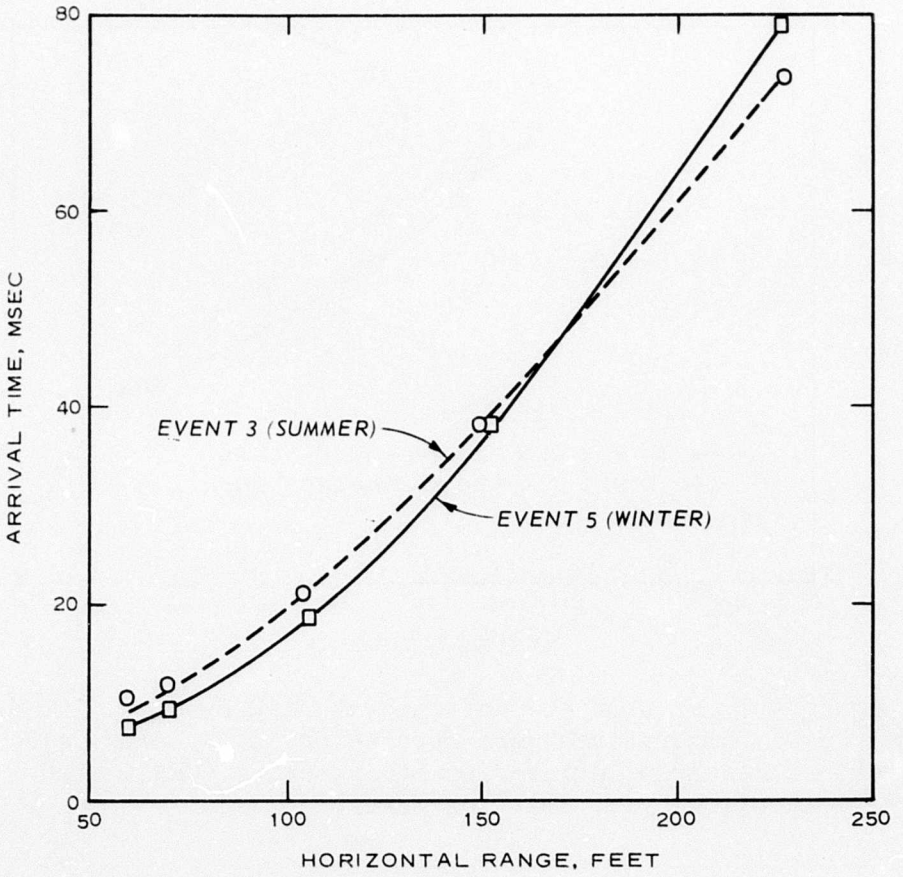

Figure 4.2 Ground-shock arrival time versus horizontal range, 1.5-foot depth, Events 3 and 5.

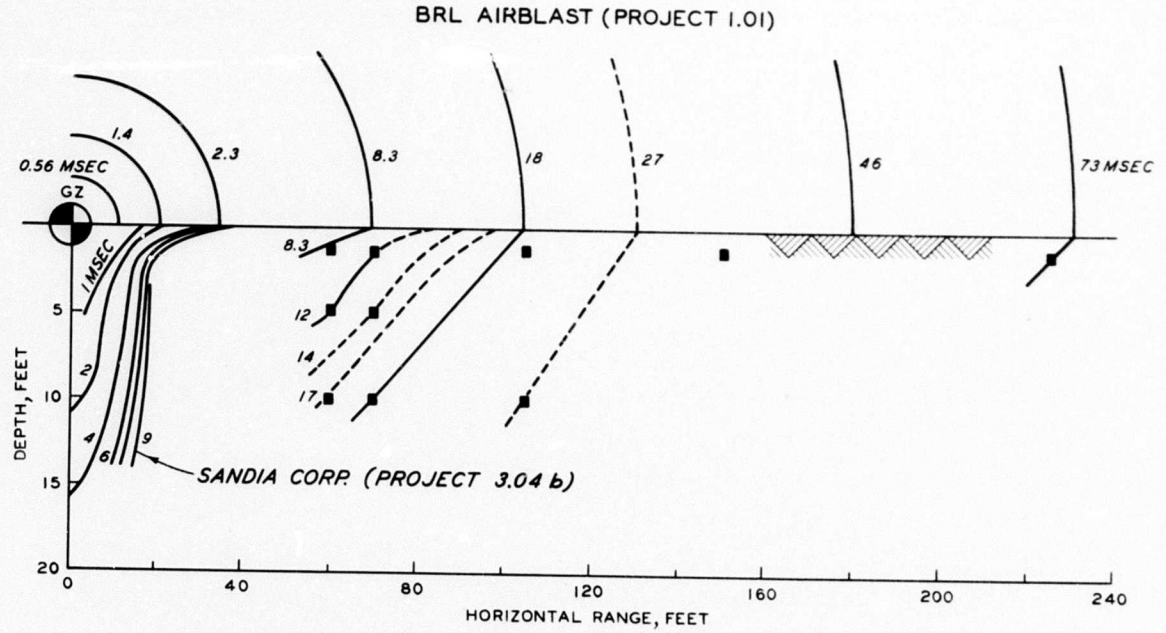

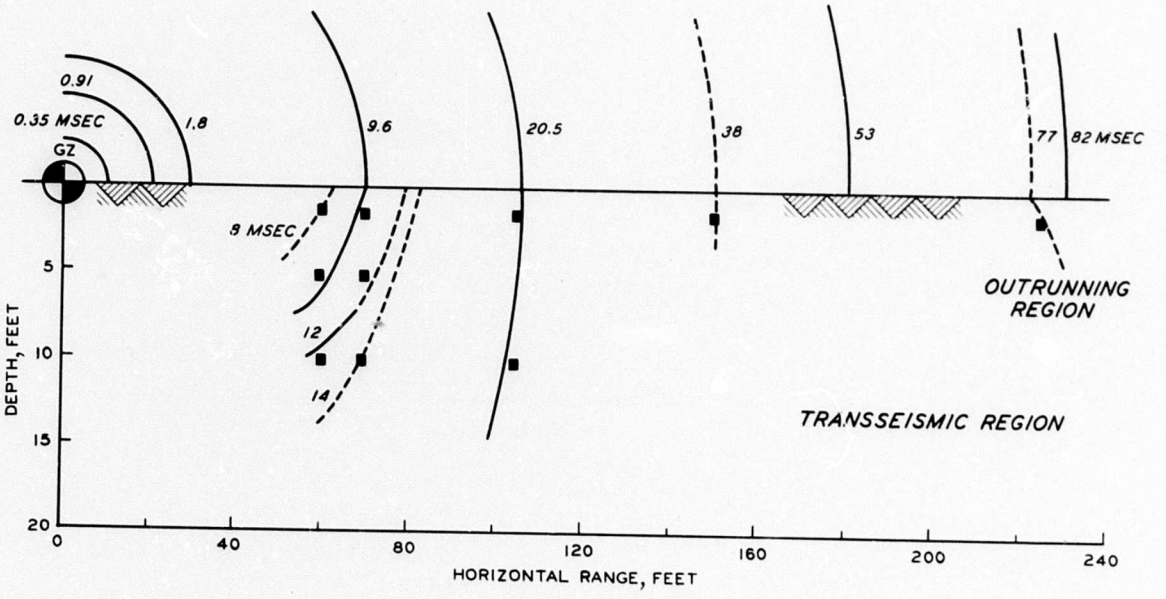

Figure 4.3 Ground-shock profiles, Events 3 and 5.

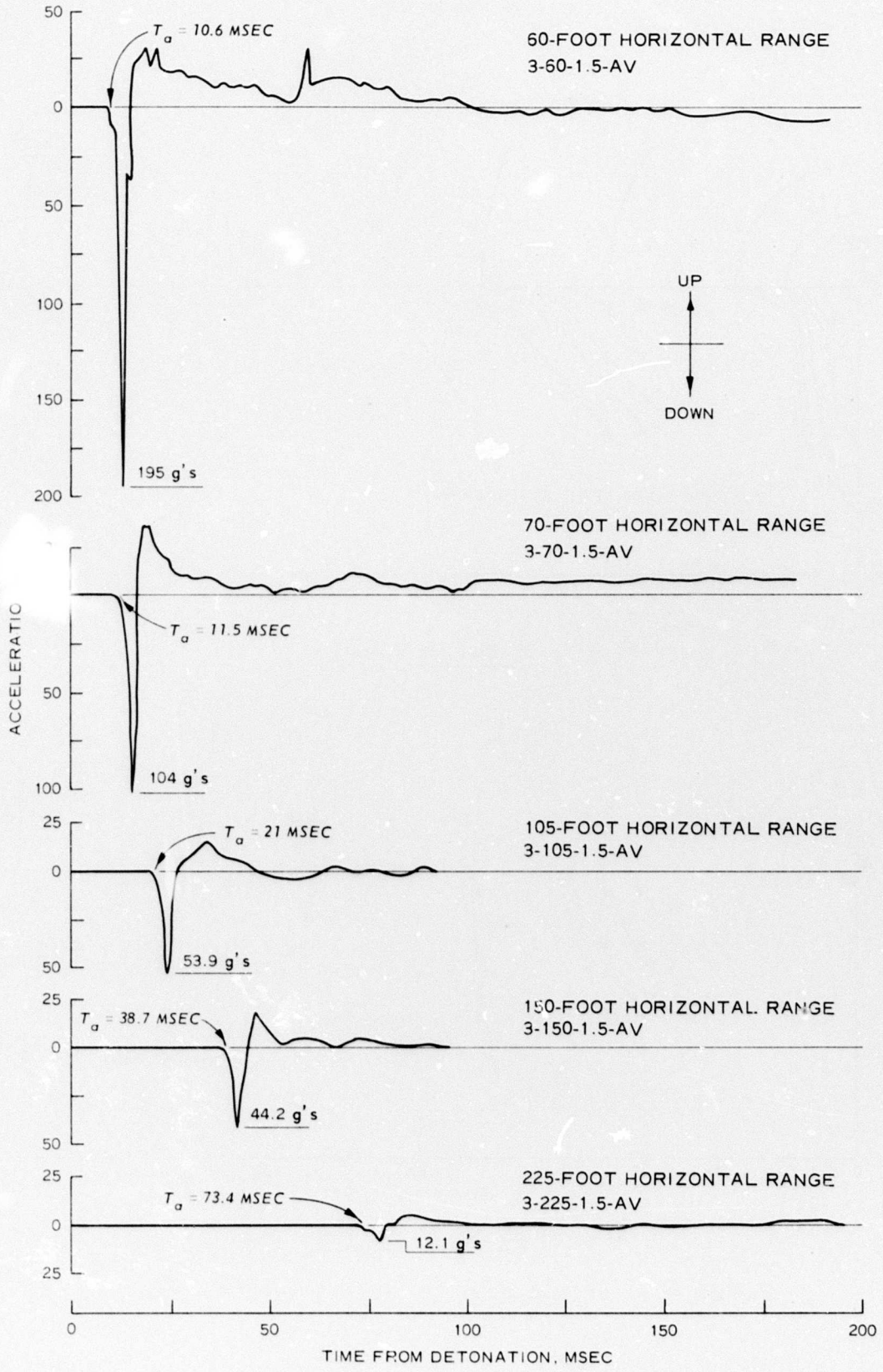

Figure 4.4 Vertical accelerograms, 1.5-foot depth, Event 3.

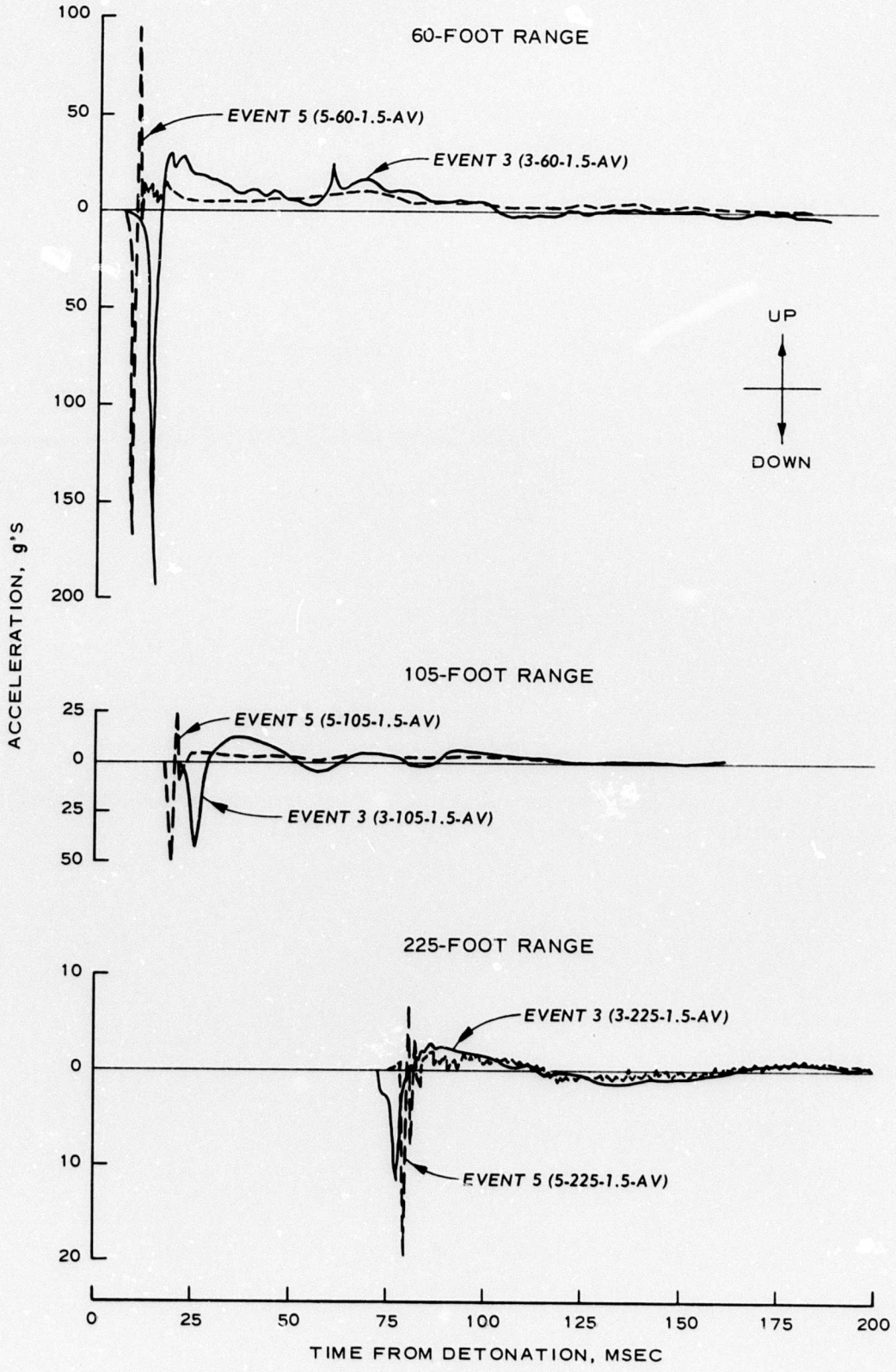

Figure 4.5 Comparison of vertical accelerograms, 1.5-foot depth, Events 3 and 5.

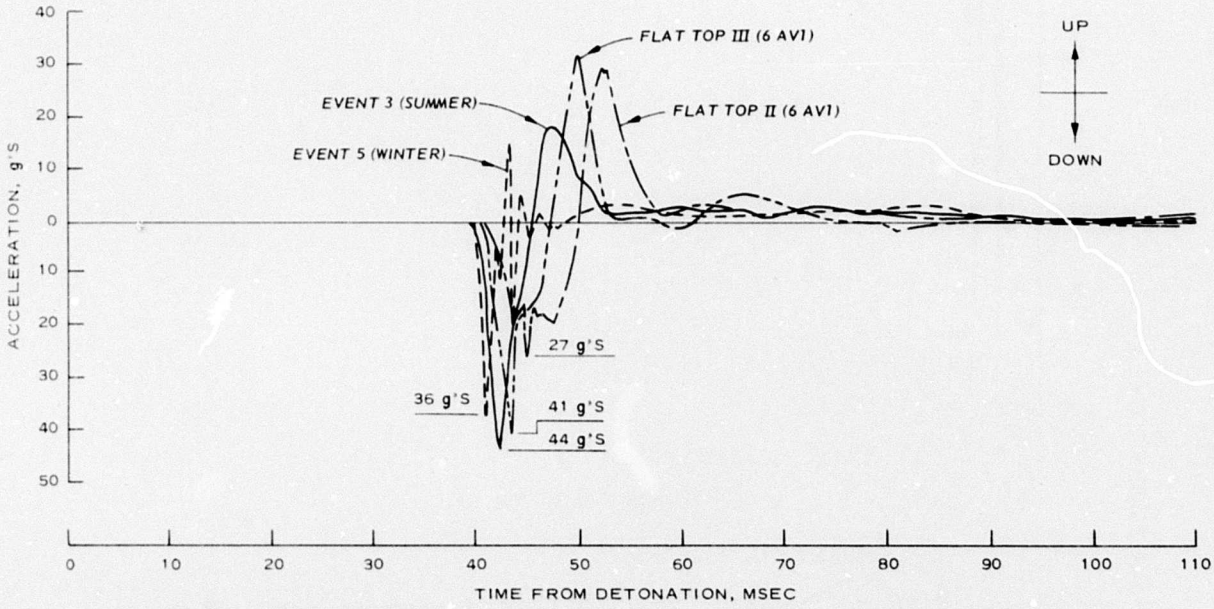

Figure 4.6 Vertical accelerograms at 150-foot range, near-surface, Distant Plain Events 3 and 5 and Flat Top II and III.

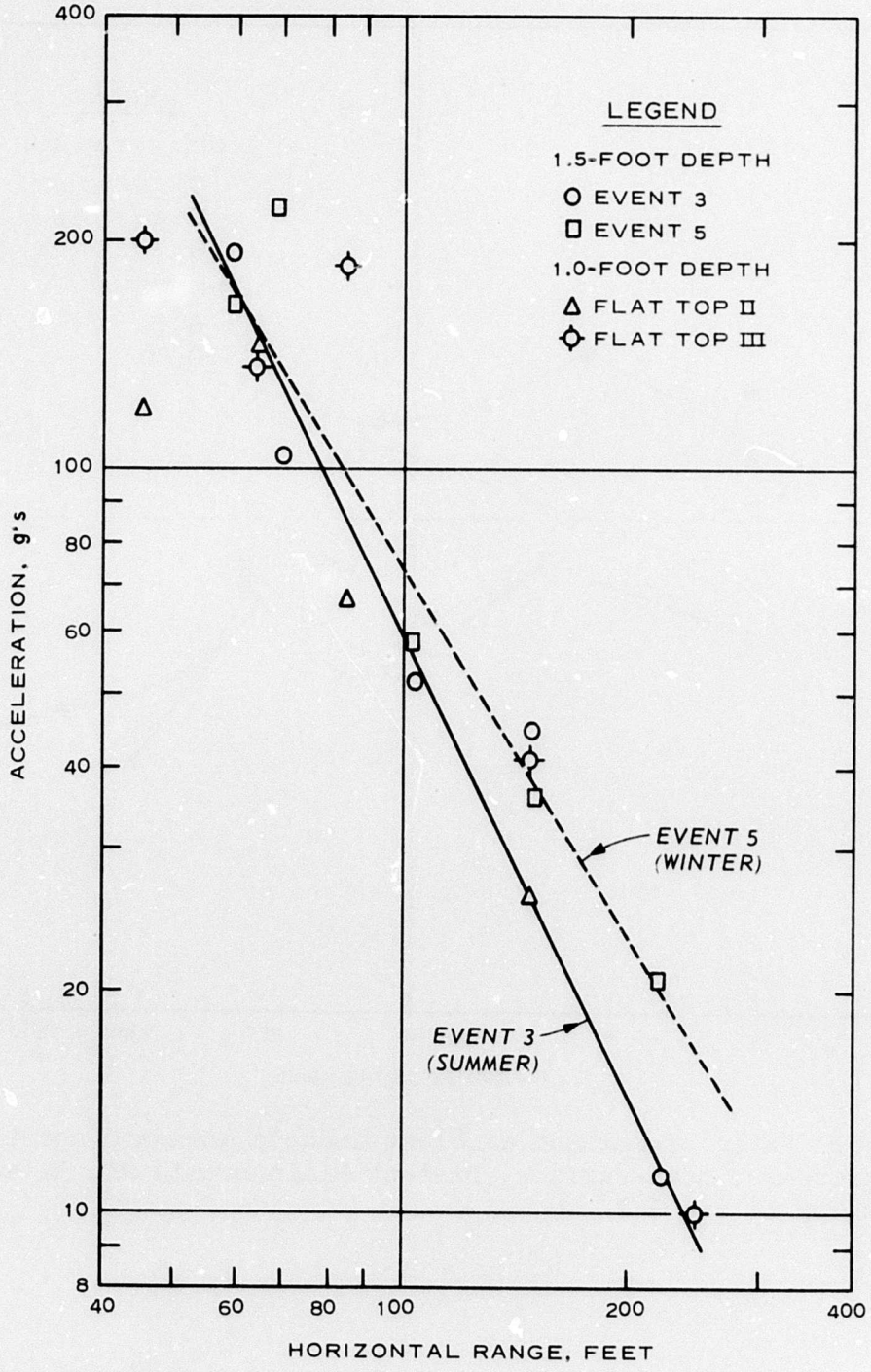

Figure 4.7 Peak airblast-induced downward acceleration versus horizontal range, near-surface, Distant Plain Events 3 and 5 and Flat Top II and III.

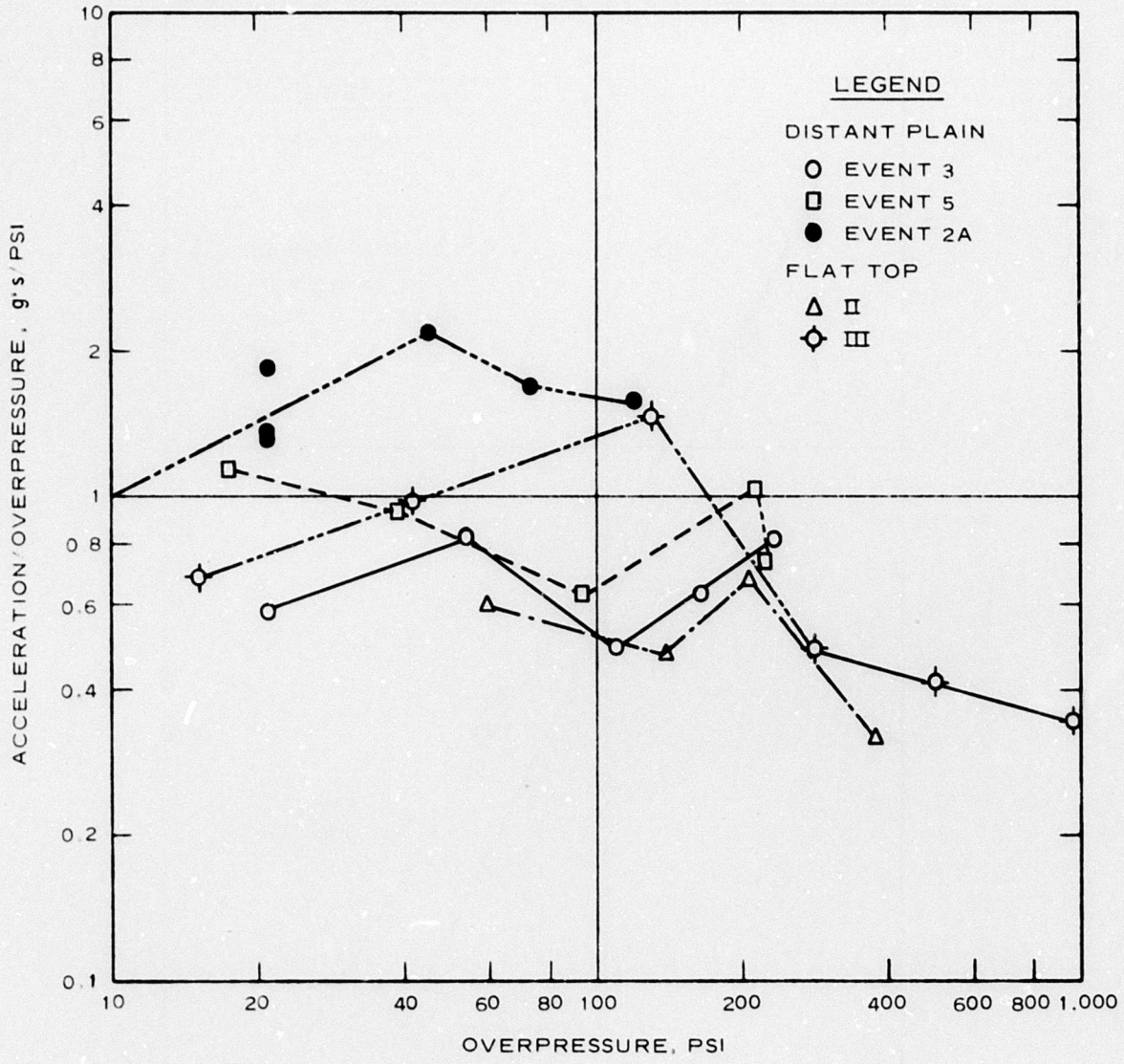

Figure 4.8 Ratio of maximum airblast-induced downward acceleration to overpressure, near-surface, Distant Plain Events 2A, 3, and 5 and Flat Top II and III.

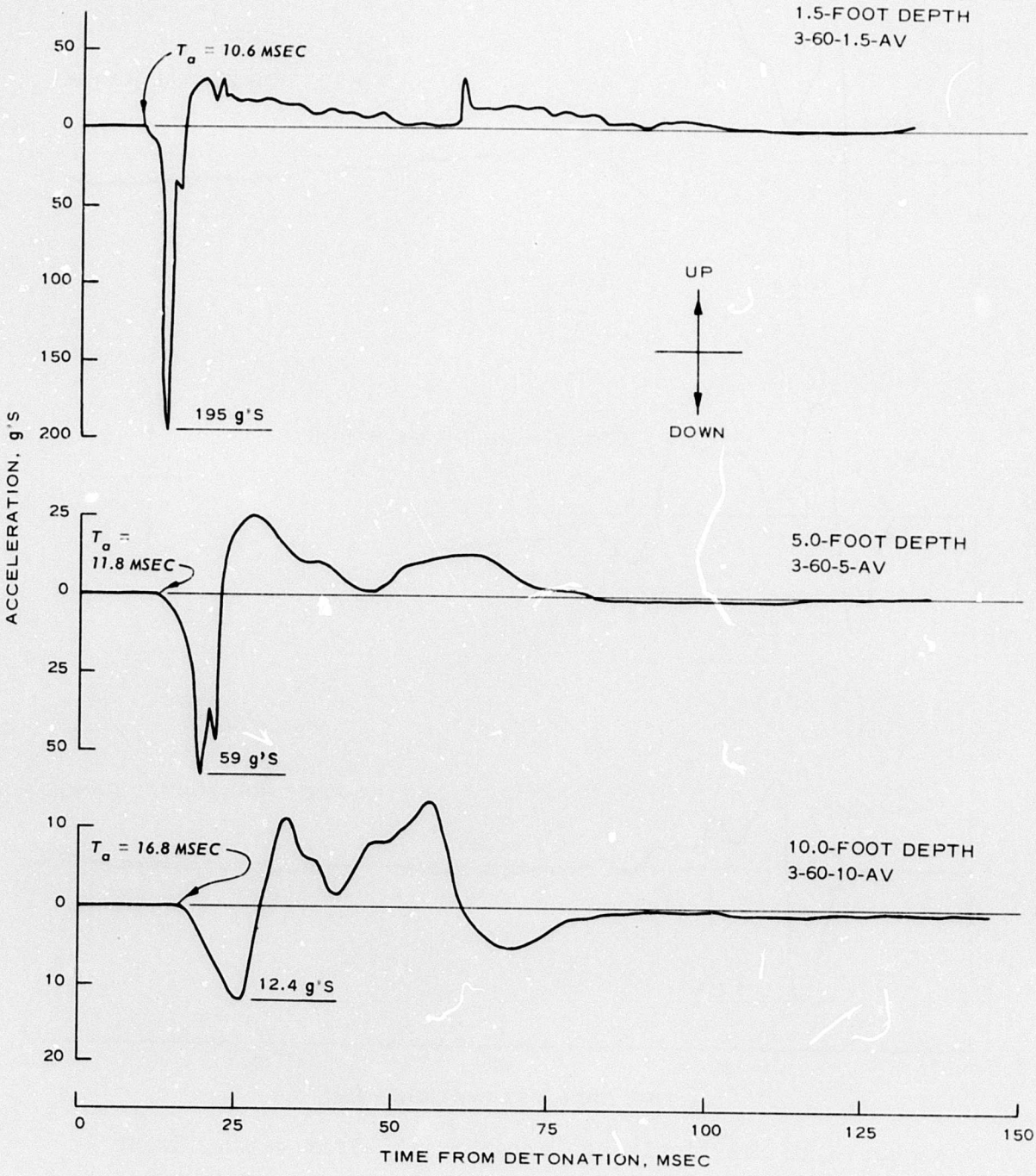

Figure 4.9 Vertical acceleration waveform modification with depth, 60-foot range, Event 3.

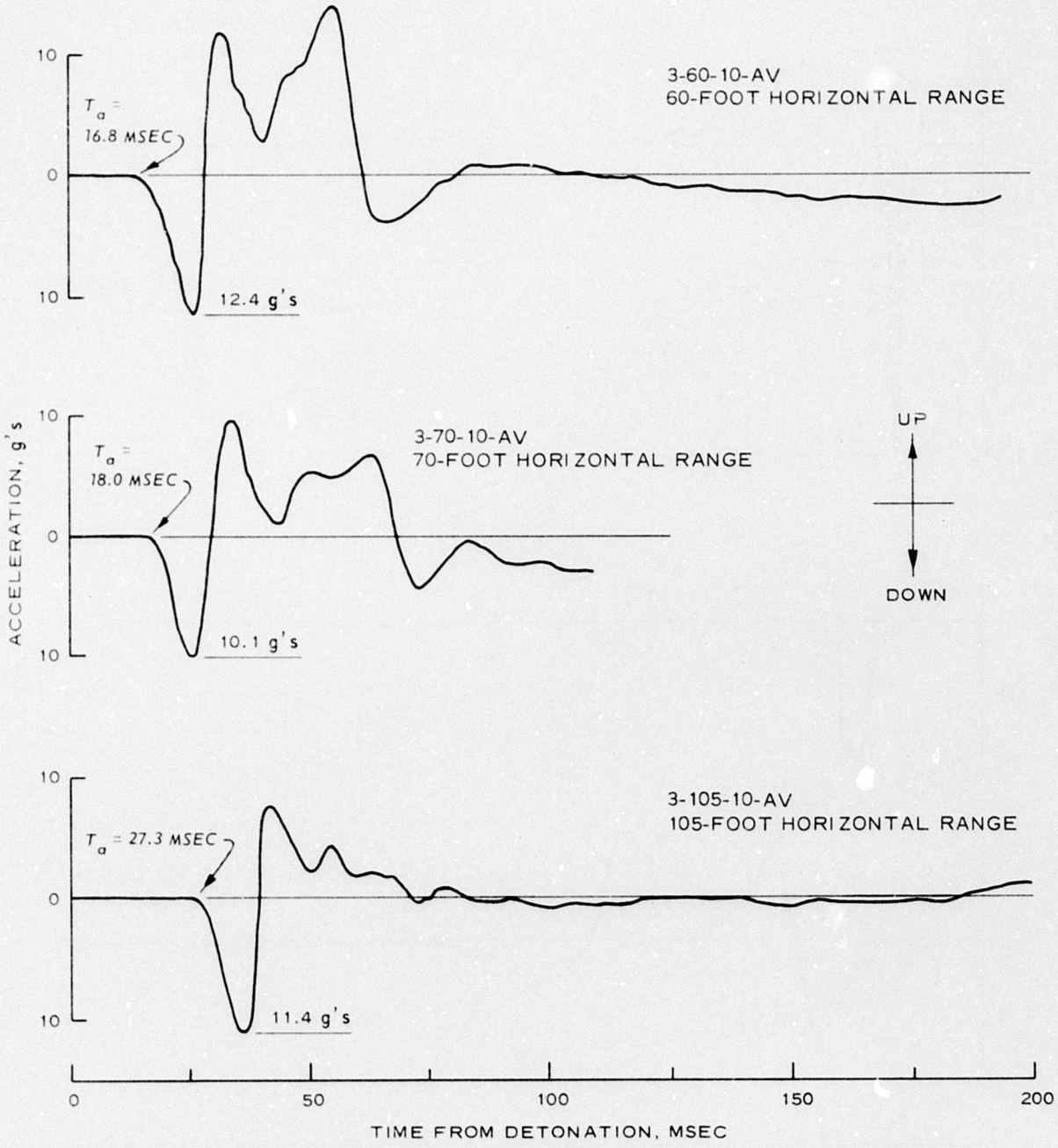

Figure 4.10 Vertical accelerograms, 10-foot depth, Event 3.

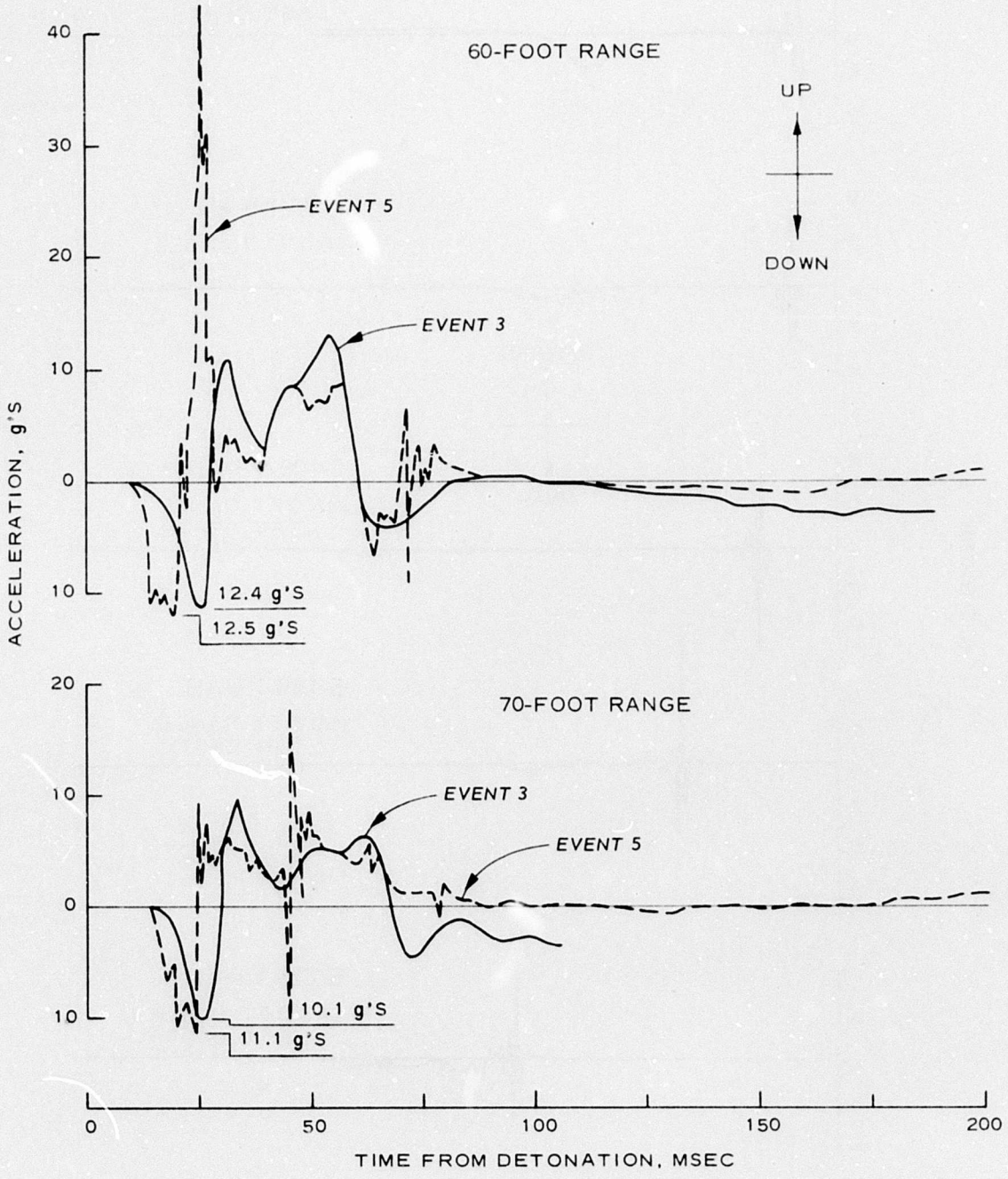

Figure 4.11 Comparison of vertical accelerograms, 10-foot depth, Events 3 and 5.

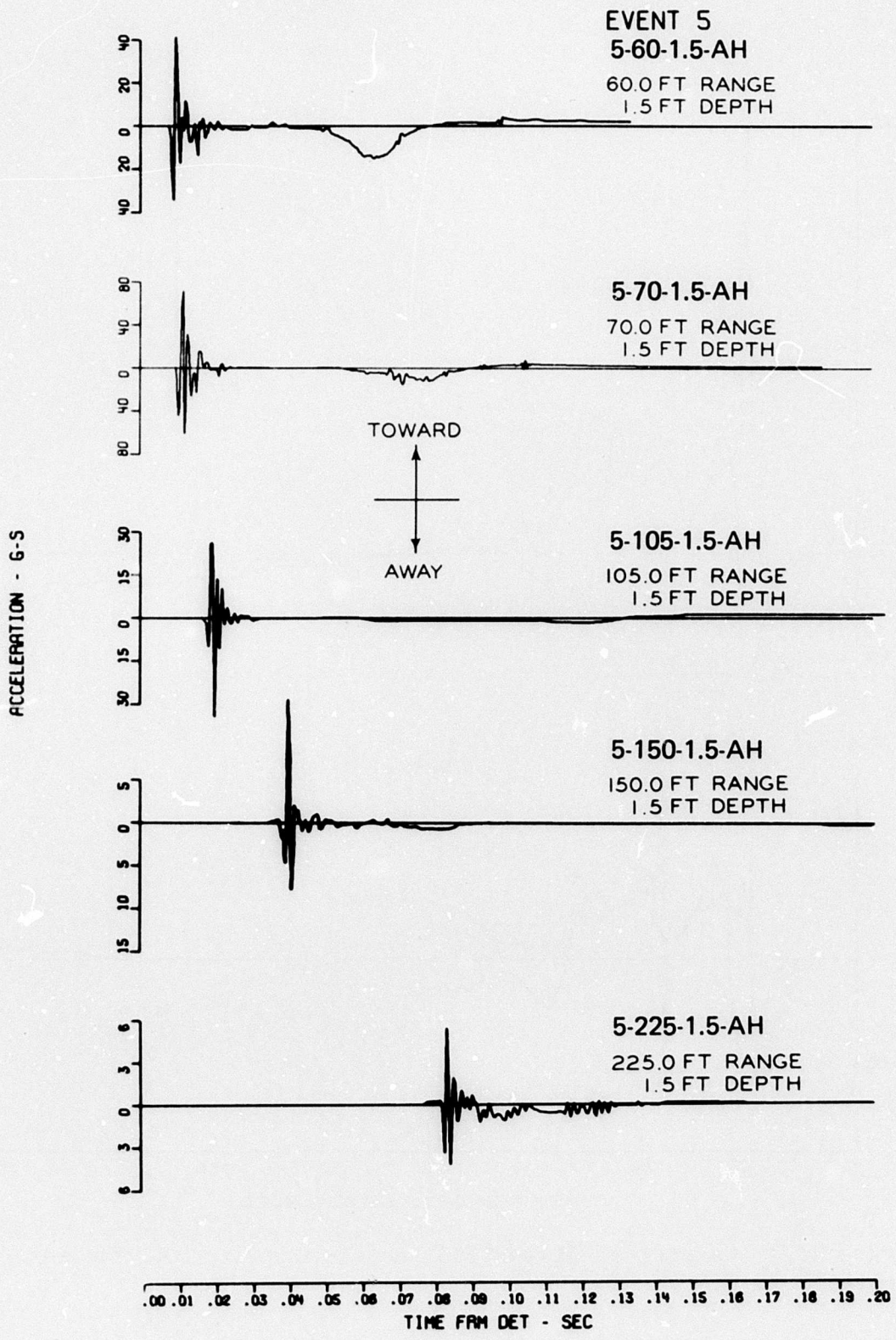

Figure 4.12 Horizontal accelerograms, 1.5-foot depth, Event 5.

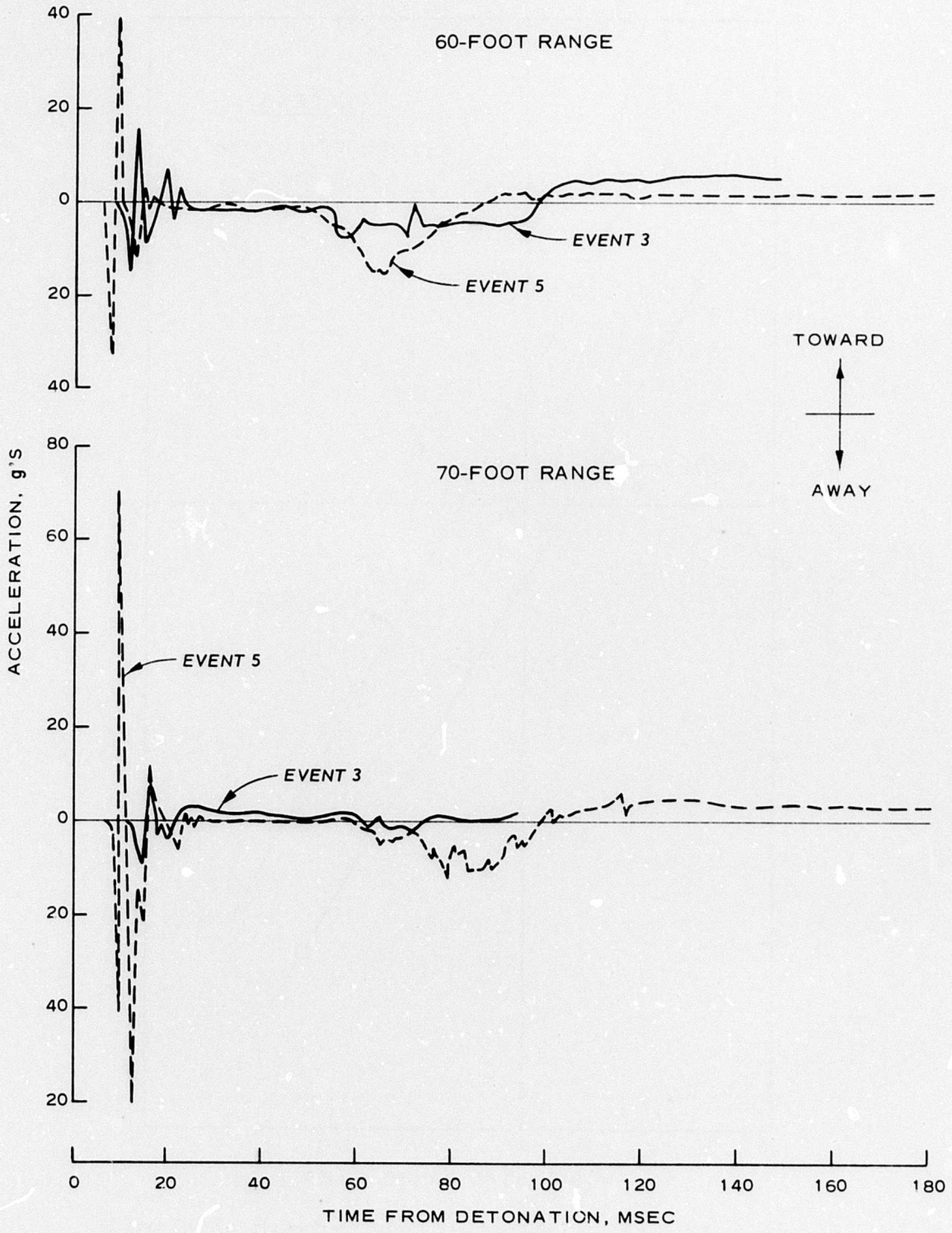

Figure 4.13 Comparison of horizontal accelerograms, 1.5-foot depth, Events 3 and 5.

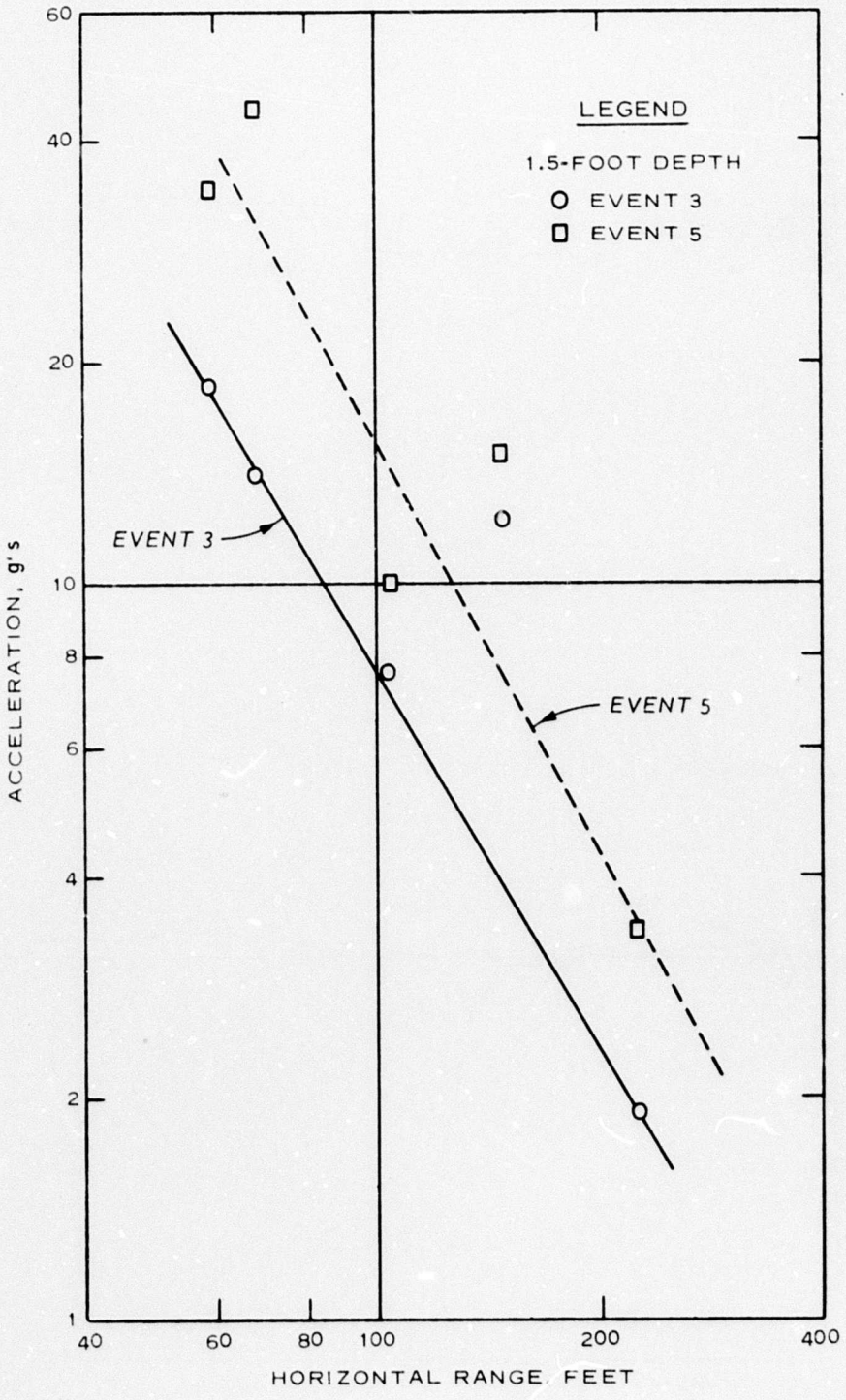

Figure 4.14 Peak airblast-induced outward acceleration versus horizontal range, 1.5-foot depth, Events 3 and 5.

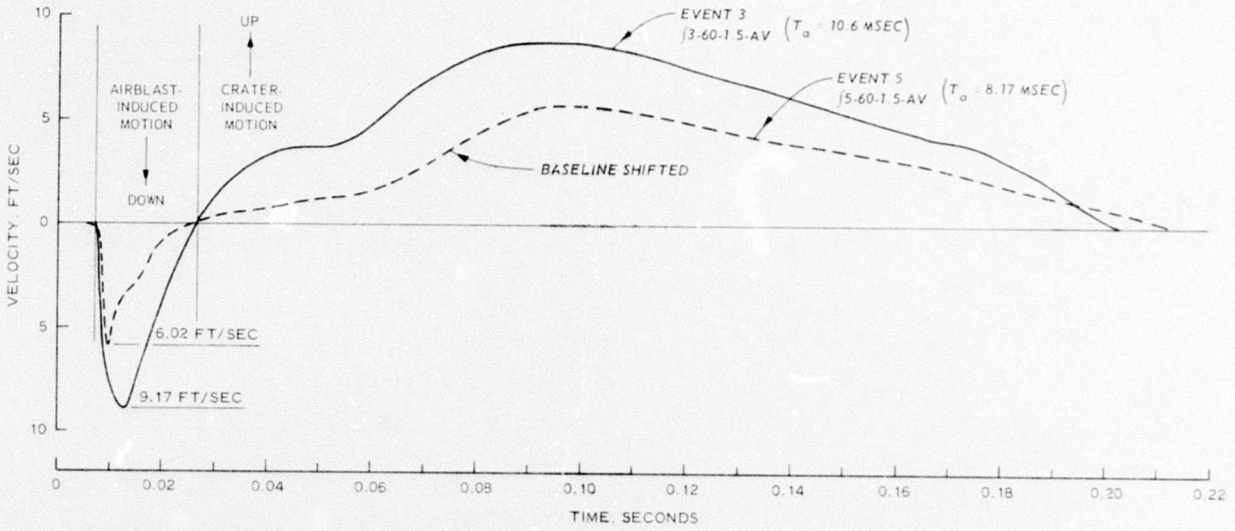

Figure 4.15 Vertical velocity waveforms from integrated acceleration, 1.5-foot depth, 60-foot range, Events 3 and 5.

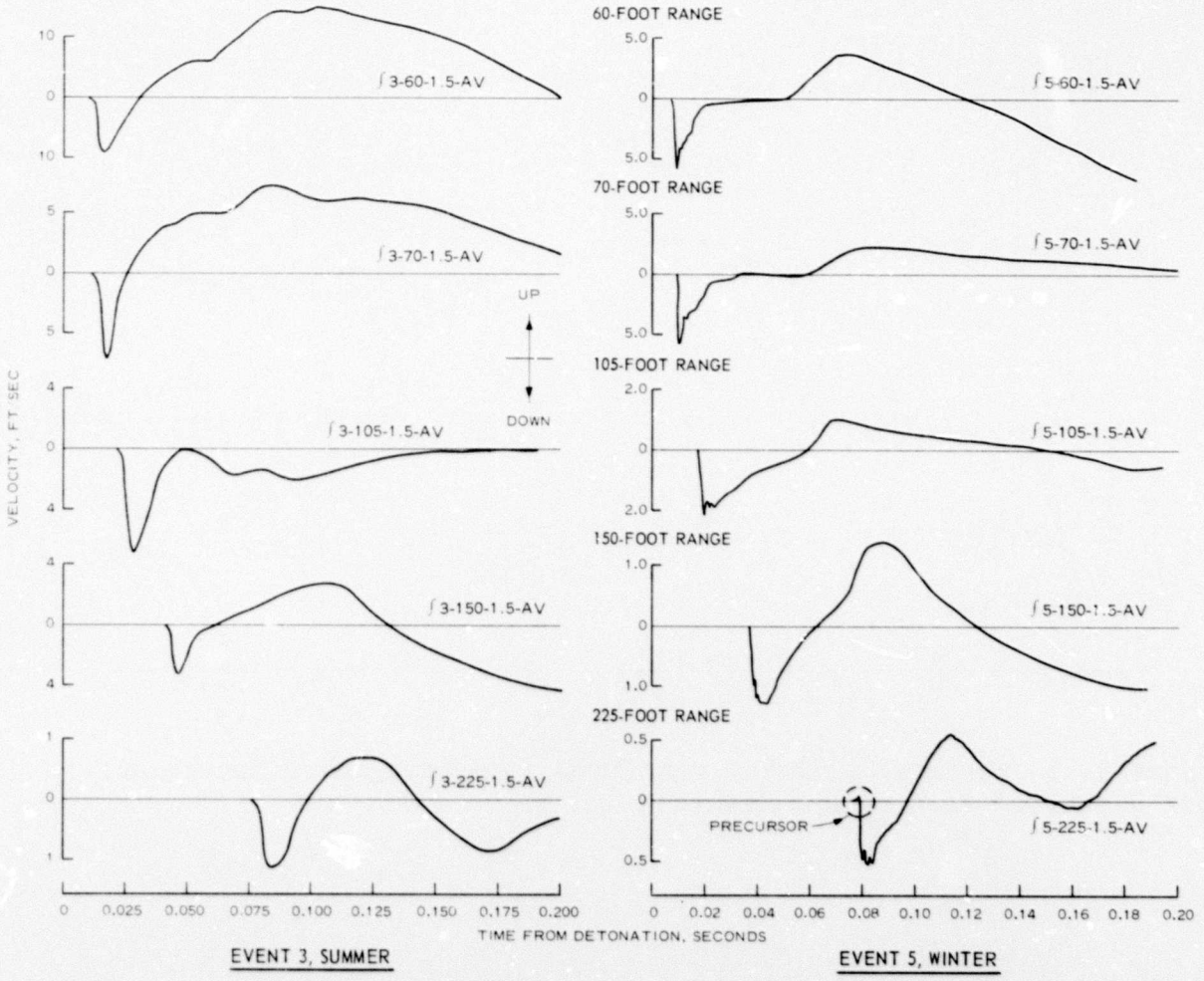

Figure 4.16 Vertical velocity waveforms from integrated acceleration, 1.5-foot depth, various ranges, Events 3 and 5.

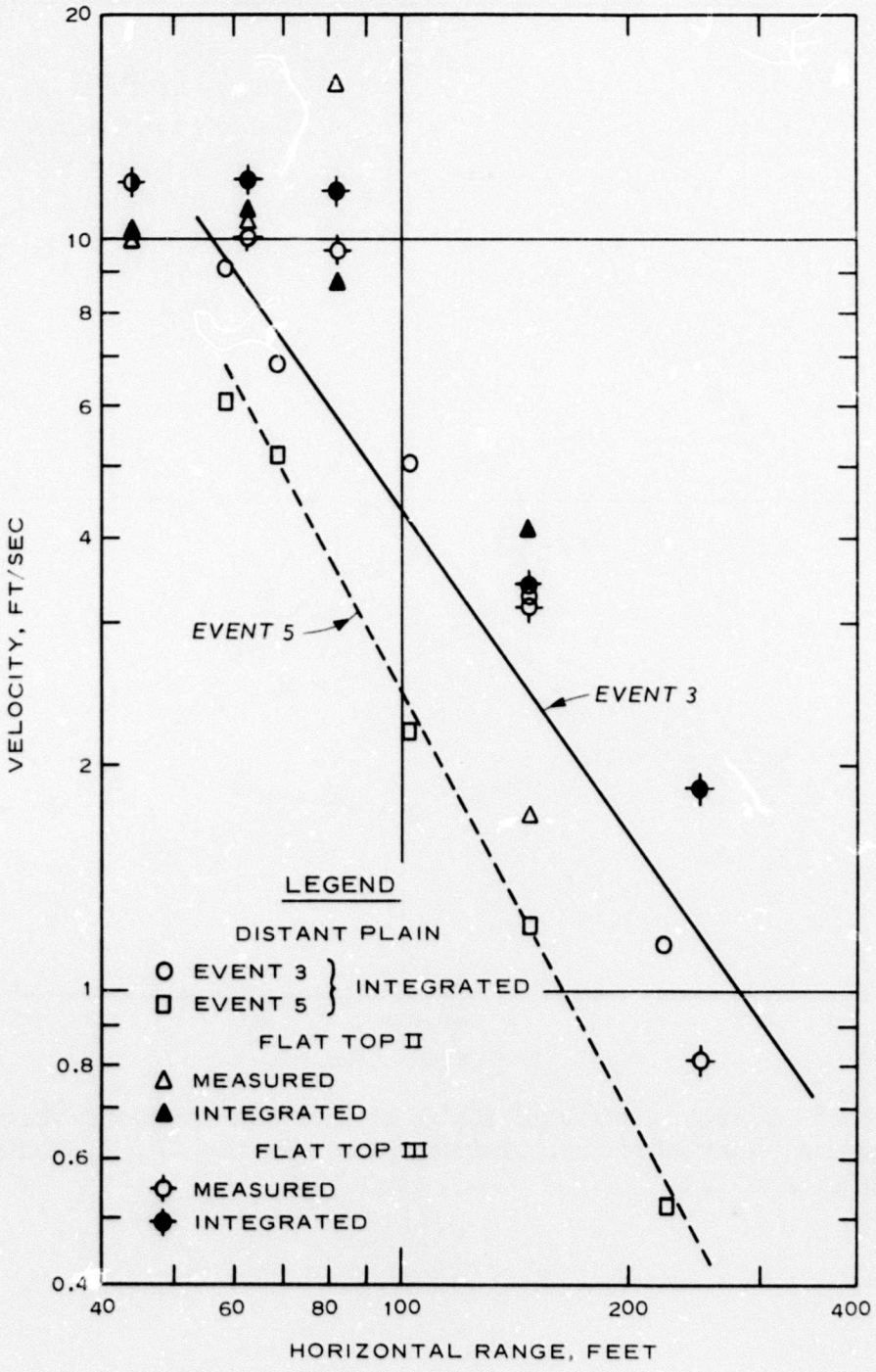

Figure 4.17 Peak airblast-induced downward velocity (integrated values) versus horizontal range, near-surface, Distant Plain Events 3 and 5 and Flat Top II and III.

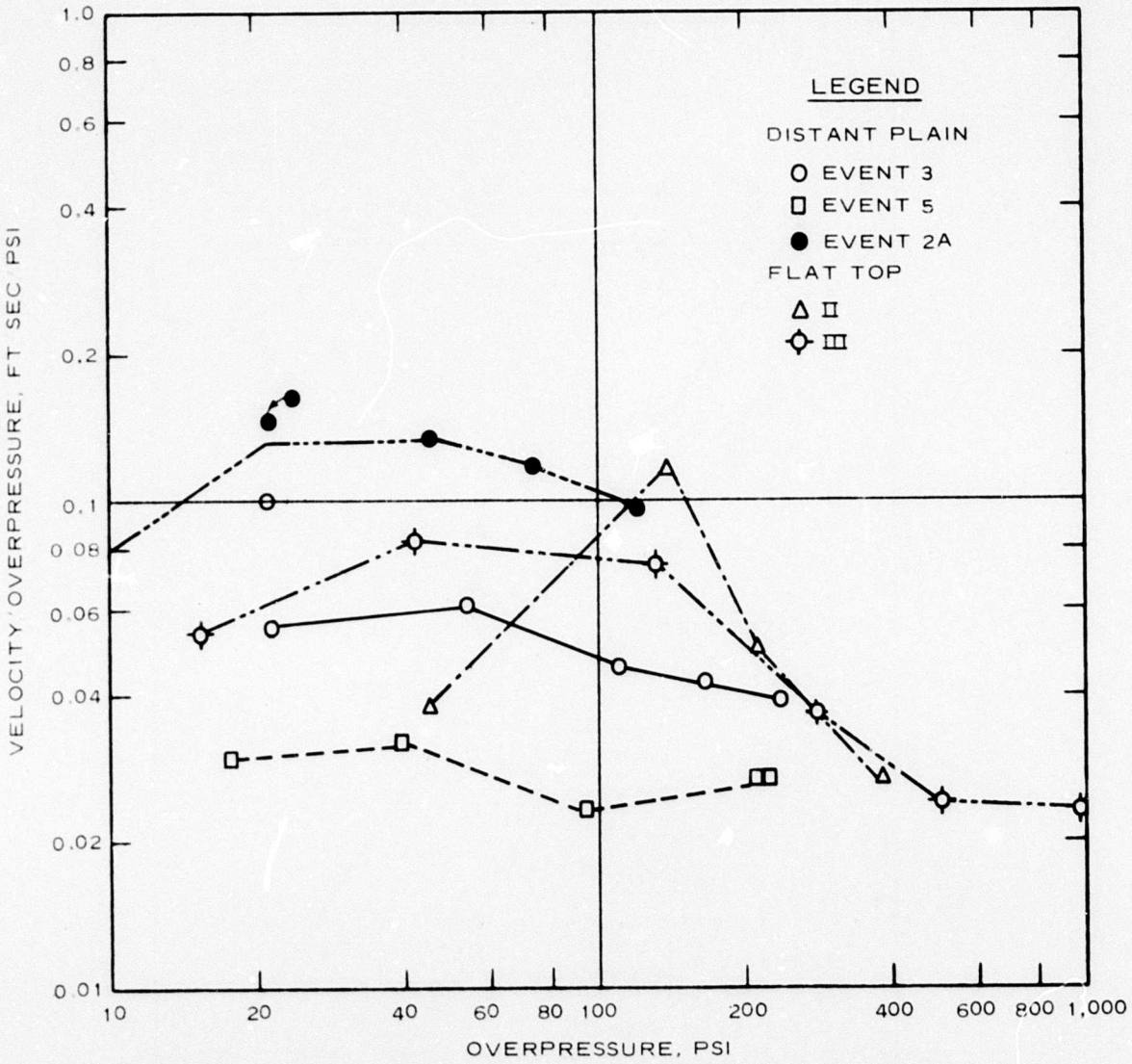

Figure 4.18 Ratio of maximum airblast-induced downward velocity to overpressure, near-surface, Distant Plain Events 2A, 3, and 5 and Flat Top II and III.

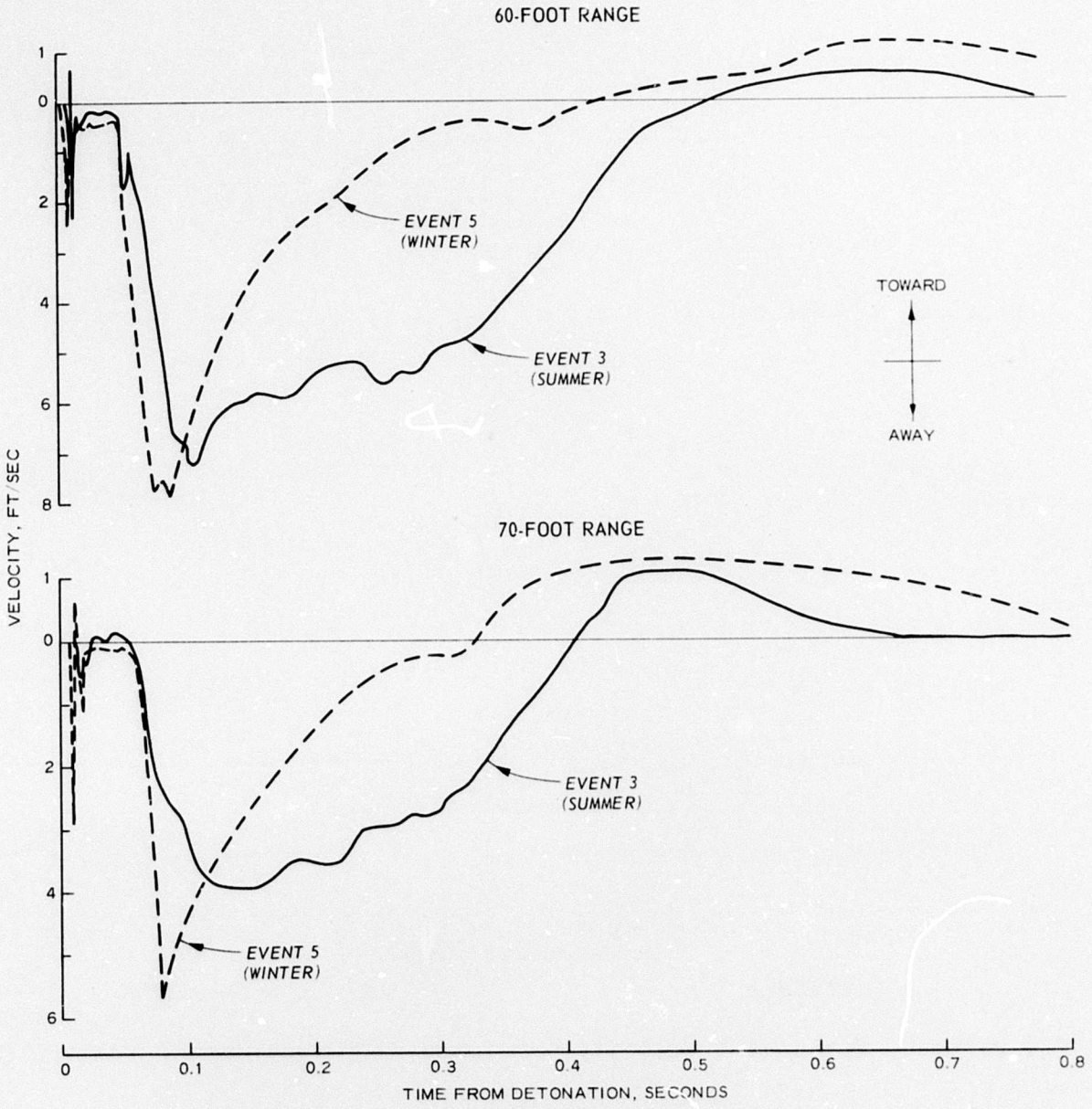

Figure 4.19 Horizontal velocity waveforms, 1.5-foot depth, Events 3 and 5.

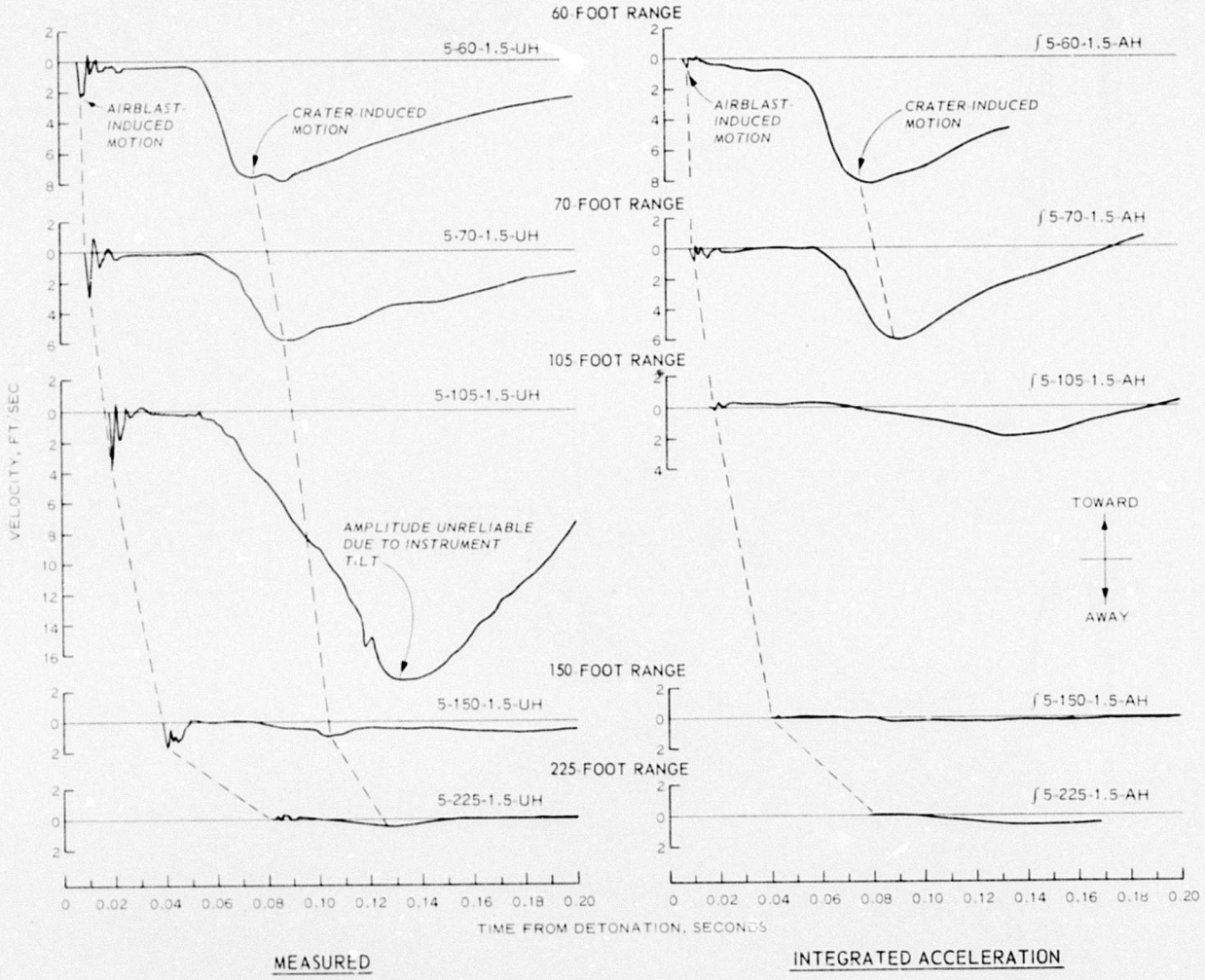

Figure 4.20 Horizontal velocity waveforms, 1.5-foot depth, Event 5.

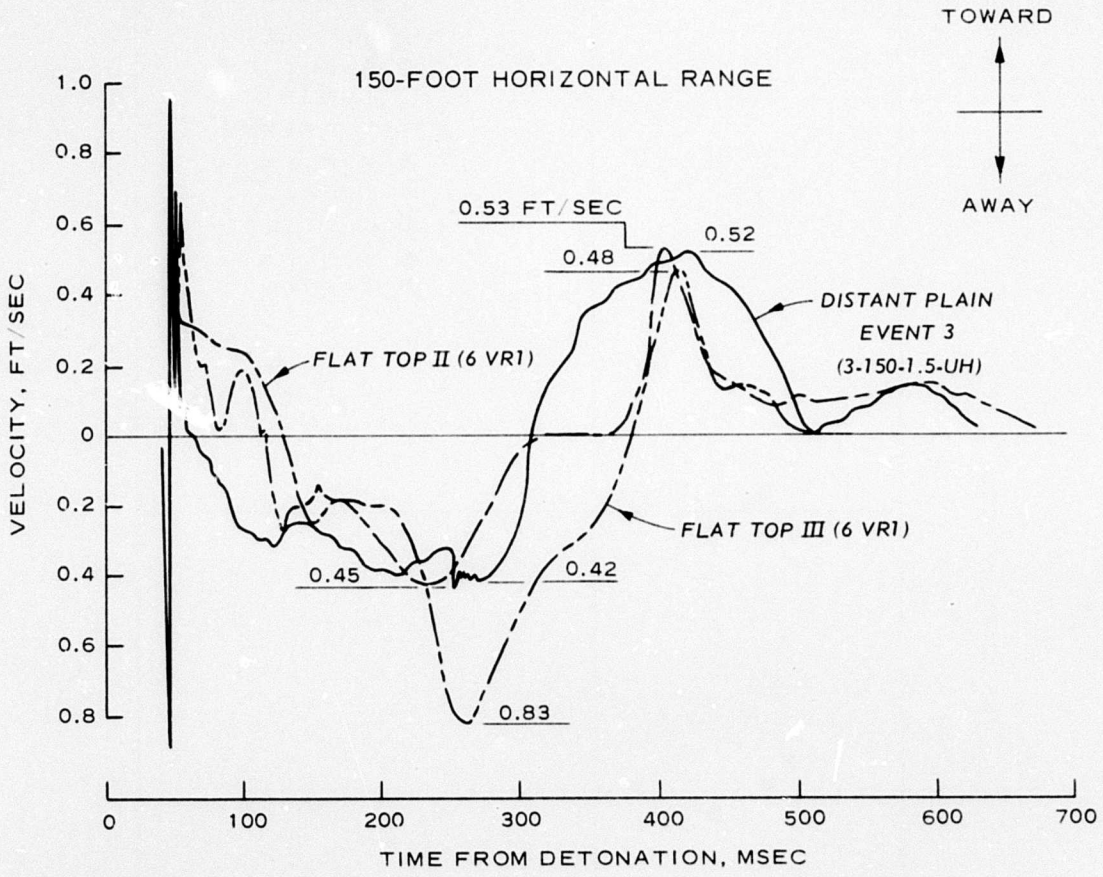

Figure 4.21 Horizontal velocity waveform comparison, near-surface, 150-foot range, Distant Plain Event 3 and Flat Top II and III.

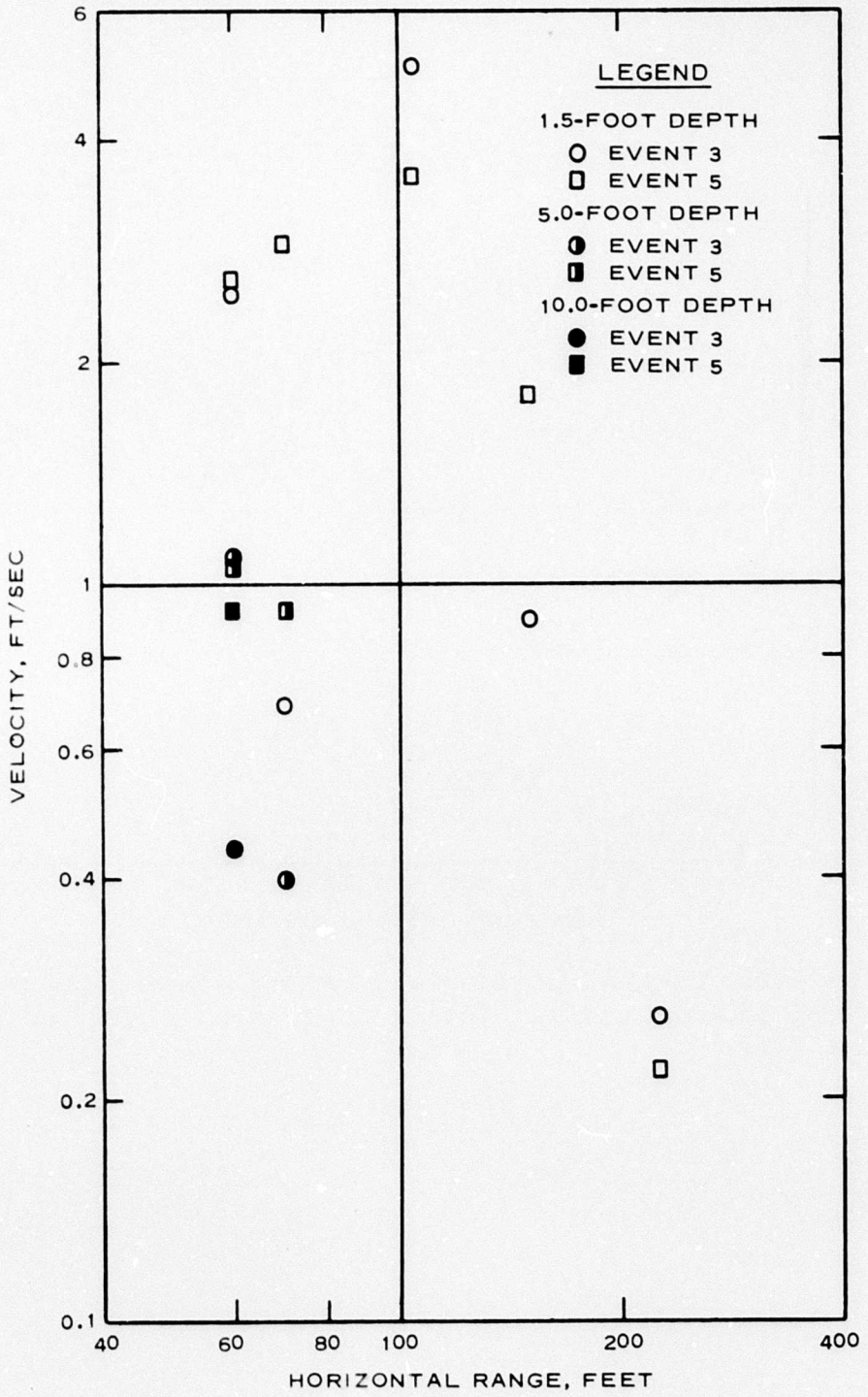

Figure 4.22 Peak airblast-induced outward particle velocity versus range, Events 3 and 5.

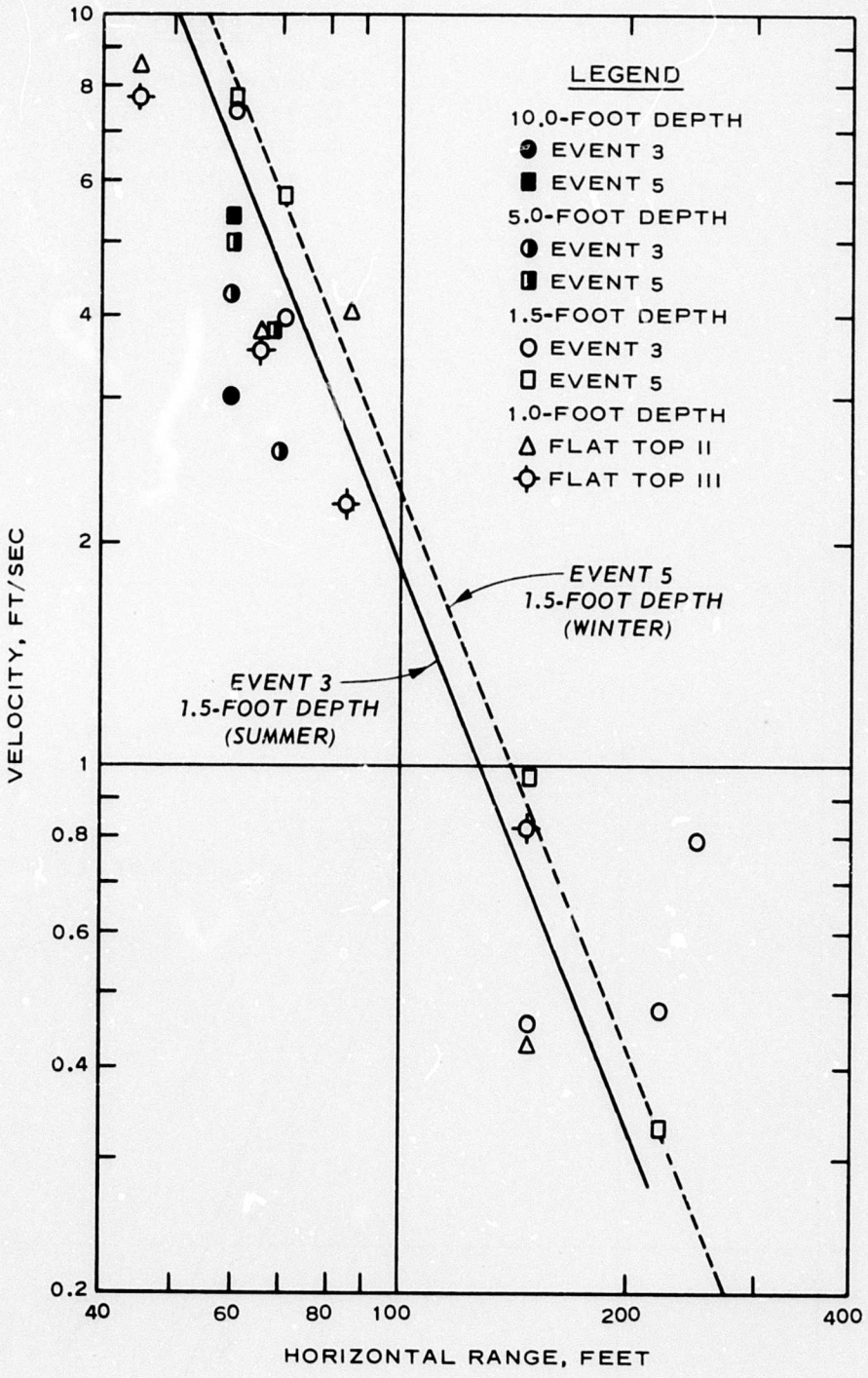

Figure 4.23 Peak crater-induced outward particle velocity versus range, Distant Plain Events 3 and 5 and Flat Top II and III.

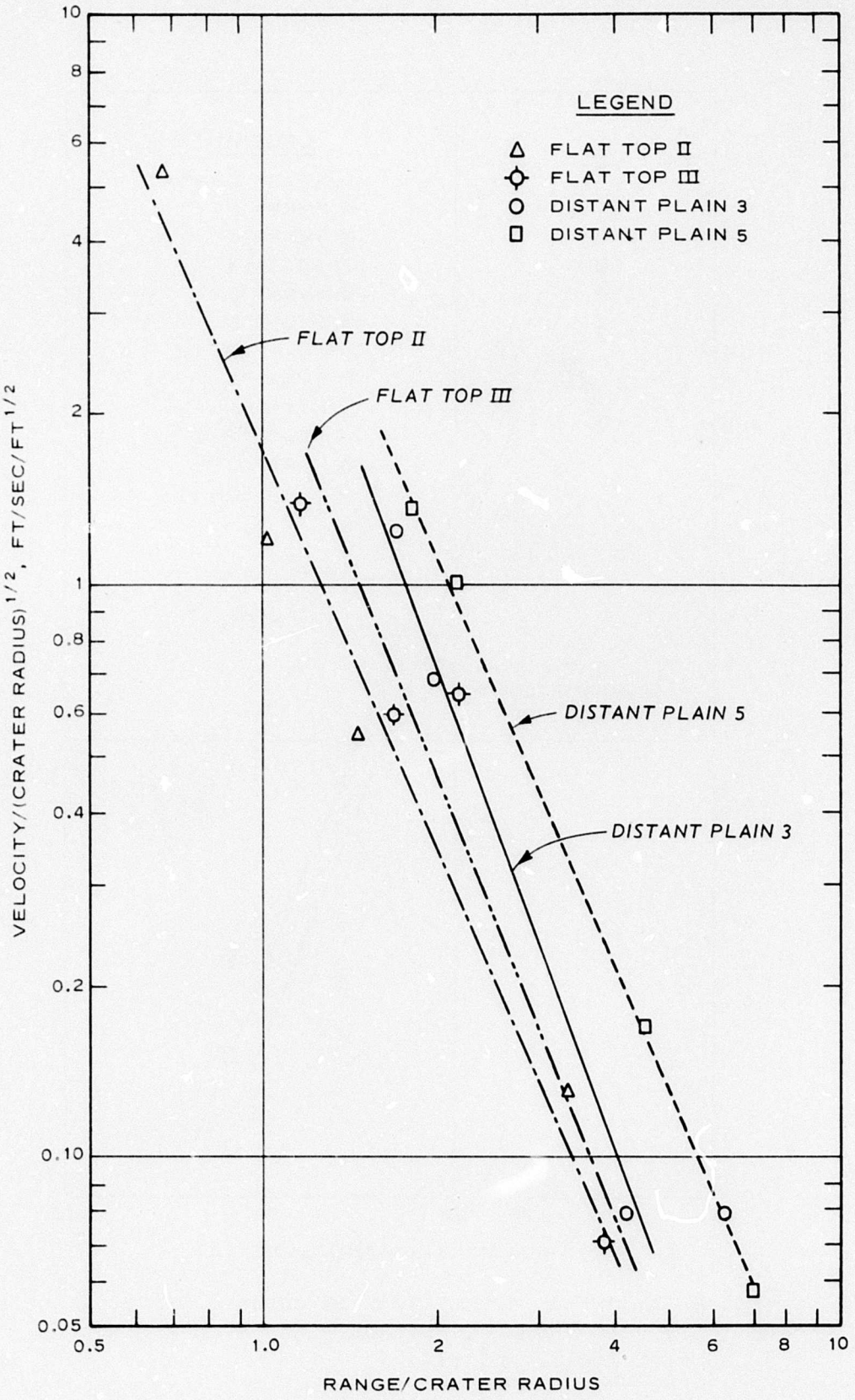

Figure 4.24 Peak crater-induced outward particle velocity normalized to crater radius, Distant Plain Events 3 and 5 and Flat Top II and III.

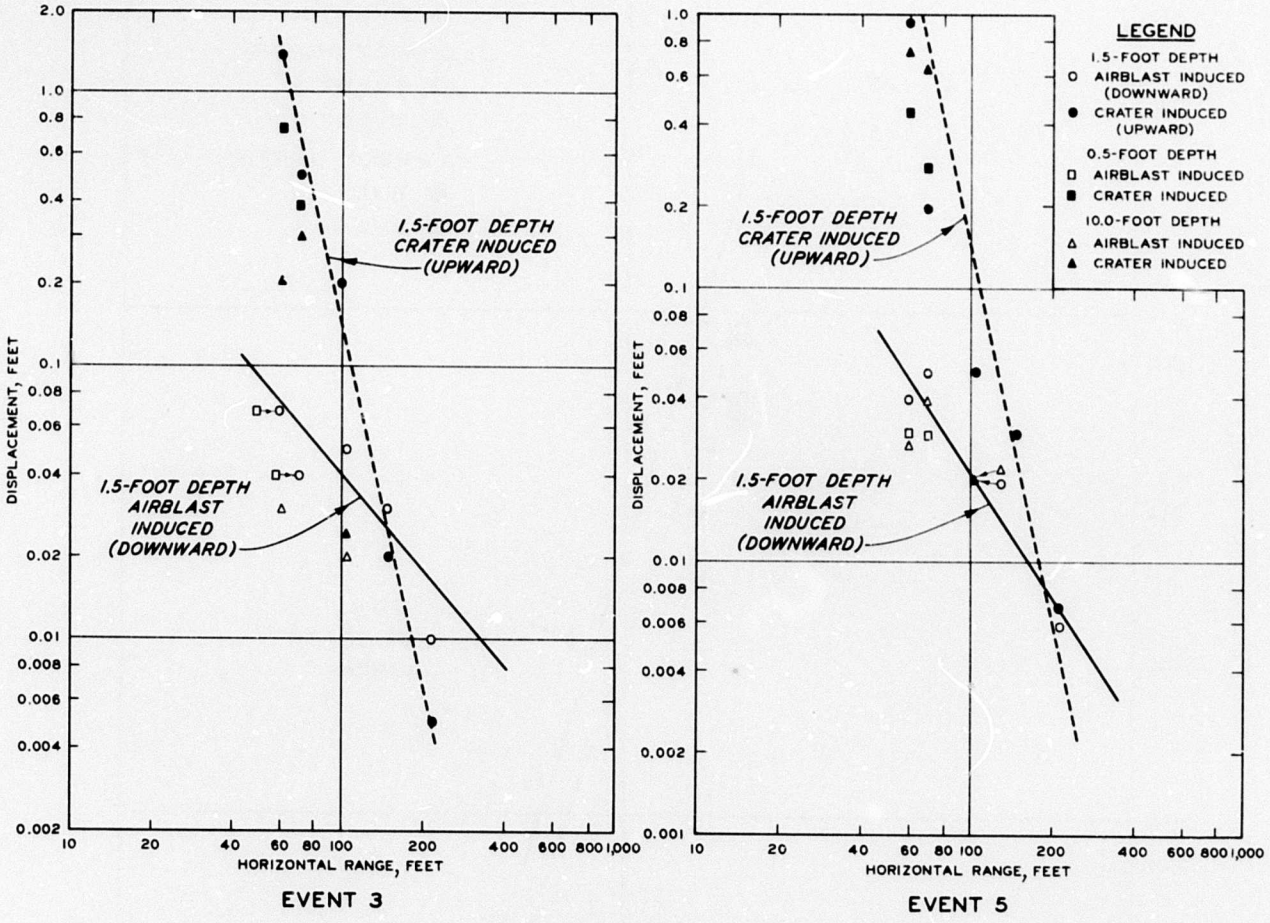

Figure 4.25 Peak vertical displacement versus horizontal range, Events 3 and 5.

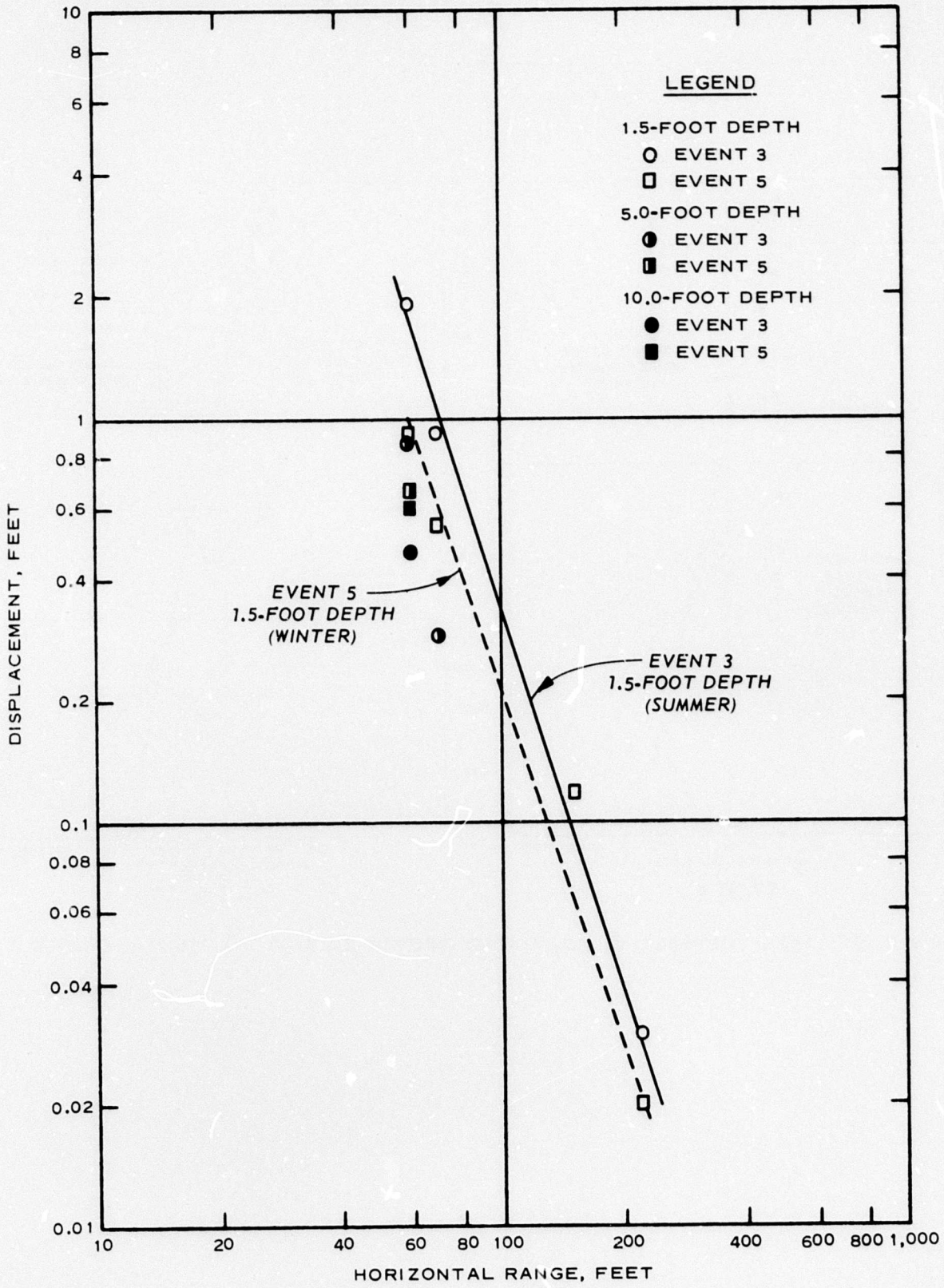

Figure 4.26 Peak crater-induced horizontal displacement versus horizontal range, Events 3 and 5.

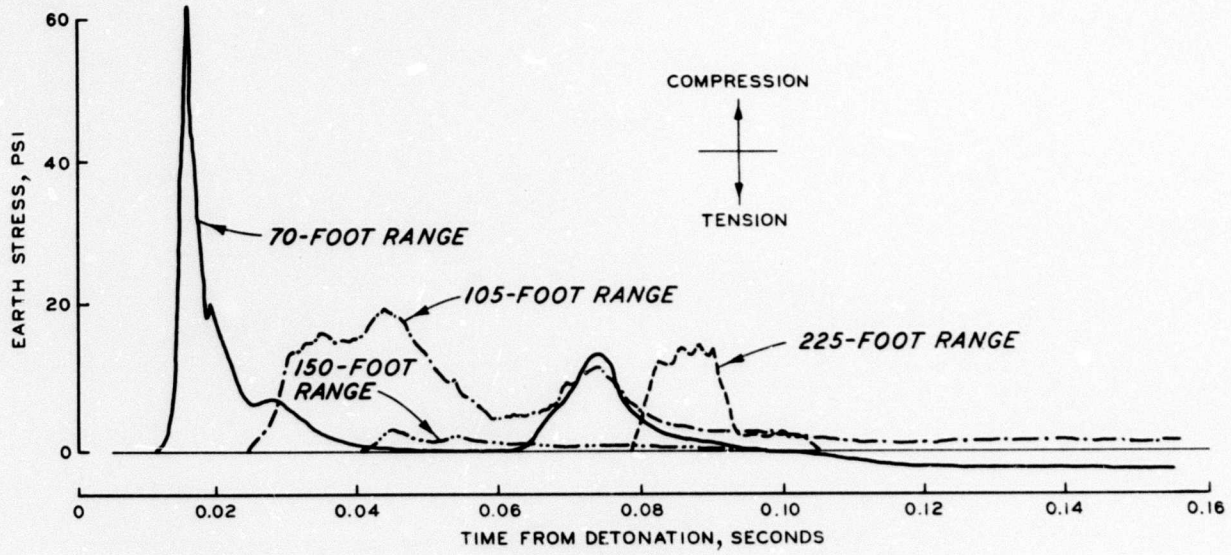

EVENT 3

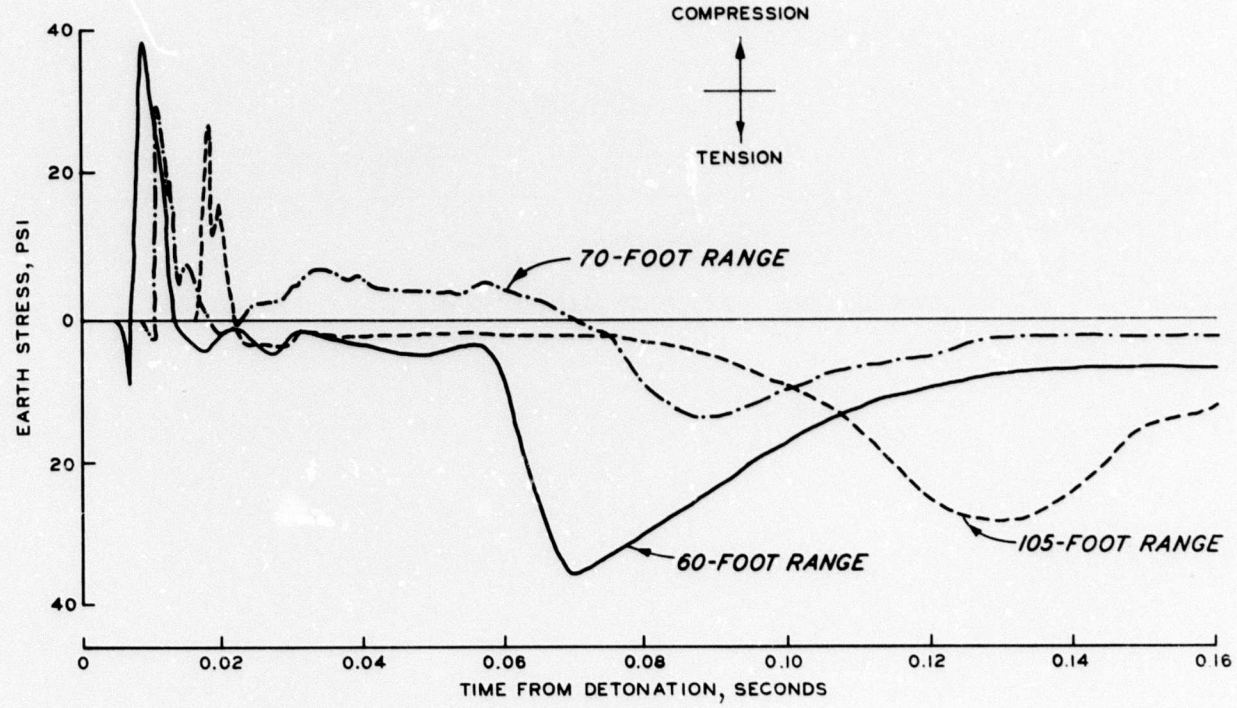

EVENT 5

Figure 4.27 Composite stress plot, 1.5-foot depth, Events 3 and 5.

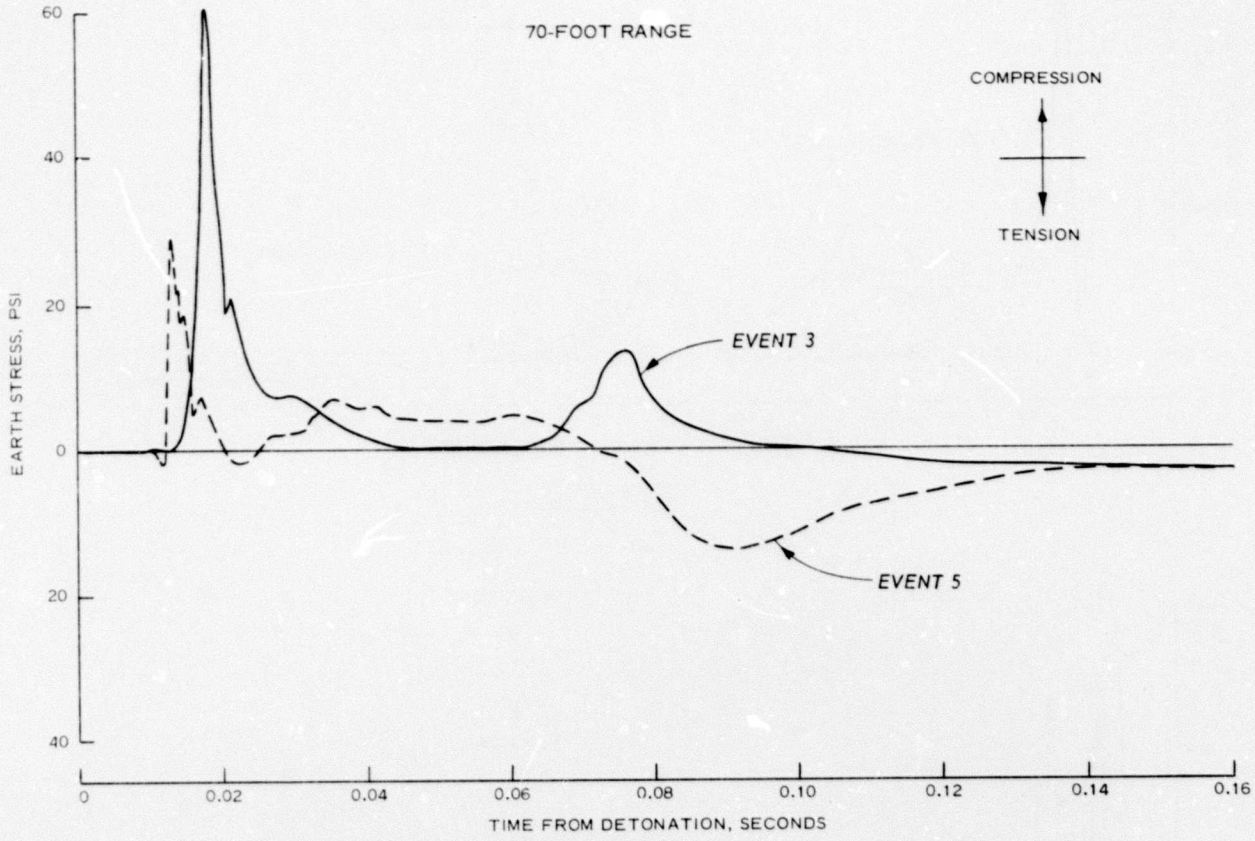

Figure 4.28 Vertical stress waveform comparison, 1.5-foot depth, 70-foot range, Events 3 and 5.

CHAPTER 5

RESULTS, EVENT 4

5.1 DATA RECOVERY

Data recovery for this event was good. Only one channel out of 36 failed to produce data. Due to a 1-1/2-hour delay in detonation, the trace (an accelerometer) drifted beyond its range. Reentry into the test area was not permitted at that time and no adjustments could be made. A large number of particle impacts (ejecta) were noted upon postshot site inspection. All but one of the cleared-sector instrument cables were severed near the recording bunker shortly after detonation. Fortunately, the cable damage occurred late enough not to interfere with the data.

It should be noted that the transducers employed for Event 4 were high-range gages utilized from the Drowning Ford (Events 1 and 2A) instrument packages. Initial set range values were later reduced and no compensation could be made for the higher range calibration resistor sealed inside the instrument canisters. Sufficient signal level could be achieved only by increasing amplifier gain. Motions were lower than expected, resulting in low signal-to-noise ratios. Additionally, ground runs for the primary power supplies for all project bunkers were strung on top of the saturated ground (some actually submerged in pools of water), resulting in considerable stray currents induced in most signal cables. Induced transient voltage levels in these cables ran as high as 38 volts.

The overall effect of the aforementioned conditions was high noise level and amplifier drift. Consequently, numerical integrations of the data contain inherent inaccuracies which limit the reliability. Error accumulation was such that second integrals are useful, in large measure, only for qualitative purposes. Significant baseline shifts occurred on a major portion of the recorded data, rendering even first integrals highly suspect at all but very early times. Treatment of the data in this section, therefore, will concern primarily the measurand. Newly developed digital filtering techniques will allow retrieval of much data contained within the noise; however, due to the additional effort and costs involved, it is not planned to reprocess the data at this time. Listings of peak values for

the data taken are given in Tables 5.1, 5.2, and 5.3.

5.2 GROUND-SHOCK ARRIVAL TIME

Arrival times (Table 5.1) for the near-surface (1.5-foot depth) accelerations ranged from 71 msec at 240-foot horizontal range to 393 msec at 700-foot horizontal range in the forested sector. For the same region, the times ranged from 63 to 351 msec in the cleared sector. Both initial and peak motion arrival times were earlier for the cleared sector (Figure 5.1). This is in agreement with surface airblast measurements made by BRL Project 1.01 (References 1 and 15).

The computed near-surface horizontal propagation velocity was higher in the cleared sector than in the forested sector, 1,610 versus 1,430 ft/sec. This was also noted in Project 1.01 surface airblast which propagated at a rate of approximately 2,080 ft/sec in the cleared sector, compared with 1,780 ft/sec in the forested sector. Outrunning ground motion was observed for both instrument lines, with surface emergence (i.e., the projected point on the ground surface where outrunning first occurs) closer for the cleared sector. This is shown graphically in Figure 5.2. The probable critical path is indicated by a dashed line. Significantly higher refraction is seen in the cleared sector, indicating a very high-velocity (probably saturated) layer occurring near the 15-foot depth with accompanying higher impedance in the upper layers. Seismic profiles were not taken for this event.

5.3 PARTICLE ACCELERATION

A prime objective was to measure the upthrust ground-shock component (caused by cratering action and refraction) and to attempt a determination of its effect on the tree blowdown mechanism. To accomplish this, two components of acceleration and one of velocity were measured along radial lines in both the forested and cleared sectors. Peak accelerations are listed in Table 5.1.

5.3.1 Vertical Acceleration. Peak downward accelerations are plotted against horizontal range in Figure 5.3 and range from about 11 g's at the 1.5-foot depth and 240-foot horizontal range to 3 g's at the 1.5-foot depth

and 700-foot horizontal range for the forested sector. At comparable ranges in the cleared sector, values were 5 g's at the 5.0-foot depth and 2.5 g's at the 1.5-foot depth. A trend of attenuation with increasing range is noted for the 1.5-foot-deep gages in both sectors. Little attenuation of the vertical component is observed at depths greater than 1.5 feet.

Peak upward acceleration is plotted against horizontal range in Figure 5.4. The 1.5-foot-depth data do not show any trend of attenuation with increasing range in the forested sector. All other locations show the expected attenuation.

Peak downward and upward accelerations were normalized to surface overpressure directly above the point of measurement. Surface overpressures were extrapolated where measurement locations did not coincide. Ratios in no case exceeded 0.8 g's/psi, with forested sector values generally exceeding those of the cleared areas (Table 5.4). Normalized data are plotted versus overpressure in Figure 5.5 and show little change for the downward near-surface (1.5-foot depth) motion. Data at the 5-foot depth and below appear to increase with decreasing overpressure; however, only two data points are available for this depth in each test area, limiting their statistical significance. The upward motion generally increases with decreasing overpressure at all depths for which a pattern could be established except 5 feet in the forested area.

Downward acceleration was ratioed against the upward component (Table 5.5) and plotted versus ground range in Figure 5.6. The ratio is seen to attenuate with range in both sectors at the shallow depth (1.5 feet), indicating an increase in direct (upward) ground-shock retransmission at larger distances due to energy refraction and surface airblast attenuation. The direct-transmitted energy at the 5-foot depth attenuated rapidly between the two locations monitored (240- and 320-foot horizontal ranges) in both sectors, resulting in an increase in the acceleration ratios. The ratio attenuated rapidly from near-surface downward to the 10-foot depth at the close-in stations.

Vertical waveforms are compared between both sectors in Figures 5.7

and 5.8. A secondary spike is seen at later times, first downward, then upward.

5.3.2 Horizontal Acceleration. Horizontal accelerations are plotted versus range in Figure 5.9. Peak outward values ranged from 5 to 0.6 g in the forest and from 1.5 to 0.5 g in the cleared sector for the ranges instrumented.

Waveform comparisons between the two sectors are shown in Figures 5.10 and 5.11. The waveforms exhibit rather typical shapes, a leading high-frequency outward-going spike followed by an apparent inward motion of about the same magnitude or greater than the initial motion. Frequencies of early motion components tend to be lower in the forested sector, with corresponding lower amplitude. In all cases, first motions were outward going (away from the charge). The deeper gages along the forested sector generally exhibited a more oscillatory character at early times than companion gages along the cleared sector.

Both peak vertical and horizontal accelerations in the forested sector exhibited a low value out of the normal data trend at the 320-foot range and 1.5-foot depth. This was not evidenced by the horizontal velocity measurement at the same point. (Compare in Figures 5.7, 5.10, and 5.15.)

5.4 PARTICLE VELOCITY

5.4.1 Vertical Velocity. No vertical velocity gages were used for this event. Consequently, data presented were obtained solely from integrated acceleration. Low signal-to-noise ratios and instrument drift created much difficulty in producing realistic late-time portions of the velocity envelope. First peaks are reasonably accurate, but reliability steadily degrades with increasing time.

Derived peak airblast-induced vertical velocities are listed in Table 5.2. The 1.5-foot data plotted as a function of range (Figure 5.12) attenuated with increasing range. No clear trend was indicated for greater depths. Forest sector amplitudes were higher near surface (1.5 feet), but lower at the 5-foot depth than those from the cleared sector.

Ratios of peak vertical velocity to surface overpressure above the point of measurement (Table 5.6) are plotted as a function of range in

Figure 5.13. Little attenuation is indicated for near-surface measurements, but considerable attenuation is seen at depth.

5.4.2 Horizontal Velocity. Horizontal velocities (Table 5.2) were directly measured and enjoy higher confidence than the vertical computation. Horizontal data were higher in the forested sector near surface and about equal at a depth of 5 feet as evidenced by the velocity-range plot of Figure 5.14.

Forest and cleared area near-surface horizontal velocity waveforms are compared in Figure 5.15. A pronounced outward-going spike predominates out to a range of 450 feet. Beyond this station, inward and outward motions become nearly equal. Waveforms from deeper locations are compared in Figure 5.16. Waveforms are quite similar except for 4-320-5-F-UH which appears to have lost part of the energy. Improper coupling of the instrument package to the soil or a soft area in front of and near the package could have contributed to this response.

In some cases, reasonable integrations were performed on acceleration-time histories. Selected comparisons are made for directly measured horizontal velocity and integrated acceleration in Figure 5.17. Excellent comparison is had at the 240-foot range station, cleared sector, at 10-foot depth as seen in the upper portion of Figure 5.17a. The measured and integrated histories are superposed for the first cycle and a half, with phase shift occurring past that point. Both yielded 0.39-ft/sec peak outward velocity caused by direct-coupled (crater-induced) energy. Coincidentally, these stations are exceptions in that the cratering energy was dominant. The velocity values listed in Table 5.2 and plotted in Figures 5.12 and 5.14 are related to the surface airblast loading. Figure 5.17b compares the same location for the forest sector. Amplitude disparities exist at all points for this comparison, the integrated values being about twice those of the direct measurement.

TABLE 5.1 ACCELERATION DATA, EVENT 4

Gage	Ground Range	Depth	Forested Sector					Cleared Sector					Prediction Value
			Arrival Time	Positive		Negative		Arrival Time	Positive		Negative		
				Peak Value	Peak Time	Peak Value	Peak Time		Peak Value	Peak Time	Peak Value	Peak Time	
	feet	feet	msec	g's	msec	g's	msec	msec	g's	msec	g's	msec	g's
Vertical (Positive Downward):													
4-240-1.5-__[a]AV	240	1.5	71.2	10.8	75.8	1.80	111.0	--	--	--	--	--	52.0
4-240-5-__AV		5.0	77.2	1.75	89.0	1.31	114.0	63.5	4.91	70.8	1.67	80.4	14.0
4-240-10-__AV		10.0	[b]	[b]	[b]	[b]	[b]	64.6	2.34	72.8	1.24	83.6	5.7
4-320-1.5-__AV	320	1.5	120.0	4.58	128.0	1.90	140.0	107.0	11.20	109.0	1.59	126.0	22.0
4-320-5-__AV		5.0	99.7	2.47	131.0	0.74	146.0	91.0	5.40	118.0	1.50	136.0	6.1
4-450-1.5-__AV	450	1.5	232.0	6.06	236.0	2.35	242.0	--	--	--	--	--	9.3
4-700-1.5-__AV	700	1.5	393.0	2.97	398.0	1.72	404.0	351.0	2.49	355.0	0.63	358.0	3.6
Horizontal (Positive Outward):													
4-240-1.5-__AH	240	1.5	71.7	4.85	74.8	--	--	--	--	--	--	--	34.0
4-240-5-__AH		5.0	71.4	0.56	86.0	--	--	61.4	1.49	67.7	--	--	9.4
4-240-10-__AH		10.0	69.5	1.40	80.0	--	--	62.6	1.41	69.5	--	--	3.7
4-320-1.5-__AH	320	1.5	122.0	0.62	132.0	--	--	107.0	0.79[c]	110.0	--	--	20.0
4-320-5-__AH		5.0	103.0	0.73[d]	--	--	--	110.0	0.95	119.0	--	--	5.5
4-450-1.5-__AH	450	1.5	232.0	1.22	236.0	--	--	--	--	--	--	--	12.0
4-700-1.5-__AH	700	1.5	284.0	0.63	395.0	--	--	351.0	0.54	352.0	--	--	7.4

[a] F for forested; C for cleared
[b] No record.
[c] Questionable record.
[d] Second positive peak.

TABLE 5.2 VELOCITY DATA, EVENT 4

Peak values for UH are for airblast-induced motion.

Gage	Ground Range	Depth	Forested Sector					Cleared Sector					Prediction Value
			Arrival Time	Positive		Negative		Arrival Time	Positive		Negative		
				Peak Value	Peak Time	Peak Value	Peak Time		Peak Value	Peak Time	Peak Value	Peak Time	
	feet	feet	msec	ft/sec	msec	ft/sec	msec	msec	ft/sec	msec	ft/sec	msec	ft/sec
Vertical (Positive Downward):													
f4-240-1.5-__[a]AV	240	1.5	--	1.38	--	--	--	--	--	--	--	--	--
f4-240-5-__AV		5.0	--	0.70	--	--	--	--	0.78	--	--	--	--
f4-240-10-__AV		10.0	[b]	[b]	[b]	[b]	[b]	--	0.50	--	--	--	--
f4-320-1.5-__AV	320	1.5	--	1.07	--	--	--	--	0.97	--	--	--	--
f4-320-5-__AV		5.0	--	0.69	--	--	--	--	0.85	--	--	--	--
f4-450-1.5-__AV	450	1.5	--	0.68	--	--	--	--	--	--	--	--	--
f4-700-1.5-__AV	700	1.5	--	0.41	--	--	--	--	0.28	--	--	--	--
Horizontal (Positive Outward):													
4-240-1.5-__UH	240	1.5	72.2	2.83	78.9	0.50	340.0	--	--	--	--	--	1.4
4-240-5-__UH		5.0	76.8	1.12	94.0	0.28	--	66.6	1.26	73.5	0.29	--	0.88
4-240-10-__UH		10.0	70.8	0.16	82.0	0.32	--	64.8	0.26	70.0	0.37	--	0.66
4-320-1.5-__UH	320	1.5	114.0	1.09	131.0	0.24	--	109.0	0.41	125.0	0.25	--	0.80
4-320-5-__UH		5.0	123.0	0.23	136.0	0.07	--	103.0	0.26	129.0	0.11	--	0.53
4-450-1.5-__UH	450	1.5	234.0	0.38	240.0	0.20	--	--	--	--	0.16	--	0.49
4-700-1.5-__UH	700	1.5	396.0	0.27	442.0	0.39	--	352.0	0.14[c]	361.0	--	--	0.30

[a] F for forested; C for cleared.
[b] No record.
[c] Questionable record.

TABLE 5.3 DISPLACEMENT DATA, EVENT 4

Gage	Ground Range	Depth	Peak Displacement			
			Forested Sector		Cleared Sector	
			Positive	Negative	Positive	Negative
	feet	feet	feet	feet	feet	feet
Vertical (Positive Downward):						
∫∫4-240-1.5-__[a]AV	240	1.5	0.036	--	--	--
∫∫4-240-5.0-__AV		5.0	0.014	--	0.012	--
∫∫4-240-10-__AV		10.0	[b]	--	0.008	--
∫∫4-320-1.5-__AV	320	1.5	0.050[c]	--	0.050[c]	--
∫∫4-320-5.0-__AV		5.0	0.050	--	0.040	--
∫∫4-450-1.5-__AV	450	1.5	0.007	--	--	--
∫∫4-700-1.5-__AV	700	1.5	0.004	--	[d]	--
Horizontal (Positive Outward):						
∫4-240-1.5-__UH	240	1.5	0.023	[d]	--	--
∫4-240-5.0-__UH		5.0	0.012	[d]	0.012	0.013
∫4-240-10-__UH		10.0	0.017[e]	0.062	0.032	0.014
∫4-320-1.5-__UH	320	1.5	0.010	0.034	0.028	[d]
∫4-320-5.0-__UH		5.0	0.031	0.070	0.017	[d]
∫4-450-1.5-__UH	450	1.5	0.008	0.005	0.002	0.004
∫4-700-1.5-__UH	700	1.5	0.059	0.032	--	--

[a] F for forested; C for cleared.
[b] No record.
[c] Approximate.
[d] Indeterminate.
[e] Second peak.

TABLE 5.4 AIRBLAST-INDUCED VERTICAL ACCELERATION RATIOS, EVENT 4

Overpressure		Depth	Maximum Acceleration/Overpressure			
			Downward		Upward	
Forested Sector	Cleared Sector		Forested Sector	Cleared Sector	Forested Sector	Cleared Sector
psi	psi	feet	g's/psi	g's/psi	g's/psi	g's/psi
24.0	40.0	1.5	0.450	[a]	0.075	[a]
		5.0	0.073	0.123	0.055	0.042
		10.0	[b]	0.058	[b]	0.031
14.0	20.0	1.5	0.328	0.560	0.136	0.080
		5.0	0.177	0.270	0.053	0.075
9.5	11.0	1.5	0.640	[a]	0.248	[a]
4.8	5.0	1.5	0.620	0.497	0.359	0.126

[a] Not instrumented.
[b] No record.

TABLE 5.5 RATIO OF MAXIMUM DOWNWARD TO UPWARD ACCELERATION, EVENT 4

Ground Range	Depth	Acceleration Ratio AV Down/AV Up	
		Forested Sector	Cleared Sector
feet	feet		
240	1.5	8.0	[a]
	5.0	1.3	2.9
	10.0	[b]	1.9
320	1.5	2.4	7.0
	5.0	3.3	3.6
450	1.5	2.6	[a]
700	1.5	1.7	3.9

[a] Not instrumented.
[b] No record.

TABLE 5.6 AIRBLAST-INDUCED VERTICAL VELOCITY RATIOS, EVENT 4

Overpressure		Depth	Maximum Velocity/Overpressure	
Forested Sector	Cleared Sector		Forested Sector	Cleared Sector
psi	psi	feet	ft/sec/psi	ft/sec/psi
24.0	40.0	1.5	0.058	[a]
		5.0	0.029	0.020
		10.0	[b]	0.013
14.0	20.0	1.5	0.079	0.059
		5.0	0.051	0.043
9.5	11.0	1.5	0.097	[a]
4.8	5.0	1.5	0.086	0.056

[a] Not instrumented.
[b] No record.

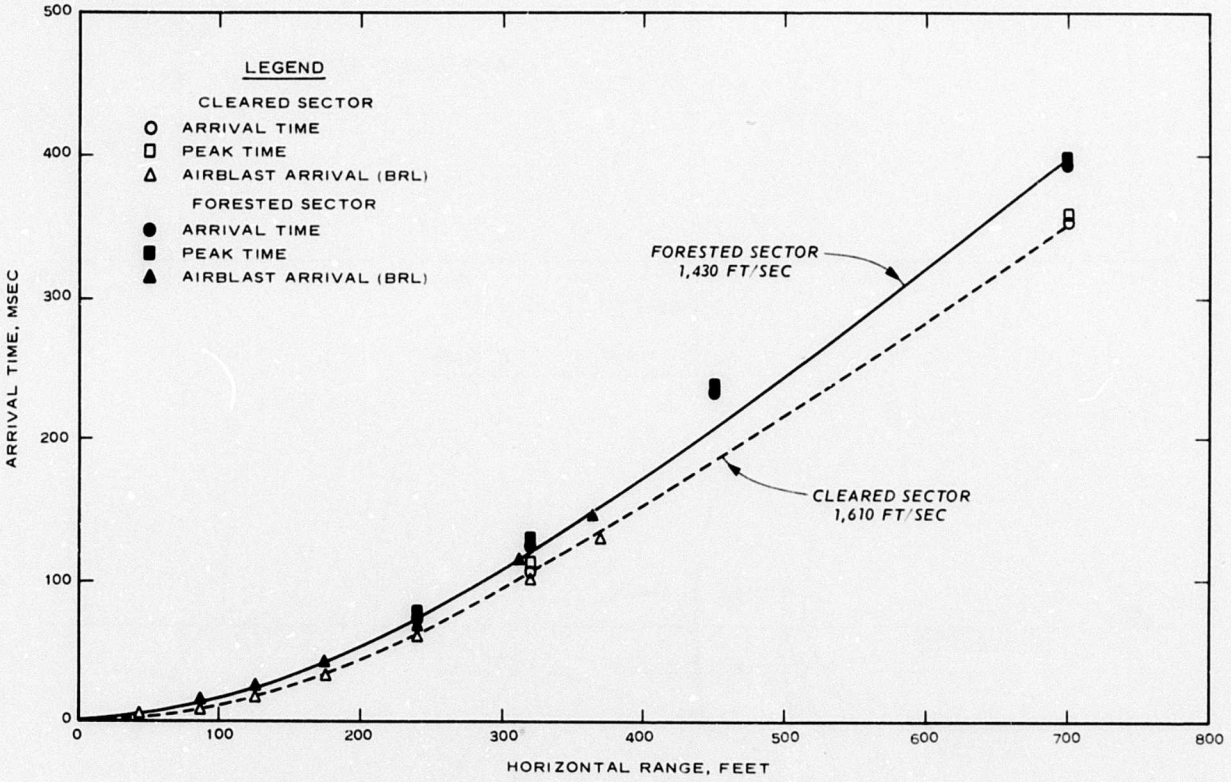

Figure 5.1 Ground-shock arrival time versus horizontal range, 1.5-foot depth, Event 4.

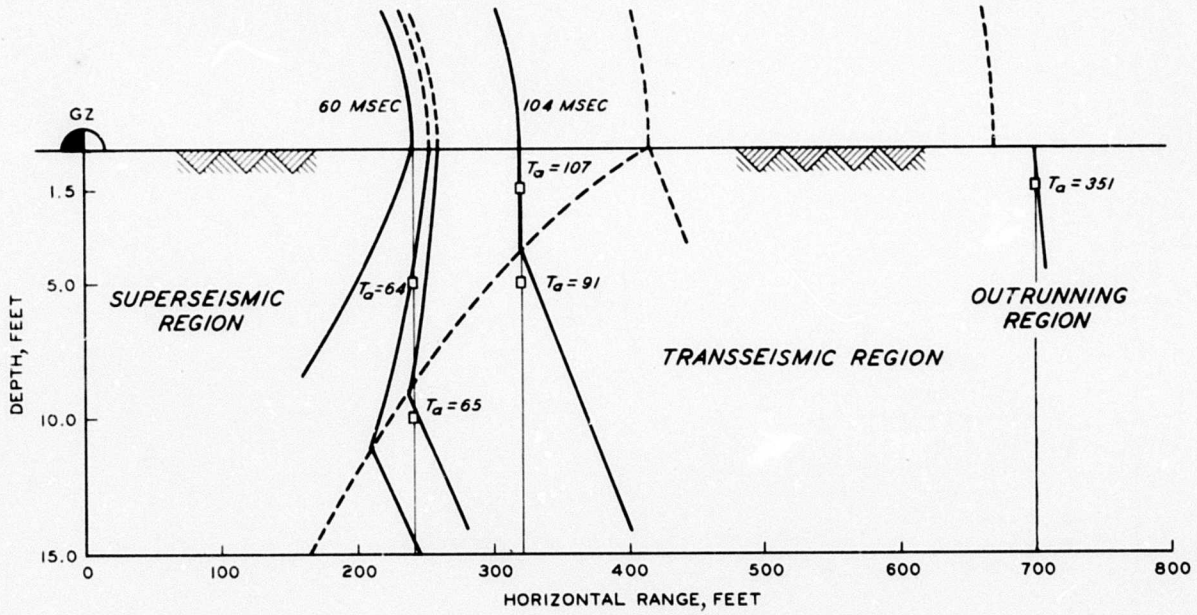

a. CLEARED SECTOR

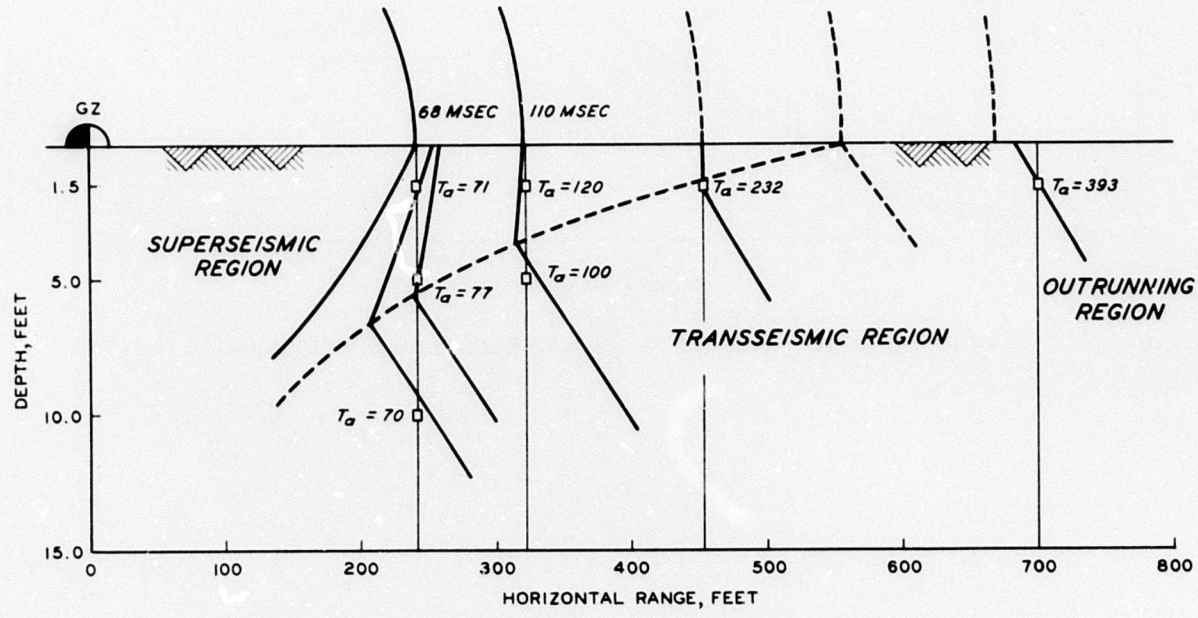

b. FORESTED SECTOR

Figure 5.2 Ground-shock profiles, Event 4.

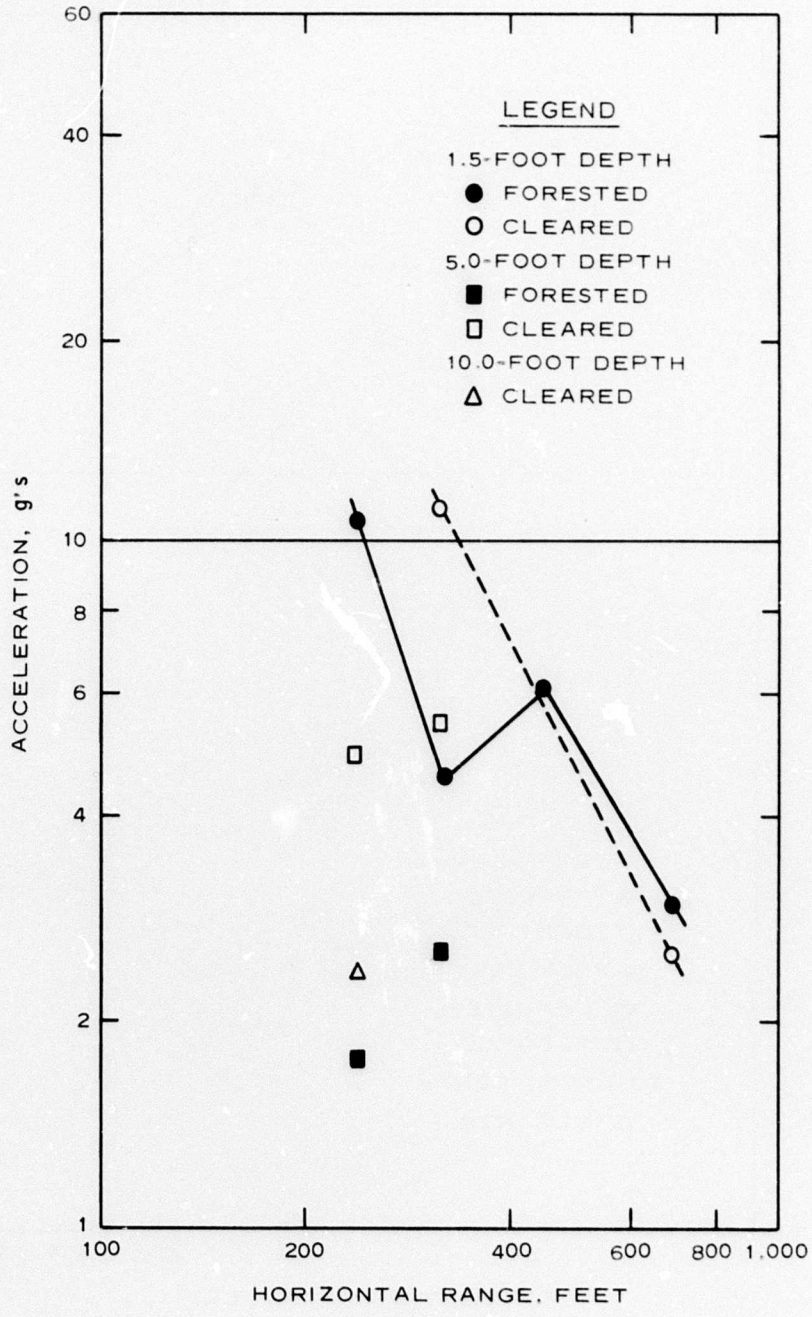

Figure 5.3 Peak airblast-induced downward acceleration versus horizontal range, Event 4.

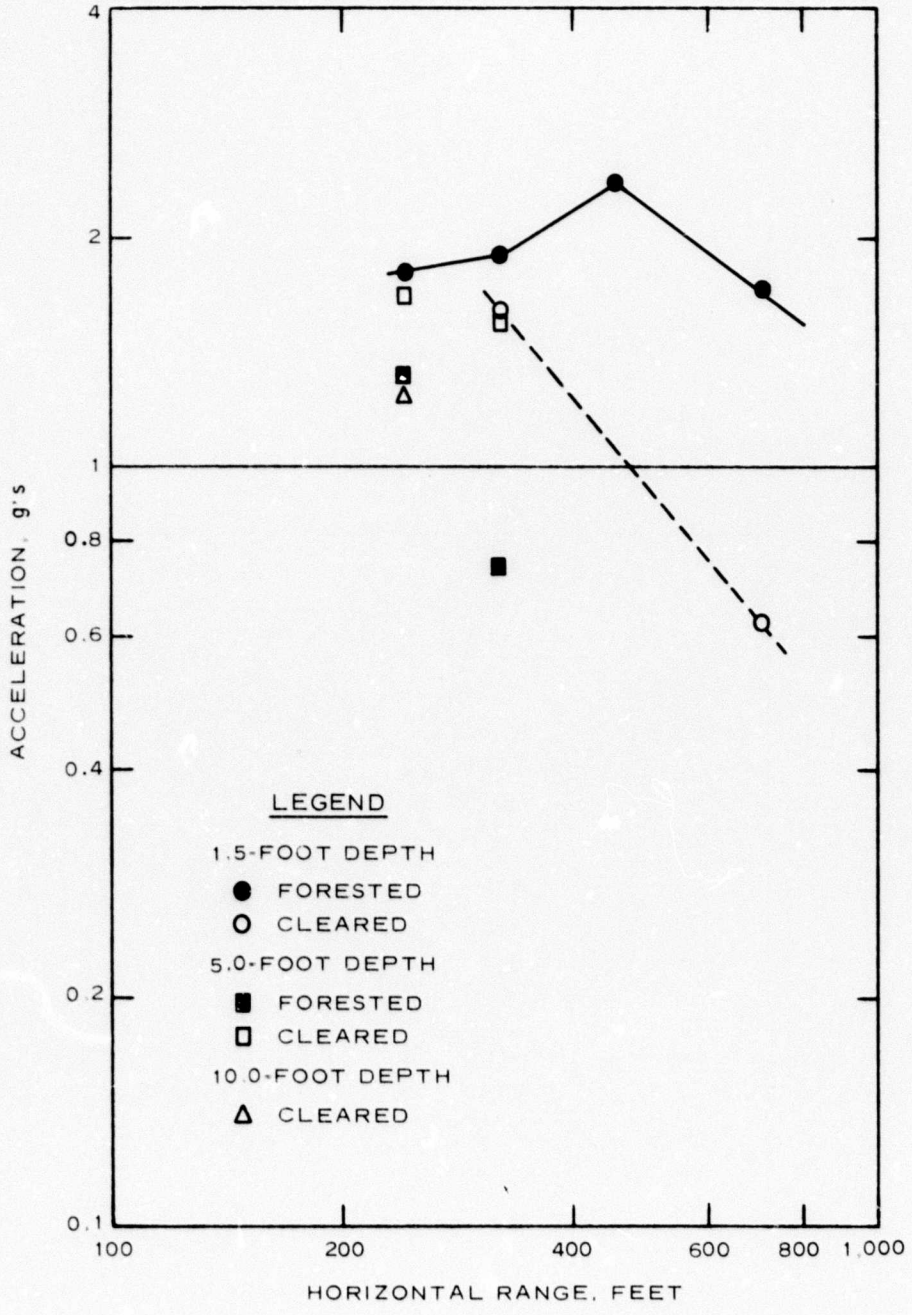

Figure 5.4 Peak crater-induced upward acceleration versus horizontal range, Event 4.

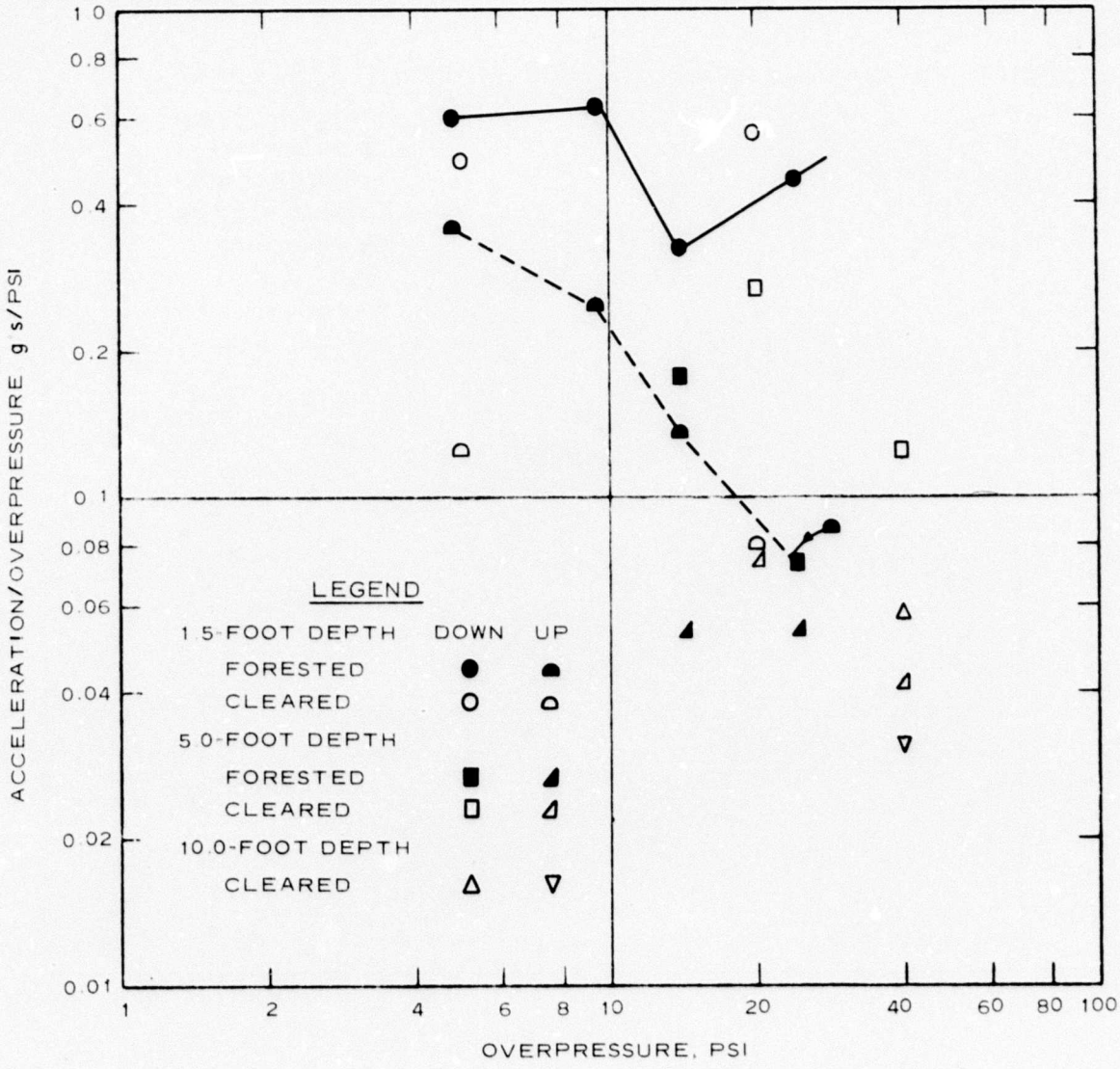

Figure 5.5 Ratio of maximum vertical acceleration to surface overpressure, Event 4.

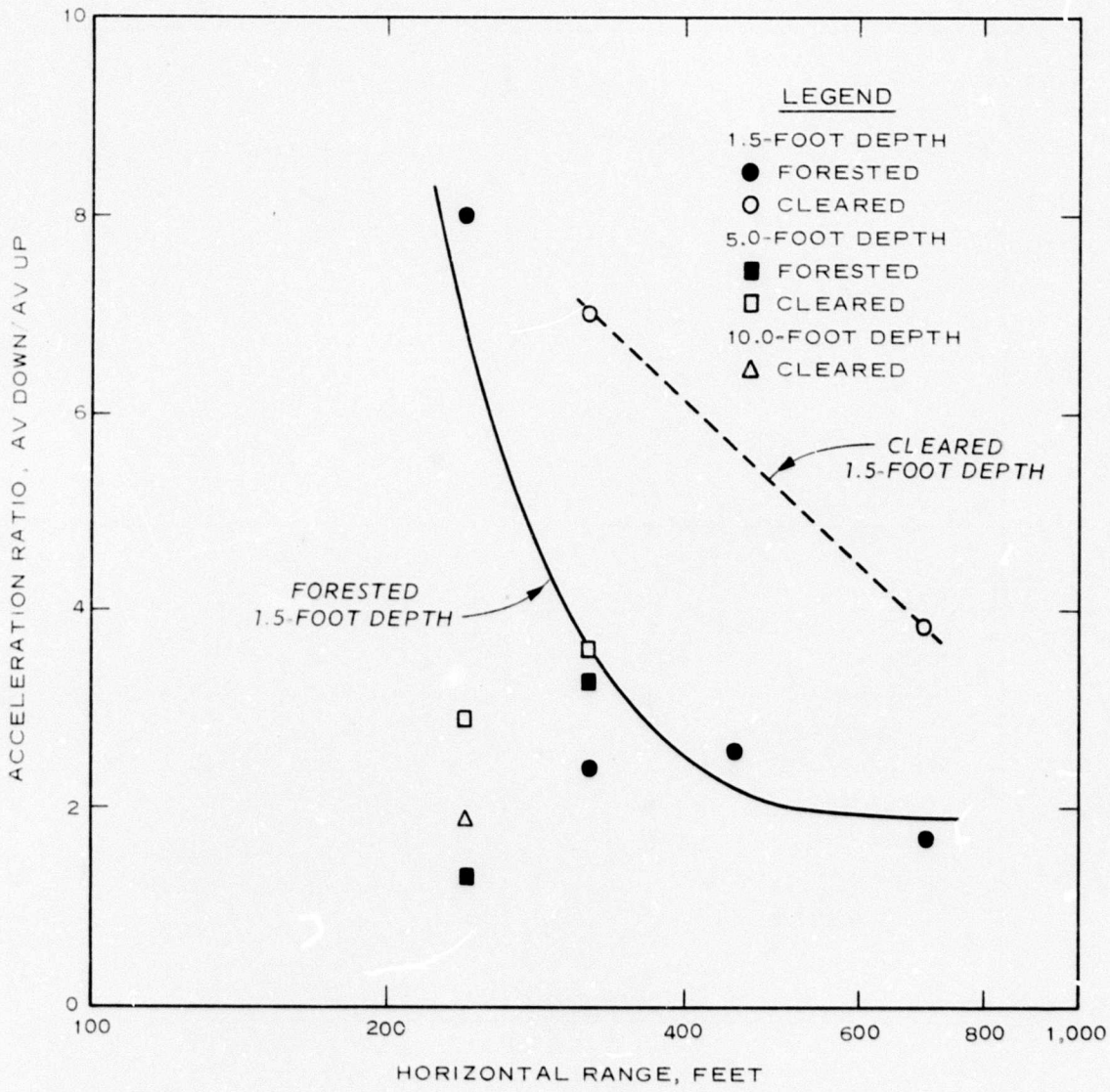

Figure 5.6 Vertical acceleration ratio as a function of ground range, Event 4.

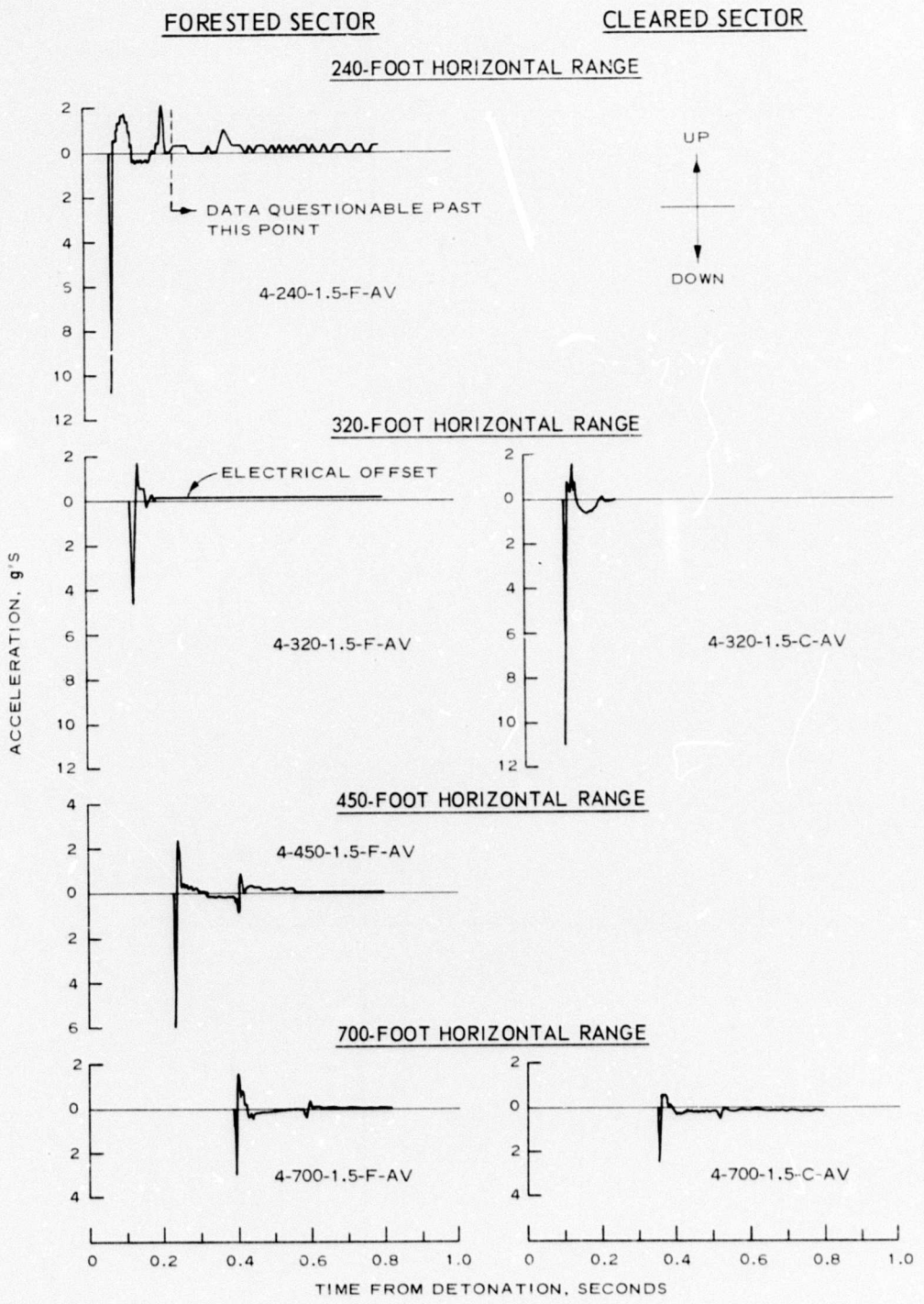

Figure 5.7 Vertical acceleration waveform comparisons, forested and cleared sectors, 1.5-foot depth, Event 4.

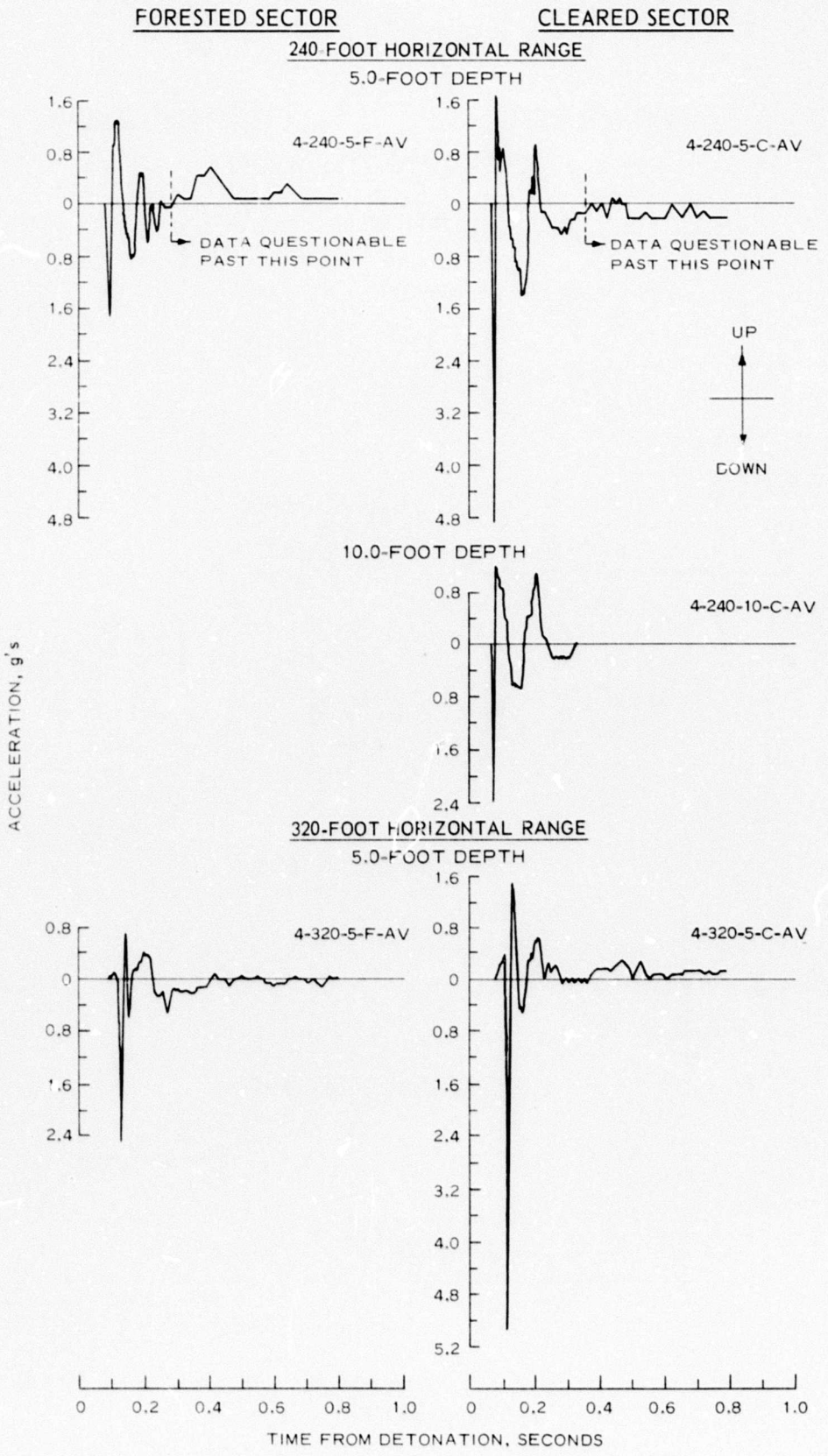

Figure 5.8 Vertical acceleration waveform comparisons, forested and cleared sectors, 5.0- and 10.0-foot depths, Event 4.

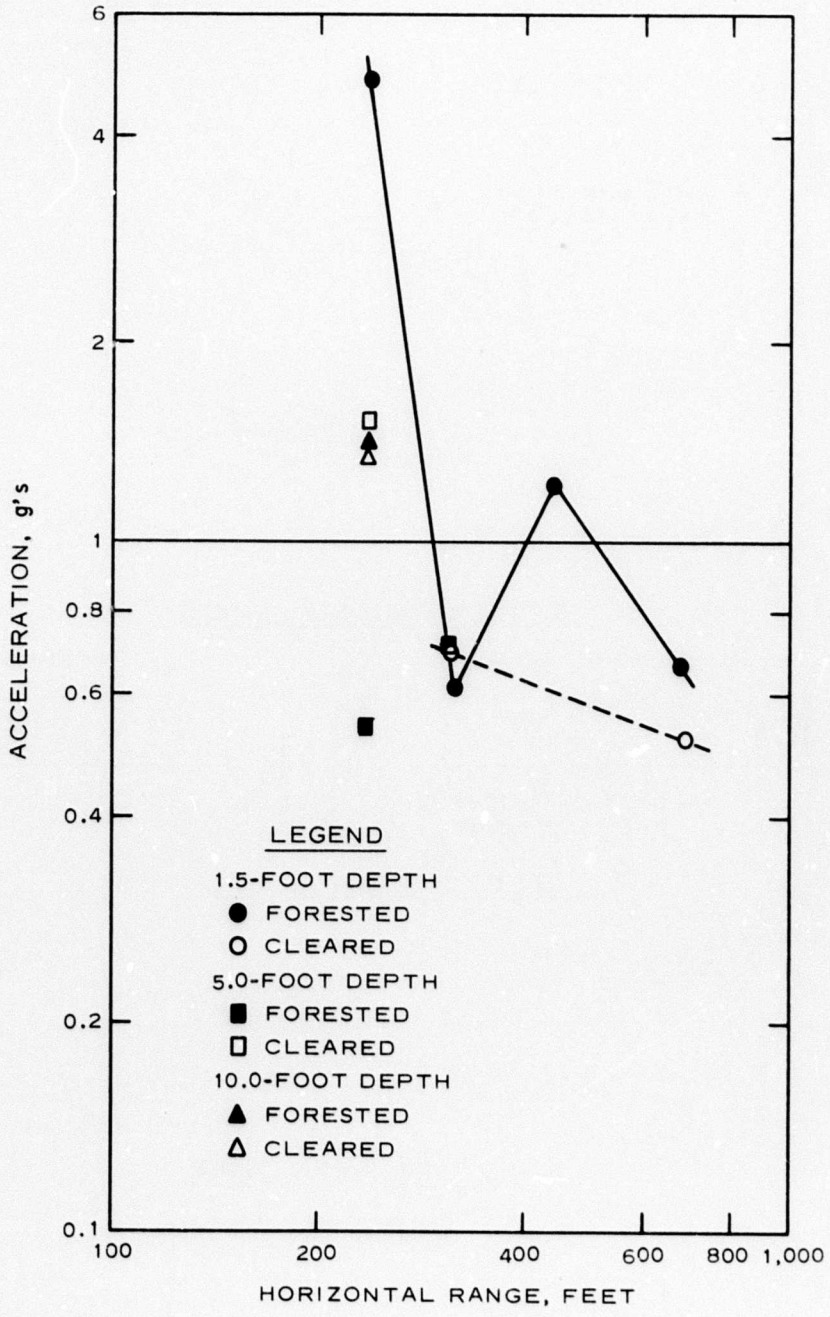

Figure 5.9 Peak airblast-induced outward acceleration versus horizontal range, Event 4.

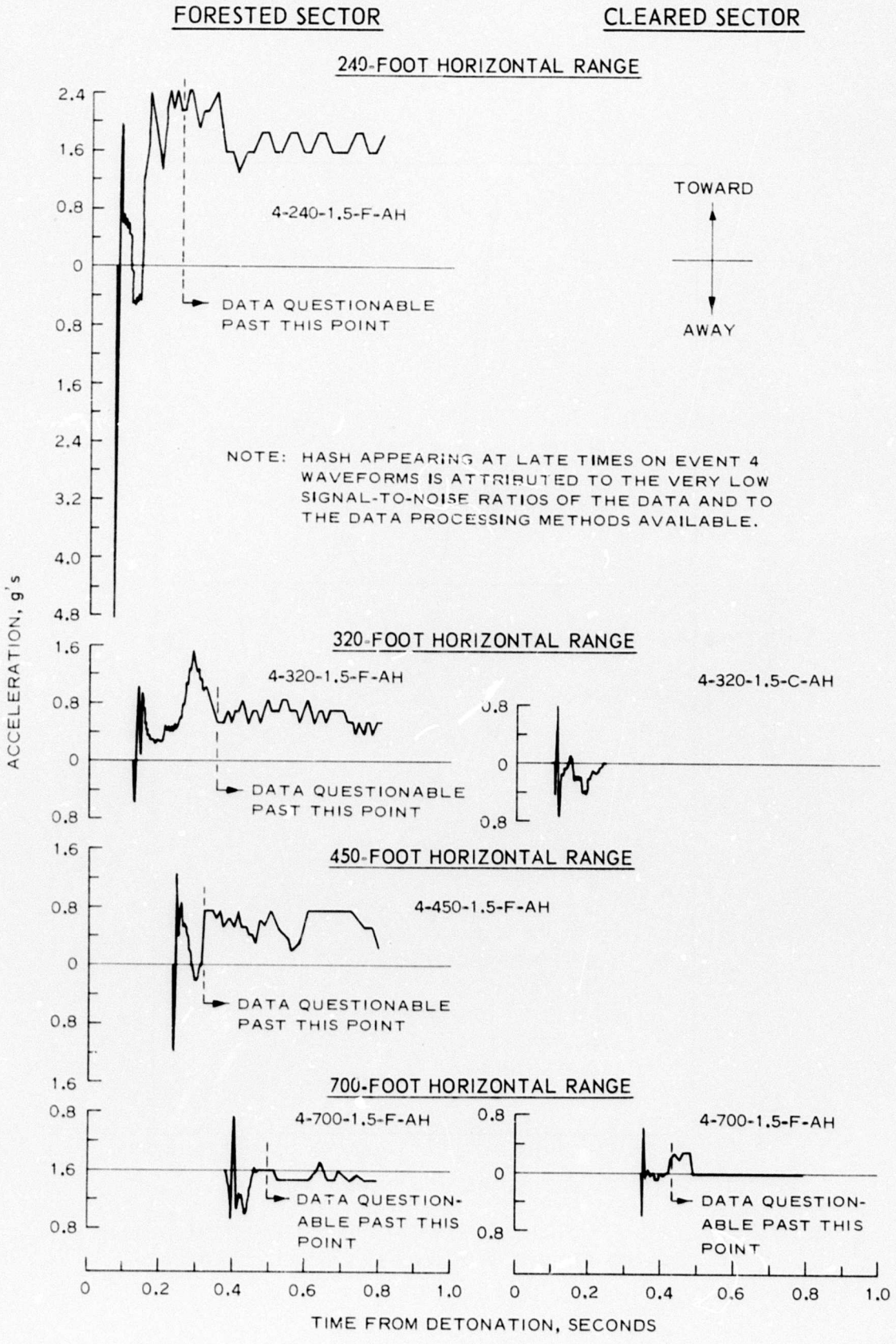

Figure 5.10 Horizontal acceleration waveform comparisons, forested and cleared sectors, 1.5-foot depth, Event 4.

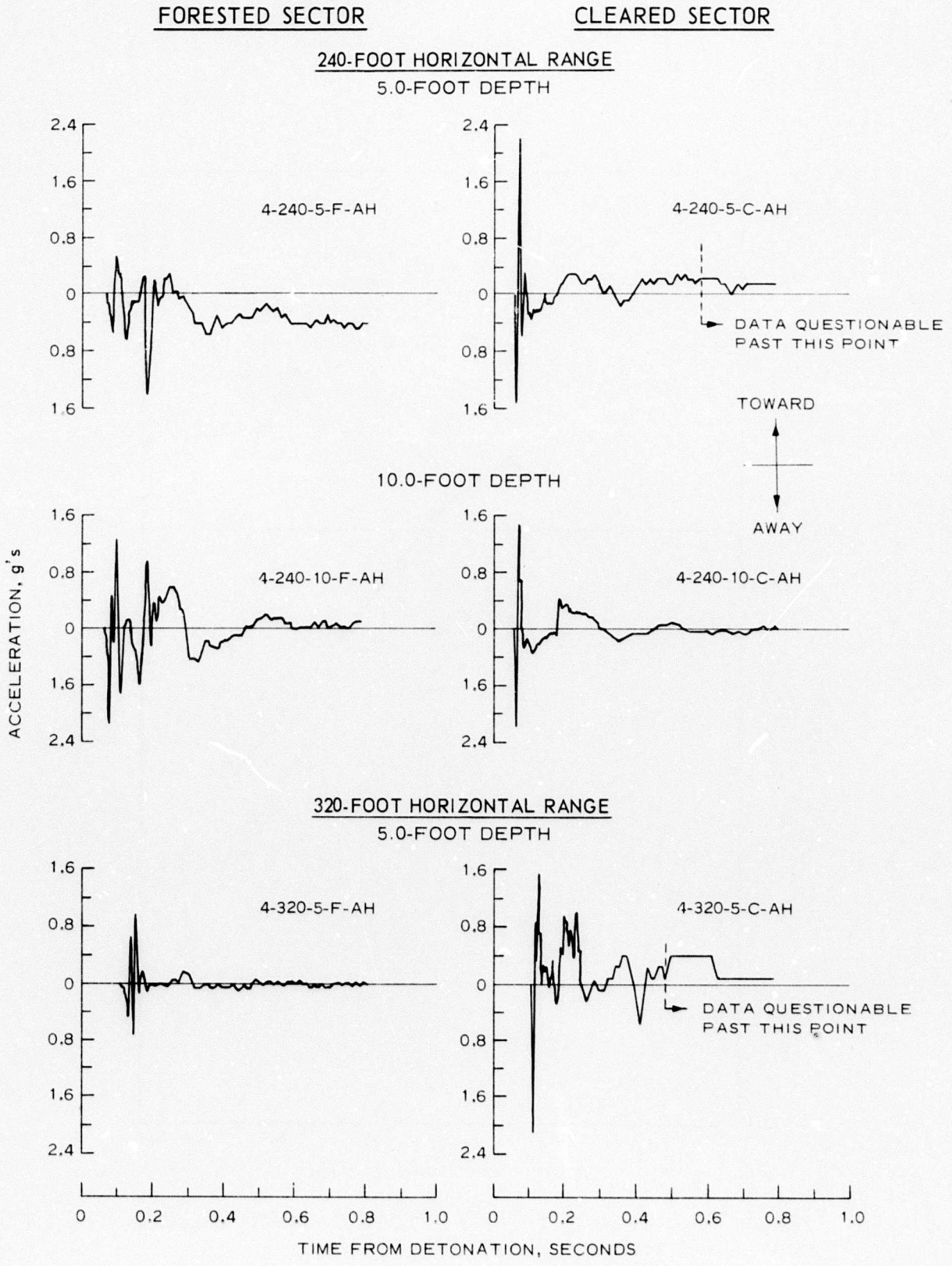

Figure 5.11 Horizontal acceleration waveform comparisons, forested and cleared sectors, 5.0- and 10.0-foot depths, Event 4.

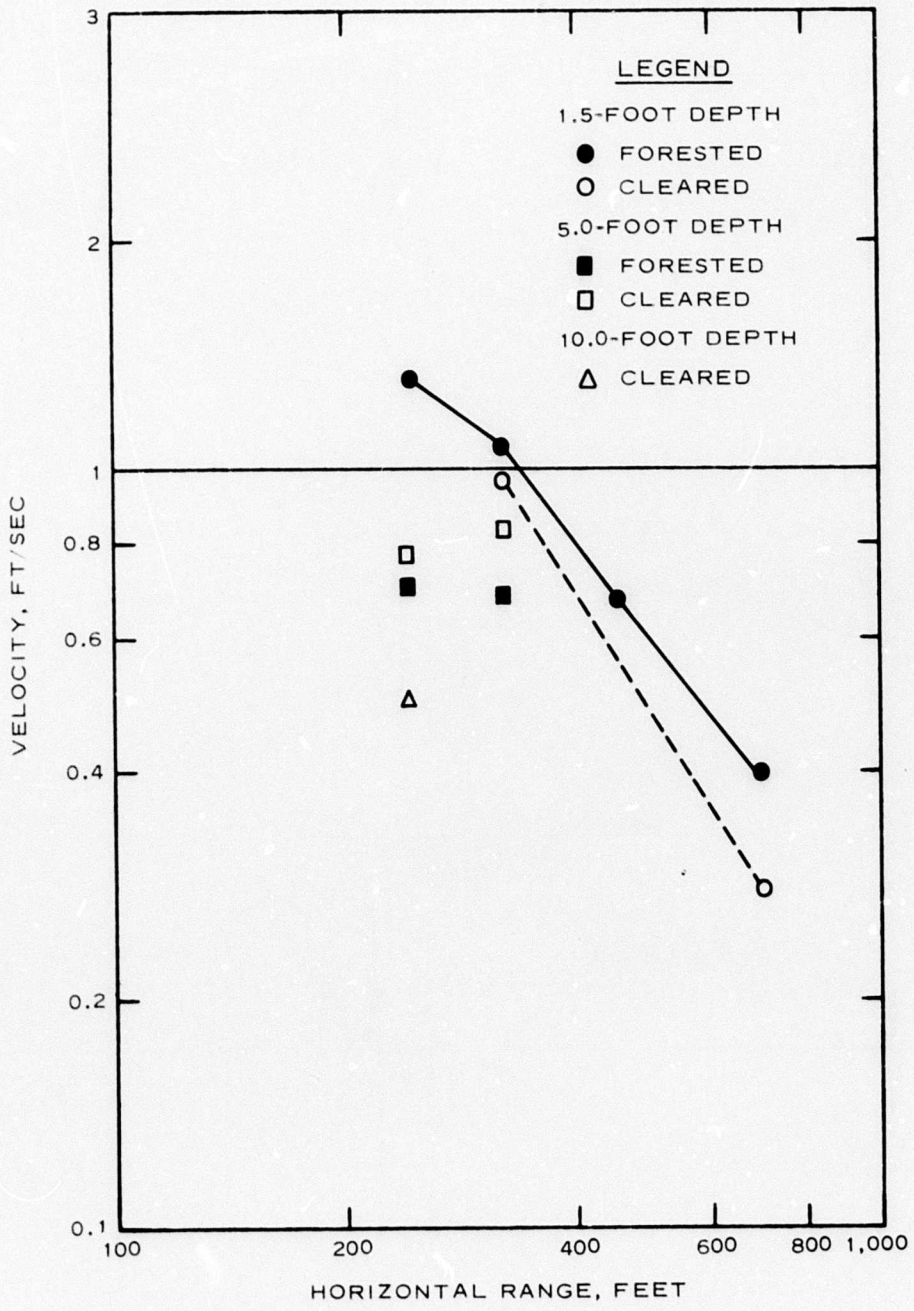

Figure 5.12 Peak airblast-induced downward velocity versus horizontal range, Event 4.

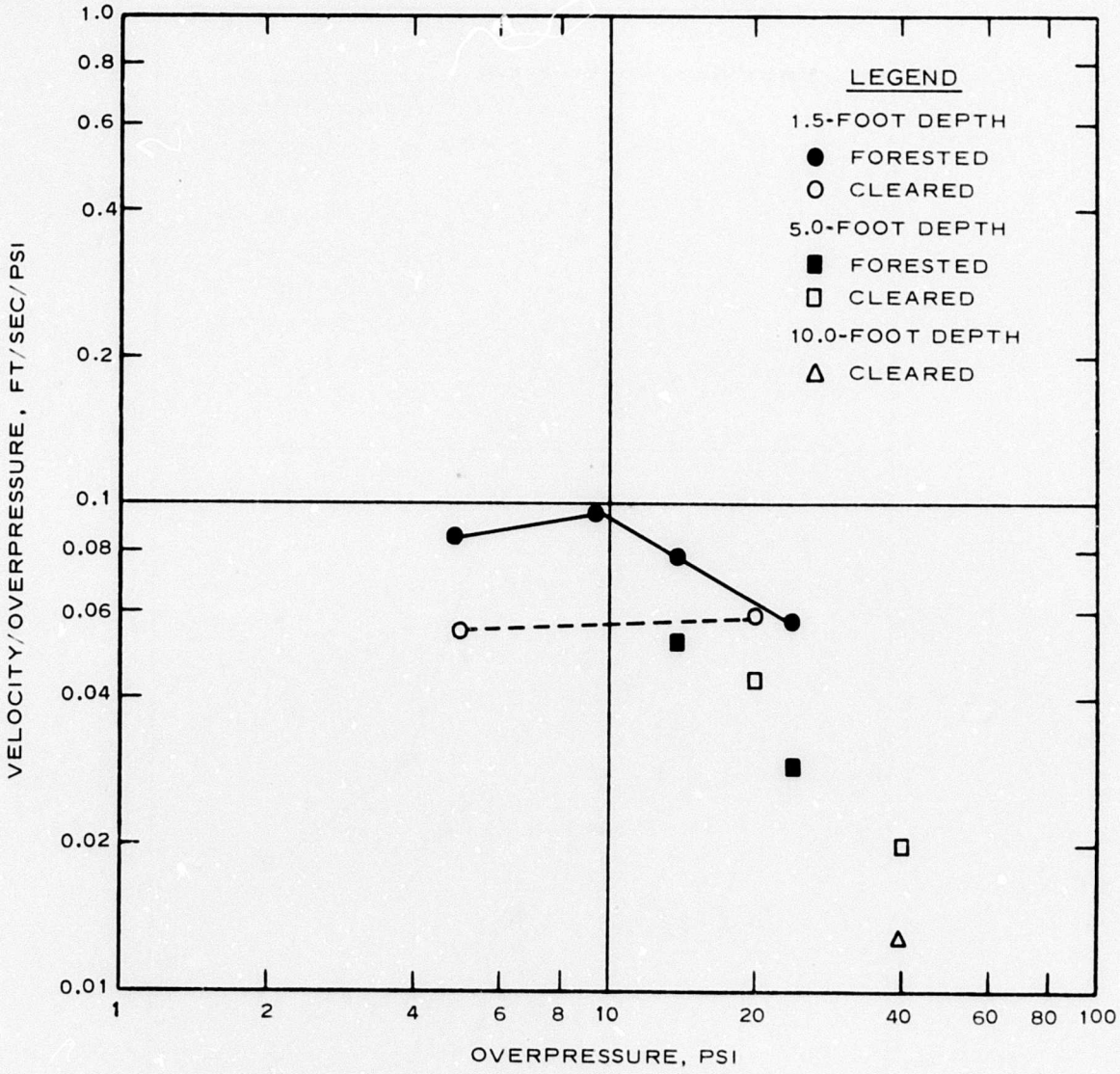

Figure 5.13 Ratio of maximum airblast-induced downward velocity to overpressure, Event 4.

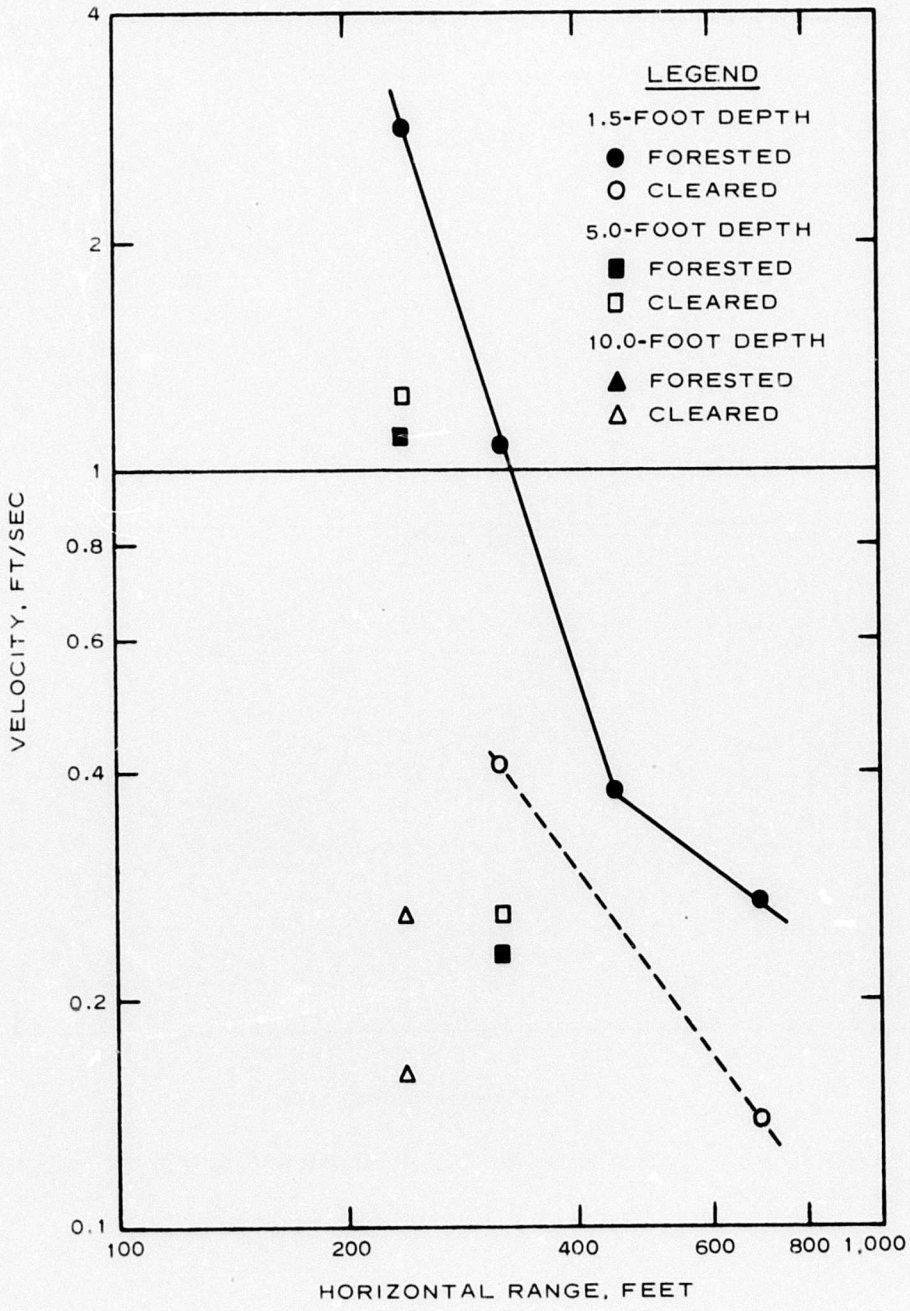

Figure 5.14 Peak airblast-induced outward velocity versus horizontal range, Event 4.

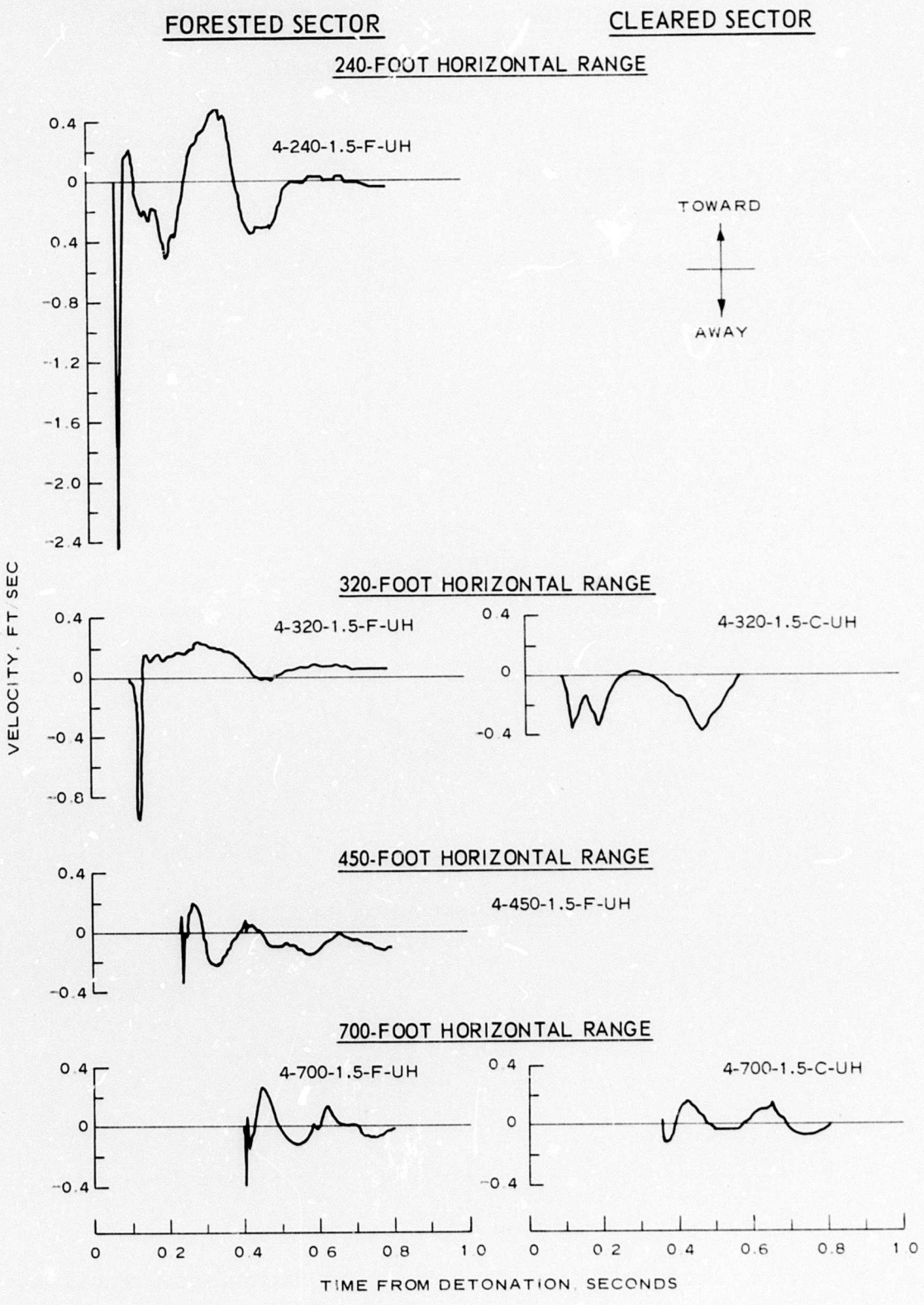

Figure 5.15 Horizontal velocity waveform comparisons, forested and cleared sectors, 1.5-foot depth, Event 4.

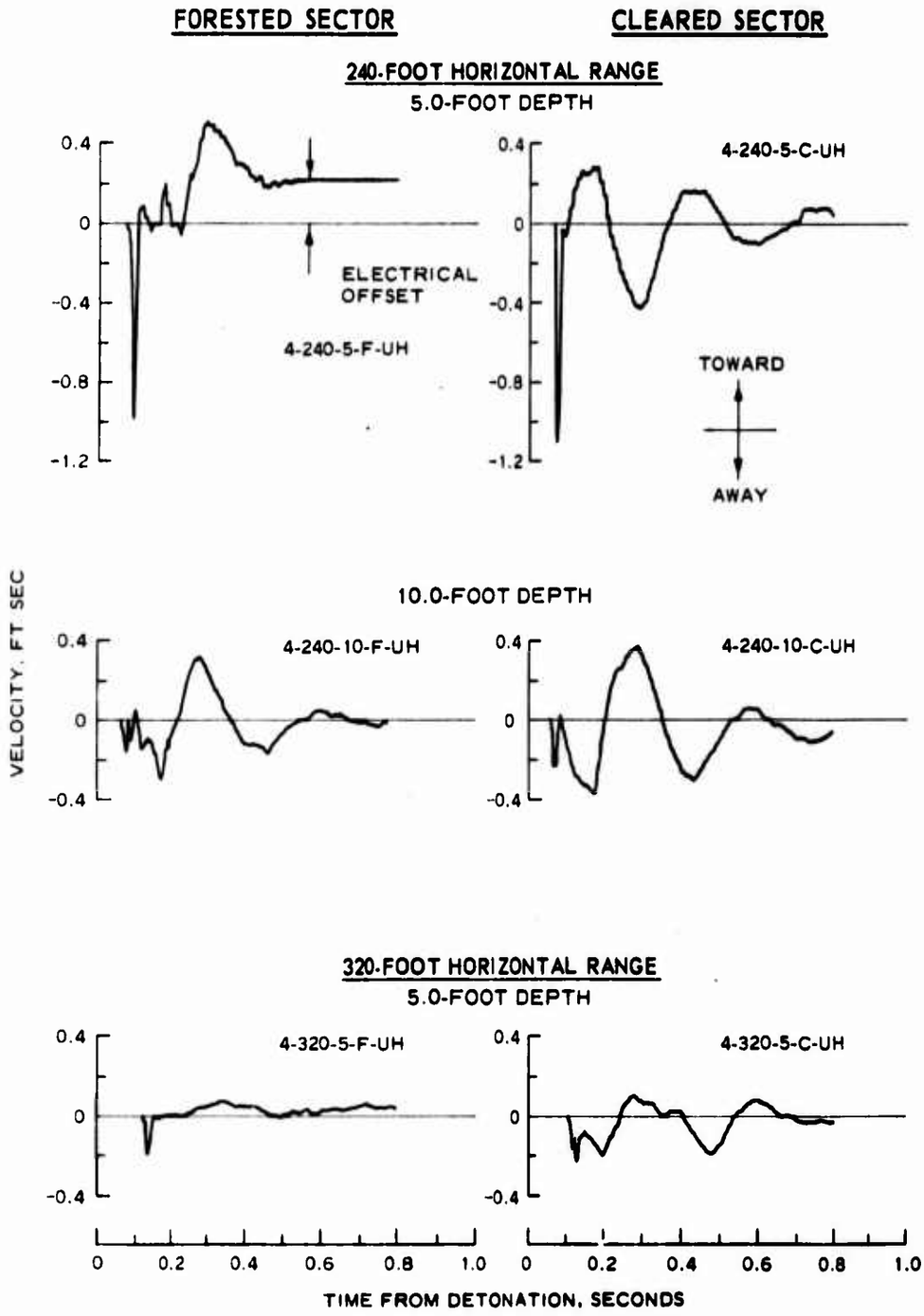

Figure 5.16 Horizontal velocity waveform comparisons, forested and cleared sectors, 5.0- and 10.0-foot depths, Event 4.

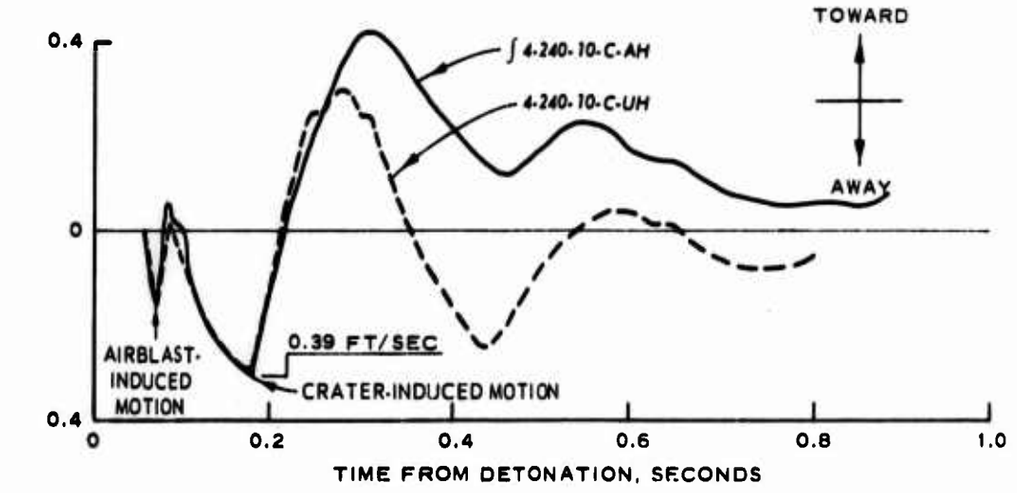

a. CLEARED SECTOR

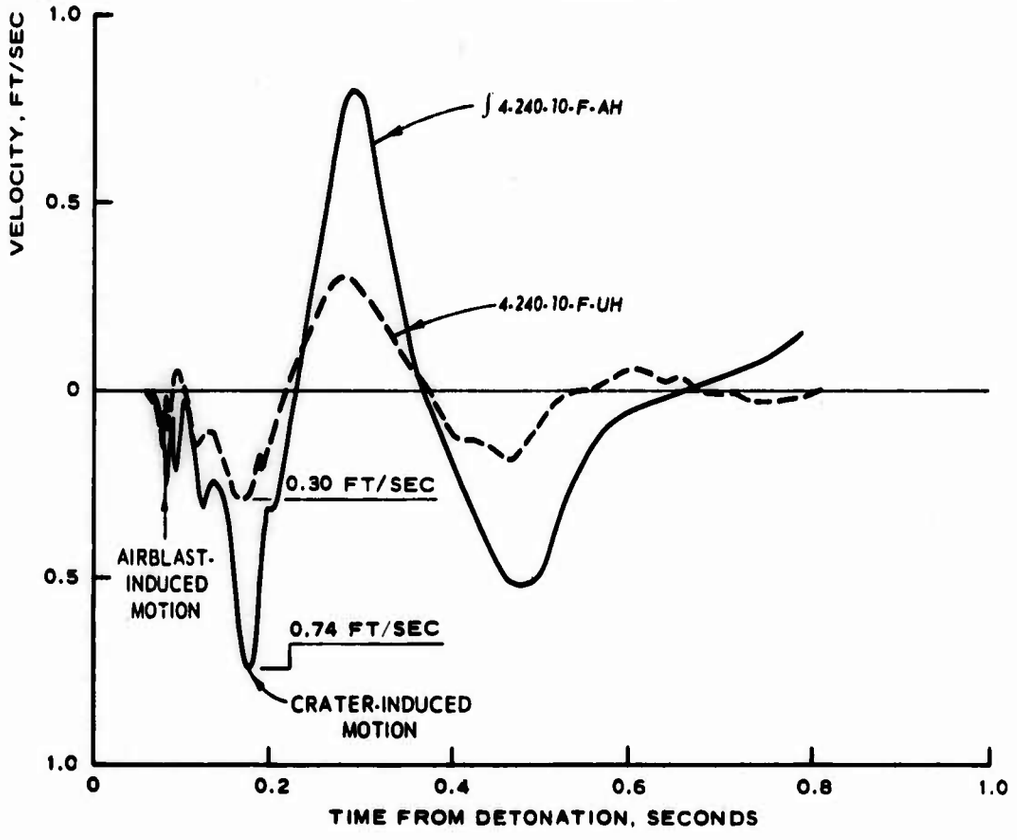

b. FORESTED SECTOR

Figure 5.17 Measured horizontal velocity waveforms compared to integrated acceleration, 10-foot depth, cleared and forested sectors, Event 4.

CHAPTER 6

CONCLUSIONS

Project 3.02a failed to record any data from Event 1. Failure to either receive or properly translate sequence start signals from DRES timing and control resulted in no equipment turn on. The equipment was set for automatic mode and the bunker was not manned. On all subsequent tests except Event 4, the instrument bunkers were fully manned.

Ground motions at the Drowning Ford Test Site were similar for Events 3 and 5, although Event 5 exhibited higher frequency signals and somewhat higher output in the horizontal plane near the ground surface. This was an influence of the thin frozen surface layer which allowed greater coupling and transmission of the high-frequency components. High-frequency perturbations are normally attenuated quite rapidly by dry alluvial soils.

Distant Plain Events 3 and 5 correlated well with the Flat Top Series on all motion parameters in both amplitude and waveform. Observed disparities and scatter are largely attributed to slight differences in test site soils, explosive coupling, and instrument canister placement. Airblast induction predominated in vertical and horizontal acceleration over the ranges instrumented, while crater induction predominated in horizontal displacement out to a range of 150 feet for Event 3 and to 190 feet for Event 5. Vertical velocity was influenced about equally by both loading modes.

The detonable gas bag experiment (Event 2A) produced no crater. Airblast-induced ground motions for this event were greater than for Events 3 and 5 or Flat Top. This was a result of significant explosive energy going directly into airblast formation rather than partitioning to the ground through crater formation coupled with a much larger initial volume and effective area loaded.

Stress measurements attempted in this test series yielded only limited success. Amplitude attenuation with depth appeared to be excessively rapid, but is supported by recent findings as discussed in Reference 15. Stresses were higher for Event 3 than for Event 5, but both were significantly lower than the surface airblast. Event 2A stresses, however, were

very nearly the magnitude of the airblast above the point of measurement. Stress measurements below 1.5 feet were generally of marginal signal level, which limited resolution.

Ground shock was not found to be a significant factor influencing the tree blowdown mechanism on Event 4. Primary motions in the blowdown region were down and away from the point of detonation at early times, then upward due to elastic rebound and, later, due to cratering action and refracted energy from depth. Measured upthrust motions were small in the regions instrumented and are felt to have provided only minimal enhancement to the translation effects imposed on the trees by airblast drag forces.

BLANK PAGE

APPENDIX A

DATA WAVEFORMS, EVENTS 2A, 3, AND 5

The data presented in this appendix are uncorrected for baseline shift and are representative of the original data recorded.

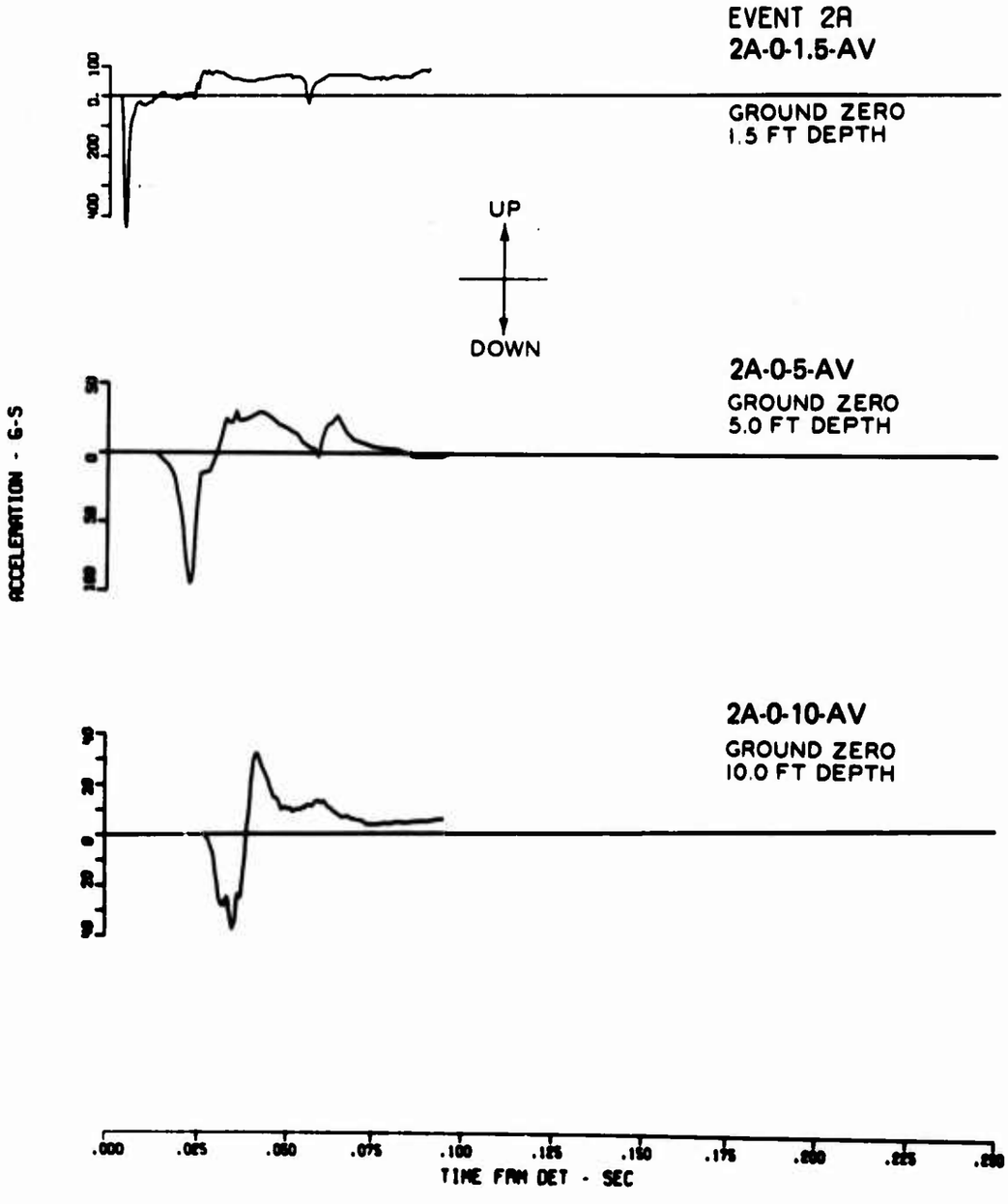

Figure A.1 Vertical acceleration, Event 2A (Sheet 1 of 6).

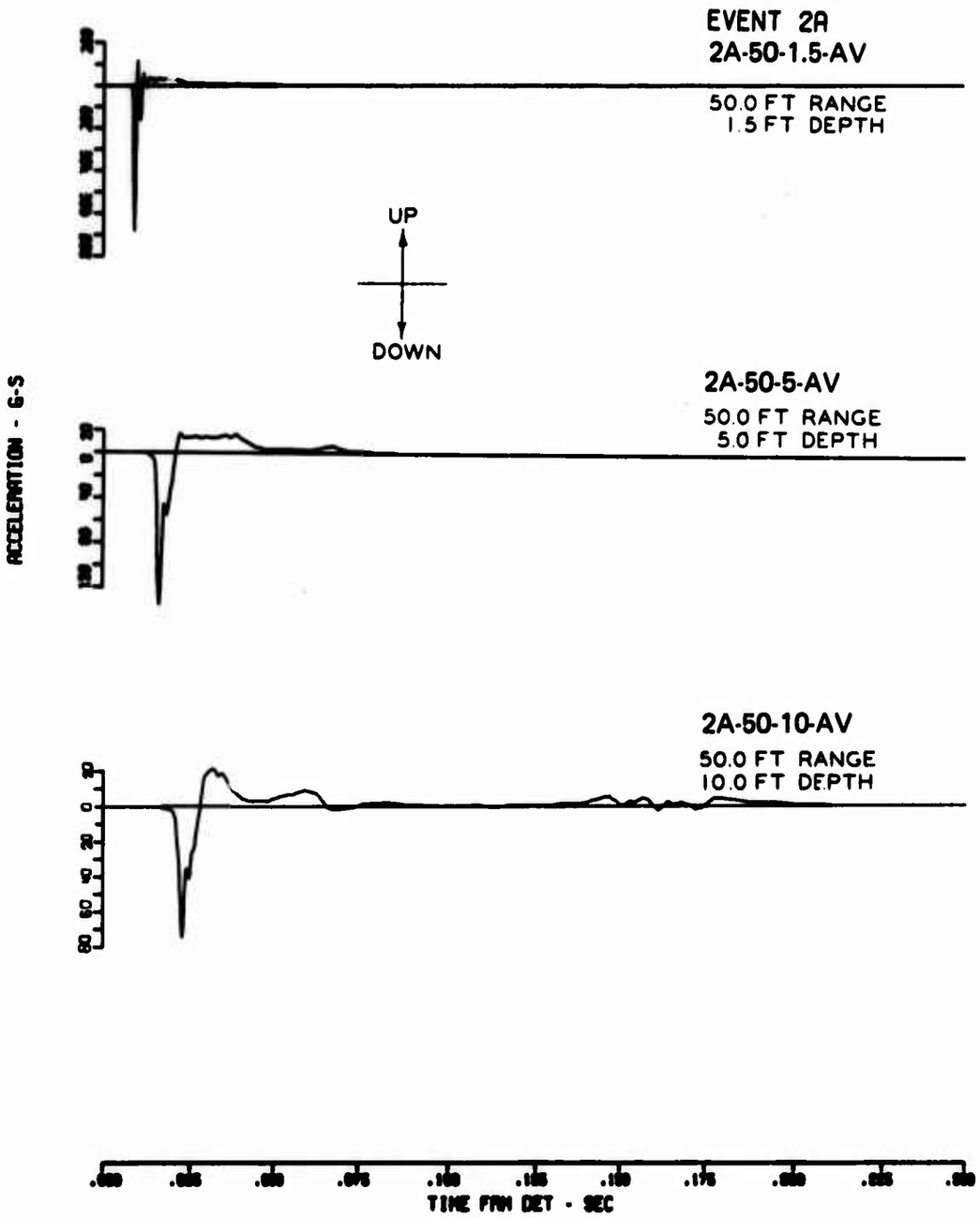

Figure A.1 (Sheet 2 of 6).

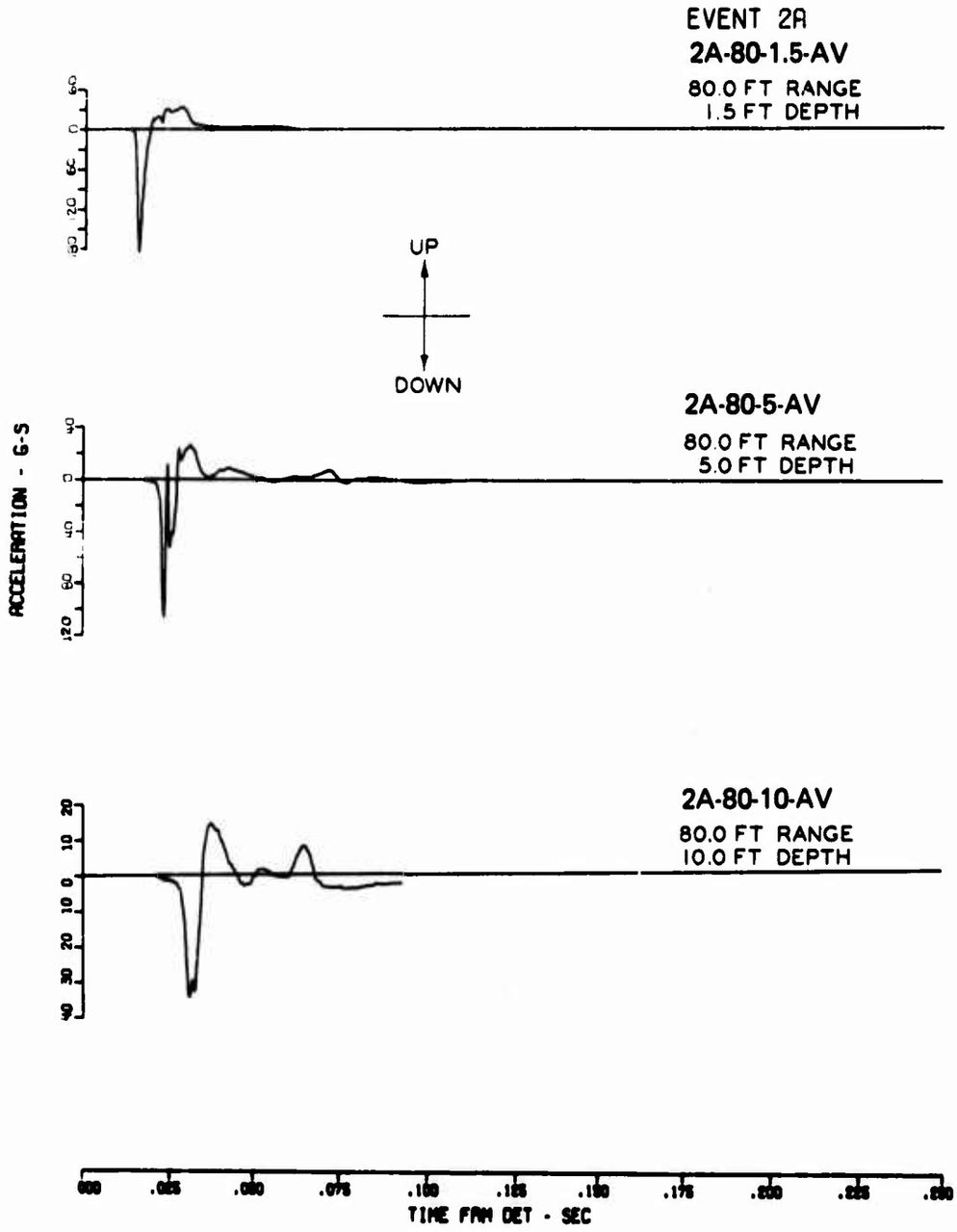

Figure A.1 (Sheet 3 of 6).

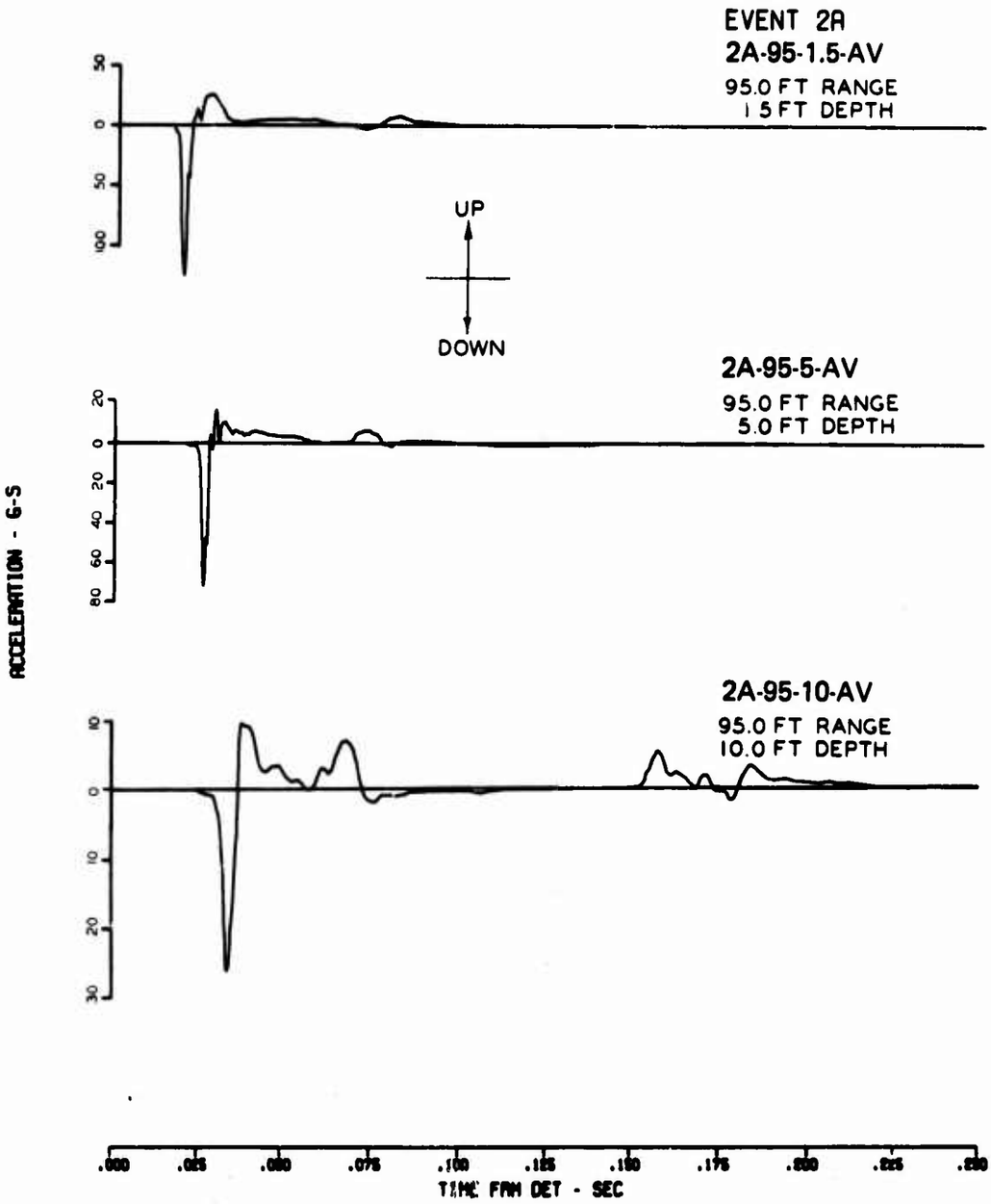

Figure A.1 (Sheet 4 of 6).

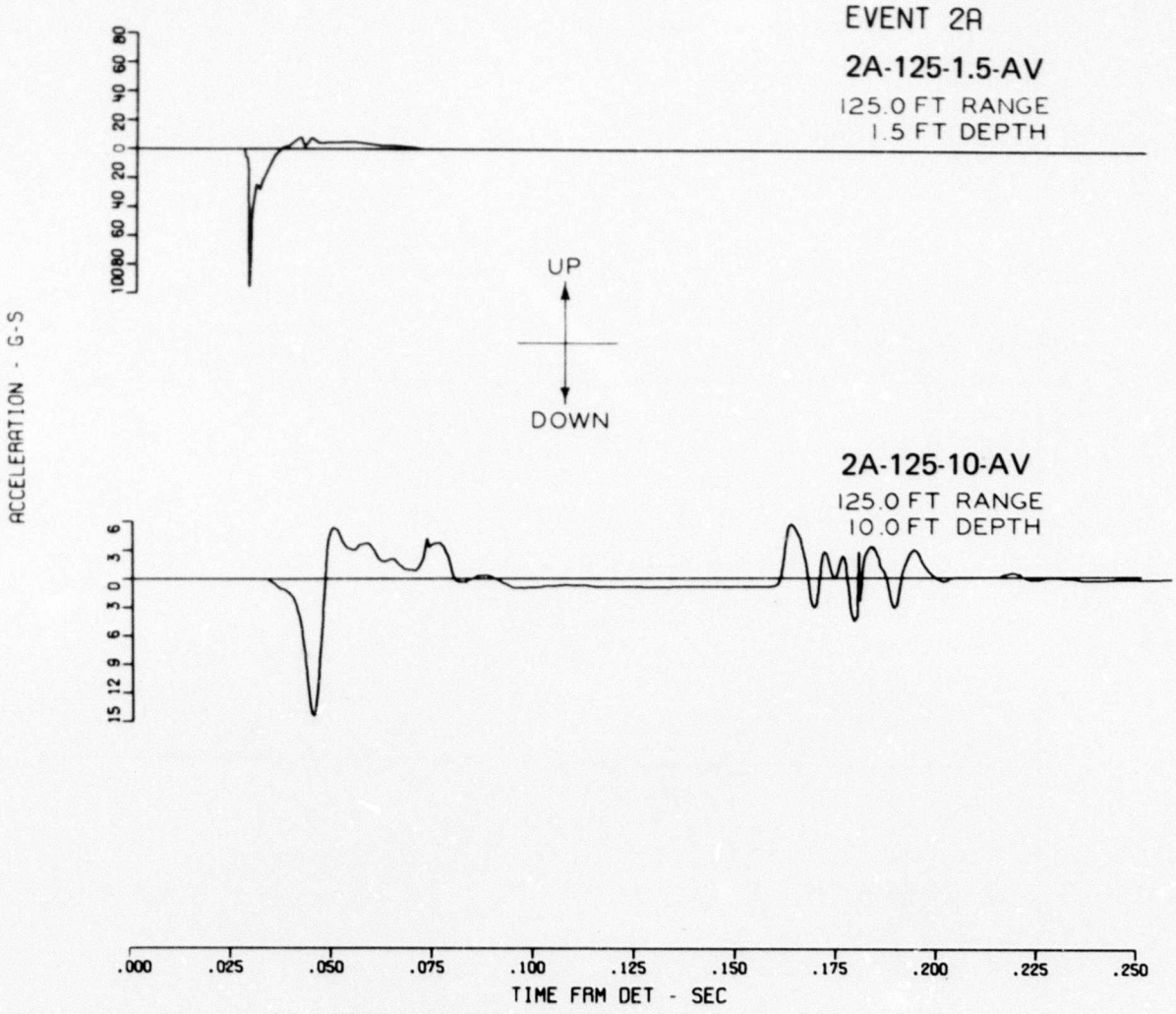

Figure A.1 (Sheet 5 of 6).

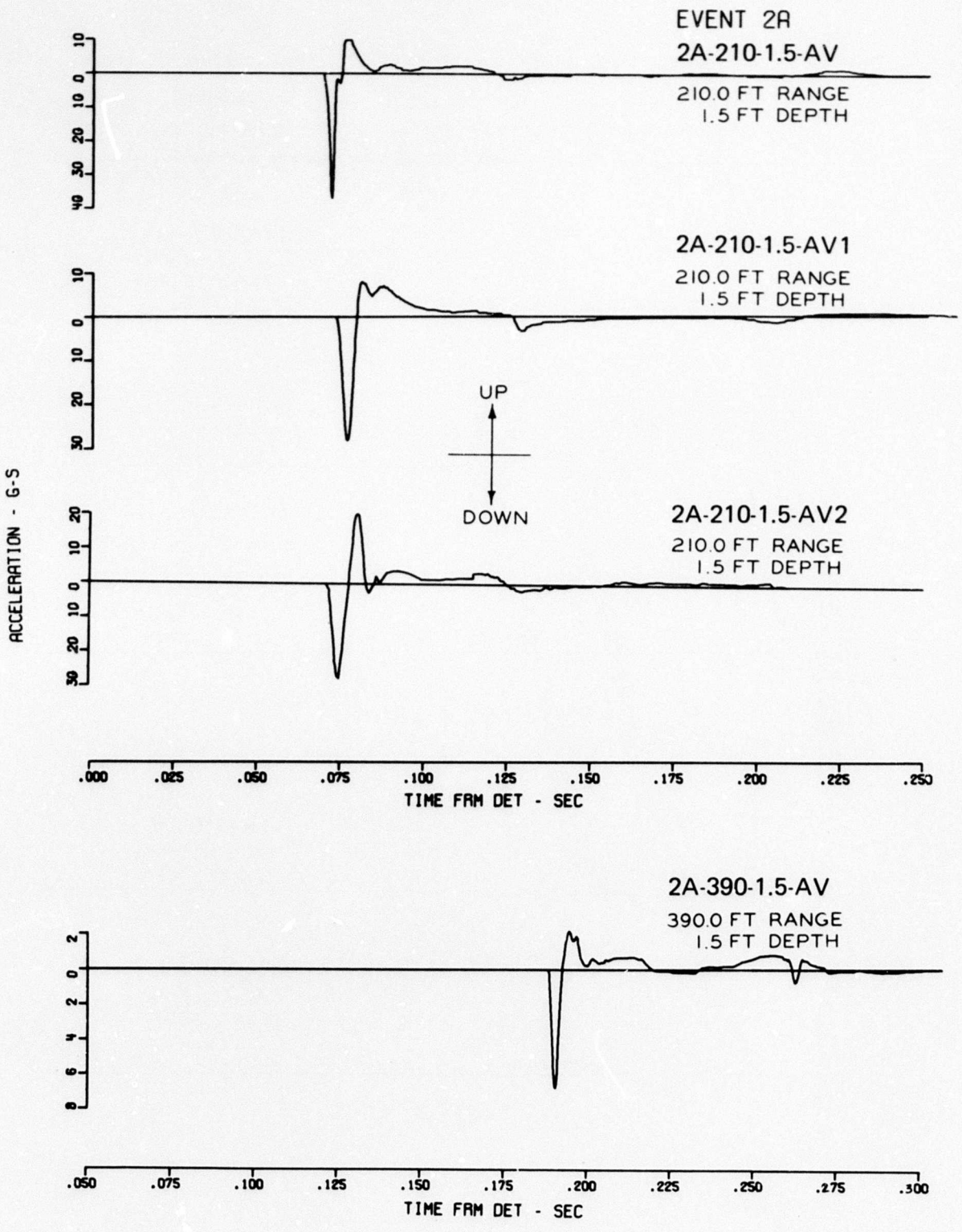

Figure A.1 (Sheet 6 of 6).

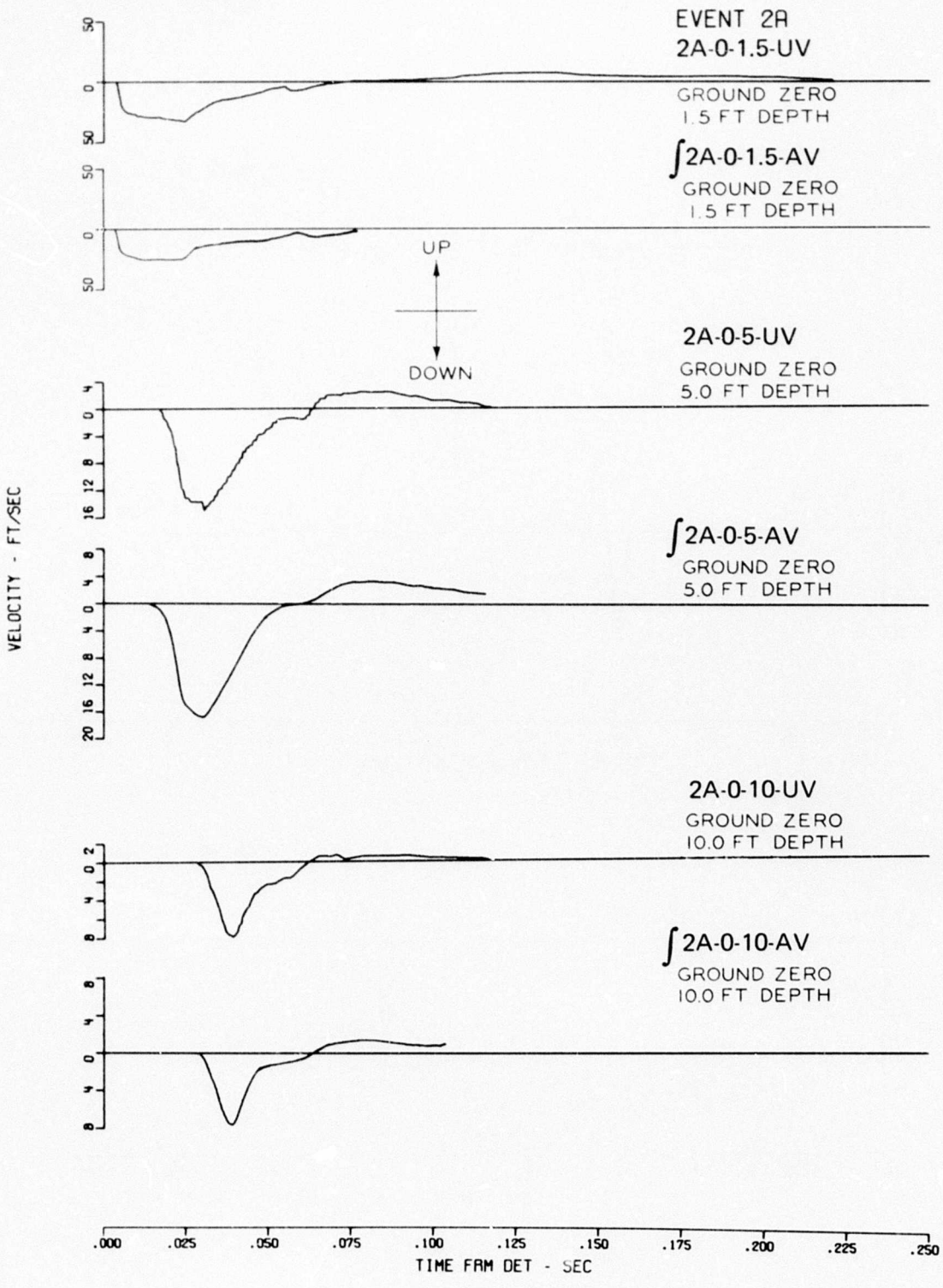

Figure A.2 Vertical velocity, Event 2A (Sheet 1 of 4).

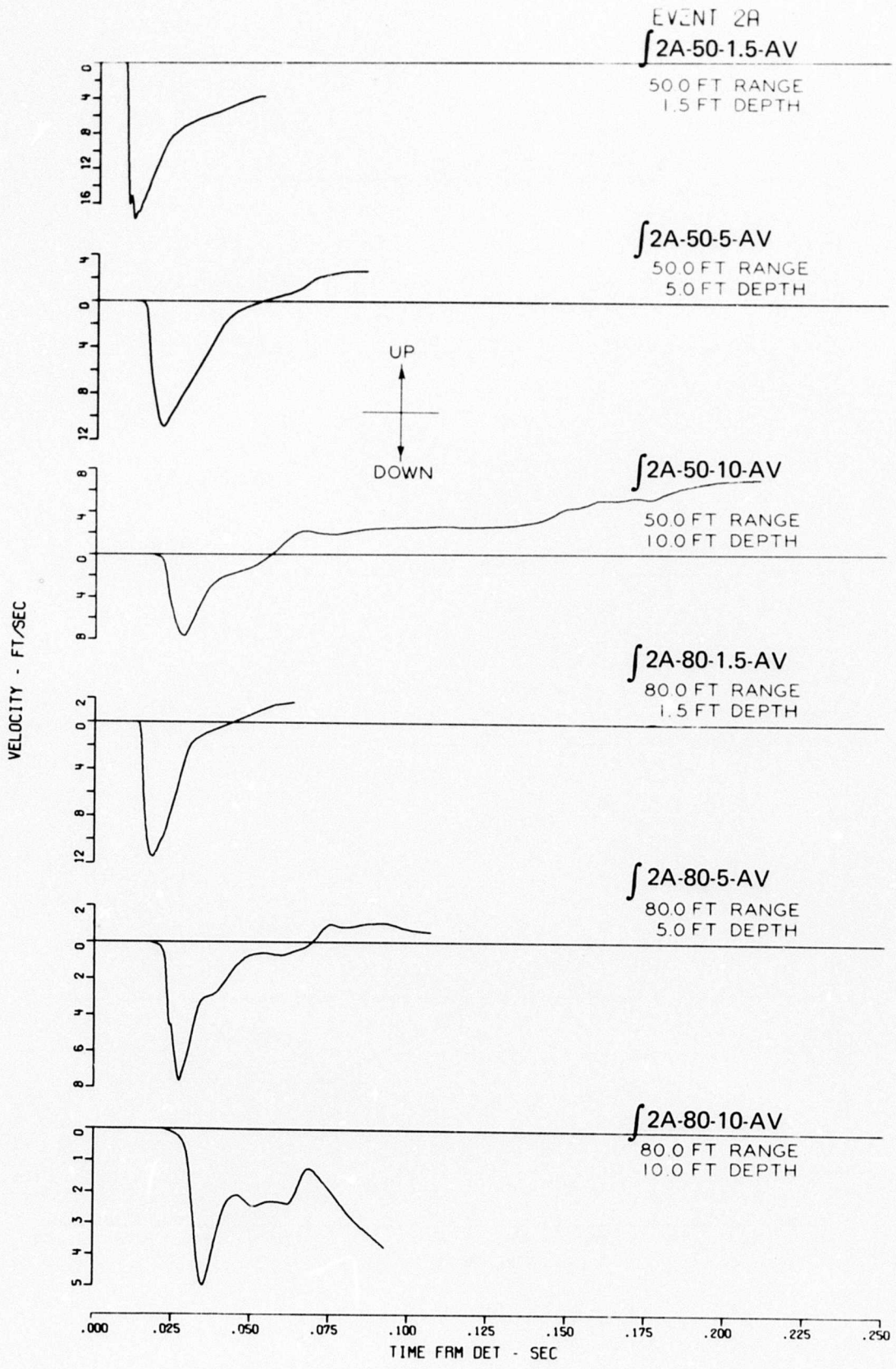

Figure A.2 (Sheet 2 of 4).

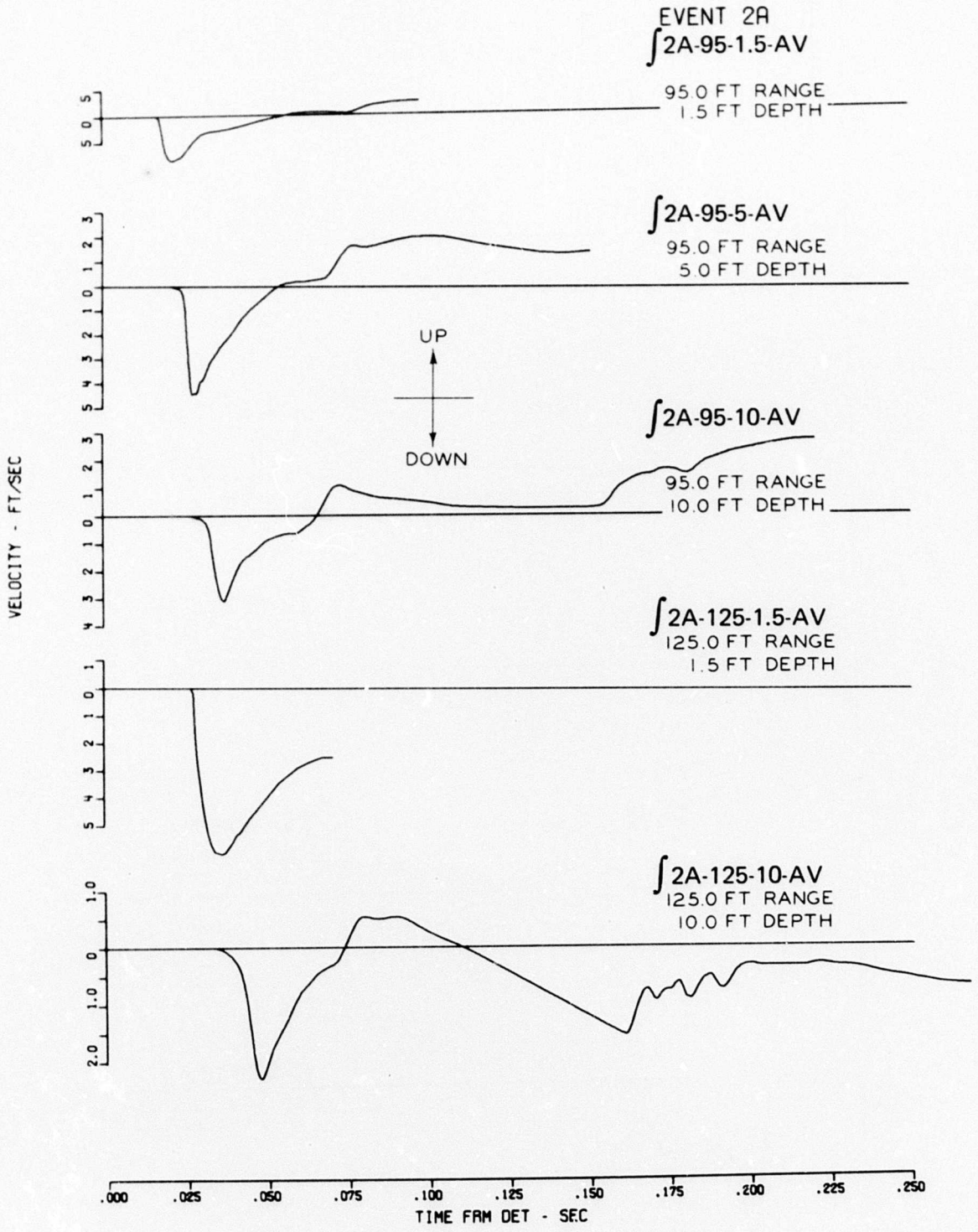

Figure A.2 (Sheet 3 of 4).

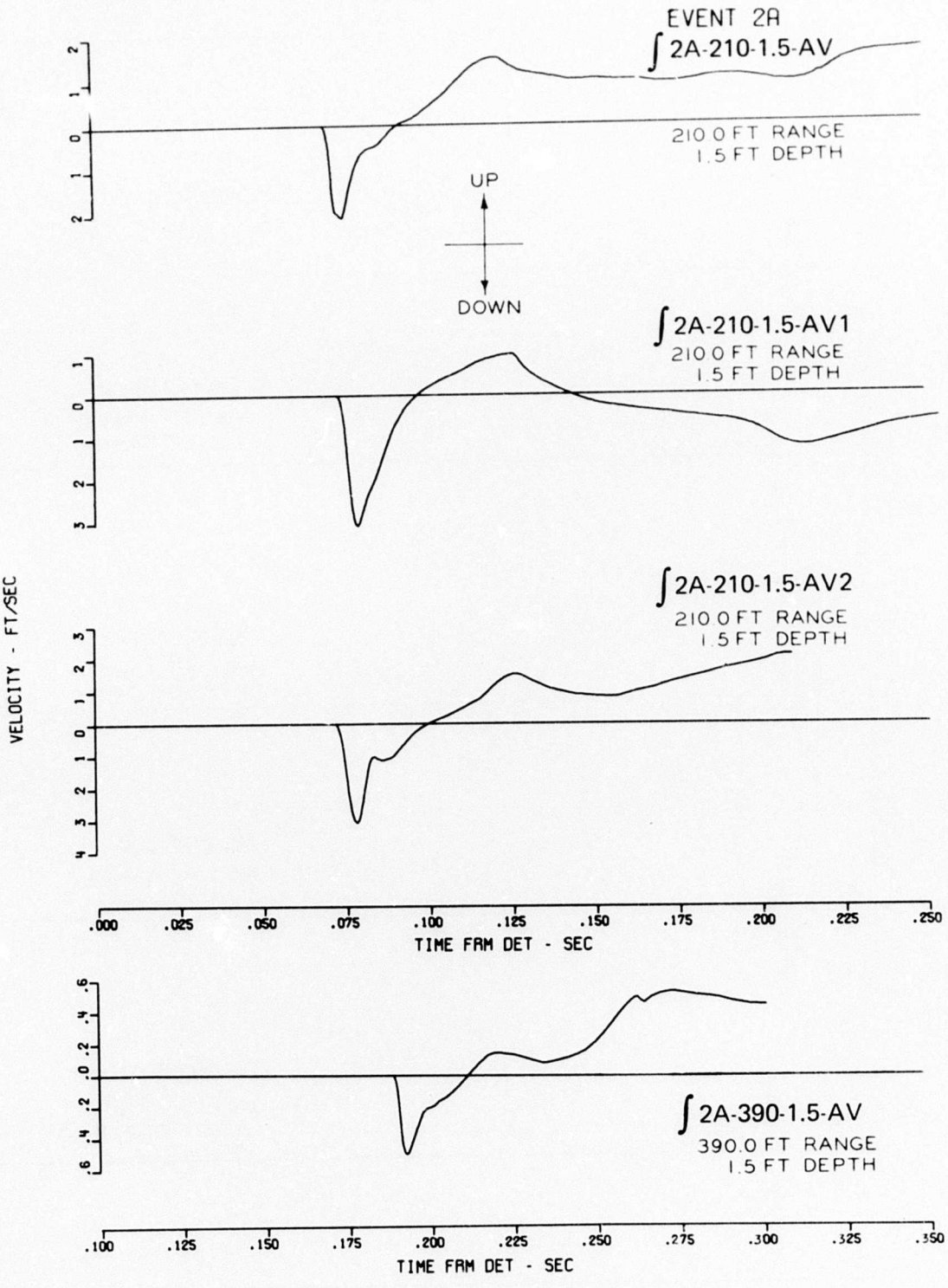

Figure A.2 (Sheet 4 of 4).

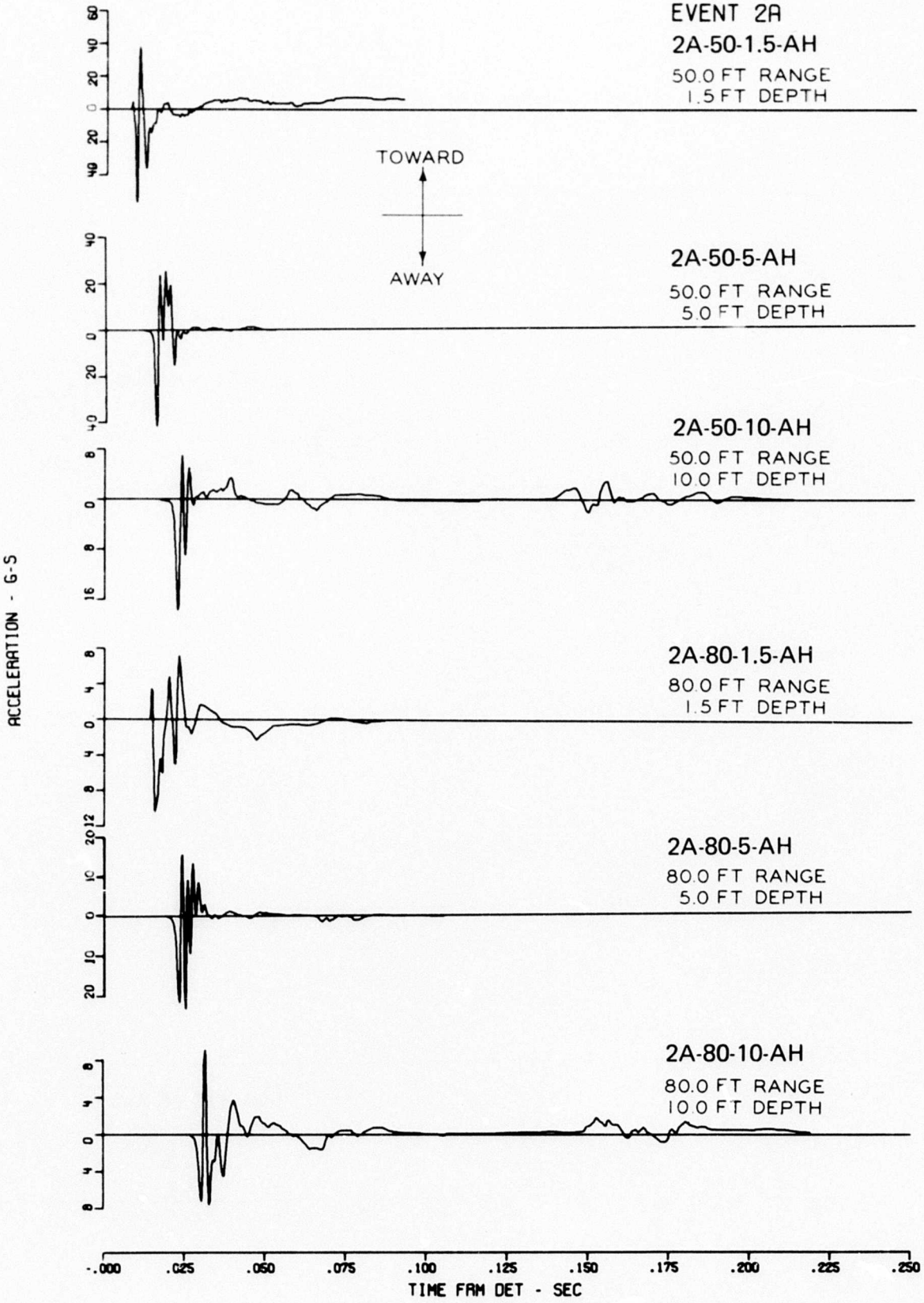

Figure A.3 Horizontal acceleration, Event 2A (Sheet 1 of 3).

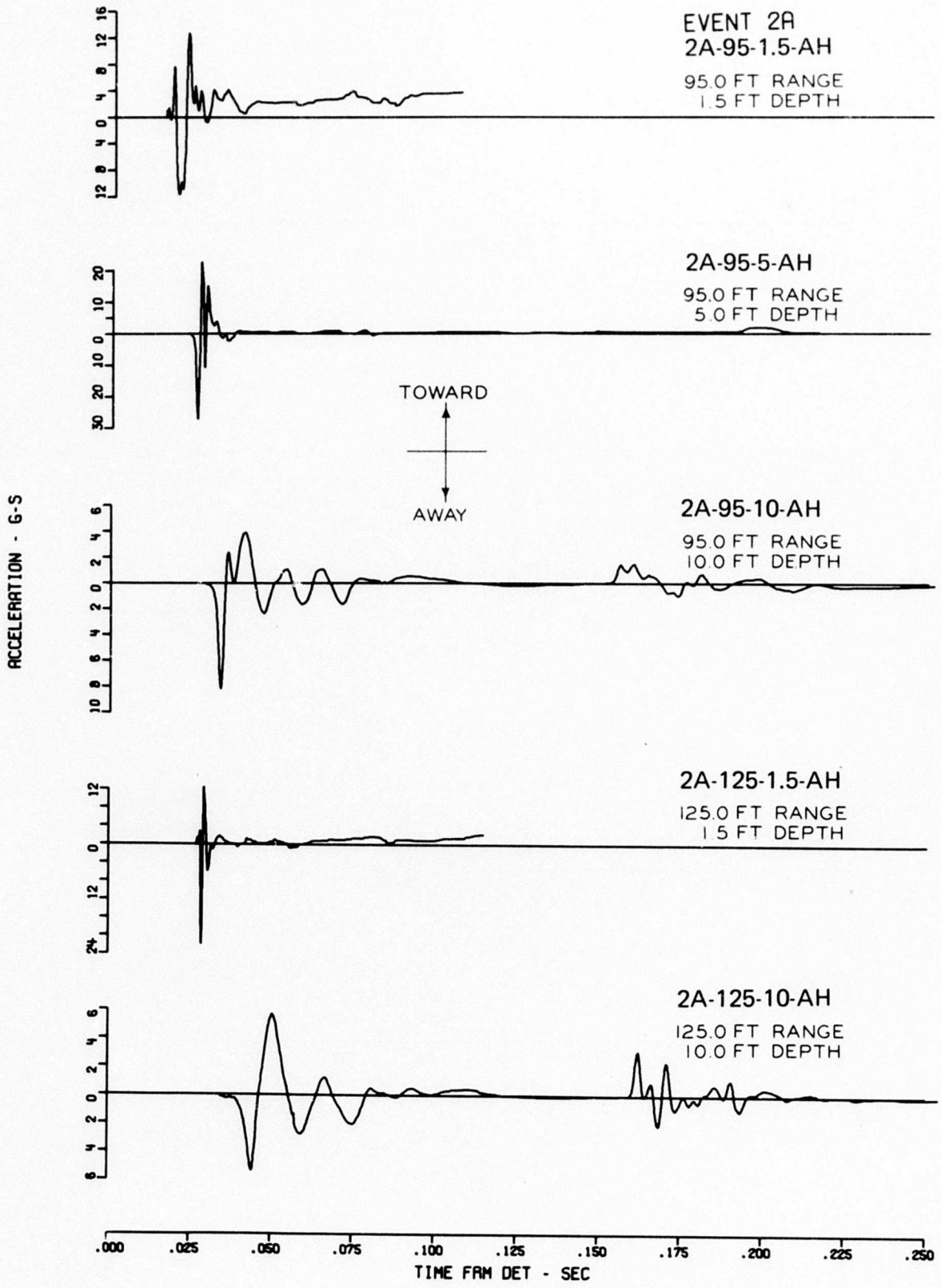

Figure A.3 (Sheet 2 of 3).

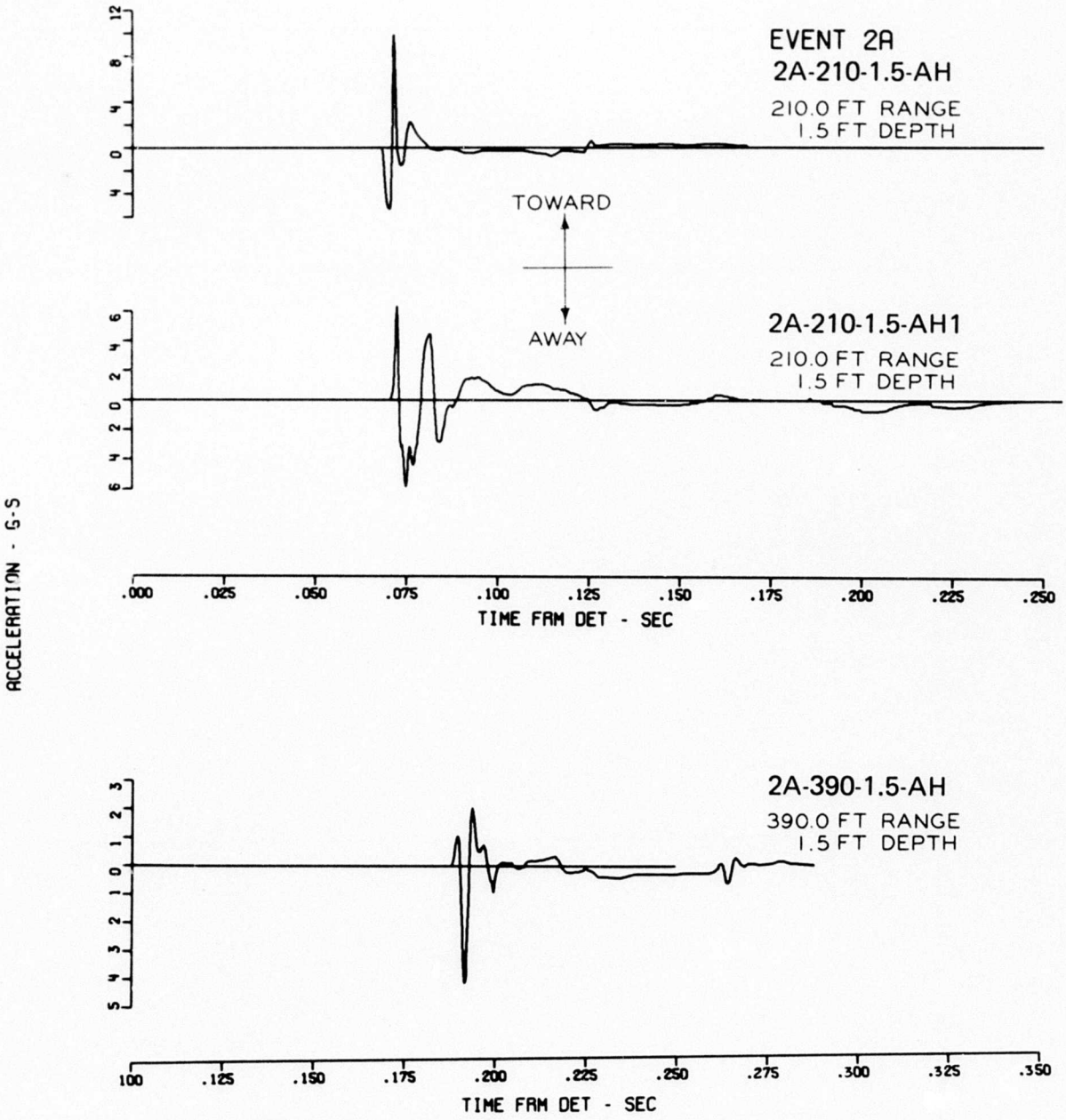

Figure A.3 (Sheet 3 of 3).

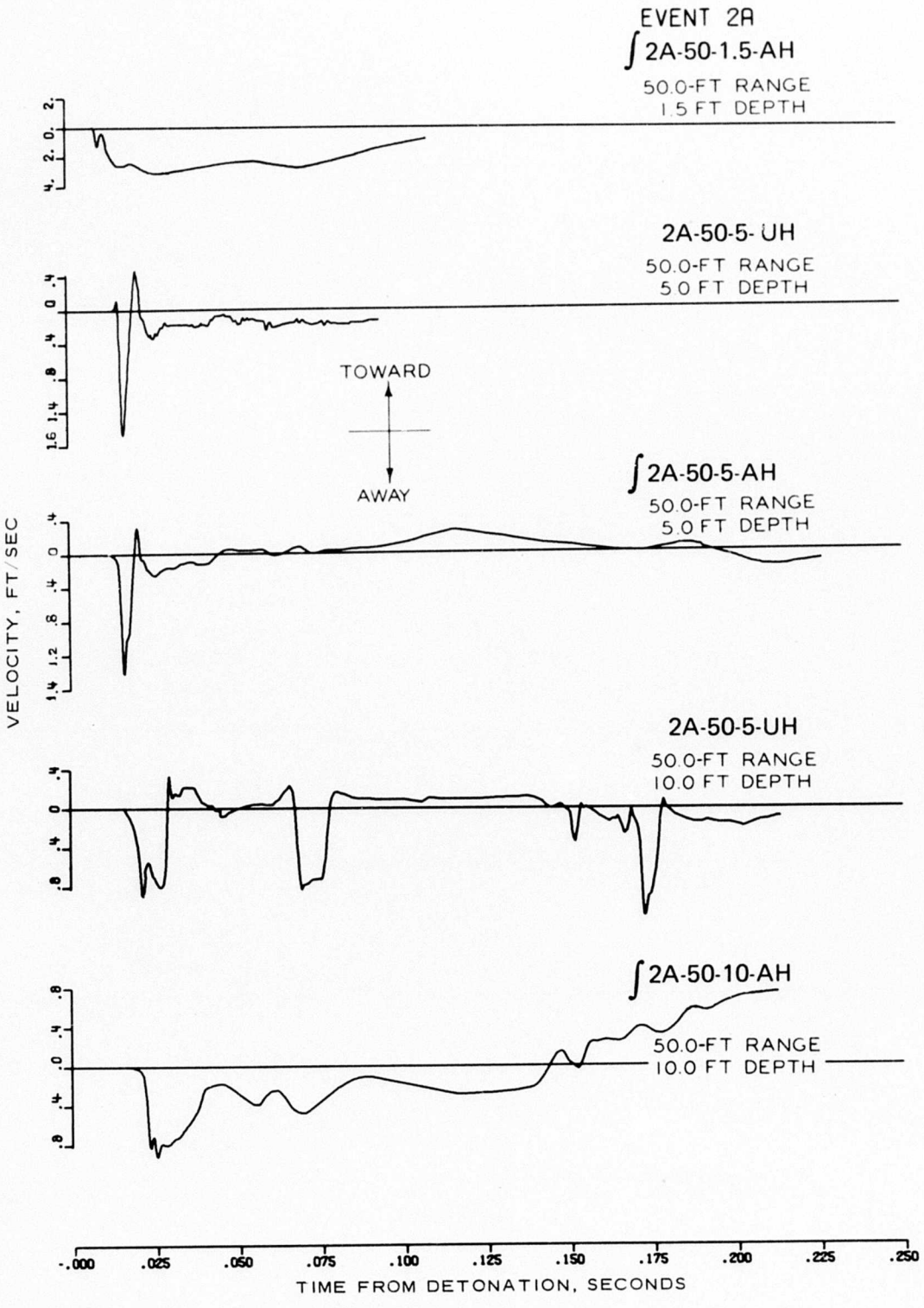

Figure A.4 Horizontal velocity, Event 2A (Sheet 1 of 5).

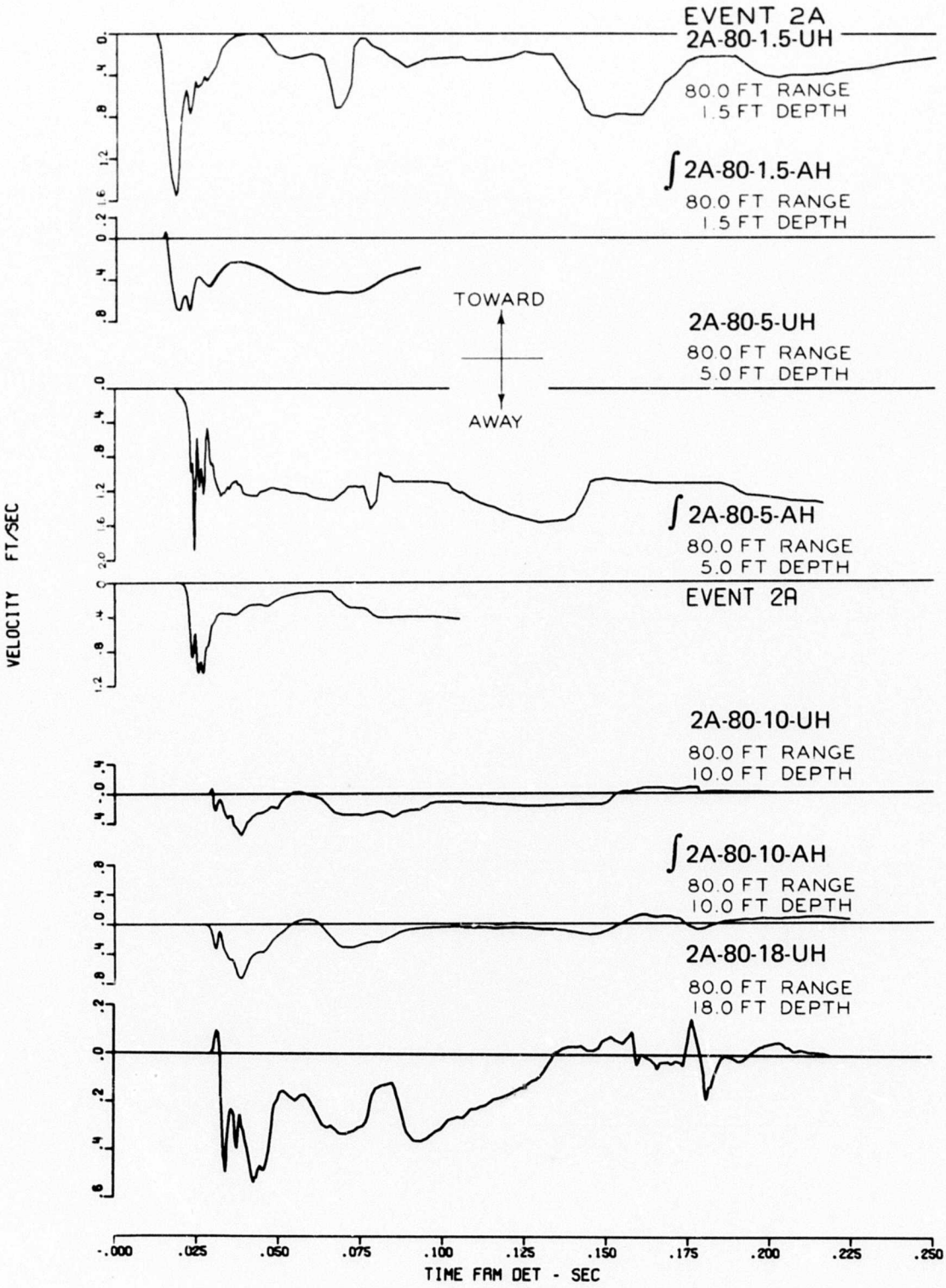

Figure A.4 (Sheet 2 of 5).

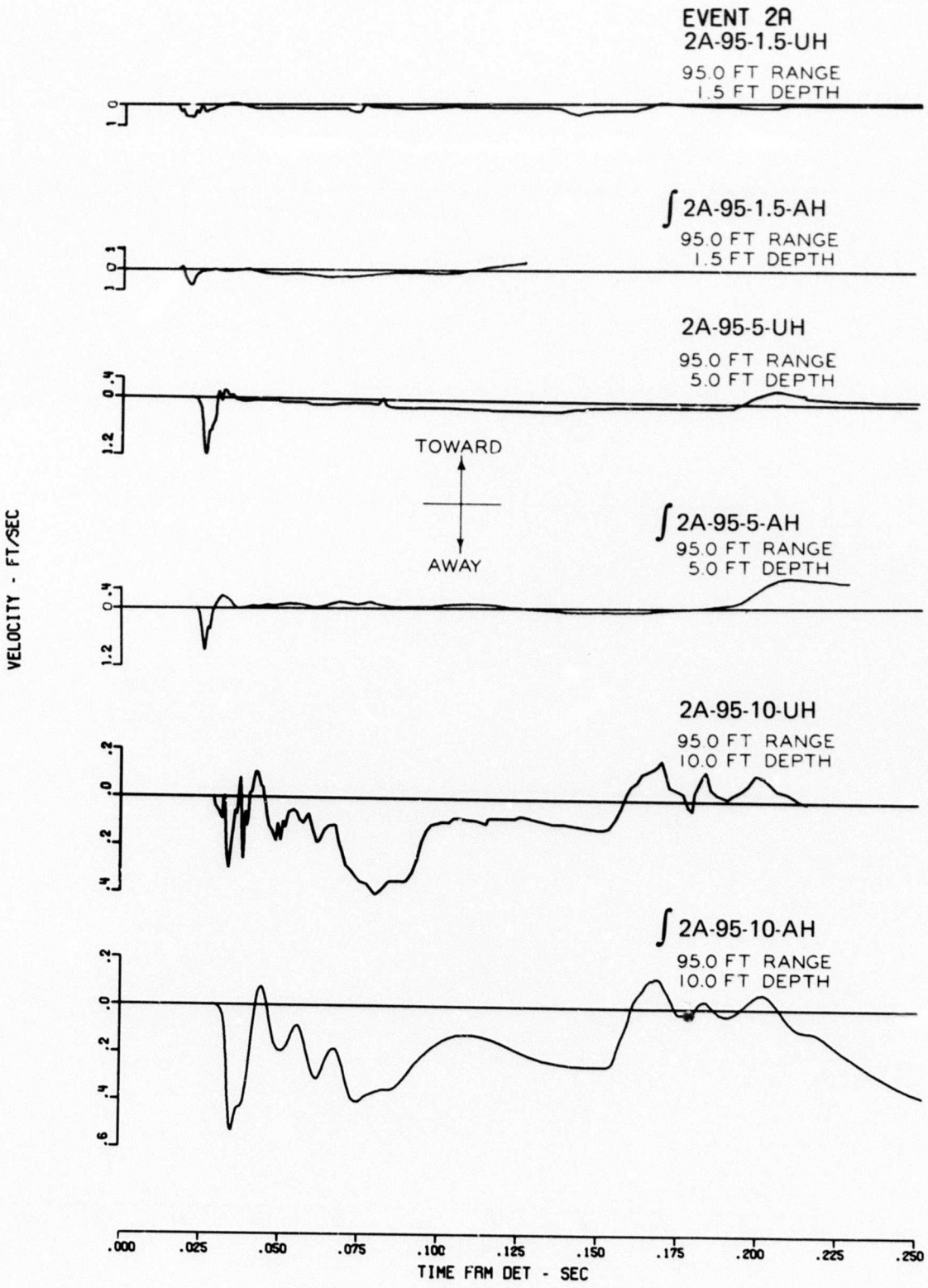

Figure A.4 (Sheet 3 of 5).

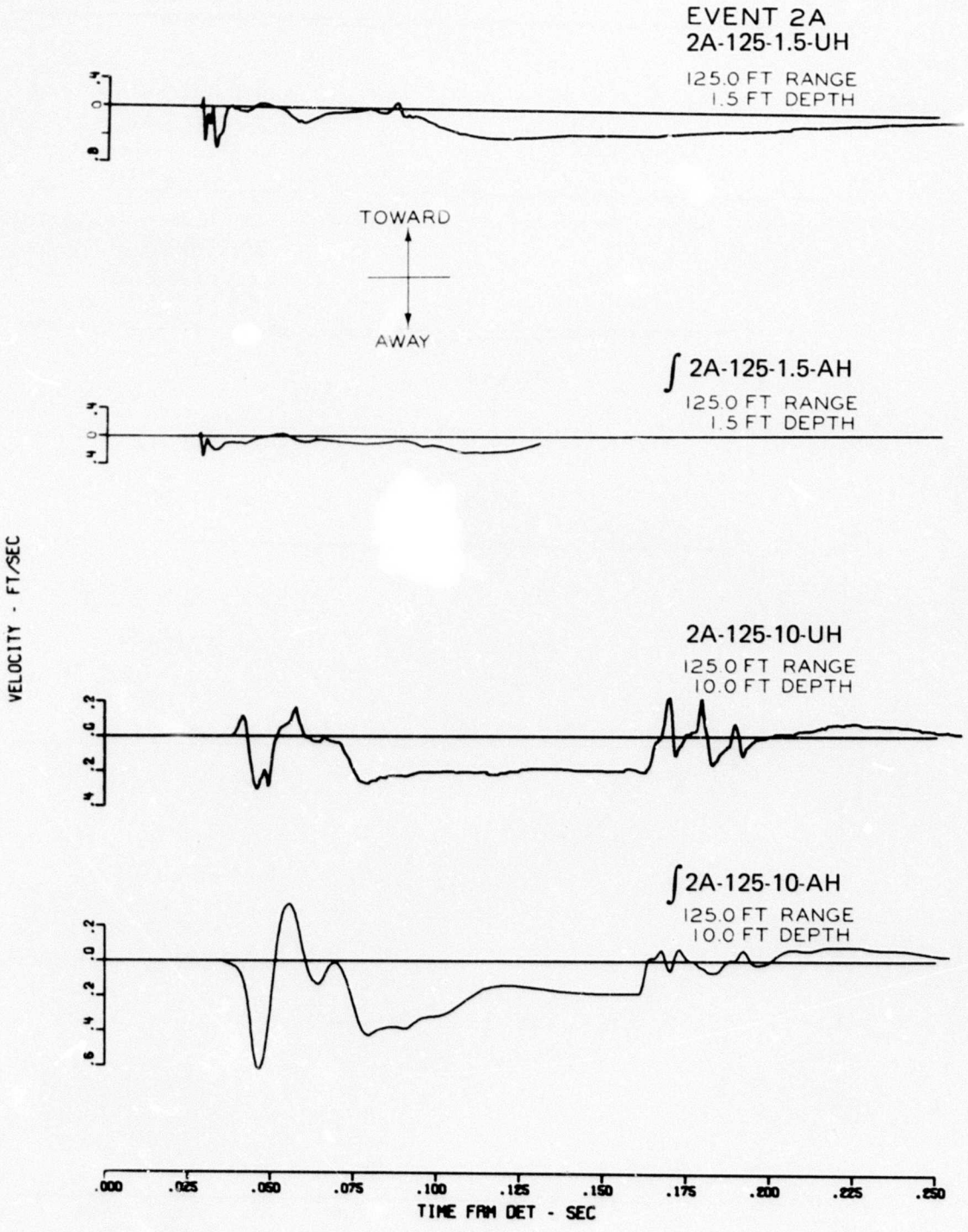

Figure A.4 (Sheet 4 of 5).

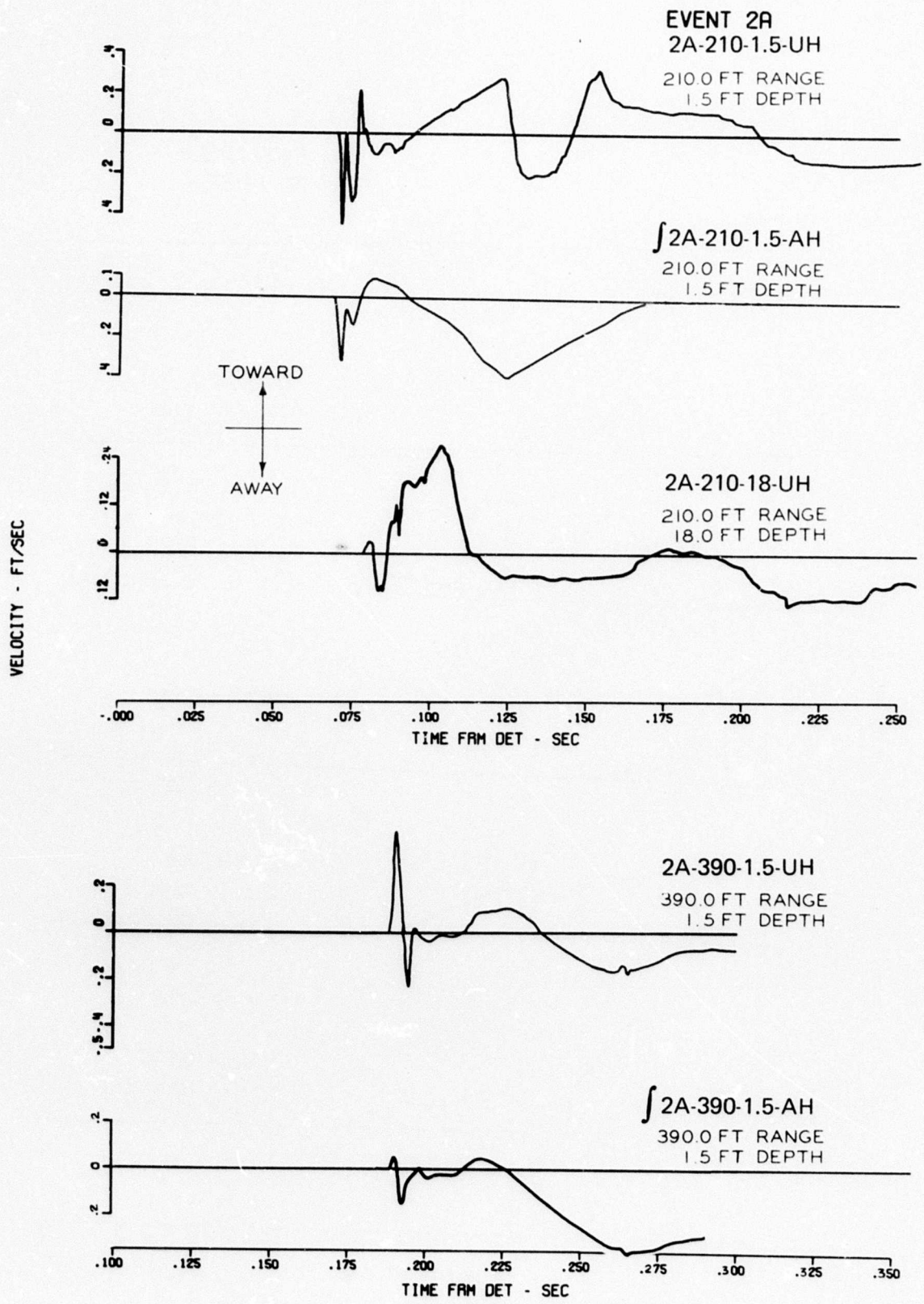

Figure A.4 (Sheet 5 of 5).

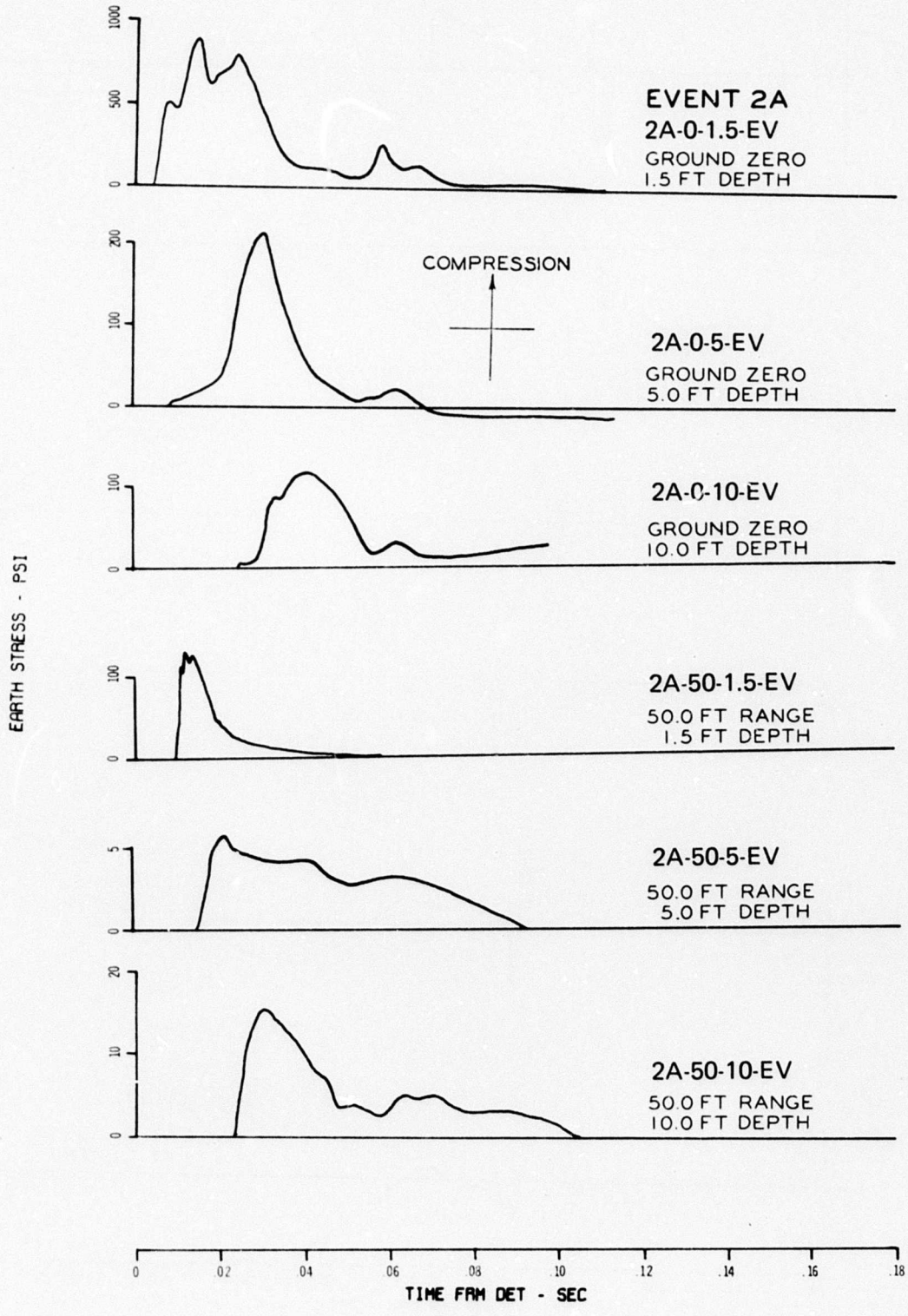

Figure A.5 Vertical stress, Event 2A (Sheet 1 of 2).

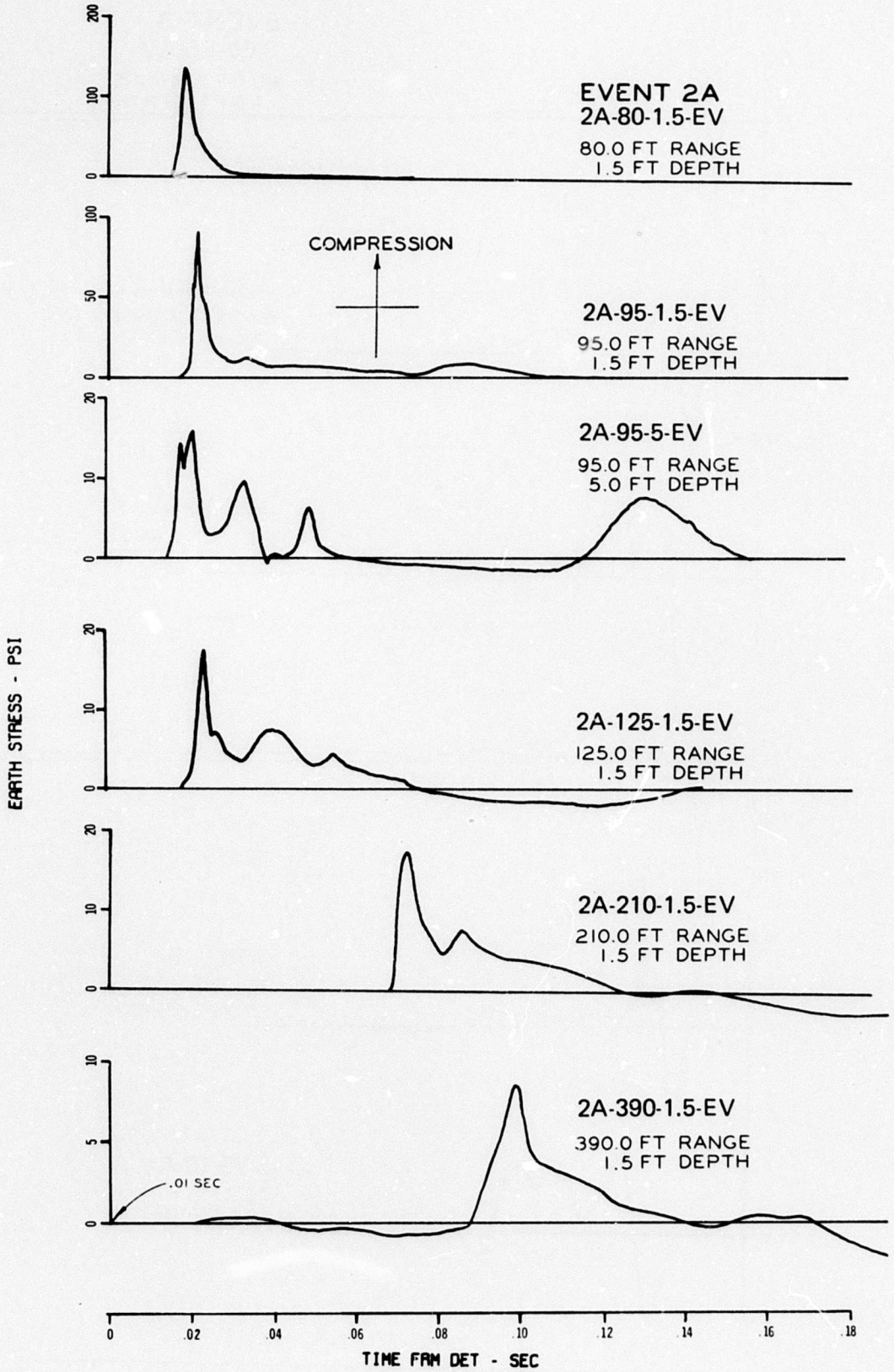

Figure A.5 (Sheet 2 of 2).

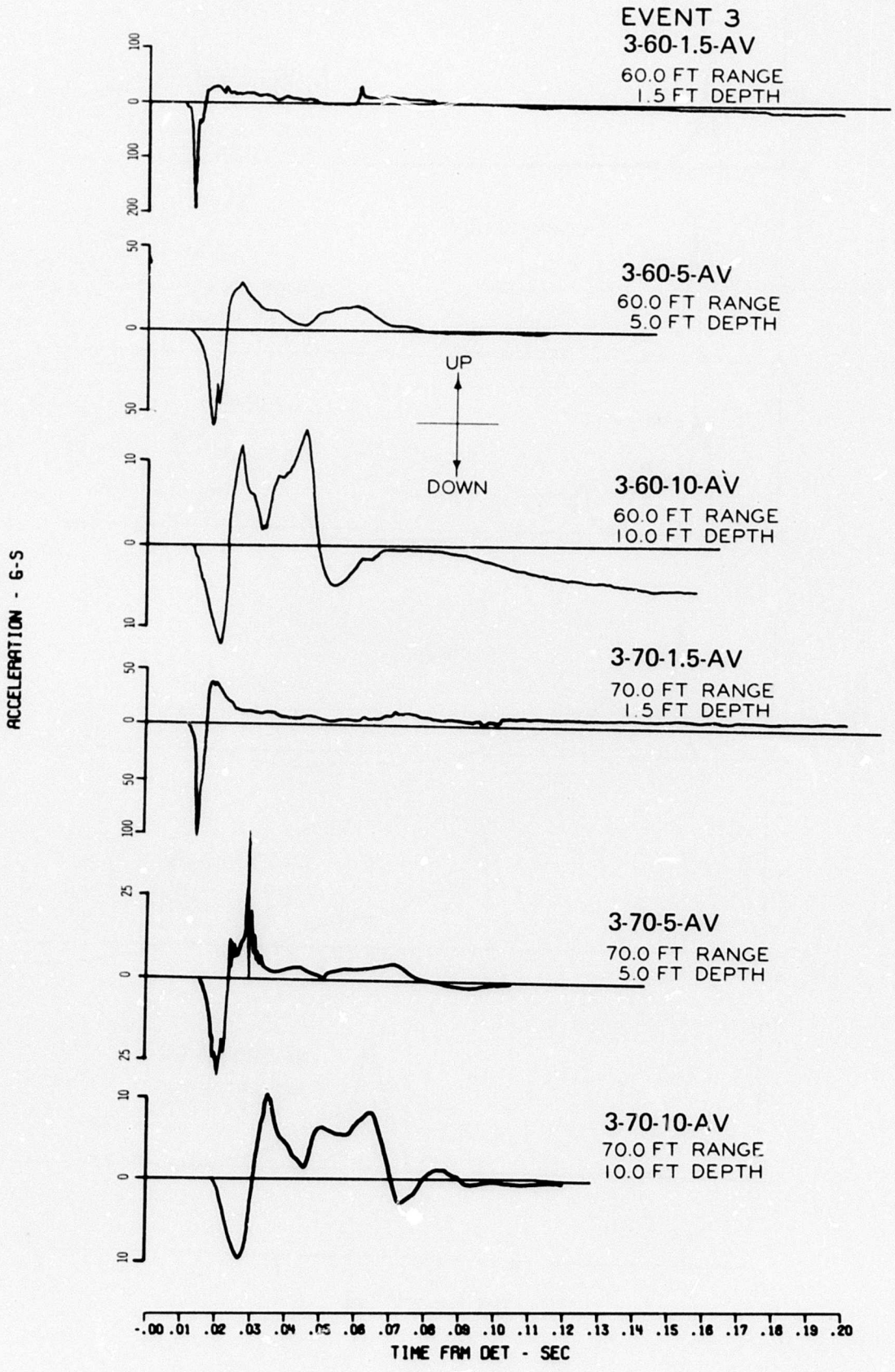

Figure A.6 Vertical acceleration, Event 3 (Sheet 1 of 2).

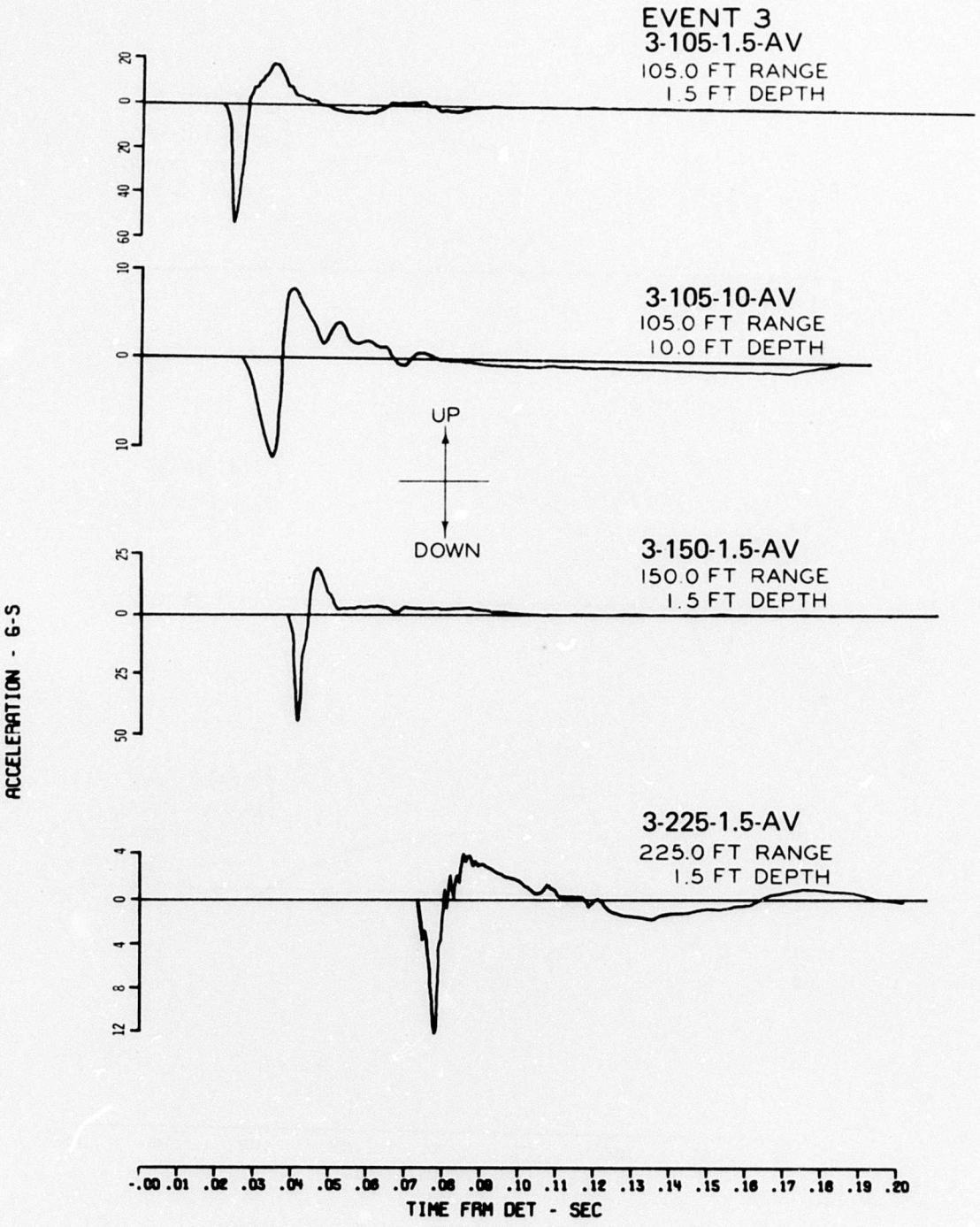

Figure A.6 (Sheet 2 of 2).

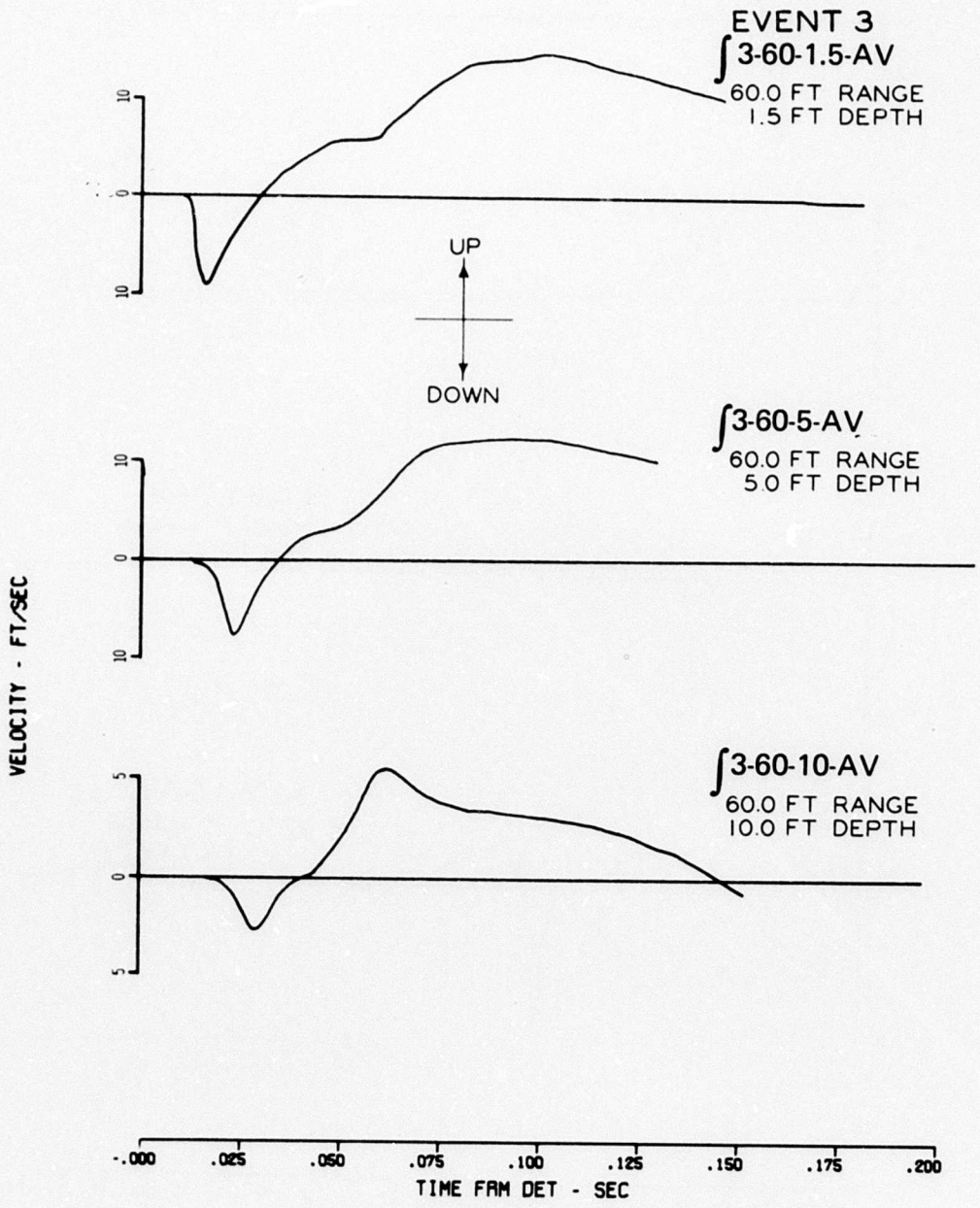

Figure A.7 Vertical velocity, Event 3 (Sheet 1 of 2).

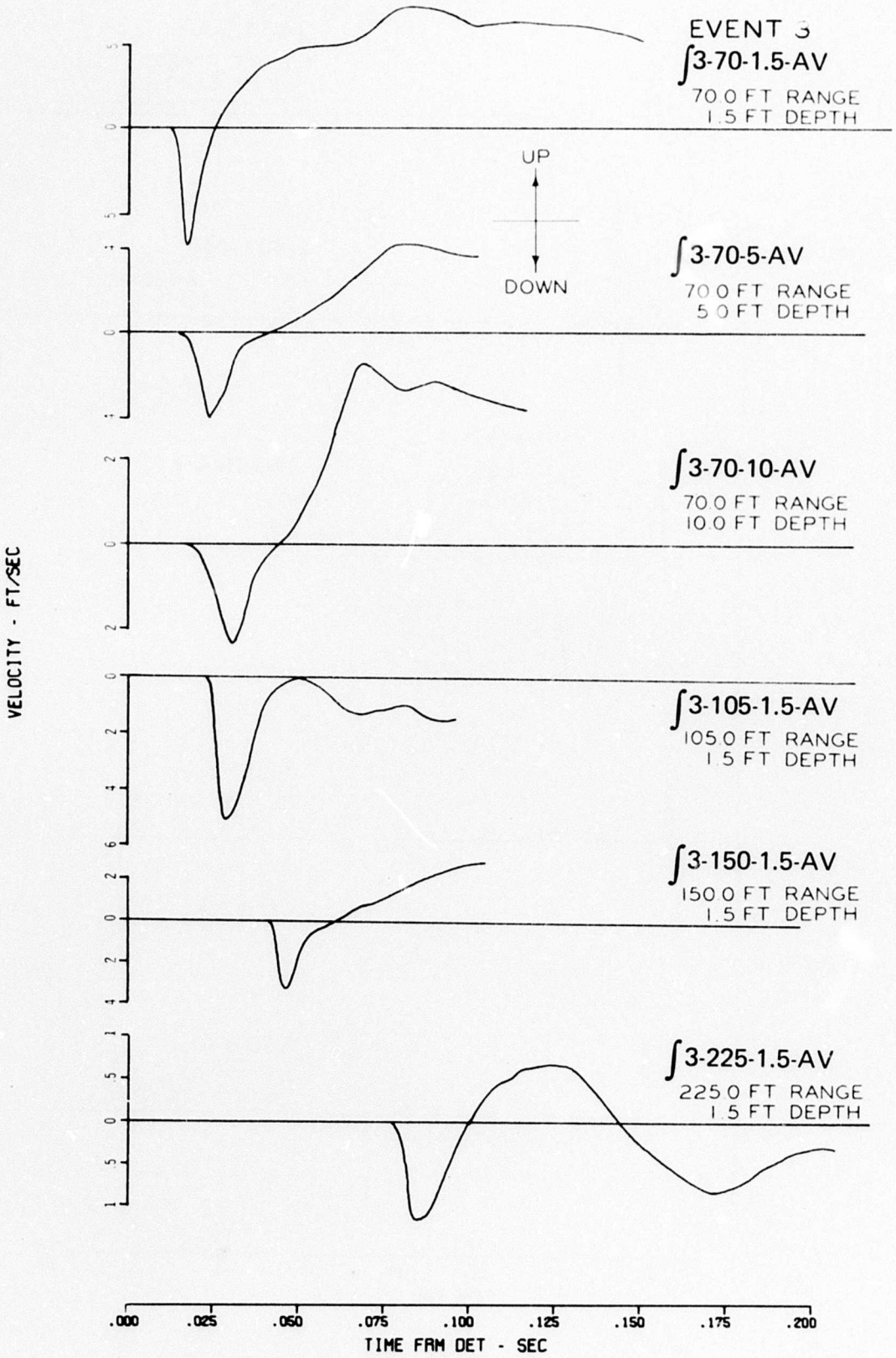

Figure A.7 (Sheet 2 of 2).

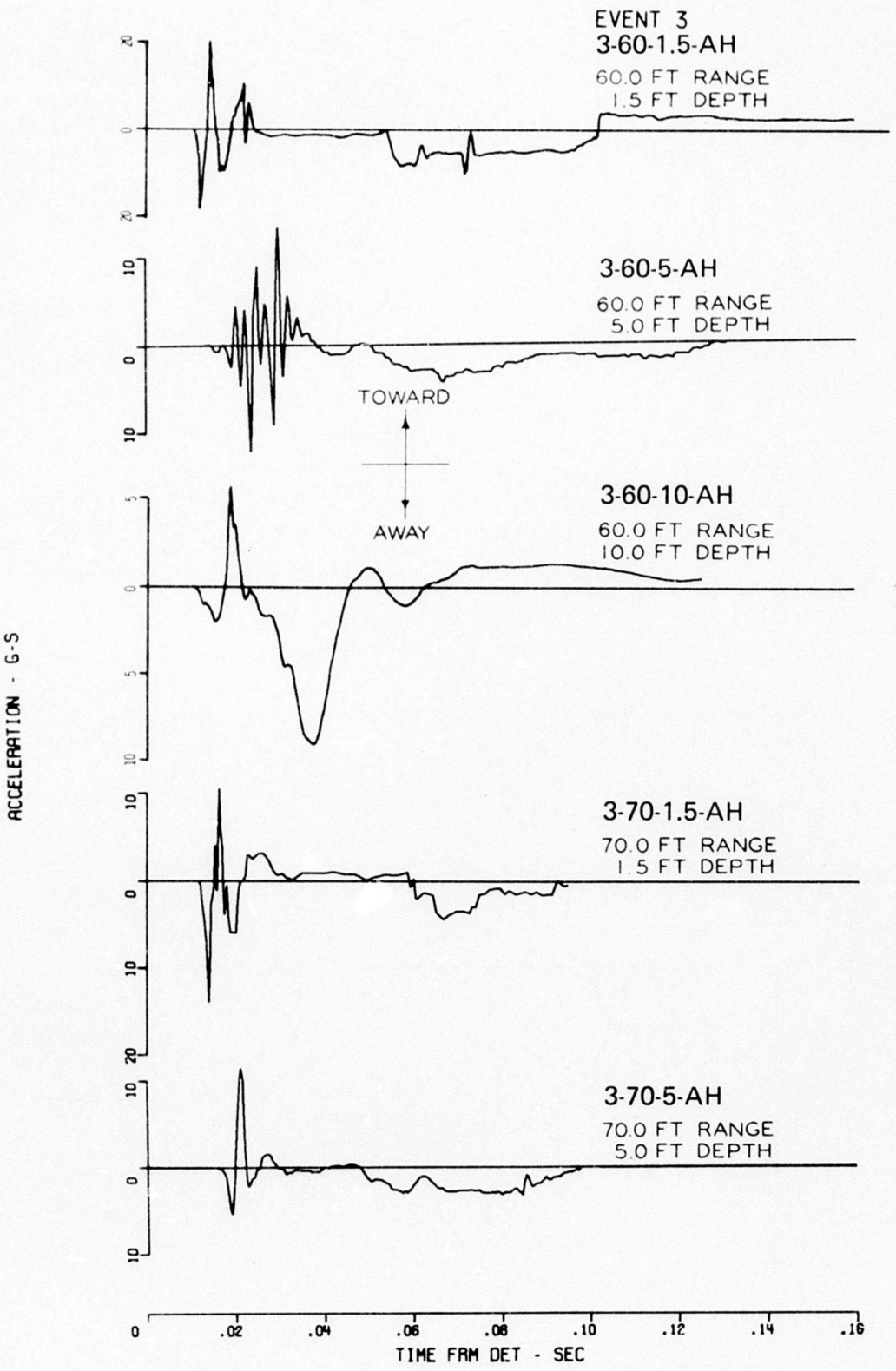

Figure A.8 Horizontal acceleration, Event 3 (Sheet 1 of 2).

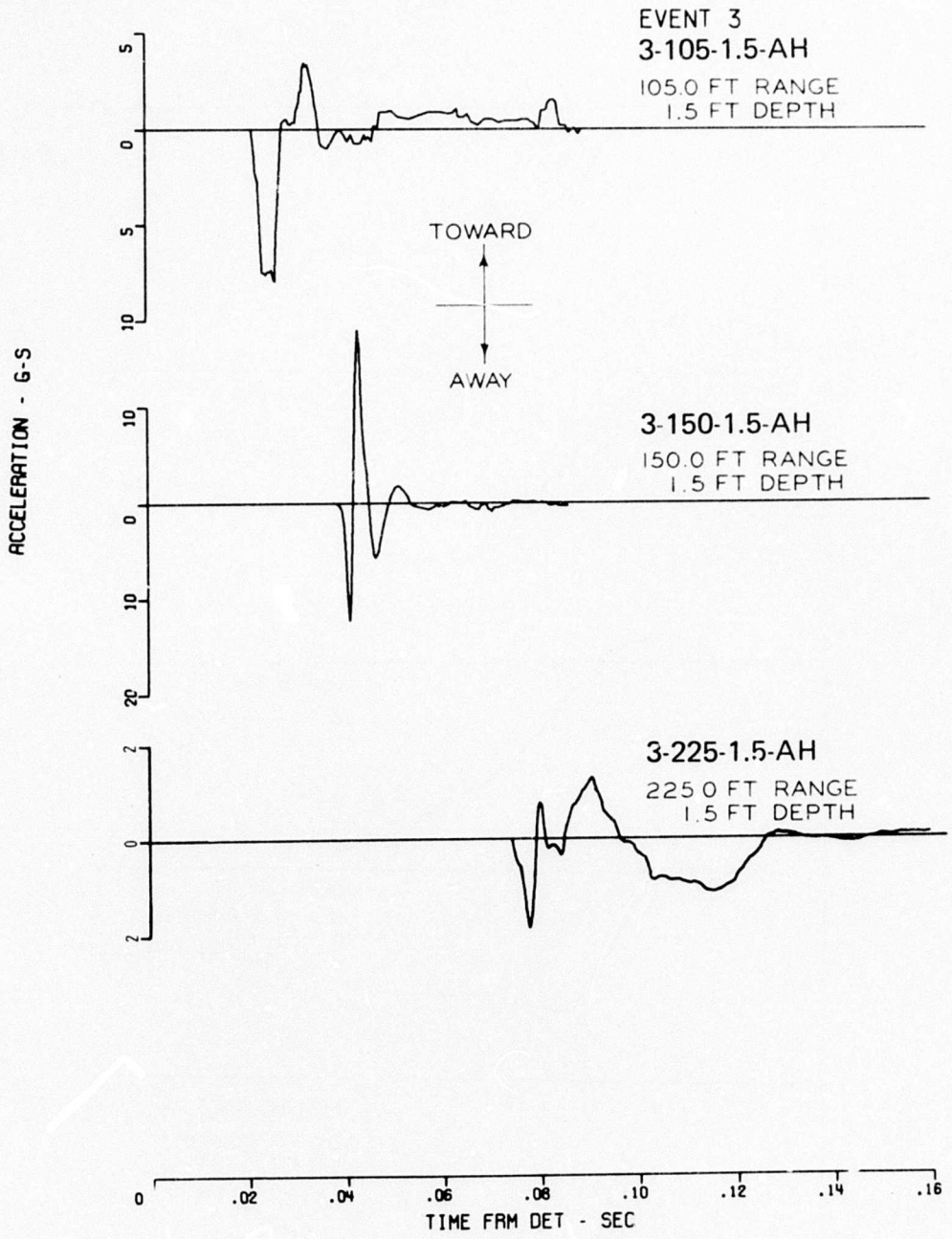

Figure A.8 (Sheet 2 of 2).

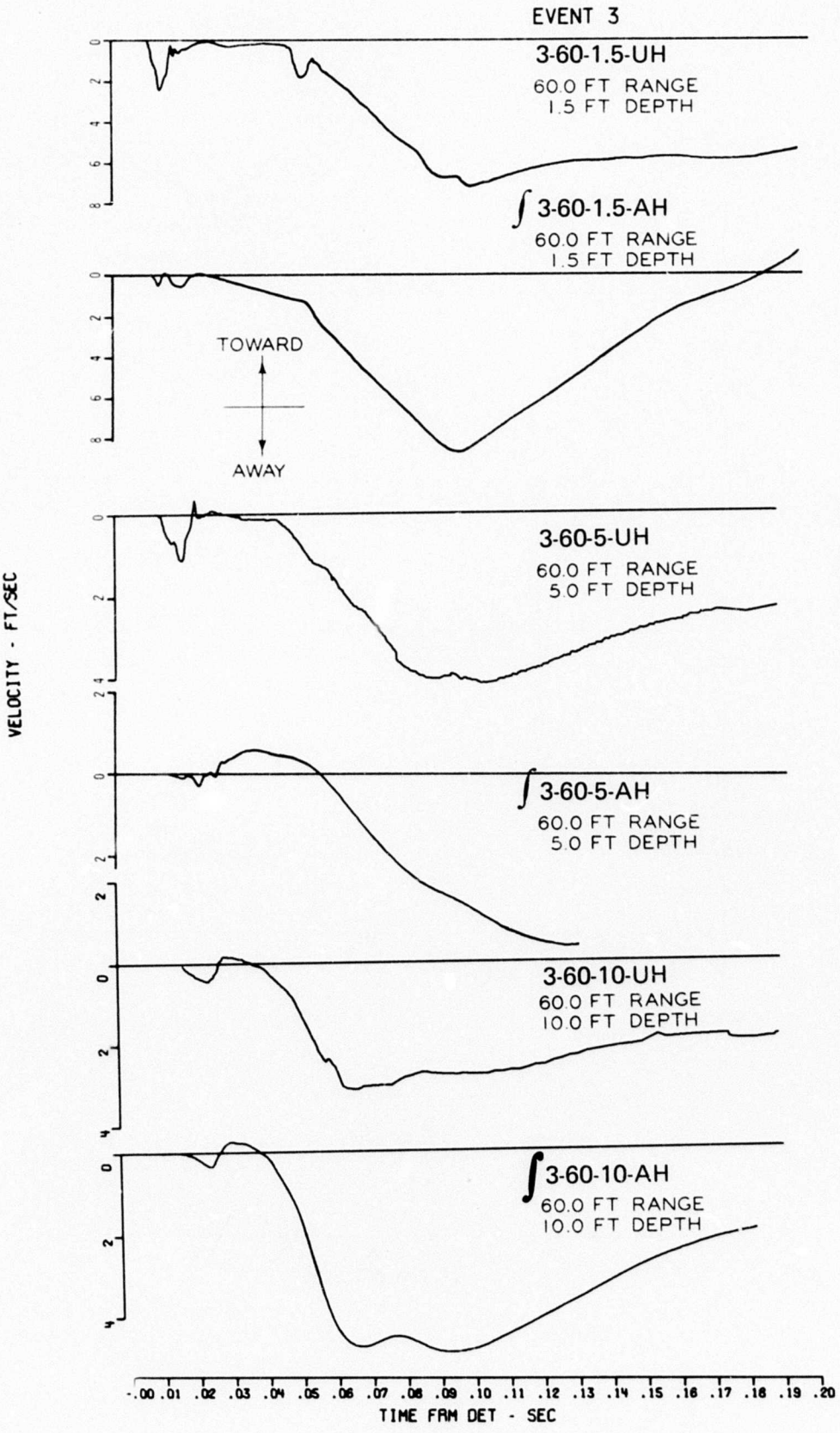

Figure A.9 Horizontal velocity, Event 3 (Sheet 1 of 3).

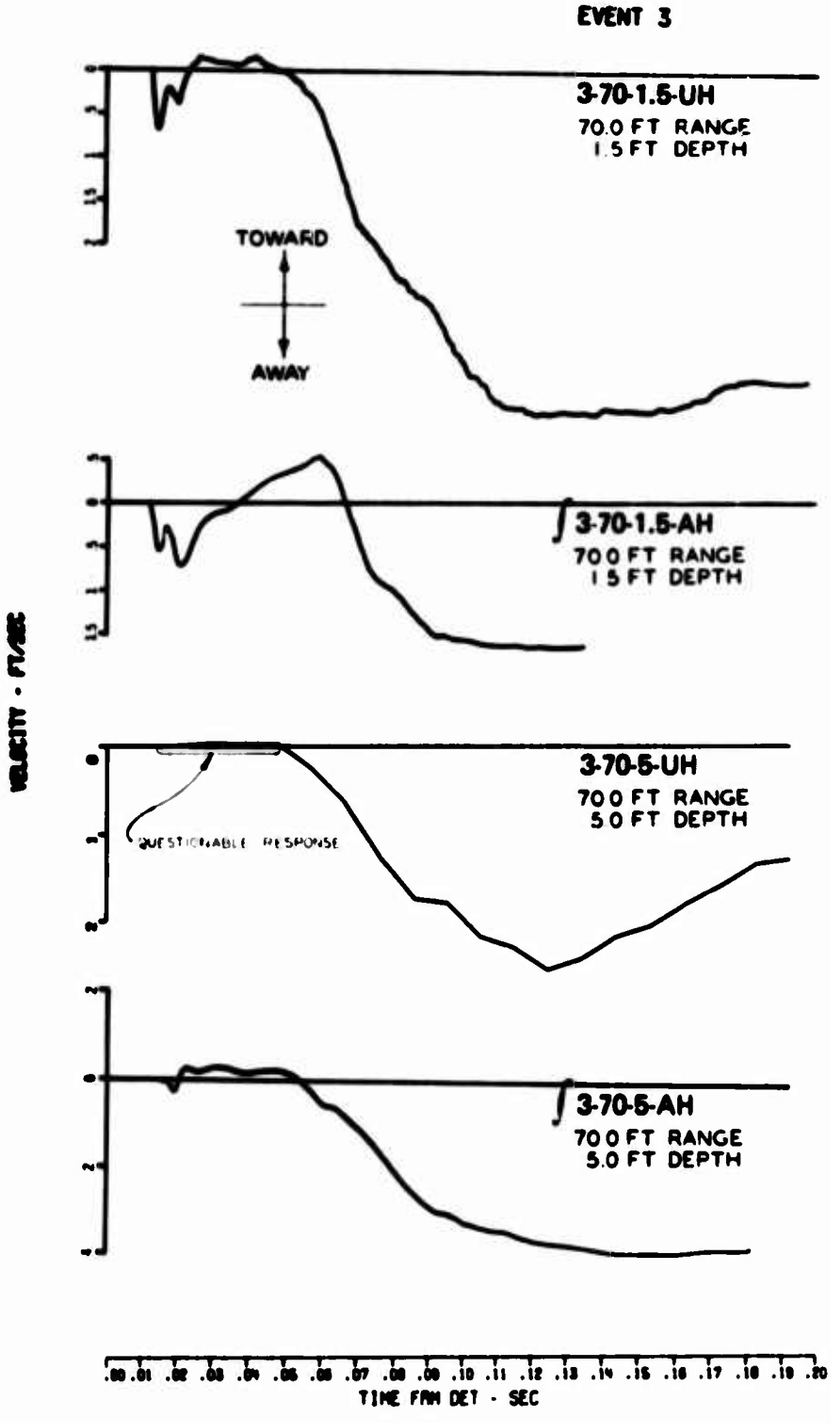

Figure A.9 (Sheet 2 of 3).

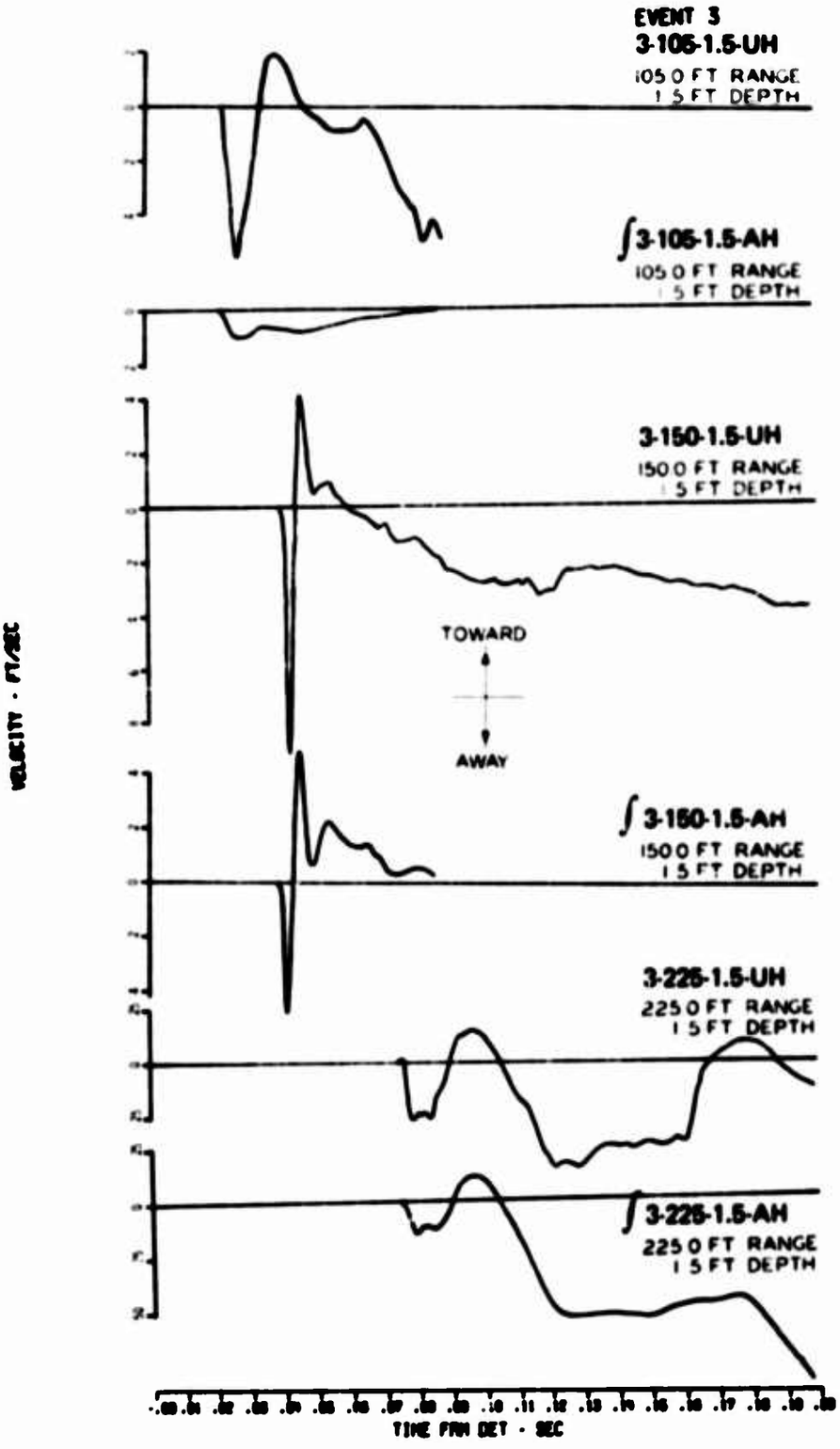

Figure A.9 (Sheet 3 of 3).

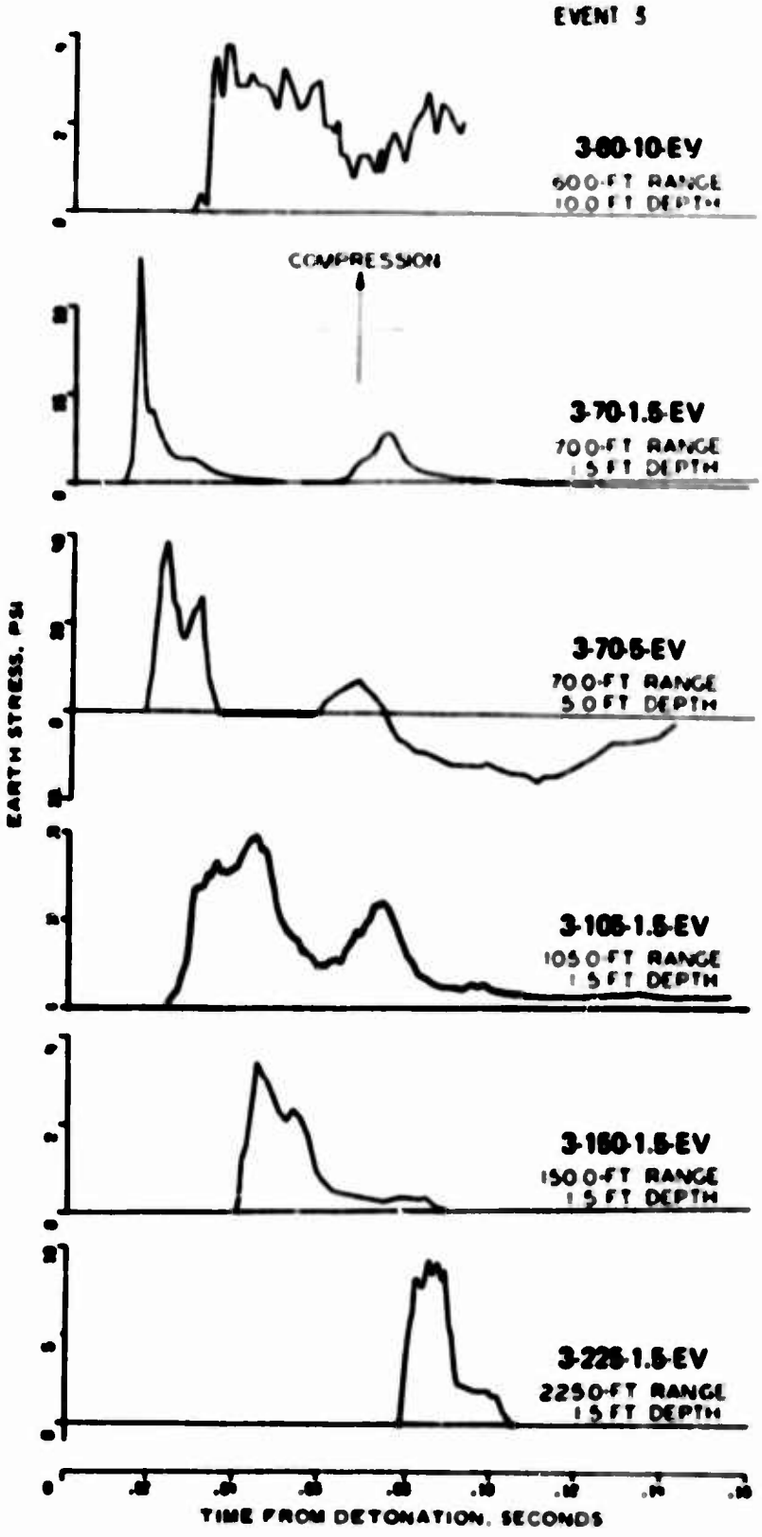

Figure A.10 Vertical stress, Event 5.

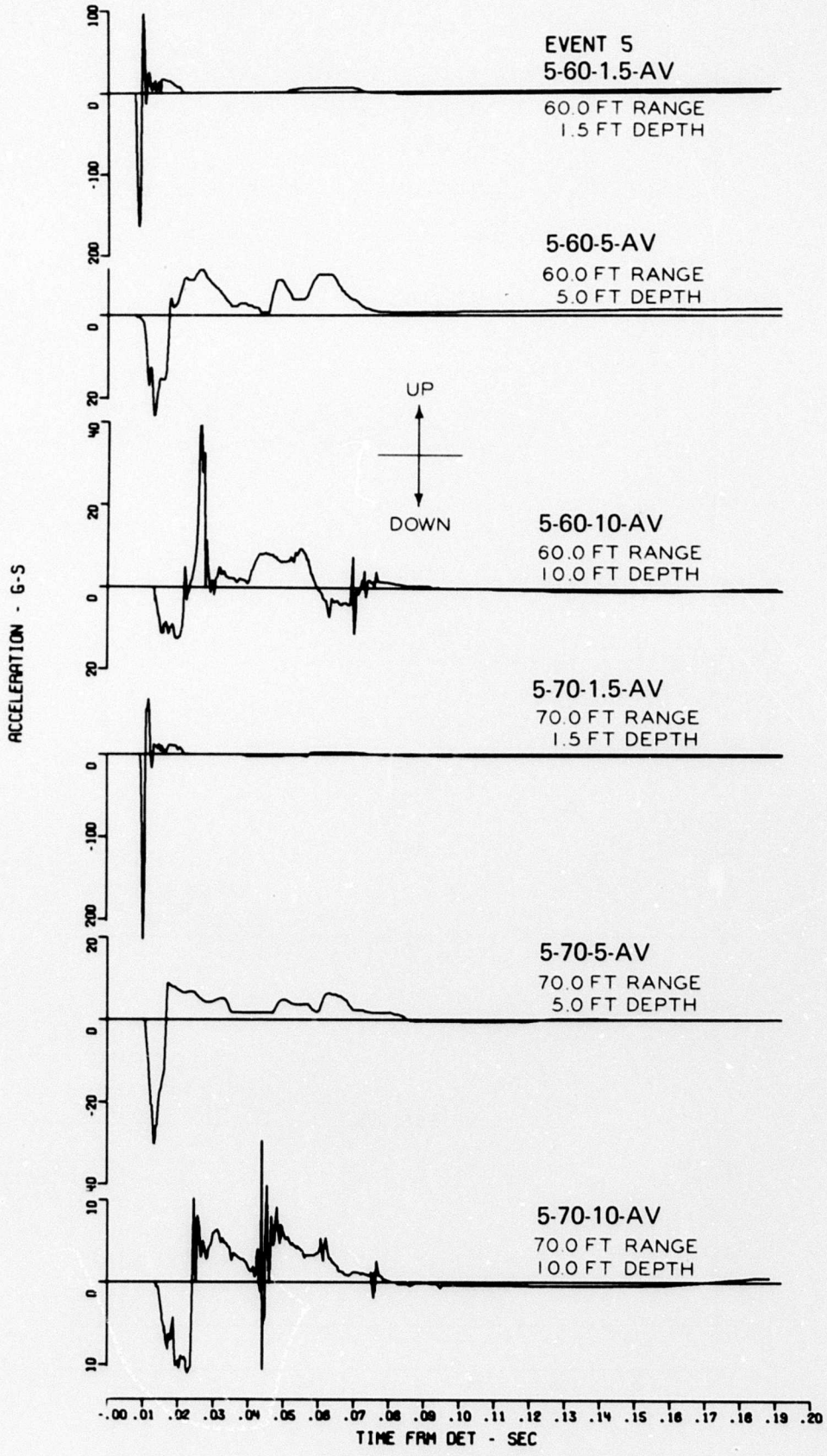

Figure A.11 Vertical acceleration, Event 5 (Sheet 1 of 2).

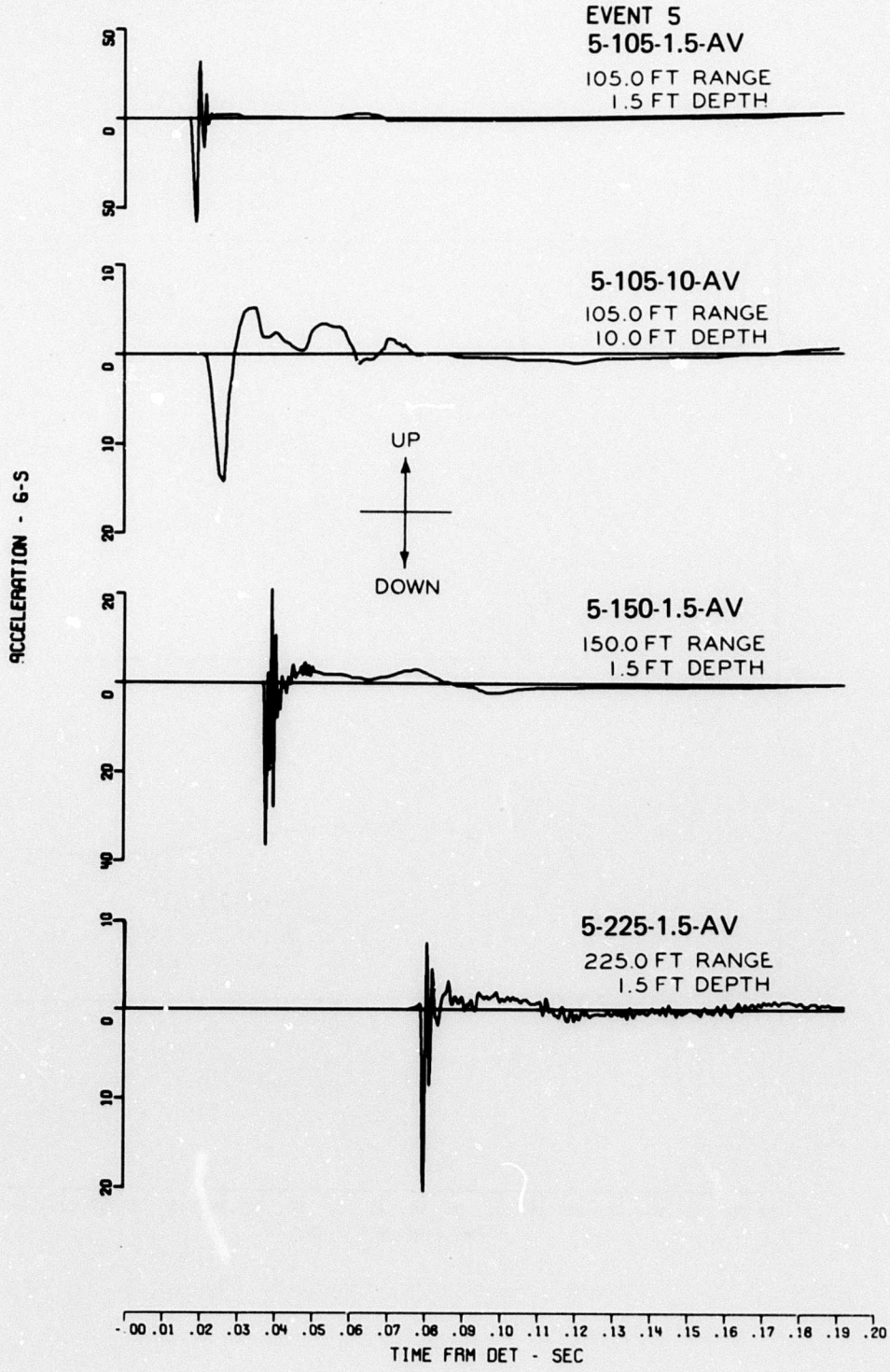

Figure A.11 (Sheet 2 of 2).

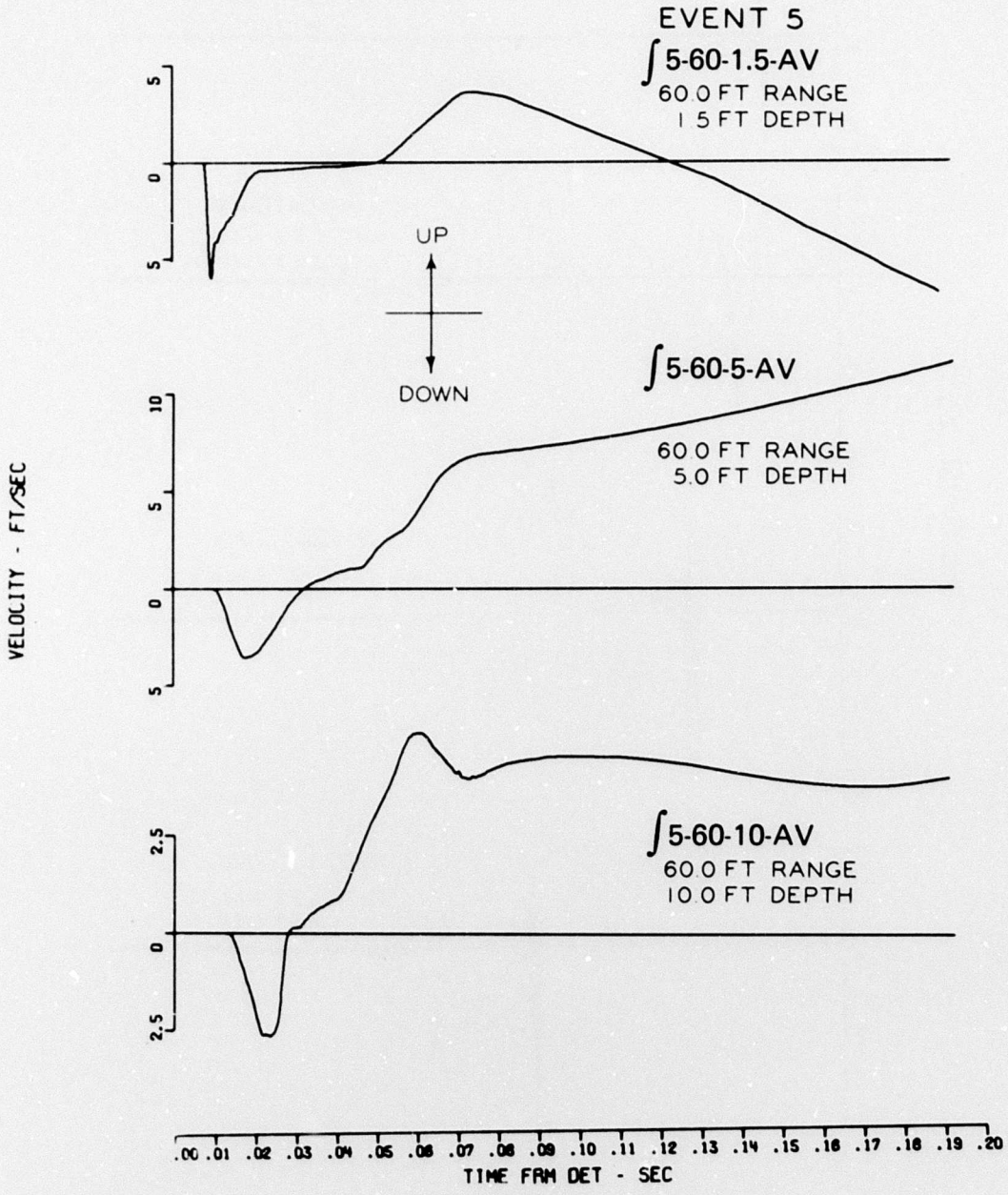

Figure A.12 Vertical velocity, Event 5 (Sheet 1 of 3).

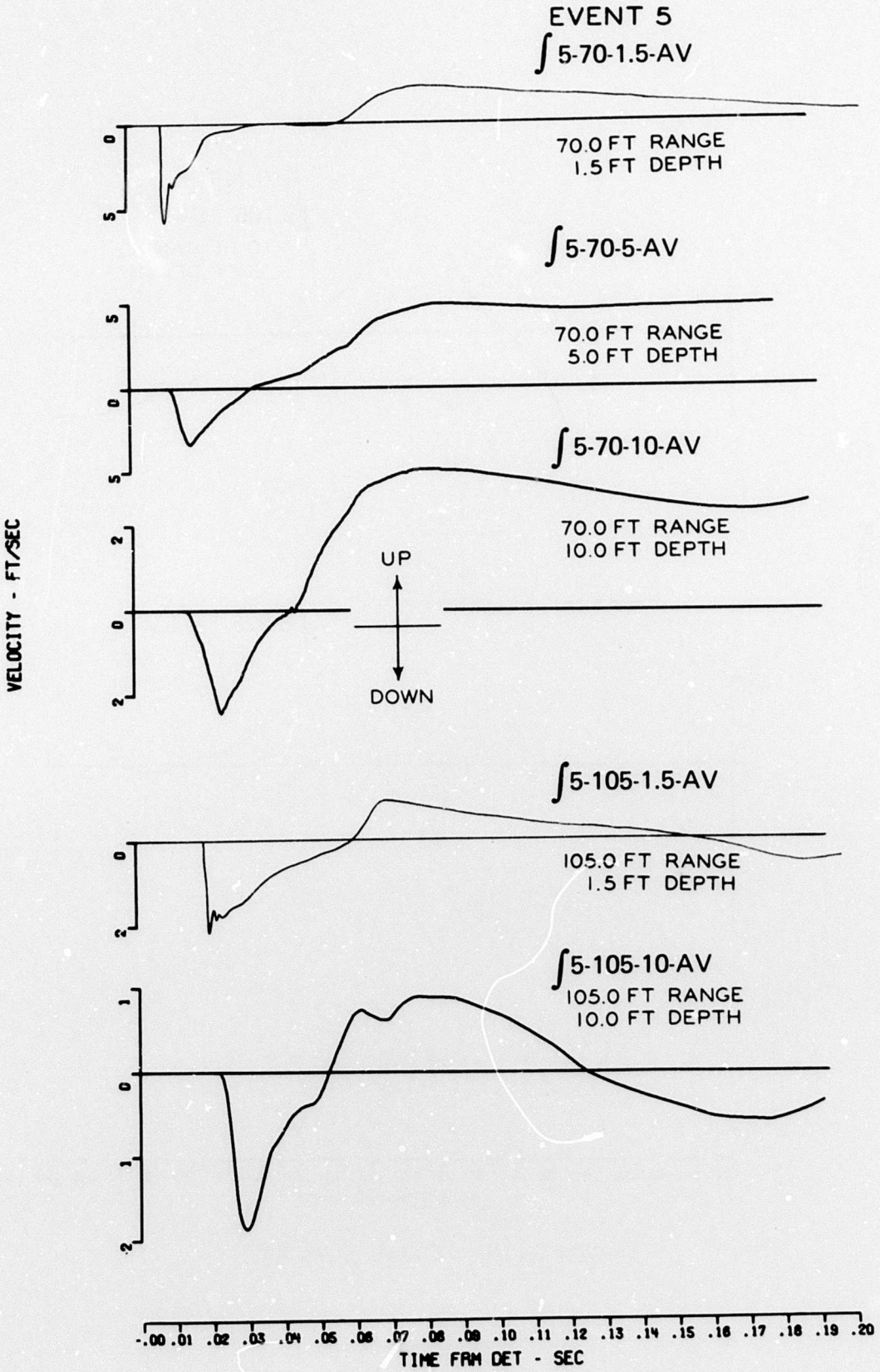

Figure A.12 (Sheet 2 of 3).

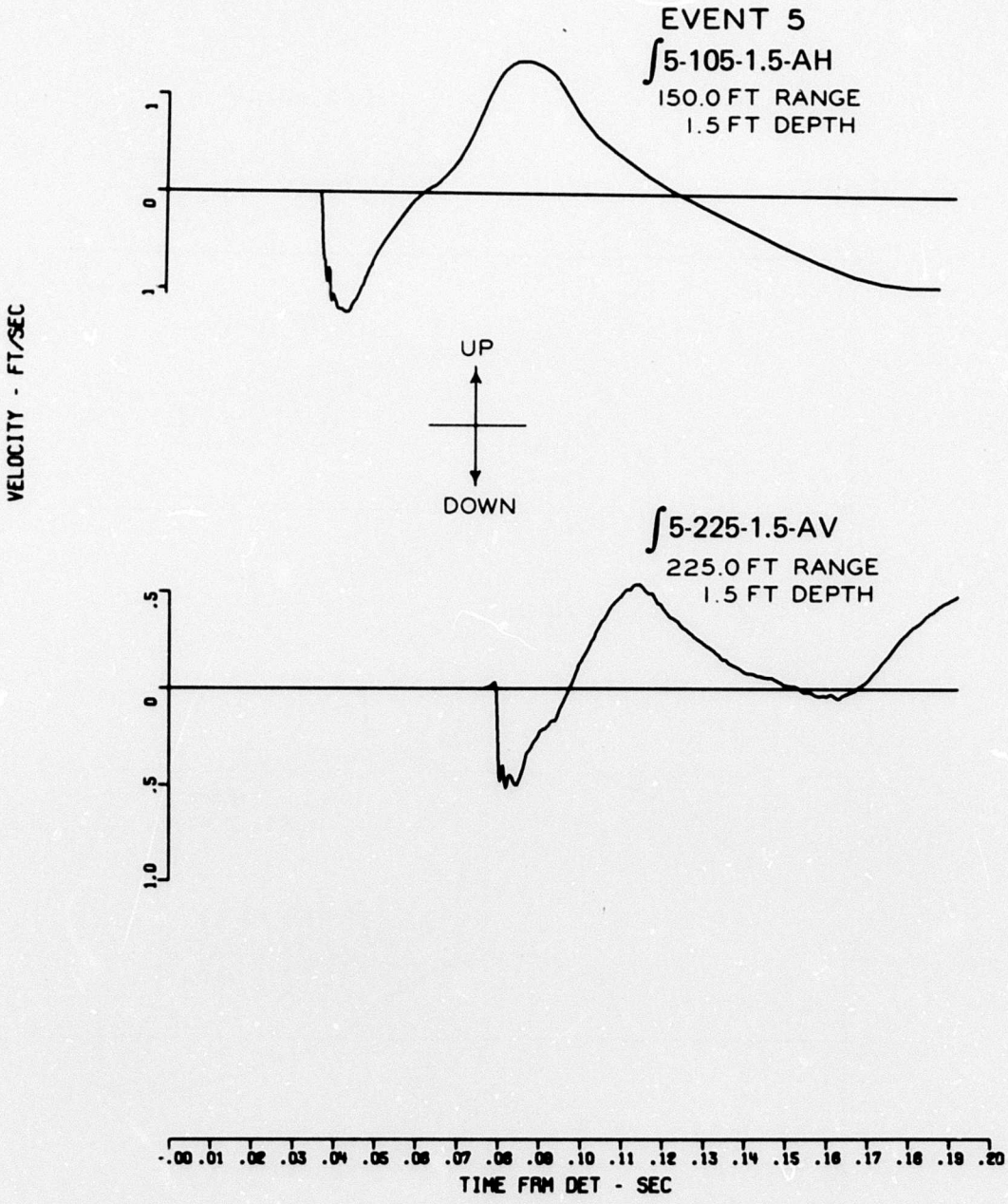

Figure A.12 (Sheet 3 of 3).

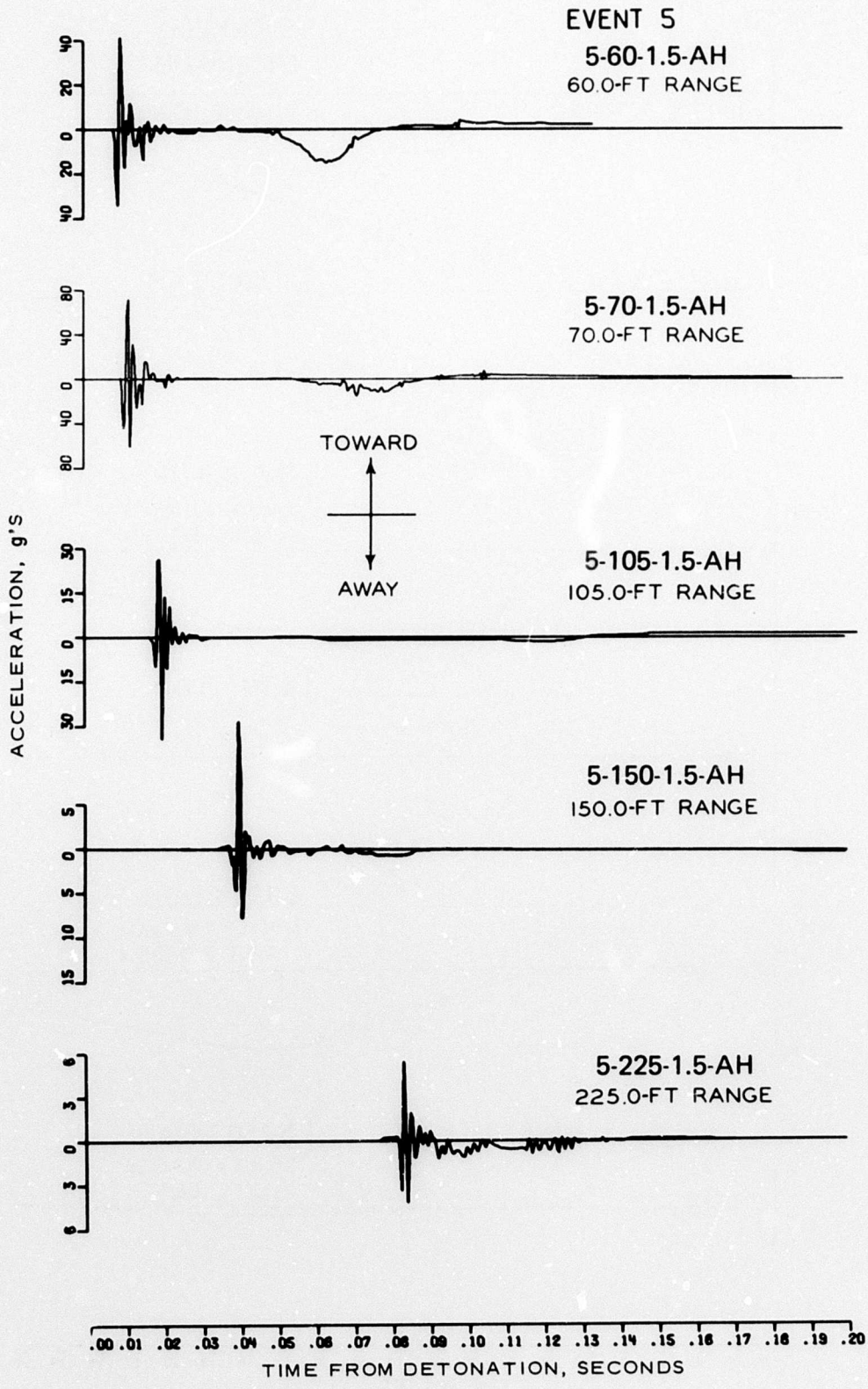

Figure A.13 Horizontal acceleration, Event 5.

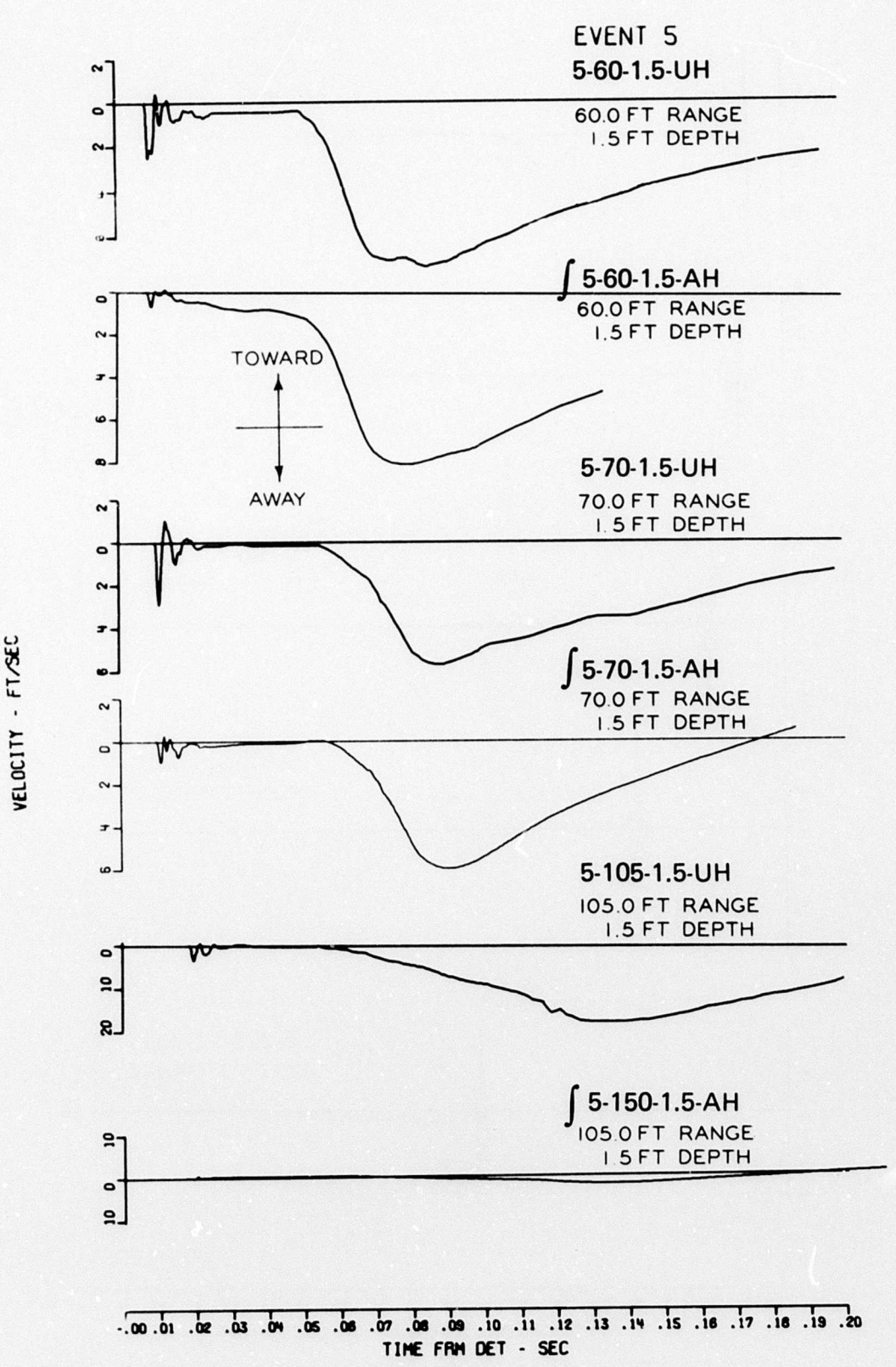

Figure A.14 Horizontal velocity, Event 5 (Sheet 1 of 3).

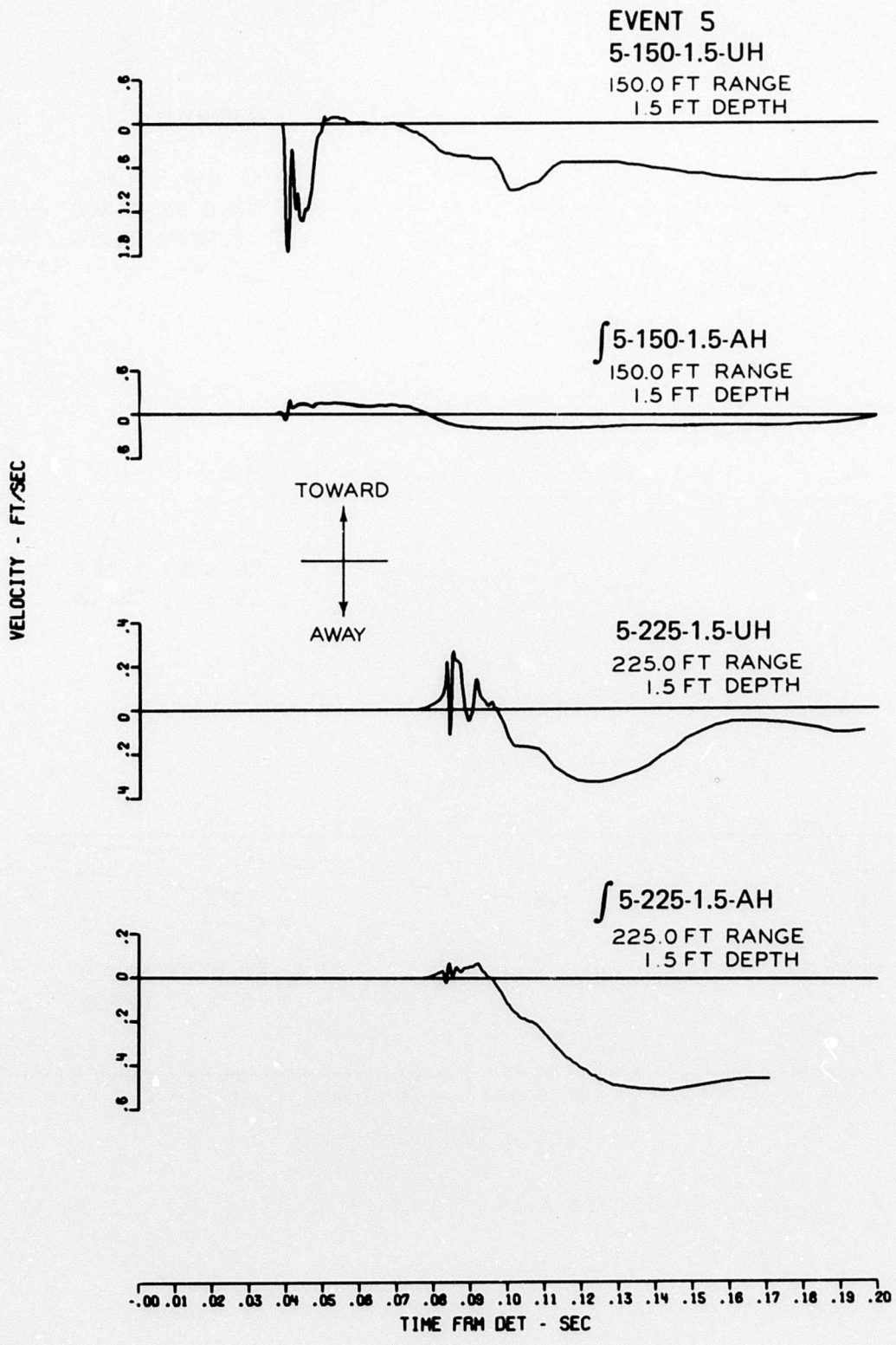

Figure A.14 (Sheet 2 of 3).

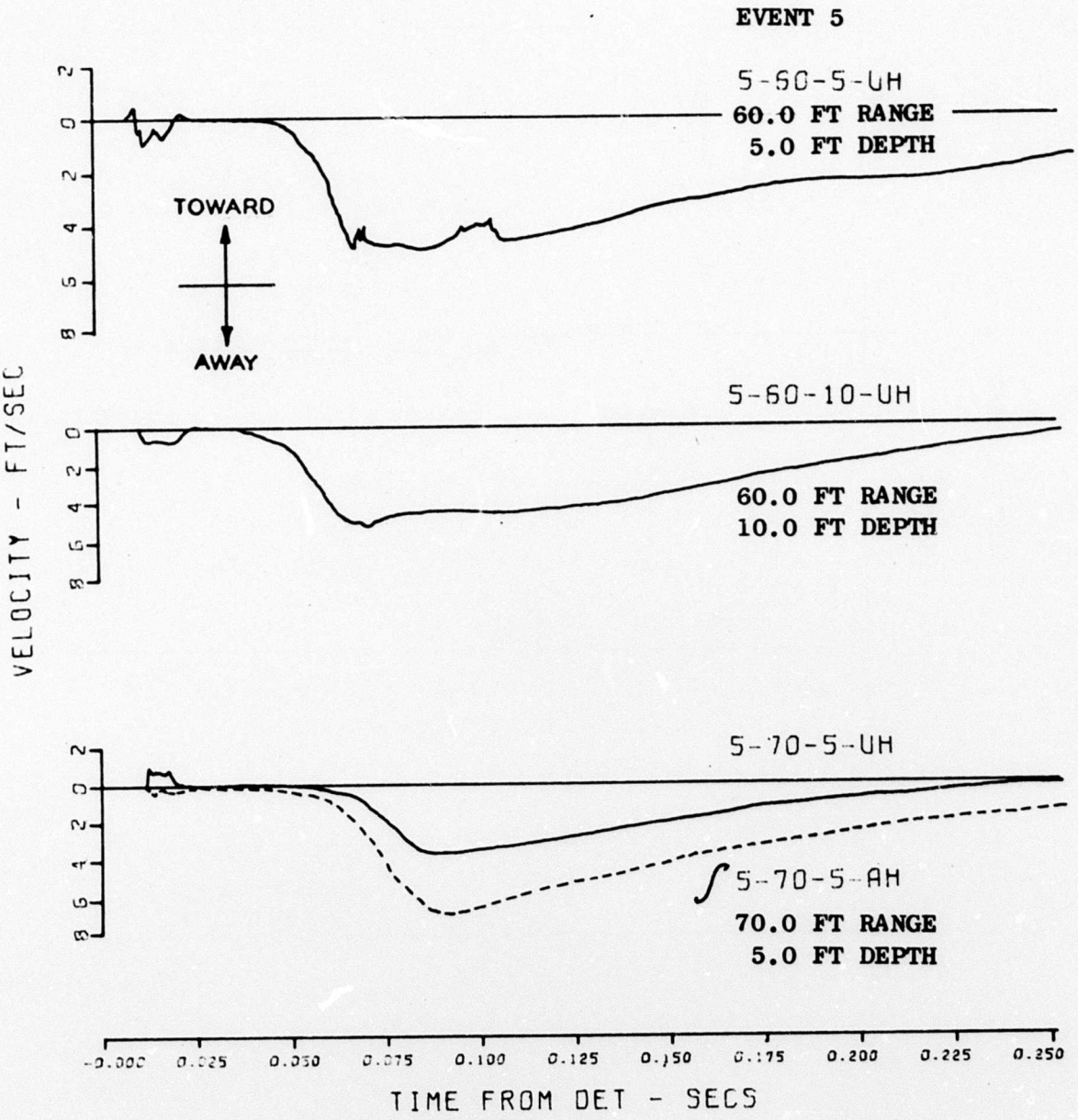

Figure A.14 (Sheet 3 of 3)

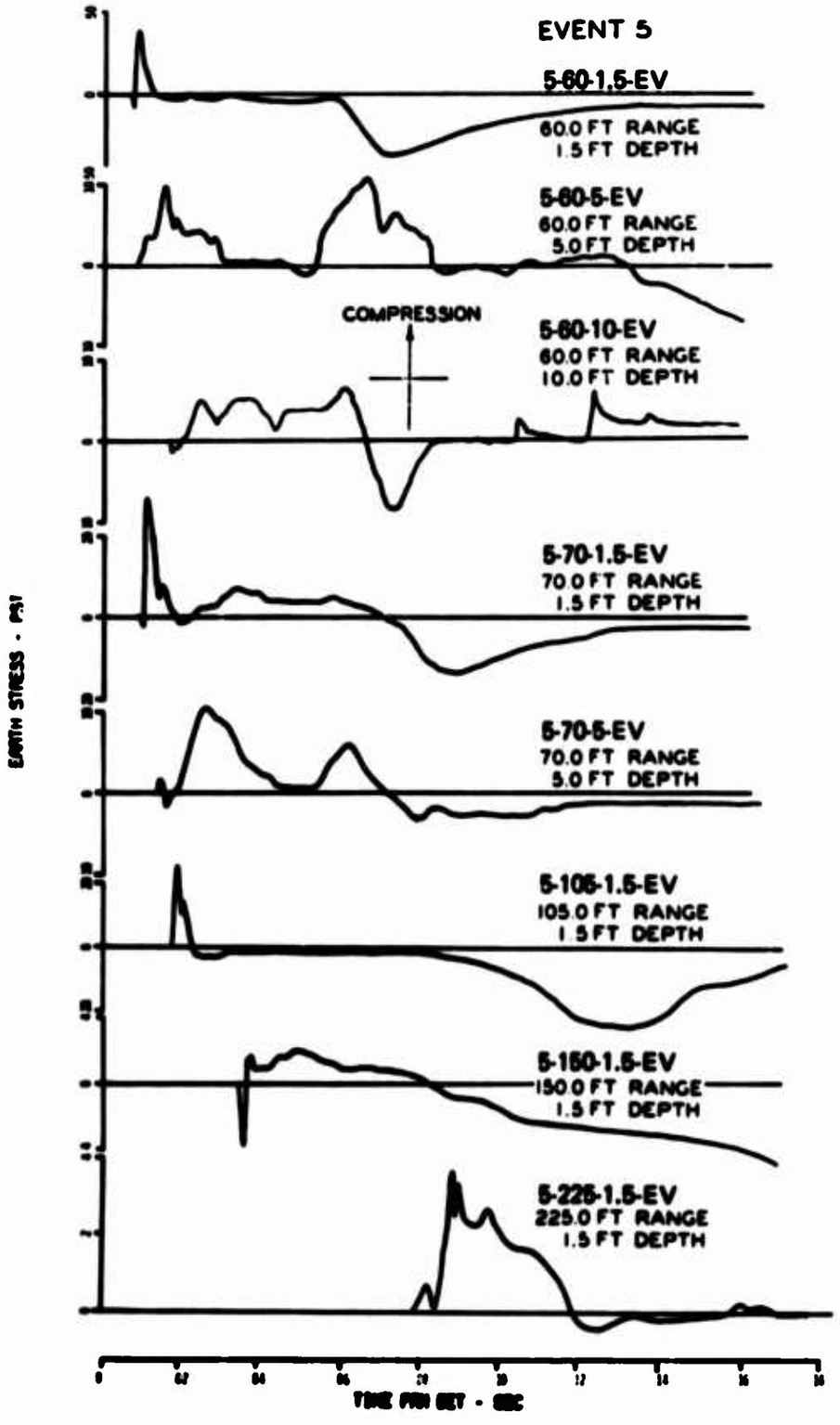

Figure A.15 Vertical stress, Event 5.

REFERENCES

1. F. M. Sauer and C. T. Vincent; "Ferris Wheel Series, Flat Top Event, Project Officer's Report - Project 1.2/1.3a, Earth Motion and Pressure Histories"; POR-3002 (WT-3002), 12 April 1967; Stanford Research Institute, Menlo Park, California; Unclassified.

2. W. R. Perrett and V. L. Gentry; "Free-Field Measurements of Earth Stress, Strain and Ground Motion"; Operation UPSHOT-KNOTHOLE, Project 1.4, WT-716, February 1955, Sandia Corporation, Albuquerque, New Mexico, Unclassified.

3. N. M. Newmark and J. D. Haltiwanger; "Air Force Design Manual: Principles and Practices for Design of Hardened Structures"; AFSWC-TDR-62-138, December 1962; Air Force Special Weapons Center, Kirtland Air Force Base, Albuquerque, New Mexico; Unclassified.

4. "Operation Distant Plain Preliminary Report"; DASA 1876-1 (DASIAC Special Report 53-1), Volume I, December 1966; Defense Atomic Support Agency Information and Analysis Center, General Electric, TEMPO, Santa Barbara, California; For Official Use Only.

5. "Operation Distant Plain Symposium"; DASA 1947-1 (DASIAC Special Report 60-1), Volume I, September 1967; Defense Atomic Support Agency Information Analysis Center, General Electric, TEMPO, Santa Barbara, California; For Official Use Only.

6. "Pace A-18 Accelerometer Tech Bulletin"; Revised February 1965, Pace Engineering Co., North Hollywood, California; Unclassified.

7. J. W. Wistor; "An Extended Range Velocity Gage for Measurements in High-Shock Environment"; Sandia Corporation, Albuquerque, New Mexico; Unclassified.

8. J. K. Ingram; "Procedure for Assembling SE-Type Soil Stress Gages"; Instruction Report No. 8, March 1967; U. S. Army Engineer Waterways Experiment Station, CE, Vicksburg, Mississippi; Unclassified.

9. J. K. Ingram; "Development of a Free-Field Soil Stress Gage for Static and Dynamic Measurements"; Technical Report No. 1-814, Februar, 1968; U. S. Army Engineer Waterways Experiment Station, CE, Vicksburg, Mississippi; Unclassified.

10. R. E. Reisler and others; "Airblast Parameters for Summer and Winter 20-Ton Explosions, Operation Distant Plain, Events 3 and 5"; Memorandum Report No. 1894, November 1967; U. S. Army Materiel Command, Ballistic Research Laboratories, Aberdeen Proving Ground, Maryland; Unclassified.

11. "Operation Distant Plain Preliminary Report"; DASA 1876-3, Volume III, January 1968; Defense Atomic Support Agency Information and Analysis Center, General Electric, TEMPO, Santa Barbara, California; For Official Use Only.

12. M. J. Dudash, ed.; "Operation Distant Plain Symposium II";

DASA 2207 (DASIAC Special Report 83), May 1968; Defense Atomic Support Agency Information and Analysis Center, General Electric, TEMPO, Santa Barbara, California; For Official Use Only.

13. F. M. Sauer, G. B. Clark, and D. C. Anderson; "Nuclear Geophysics; Part Four, Empirical Analysis of Ground Motion and Cratering"; DASA 1285(IV), May 1964; Stanford Research Institute, Menlo Park, California; Unclassified.

14. J. M. McCormick, M. L. Baron, and I. Nelson; "Studies on the Distant Plain 1A Event"; DASA 2213, July 1968; Paul Weidlinger Consulting Engineer, New York, New York; Unclassified.

15. "Operation Distant Plain Preliminary Report"; DASA 1876-2 (DASIAC Special Report 53-2), February 1967; Defense Atomic Support Agency Information and Analysis Center, General Electric, TEMPO, Santa Barbara, California; For Official Use Only.